IAEA-TECDOC-1363

Guidelines for radioelement mapping using gamma ray spectrometry data

INTERNATIONAL ATOMIC ENERGY AGENCY IAEA

July 2003

The originating Section of this publication in the IAEA was:

Nuclear Fuel Cycle and Materials Section
International Atomic Energy Agency
Wagramer Strasse 5
P.O. Box 100
A-1400 Vienna, Austria

GUIDELINES FOR RADIOELEMENT MAPPING USING
GAMMA RAY SPECTROMETRY DATA

IAEA, VIENNA, 2003
IAEA-TECDOC-1363
ISBN 92–0–108303–3
ISSN 1011–4289

Printed by the IAEA in Austria
July 2003

FOREWORD

Gamma rays are the most penetrating radiation from natural and man-made sources, and gamma ray spectrometry is a powerful tool for the monitoring and assessment of the radiation environment. Gamma ray surveys are carried out from aircraft, field vehicles, on foot, in boreholes, on the sea bottom and in laboratories. Ground and airborne gamma ray measurements cover large areas of the earth's surface, and many national and regional radiometric maps have been compiled and published. Standardized maps of terrestrial radiation and radioelement concentrations can be compared and regionally unified, showing general regional trends in radionuclide distribution and making the radiological assessment of the environment possible.

Radiometric surveys and maps are applicable in several fields of science. They retain their geological and geophysical information for mineral prospecting, geochemical mapping and structural geology, and enable the comparison of geological features over large regions. Although the gamma ray method was originally developed for geoscience, it has also been successfully applied in emergency situations for mapping the contamination from nuclear fallout and for the location of lost radioactive sources.

The use of modern computer data processing has enabled the introduction of new interpretation methods and the achievement of greater reliability in solving geological and environmental problems. The purpose and scope of this report is to introduce the theoretical background of gamma ray spectrometry in its application to the radiation environment, and to emphasize and illustrate new procedures in this field based on current knowledge. The report introduces the principles of radioactivity, contemporary radiation units, and the fundamentals of gamma ray spectrometry and its application to airborne, ground, car-borne, borehole and laboratory measurements. Examples of the use of gamma ray spectrometry in environmental studies and geological mapping illustrate the conditions, requirements and procedures for data acquisition, processing and reporting using this method.

For many years the International Atomic Energy Agency (IAEA) has been involved in the treatment of exploration data and their multiple applications related to mineral exploration, agricultural, and environmental assessment. Recognizing that techniques and methods are rapidly progressing in this field, the IAEA invited a group of specialists to write a comprehensive report on radioelement mapping using gamma ray spectrometry. The authors of this publication are known and recognized specialists from four countries involved in mapping and data treatment using spectrometry. They all have extensive experience in the application and use of gamma ray spectrometry for radioelement mapping.

This TECDOC is one of a series of IAEA publications covering all aspects of the uranium mining industry, from exploration to exploitation, decommissioning, and the application of techniques in other non-uranium resources areas.

The IAEA officers responsible for this publication were J.-P. Nicolet and G. Erdi-Krausz of the Division of Nuclear Fuel Cycle and Waste Technology.

EDITORIAL NOTE

The use of particular designations of countries or territories does not imply any judgement by the publisher, the IAEA, as to the legal status of such countries or territories, of their authorities and institutions or of the delimitation of their boundaries.

The mention of names of specific companies or products (whether or not indicated as registered) does not imply any intention to infringe proprietary rights, nor should it be construed as an endorsement or recommendation on the part of the IAEA.

CONTENTS

1. INTRODUCTION

The use of gamma ray spectrometry as a tool for mapping radioelement concentrations has found widespread acceptance in diverse fields. The method has evolved over several decades and continues to be developed. The method has benefited from continuing advances in instrumentation, field procedures, and calibration and data processing procedures. Gamma ray spectrometry is widely used for environmental mapping, geological mapping and mineral exploration.

1.1. Purpose of the report

The past decade has seen several significant changes in both instrumentation and methodology. Modern spectrometers now have automatic gain stabilization on individual detector crystals. Increases in computer processing capability have seen the implementation of full spectrum methods for statistical noise reduction and for routine data processing. New methods for enhancing and displaying the data have also been developed. These improvements have greatly increased the amount of useful information that can be extracted from gamma ray spectrometric data. This had led to a renewed interest in the application of the method to geological and environmental mapping.

The purpose of this report is to provide an up-to-date review on the use of gamma ray spectrometry for radioelement mapping and, where appropriate, provide guidelines on the correct application of the method. The report is timely, as recent years have seen several significant improvements to the method – particularly in the application of statistical smoothing techniques to the reduction of noise in raw gamma ray spectra, and in the application of image processing techniques to the enhancement and interpretation of radioelement data. The report will be a useful training guide for those new to the method. It gives a broad coverage of all aspects of the gamma ray method and provides a comprehensive list of references. Those familiar with the method will find the report a useful reference, and will benefit from the coverage of recent developments in this field.

1.2. Historical review

Martin Klaproth, a German chemist, discovered the element uranium in 1789. Henri Becquerel, a French physicist, discovered radioactivity in 1896. This led to further research into the nature of matter and gave birth to nuclear physics. The development of techniques for the measurement of radioactivity soon followed. The first tube detectors were developed in the first decade of the twentieth century, and these led to the development of portable field instruments. Measurement sensitivity increased significantly when scintillation detectors were developed during the 1940s.

Intensive uranium exploration led to the first airborne radiometric surveys in the USA, Canada and former USSR in 1947 and in Australia in 1951. Airborne, ground and laboratory gamma ray spectrometry were developed and applied to mineral exploration and environmental monitoring in the 1960s and 1970s. This enabled the in situ estimation of the radioelement concentrations of potassium, uranium and thorium in the field. Subsequent developments included the use of multichannel analyzers, digital recording, the development of semiconductor detectors, and improvements in data processing.

1.3. Gamma ray methods

The remote sensing of environmental radioactivity is achieved mainly through the detection of gamma radiation. Gamma rays are the most penetrating radiation from natural and man-made sources. Individual radionuclides emit gamma rays of specific energies that are characteristic for an element and isotope. Gamma ray measurements can be conducted in two modes. Total count measurements register gamma rays of all energies. These are used to monitor the gross level of the gamma radiation field and to detect the presence of anomalous sources. Spectrometers, on the other hand, measure both the intensity and energy of radiation, and this enables the source of the radiation to be diagnosed. Gamma ray spectrometry is thus a powerful tool for monitoring the radiation environment.

There are many types of gamma ray surveys. Spectrometers can be mounted in aircraft or motor vehicles. Hand-held portable spectrometers for ground measurements, and borehole spectrometers for down-hole measurements are available. Sea-bottom surveys are also possible, and laboratory spectrometers can accurately measure rock and soil samples. Large areas of the world have been covered by ground and airborne gamma ray surveys, and many national and regional radiometric maps have been compiled and published (IAEA, 1995, IAEA, 1997, Green et al., 1993). Survey results are usually reported in units of gamma ray dose rate (total-count surveys) or concentrations of the radioelements (spectrometer surveys). This requires that instruments are adequately calibrated. The IAEA has been instrumental in the introduction of standards for the calibration of gamma ray field instruments and the design and preparation of geological reference materials for laboratory gamma ray spectrometry (IAEA, 1989, IAEA 1987). The advantage of standardized procedures for calibration and data processing are that the results of different surveys can be combined and compared. This enables the interpretation of regional trends in radionuclide distribution.

Gamma ray surveys are used in several fields of science. They are used for geological, geochemical, and environmental mapping, and allow the interpretation of regional features over large areas. Gamma ray surveys are used in soil mapping and for mineral exploration. They may be used to estimate and assess the terrestrial radiation dose to the human population and to identify areas of potential natural radiation hazard. They have, for example, been used to delineate areas at risk from atmospheric radon. Regional surveys provide a base against which man-made contamination can be estimated. For example, surveys are regularly carried out around nuclear facilities such as power plants to provide a baseline against which any accidental release of radioactive material can be measured. Similar surveys are used to assess the contamination in areas of former mining, and of industrial areas. The gamma ray method has been successfully applied to mapping the fallout from nuclear accidents, and for the location of lost radioactive sources.

1.4. Scope of the report

This report gives an overview of the theoretical background to radioactivity and the gamma ray spectrometric method. This is followed by a review of the application of the method to mapping the radiation environment.

Chapter 2 gives a brief outline of the principles of radioactivity, the interaction of gamma rays with matter, instrumentation applied to the measurement of gamma rays, and the quantities and units in contemporary use in gamma ray spectrometry. This is followed by a review of the fundamentals of gamma ray spectrometry (Chapter 3), and its application to ground (Chapter 4) and airborne (Chapter 5) mapping. These chapters cover all aspects of the calibration and

data processing procedures required for estimating the ground concentrations of the radioelements.

Chapter 6 describes the procedures required for the recovery of older survey data, and the "back-calibration" of these data. These are the procedures required to enable the reporting of older survey data in the correct physical units. The chapter includes a section on the merging of surveys to create regional compilations.

Chapter 7 gives an overview of data presentation and integration for mapping applications. It covers areas such as map projections, profile and map presentations, gridding, and the application of image processing techniques to the presentation of gamma ray spectrometric data. Data analysis and interpretation methodology are covered in Chapter 8. The application of gamma ray spectrometric data to mapping the natural radiation environment and man-made sources of radiation are reviewed in Chapters 9 and 10, respectively.

2. PRINCIPLES OF RADIOACTIVITY

The application of radioactivity in geoscience is based on knowledge of the physical properties of radiation sources, and our ability to detect these sources through the analysis of remotely sensed data. This chapter reviews the principles of radioactivity and its detection. Quantities and units in contemporary use in radioactivity are reviewed.

2.1. Basic radioactivity

Atoms are the smallest particles of mass with distinctive chemical properties. An atom consists of a nucleus surrounded by electrons. The nucleus consists of positively charged protons, and uncharged neutrons. The diameter of an atom is of the order 10^{-10} m, and the diameter of a nucleus is of the order 10^{-15} m. Protons and neutrons have a mass of 1.67×10^{-27} kg. The mass of negatively charged electrons is 9.11×10^{-31} kg. The elementary charge is 1.602×10^{-19} C.

The number of protons in a nucleus of an element, X, is the proton number Z (also called the atomic number). The sum of the protons and neutrons (nucleons) is the mass number, A, of an atom. Atoms of an element having the same atomic number but different numbers of neutrons (i.e. different mass numbers) are called *isotopes*. Isotopes are denoted by their chemical symbol and their mass number as follows - ^{A}X. Isotopes have identical chemical properties, but different physical properties. Atoms having identical numbers of protons and neutrons are named nuclides.

The atomic nuclei of some isotopes have a surplus of energy, are unstable, and disintegrate to form more stable nuclei of a different isotope. This process is accompanied by the emission of particles or energy, termed nuclear radiation. Nuclides with this feature are called radionuclides, and the process is called nuclear decay or disintegration.

The radioactivity decay law expresses the decrease in the number of atoms of a radionuclide with time:

$$N_t = N_0 e^{-\lambda t} \tag{2.1}$$

where N_t = the number of atoms present after time t (s);
N_0 = the number of atoms present at time $t = 0$;
λ = the decay constant of a radionuclide (s^{-1}),

A related constant, the half-life $T_{1/2}$ (s), is the time taken for half the radionuclides to decay:

$$T_{1/2} = \frac{0.693}{\lambda} \tag{2.2}$$

The product λN gives the activity (Bq) of the radionuclide. Radioactive decay is independent of other physical conditions.

2.2. Types of radioactive decay

There are several types of radioactive decay. *Alpha decay* is accompanied by the release of an alpha particle consisting of 2 protons and 2 neutrons. *Beta$^-$ decay* is realized by the emission of a beta particle identical to a negatively charged electron. *Beta$^+$ decay*, which is less

frequent, is accompanied by the emission of a positively charged positron. *Electron capture* occurs through the absorption of an orbital electron of an atom by the atomic nucleus. The replacement of the vacant electron position is followed by the emission of characteristic radiation (electromagnetic radiation of low energy). Spontaneous fission occurs through the splitting of heavy atoms into two fragments and the subsequent release of neutrons and energy. The decay of a radionuclide usually leaves the newly formed nucleus in an energy excited state, and the surplus energy is radiated as gamma rays.

The type of decay of unstable nuclides determines the nature of the newly formed atoms. The equations representing transitions of an element X to an element Y by a specific mode of decay are summarized as follows:

$$^{A}X \rightarrow {}^{A-4}Y + \alpha \text{ (alpha emission)}, \qquad Z_Y = Z_X - 2 \tag{2.3}$$

$$^{A}X \rightarrow {}^{A}Y + \beta \text{ (beta}^{-}\text{ emission)}, \qquad Z_Y = Z_X + 1 \tag{2.4}$$

$$^{A}X \rightarrow {}^{A}Y + \text{photon (electron capture)}, \quad Z_Y = Z_X - 1 \tag{2.5}$$

Some radionuclides may have more than one mode of decay. For example, 66 percent of ^{212}Bi disintegrations are by beta particle emission to ^{212}Po, and 34 percent are by alpha particle emission to ^{208}Tl. But irrespective of the type of radiation, the observed half-life is always the same.

Radioactive decay also often occurs in a series (or chain) with a number of daughter products, which are also radioactive, and terminates in a stable isotope. In a closed system, and starting with a specified amount of a mother element, the number of atoms of daughter elements and their activity grows gradually until radioactive equilibrium of the disintegration series is reached. At this point, the activities of all the radionuclides of the series are identical. Thus the measurement of the concentration of any daughter element can be used to estimate the concentration of any other element in the decay series. Under equilibrium conditions, this relationship can be expressed as follows:

$$\lambda_1 N_1 = \lambda_2 N_2 = \lambda_3 N_3 = \ldots \qquad \lambda_i N_i \tag{2.6}$$

Examples of chain disintegration are the natural decay series ^{238}U, ^{235}U and ^{232}Th.

2.3. Statistical nature of radioactive decay

Radioactive decay is a statistical phenomenon. Each atomic disintegration during radioactive decay occurs completely independently of every other decay event, and the time interval between disintegrations is not constant. For a large number of randomly disintegrating atoms of a particular radionuclide, the frequency of radioactive decay is given by Poisson's distribution: if $\bar{n}$ is the mean decay rate, the probability, P, that the number of atomic nuclei, n, will decay within a time unit is:

$$P(n) = \frac{\bar{n}^n}{n!}\exp(-\bar{n}) \tag{2.7}$$

For Poisson's distribution it holds that the variance σ^2 of a distribution is equal to its mean value, and σ is the standard deviation. The range of $\pm 1\sigma$ about the mean encompasses 68.3 percent of the distribution, $\pm 2\sigma$ encompasses 95.5 percent of the distribution, and $\pm 3\sigma$ encompasses 99.7 percent of the distribution.

The emission of particles and gamma rays in radioactive decay is proportional to the number of disintegrating atoms, and the standard deviation may be used to estimate the range of deviations and errors of the radiometric measurements. If *N* counts are recorded in time *t*, then the standard deviation of the recorded counts is:

$$\sigma(N) = \sqrt{\overline{N}} \tag{2.8}$$

where $\overline{N}$ is the mathematical expectation of the number of counts (the mean count of repeated measurements). The fractional standard deviation of a count (error of measurement of *N*) is:

$$\frac{\sigma(N)}{\overline{N}} = \frac{1}{\sqrt{\overline{N}}}. \tag{2.9}$$

For a count rate $n = N/t$ (c/s), the standard deviation is given by

$$\sigma(n) = \frac{\sqrt{N}}{t} = \sqrt{\frac{n}{t}} \tag{2.10}$$

and the fractional standard deviation of the count rate *n* (error of measurement of *n*) is:

$$\frac{\sigma(n)}{n} = \frac{1}{\sqrt{nt}} \tag{2.11}$$

The "probable deviation" ($P = 0.5$) is 0.674 σ, a multiple of standard deviation. Equations (2.9) and (2.11) indicate that the precision of radiometric measurements can be increased by (a) increasing the counts, *N*, (b) increasing the count rate, *n,* and (c) increasing the counting time, *t*. This can be accomplished by the use of more sensitive equipment, improving the geometry of measurement, or extending the counting time. In practice, errors are also affected by background radiation. The background radiation should be kept to a minimum by shielding the detector. More detailed description of the theory of radioactivity can be found in Adams and Gasparini, 1970, Kogan et al., 1971, and Mares et al., 1984.

2.4. Natural sources of radiation

While many naturally occurring elements have radioactive isotopes, only potassium, and the uranium and thorium decay series, have radioisotopes that produce gamma rays of sufficient energy and intensity to be measured by gamma ray spectrometry. This is because they are relatively abundant in the natural environment. Average crustal abundances of these elements quoted in the literature are in the range 2-2.5% K, 2-3 ppm U and 8-12 ppm Th.

^{40}K is the radioactive isotope of potassium, and occurs as 0.012 percent of natural potassium. This isotope decays to ^{40}Ar with the emission of gamma rays with energy 1.46 MeV. Since ^{40}K occurs as a fixed proportion of K in the natural environment, these gamma rays can be used to estimate the total amount of K present. The half-life of ^{40}K is 1.3×10^{9} years.

Uranium occurs naturally as the radioisotopes ^{238}U and ^{235}U which give rise to decay series that terminate in the stable isotopes ^{206}Pb and ^{207}Pb respectively (Tables 2.1 and 2.2). The half-lives of ^{238}U and ^{235}U are 4.46×10^{9} and 7.13×10^{8} years, respectively. Thorium occurs naturally as the radioisotope ^{232}Th which gives rise to a decay series that terminates in the stable isotope ^{208}Pb (Table 2.3). The half-life of ^{232}Th is 1.39×10^{10} years. Neither ^{238}U, nor ^{232}Th emit gamma rays, and gamma ray emissions from their radioactive daughter products are used to estimate their concentrations.

2.5. Disequilibrium

Disequilibrium occurs when one or more decay products in a decay series are completely or partially removed or added to the system. Thorium rarely occurs out of equilibrium in nature, and there are no disequilibrium problems with potassium. However, in the uranium decay series disequilibrium is common, and can occur at several positions in the ^{238}U decay series: ^{238}U can be selectively leached relative to ^{234}U; ^{234}U can be selectively leached relative to ^{238}U; ^{230}Th and ^{226}Ra can be selectively removed from the decay chain; and finally ^{222}Rn (radon gas) is mobile and can escape from soils and rocks into the atmosphere. Depending on the half-lives of the radioisotopes involved, it may take days, weeks or even millions of years for equilibrium to be restored.

Disequilibrium in the uranium decay series is a serious source of error in gamma ray spectrometry. Uranium concentration estimates are based on the measurement of ^{214}Bi and ^{214}Pb isotope abundances. These occur far down in the radioactive decay chain and may not be in equilibrium with uranium. Estimates of uranium concentration are therefore usually reported as “equivalent uranium” (eU) as these estimates are based on the assumption of equilibrium conditions. Thorium is also usually reported as “equivalent thorium” (eTh), although the thorium decay series is almost always in equilibrium.

2.6. Interaction of gamma rays with matter

Radiation is comprised of a flux of elementary particles and energy quanta, and can be classified by its physical character and energy. These determine how the radiation interacts with matter.

Alpha radiation is a flux of positively charged alpha particles. Alpha particles have an initial energy of several MeV, and an initial velocity of the order 10^{7} m/s. They exhibit high ionization, and their penetration range in matter is low. Alpha particles are absorbed by about 10^{-2} m of air, and 10^{-5} m of rock. Alpha particles have a discrete energy that is specific for a particular radionuclide.

Beta radiation is a flux of electrons with a continuous energy spectrum up to a maximum energy, which depends on the particular radionuclide. The initial velocity of beta particles can approach the velocity of light. The penetration range for beta particles depends on the initial energy of the particle. For E=2 MeV, the penetration range is about 8 m in air and 1 cm in water.

TABLE 2.1. ^{238}U DECAY SERIES (simplified after Radiological Health Handbook, 1970, and Ivanovich and Harmon, 1982)

Nuclide	Half-life	Major radiation energies (MeV) and intensities*		
		α	β	γ
^{238}U	4.468×10^9y	4.15 (23%) 4.19 (77%)	–	–
^{234}Th	24.1d	–	~0.103 (19%) 0.191 (81%)	0.063 (3.5%) 0.093 (4%)
^{234}Pa	1.18m	–	2.29 (98%)	0.765 (0.30%) 1.001 (0.60%)
99.86% / 0.14%				
^{234}Pa	6.7h	–	0.53 (66%) 1.13 (13%)	0.10 (50%) 0.70 (24%) 0.90 (70%)
^{234}U	2.48×10^5y	4.72 (28%) 4.77 (72%)	–	0.053 (0.2%)
^{230}Th	7.52×10^4y	4.62 (24%) 4.68 (76%)	–	0.068 (0.6%) 0.142 (0.07%)
^{226}Ra	1602y	4.60 (5.5%) 4.78 (94.5%)	–	0.186 (4%)
^{222}Rn	3.825d	5.49 (~100%)	–	0.510 (0.07%)
^{218}Po	3.05m	6.11 (100%)	0.33 (100%)	–
99.98% / 0.02%				
^{214}Pb	26.8m	–	1.03 (6%)	0.295 (19%) 0.352 (36%)
^{218}At	2s	6.65 (6%) 6.70 (94%)	0.67 (94%)	–
^{214}Bi	19.7m	5.61 (100%)	3.26 (100%)	0.609 (47%) 1.120 (17%) 1.764 (17%)
99.96% / 0.04%				
^{214}Po	164μs	7.83 (100%)	–	0.799 (0.014%)
^{210}Tl	1.32m	–	2.3 (100%)	0.296 (80%) 0.795 (100%) 1.31 (21%)
^{210}Pb	~22y	3.7 (1.8×10^{-8}%)	0.017 (85%) 0.064 (15%)	0.047 (4%)
^{210}Bi	5.02d	4.93 (60%) 4.89 (34%) 4.59 (5%)	1.155 (100%)	–
~100% / ~.00001%				
^{210}Po	138.3d	5.30 (100%)	–	0.803 (0.0011%)
^{206}Tl	4.19m	–	1.520 (100%)	–
^{206}Pb	Stable	–	–	–

* Intensities refer to percentage of disintegrations of the nuclide itself, not to the original parent of the series.

TABLE 2.2. ^{235}U DECAY SERIES (simplified after Radiological Health Handbook, 1970, and Ivanovich and Harmon, 1982)

Nuclide	Half-life	Major radiation energies (MeV) and intensities*		
		α	β	γ
^{235}U	7.13×10^{8}y	4.36 (18%) 4.39 (57%) 4.1-4.6 (8%)	–	0.143 (11%) 0.185 (54%) 0.204 (5%)
^{231}Th	25.64h	–	0.300 (~100%)	0.026 (2%) 0.084 (10%)
^{231}Pa	3.43×10^{4}y	5.01 (<20%) 4.99 (25.4%) 4.94 (22.8%)	–	0.027 (6%) 0.29 (6%)
^{227}Ac	22y	4.95 (48.7%) 4.94 (36.1%) 4.87 (6.9%)	0.046 (100%)	0.070 (0.08%)
98.8% / 1.2%				
^{227}Th	18.17d	5.76 (21%) 5.98 (24%) 6.04 (23%)	–	0.050 (8%) 0.237 (15%) 0.31 (8%)
^{223}Fr	21m	5.34 (.005%)	1.15 (100%)	0.050 (40%) 0.080 (13%) 0.234 (4%)
^{223}Ra	11.68d	5.61 (26%) 5.71 (53.7%) 5.75 (9.1%)	–	0.149 (10%) 0.270 (10%) 0.33 (6%)
^{219}Rn	3.92s	6.42 (8%) 6.55 (11%) 6.82 (81%)	–	0.272 (9%) 0.401 (5%)
^{215}Po	1.83ms	7.38 (100%)		–
^{211}Pb	36.1m	–	0.95 (1.4%) 0.53 (5.5%) 1.36 (92.4%)	0.405 (3.4%) 0.427 (1.8%) 0.832 (3.4%)
^{211}Bi	2.16m	6.28 (17%) 6.62 (83%)	0.60 (0.28%)	0.351 (14%)
0.32% / 98.68%				
^{211}Po	0.52s	7.43 (99%)	–	0.570 (0.5%) 0.90 (0.5%)
^{207}Tl	4.79m	–	1.44 (100%)	0.897 (0.16%)
^{207}Pb	Stable	–	–	–

* Intensities refer to percentage of disintegrations of the nuclide itself, not to the original parent of the series.

TABLE 2.3. ^{232}Th DECAY SERIES (simplified after Radiological Health Handbook, 1970, and Ivanovich and Harmon, 1982)

Nuclide	Half-life	Major radiation energies (MeV) and intensities*		
		α	β	γ
^{232}Th	1.39×10^{10}y	3.95 (24%) 4.01 (76%)	–	–
↓				
^{228}Ra	5.75y	–	0.055 (100%)	–
↓				
^{228}Ac	6.13h	–	2.11 (100%)	0.34 (15%) 0.908 (25%) 0.96 (20%)
↓				
^{228}Th	1.913y	5.34 (28% 5.42 (71%)	–	0.084 (1.6%) 0.214 (0.3%)
↓				
^{224}Ra	3.64d	5.45 (5.5%) 5.68 (94.5%)	–	0.241 (3.7%)
↓				
^{220}Rn	55.6s	6.30 (~100%)	–	0.55 (0.07%)
↓				
^{216}Po	0.145s	6.78 (100%)	–	–
↓				
^{212}Pb	10.64h	–	0.580	0.239 (47%) 0.300 (3.2%)
↓				
^{212}Bi	60.5m	6.05 (70%) 6.09 (30%)	2.25 (100%)	0.040 (2%) 0.727 (7%) 1.620 (1.8%)
64.0% ↓ 36.0%				
^{212}Po	304ns	8.78 (100%)	–	–
^{208}Tl	3.1m	–	1.80 (100%)	0.511 (23%) 0.583 (86%) 0.860 (12%) 2.614 (100%)
↓				
^{208}Pb	Stable	–	–	–

* Intensities refer to percentage of disintegrations of the nuclide itself, not to the original parent of the series.

Beta radiation passing through matter loses its energy by ionization and generates electromagnetic radiation called bremsstrahlung. Positrons passing through matter combine with electrons, and generate two annihilation gamma quanta of energy 511 keV each.

Gamma radiation is part of the electromagnetic spectrum. Gamma rays travel at the speed of light (c), and have a discreet energy (E), frequency (f), and wave length (λ). These are related by:

$$E = hf = hc/\lambda \tag{2.12}$$

where h = Planck's constant 6.6261×10^{-34} Js;
c = velocity of light.

Electromagnetic radiation of energy $E < 40$ keV is denoted as X-rays. Gamma rays comprise that part of the electromagnetic spectrum where $E > 40$ keV.

Gamma rays interact with atoms of matter by three principal processes (ICRU, 1994). These are the photoelectric effect, Compton scattering and pair production. The photoelectric effect is the predominant absorption process at low energies, and results in all the energy of a gamma quantum being absorbed in a collision with an electron of an atom. Compton scattering predominates at moderate energies and corresponds to a collision of an incident photon with an electron. The incident photon loses part of its energy to the electron and is "scattered" at an angle to its original direction. Pair production occurs at energies greater than 1.02 MeV. It is the process whereby an incident photon is completely absorbed and results in the creation of an electron-positron pair in the electrostatic field of a nucleus.
The probability that a photon will interact with matter, expressed by the cross-section σ (m^2), depends on the photon energy, E, and the composition of the matter. Figure 2.1 illustrates the relationship between the scattering and absorption processes, the energy of the incident photon, and the atomic number of the absorbing medium. For gamma rays of natural terrestrial origin (E up to 2.615 MeV) and for matter comprising rock, water and air, Compton scattering is the dominant interaction process.

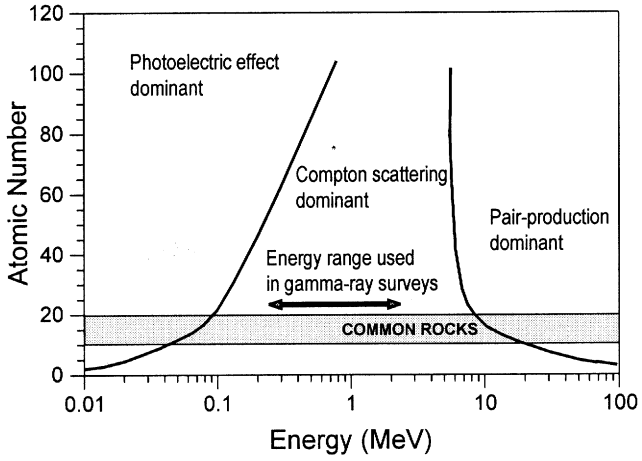

FIG. 2.1. The interaction of gamma rays with matter.

Typically, gamma ray photons lose energy through successive Compton scattering events, until eventually the resulting low-energy photons are absorbed through the photoelectric effect. As a result of the interaction of gamma rays with matter, the intensity of radiation decreases with distance from the source. The absorption of gamma rays of a specific energy in matter is described by either a linear attenuation coefficients μ (m^{-1}) or a mass attenuation coefficient μ/ρ (m^2/kg). For a narrow beam of gamma rays, the attenuation of the gamma rays can be modelled by an exponential function. The range of gamma rays of natural radionuclides is about 700 m in air, up to 0.5 m in rocks and a few cm in lead. Gamma rays have a discrete energy that is specific for a particular radionuclide. Since gamma rays are the most penetrating component of natural and man-made radiation, they are widely used in the study of the radiation environment.

2.7. Detectors and instruments

Ionizing radiation can be measured through the physical and chemical effects of its interaction with matter. Field and laboratory methods are based mainly on the ionizing properties of radiation and the use of instruments that convert the radiation to electrical signals.

Ionization chambers, proportional counters, Geiger-Muller tubes, scintillation counters, semiconductor detectors, thermoluminiscence detectors and various mechanical and chemical track detectors are used to monitor and quantify the α, β, γ and neutron radiation of the environment. The nature and character of the radiation governs the selection of a suitable detector. The efficiency of a detector is a measure of the probability that an incident photon will be absorbed in the detector. It is usually quoted as the ratio of recorded counts to incident photons. The energy resolution of a detector is a measure of its ability to distinguish between two gamma rays of only slightly different energies. This is usually defined as the full width of a photopeak at half the maximum amplitude (FWHM) divided by its energy. Instruments used in in-situ gamma ray spectrometry are usually specified by the energy resolution of the ^{137}Cs photopeak at 662 keV. Dead time refers to the finite time required for a detector to process an individual particle of radiation. During this time all incoming pulses are ignored. Dead time should thus be as small as possible.

A Geiger-Muller counter (GM counter) consists of a gas-filled tube equipped with a metal cylinder (the cathode) and a thin conductive wire (the anode) mounted along the tube axis. Normally argon, with an admixture of halogen vapour, is used as gas filling. GM counters are 2 to 30 cm long and 1 to 4 cm in diameter, and they operate with applied voltage of several hundred volts. GM counters make use of the progressive growth of ionization in a strong electric field between the anode and the cathode. An incident photon interacts with the cathode and releases an electron that may be directed into the GM tube. The growth of ionization between the anode and the cathode amplifies the signal and generates an electric current between the electrodes. This results in a voltage pulse at the anode output of the GM counter. The multiplication coefficient of the gas ionizing chain reaction is of the order of 10^6, and the output pulse is not proportional to the absorbed gamma ray energy. The detection efficiency of GM counters is very low (less than 2%) and the dead time is of the order 10^{-4} s.

Scintillation counters consist of a scintillator and a photomultiplier. An incident gamma ray photon interacts with the material of the scintillation crystal to produce scintillations. These photons of visible light induce the ejection of electrons from the photocathode of the attached photomultiplier. Their number multiplies progressively at dynodes of the photomultiplier, and an electron cloud strikes the anode. This induces a negative voltage pulse as output, with amplitude proportional to the energy of the incident photon. Scintillation counters are widely used in gamma ray spectrometry. Thallium-activated sodium iodide NaI(Tl) crystals are mainly used as detectors in field gamma ray surveys. They are transparent, with a high density (3.66 g/cm), and can be manufactured in large volumes. They have a detection efficiency of up to 100% for low-energy gamma rays but somewhat less for high-energy gamma rays. The dead time is of the order 10^{-7} s and the energy resolution for ^{137}Cs at 662 keV is in the range ranges 7-10%, depending on the volume and quality of the detector. NaI(Tl) detectors are hygroscopic, they age, they are fragile, and the photomultiplier tube function is dependent on temperature. Their large crystal volumes are an advantage in applications such as airborne surveying where measurement times are necessarily short. Thallium-activated caesium-iodide CsI(Tl) crystals are neither hygroscopic nor particularly fragile. They have a density of 4.51 g/cm^3, and a dead time of the order 10^{-9} s. But they are too expensive for widespread use. Plastic scintillators are an admixture of a scintillator and a plastic transparent material. They can be produced in large volumes, but have poor energy resolution and are not suitable for

gamma ray spectrometry. Bismuth-germanium-oxygen $Bi_4Ge_3O_{12}$ scintillation crystals have been applied to field gamma ray spectrometry in boreholes. Due to their high density (7.13 g/cm^3) they are efficient at high gamma ray energies.

Germanium semiconductor detectors use the electronic carriers (electron-ion and electron-hole pairs) created by the absorption of gamma ray photons in the germanium detector. These collect directly on the detector electrodes, causing a flow of electric current through the semiconductor and produce an output voltage pulse of amplitude proportional to the energy of the incident gamma ray photon. The detector consists of a germanium crystal mounted in a vacuum cryostat cooled to -196 °C. Cooling is by insertion of the cryostat in a dewar vessel filled with liquid nitrogen, or by electrically powered cryogenic refrigerators. The detectors are generally of small volume and used in in-situ gamma ray spectrometry. The energy resolution of these detectors is very high, but because of their small volume, their sensitivity is low and it may take tens of minutes to record a spectrum.

Independent of the type of detector, radiometric instruments used for the detection of gamma rays differ in their response to gamma radiation and in their ability to distinguish gamma rays of different energy. Count rate meters produce a voltage or electric current at the output that is proportional to the count rate. The voltage or current is usually displayed on a dial gauge. The precision of measurement is proportional to the value of the instrument time constant. Scalers give the number of detected particles and the time of measurement.

Total count instruments have an energy discrimination threshold above which all gamma rays are recorded. Any change in the energy discrimination threshold will affect the response of the instrument. For small field instruments, the energy discrimination threshold is usually set at a low energy between 30 and 150 keV. This gives the instrument a high sensitivity. However, since these instruments do not usually have automatic gain stabilization to keep the discrimination threshold at a constant level, the response may change with time. A reference radiation source may be used to adjust the gain periodically. Total count measurements can be used to estimate the overall radiation level.

Gamma ray spectrometers use the direct proportionality between the energy of an incoming gamma ray and the pulse amplitude at the output of the detector. Figure 2.2 shows a block diagram of a gamma ray spectrometer. After amplification and digitisation, the pulse amplitudes are analysed, and the output of the spectrometer is an energy spectrum of detected radiation. Since individual radionuclides emit specific gamma ray energies, gamma ray spectra can be used to diagnose the source of the radiation.

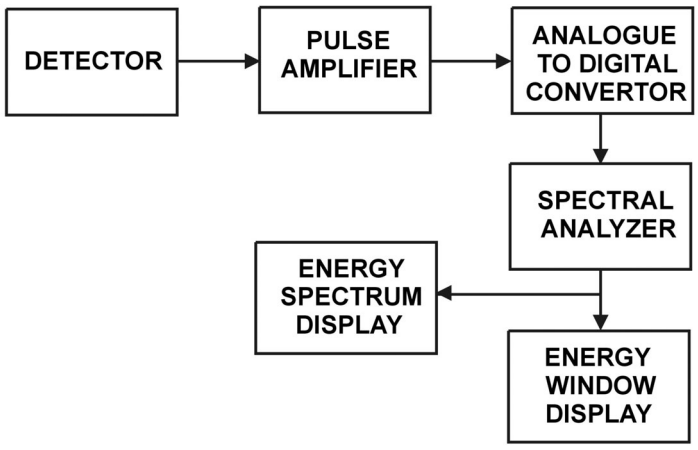

FIG. 2.2. Block diagram of a gamma ray spectrometer.

Gamma ray spectrometers are either “integral” or “differential”. Integral spectrometers record only those pulses with amplitudes exceeding a discrimination threshold. This threshold can be changed to allow the discrimination of individual radionuclides. Differential gamma ray spectrometers record pulses whose amplitudes fall within a given amplitude interval (or channel), corresponding to a discrete range of gamma ray energy. Wider energy intervals (comprising several channels) are called energy windows. Modern analyzers use as many as 256 or 512 channels, with a width of several keV per channel. Older systems are limited to recording several distinct energy windows. Gamma ray spectrometers should have amplitude gain stabilization to avoid the effect of energy spectrum drift. Gain stabilization can be accomplished by controlling the temperature of the detector, or by spectrum energy stabilization using either a reference radioactive source or the measured spectrum.

Some radiological instruments can be used for the calibration of field survey radiometric devices. Pressurised ionization chambers measure the electric current generated between two electrodes in a gas whose atoms are ionized by gamma and X-rays. The output is proportional to the environmental exposure rate.

Further descriptions of detectors and radiometric devices can be found in Adams and Lowder (1964), IAEA (1989), ICRU (1994), IAEA (1979), IAEA (1991), and Rossi and Staub (1949).

2.8. Quantities and units

Physical quantities in atomic and nuclear physics are defined and expressed in units that have been adopted by the International Organisation for Standardization (ISO), and are described in ISO (1992a) and ISO (1992b). Further references for quantities and units are recent publications of the International Commission on Radiological Protection (ICRP, 1991, 1993) and the United Nations Scientific Committee on Effects of Atomic Radiation (UNSCEAR, 1993). Apart from the SI units of nuclear physics, other units in common use in the field of radioactivity and the environment can be found in IAEA (1979) and IAEA (1989). This section describes a selection of SI and conventional units in common use in these fields.

The symbols of the basic parameters used in the published ISO standards and literature are as follows:

Z	atomic number (number of protons);
A	mass number (number of nucleons);
N	number of entities (eg. particles, pulses, counts);
n	frequency of events (eg. count rate), (1/s);
λ	decay constant (s^{-1});
$T_{1/2}$	half-life (s);
σ	effective cross section (m^2);
σ	standard deviation (eg. $\sigma(n)$ - standard deviation of a count rate);
E	energy (eV), 1 eV = 1.602×10^{-19} J;
μ	linear attenuation coefficient (m^{-1});
μ/ρ	mass attenuation coefficient (m^2/kg);
ρ	density (kg/m^3).

2.8.1. SI derived quantities and units and non-SI units accepted for use with SI

The quantities are summarised in Table 2.4 and described below in the following sequence: quantity, recommended symbol, unit, dimension, definition, comments and conversion to older units.

Activity, A, becquerel, Bq, (s^{-1}). The mean number of spontaneous nuclear transitions per unit time interval. 1 Bq = 1 disintegration per second. 1 Ci (curie) = $3.7x10^{10}$ Bq. 1 g of ^{226}Ra has an activity of $3.7x10^{10}$ Bq.

Specific activity (activity per unit mass), a, becquerel per kilogram, Bq/kg, ($kg^{-1}s^{-1}$). The number of atomic decays per unit time per unit mass. Used to describe the radionuclide content of rocks, building materials etc.

Activity concentration (activity per unit volume), c_A, becquerel per metre cubed, Bq/m^3, (m^{-3} s^{-1}). The number of atomic decays per unit time and unit volume. Used to describe the concentration of radionuclides in gases and liquids. 1Bq/litre = 1 kBq/m^3.

Surface activity (activity per unit area), a_s, becquerel per metre squared, Bq/m^2, ($m^{-2}s^{-1}$). The number of atomic decays per unit time and unit area used to describe the surface distribution of radionuclides, e.g. the contamination of the earth's surface by nuclear fallout.

Exposure, X, coulomb per kilogram, C/kg, (kg^{-1} s A). The ionizing power of electromagnetic radiation in air - defined by the ratio of the sum of electrical charges, dQ, of one sign of ions liberated indirectly by photons of gamma or X-radiation in air, and the mass, dm, of the air, X = dQ/dm. 1 R = 2.58×10^{-4} C/kg.

Exposure rate, X′, coulomb per kilogram and second (ampere per kilogram) C/(kg s) (A kg^{-1}). The ratio of an incremental exposure, dX, in a time interval, dt, to the time interval, X′ = dX/dt. Exposure rate was used for the description of terrestrial gamma radiation in μR/h, 1 μR/h = 7.17×10^{-14} A/kg. Terrestrial gamma radiation be expressed as dose rate.

Dose, *absorbed dose*, D, gray, Gy, (m^2 s^{-2}). Absorbed dose is defined as the energy imparted by radiation to a unit mass of irradiated matter. 1 Gy = 1 J/kg. The matter (air, tissue) is specified. 1 rad = 10^{-2} Gy. Conversion: 1 R = 8.69×10^{-3} Gy (in air), 1 R = 9.57×10^{-3} Gy (in tissue).

Dose rate, absorbed dose rate, D′, gray per second, Gy/s, (m^2 s^{-3}). Dose rate is defined as the ratio of an incremental dose, dD, in a time interval, dt, to the time interval, D′ = dD/dt. Gamma dose rate in air is used for the description of terrestrial radiation, and is usually expressed in nGy/h. 1 pGy/s = 3.6 nGy/h. For conversion of terrestrial exposure rate to terrestrial dose rate in air it holds: 1 μR/h = 8.69 nGy/h.

Dose equivalent, H, sievert, Sv, (m^2 s^{-2}). Expresses the biological effects of radiation on tissue, and depends on the absorbed dose, D, and the type of radiation, given by a quality factor, Q. H = DQ. 1 rem = 10^{-2}Sv. The quality factor is a function of the type of radiation and its energy. Basic values of Q, independent of the energy of the particles, are: gamma rays, X-rays and electrons: Q = 1; neutrons and protons: Q = 10; alpha particles: Q = 20.

Photon dose equivalent rate, H'_x, sievert per second, Sv/s, (m^2 s^{-3}). This is sometimes used for reporting the effect of the gamma radiation field on humans (nSv/h). The relationship to gamma dose rate in air is $H'_x = 1.15\ D'_a$.

Equivalent dose, H_T, sievert, Sv, (m^2 s^{-2}). Expresses the biological effects of radiation to organs or tissue. $H_T = w_R D_{TR}$, where w_R is the radiation weighting factor, and D_{TR} is the mean absorbed dose.

Effective dose, E, sievert, Sv, (m^2 s^{-2}). Effective dose is a sum of multiples of equivalent doses in separate human organs and particular organ weighting factors w_T. $E = \Sigma\, w_T H_T$. Effective dose is expressed in mSv and usually reported per annum. For environmental gamma radiation the estimate is $E = D'_a \times t \times 0.7 \times 10^{-6}$, where E is the effective dose (mSv), D' , is the dose rate in air (nGy/h), t is the exposure time (h) and 0.7 is the conversion coefficient (Sv/Gy) for human organs (UNSCEAR, 1988). For D'_a = 100 nGy/h, t = 8760 h (1 year), E = 0.613 mSv.

TABLE 2.4. SI DERIVED QUANTITIES AND UNITS OF RADIOACTIVITY

Quantity	Symbol	Unit	Dimension	Use/Conversion of older units
Activity	A	Becquerel (Bq)	s^{-1}	radioactivity of objects
Specific activity	a	becquerel per kilogram (Bq/kg)	$kg^{-1}s^{-1}$	radioactivity of unit mass
Activity concentration	c_A	becquerel per metre cubed (Bq/m^3)	$m^{-3}s^{-1}$	radioactivity of gases and liquids
Surface activity	a_s	becquerel per metre squared (Bq/m^2)	$m^{-2}s^{-1}$	radioactivity of unit area
Exposure	X	coulomb per kilogram (C/kg)	$kg^{-1}sA$	ionizing effect of X and gamma rays in air
Exposure rate	X´	ampere per kilogram (A/kg)	$A\ kg^{-1}$	exposure per unit time, gamma radiation field. $1\mu R/h = 7.17 \times 10^{-14} A/kg$
Dose	D	Gray (Gy)	m^2s^{-2}	absorbed dose. 1 rad=10^{-2}Gy. $1R = 8.69 \times 10^{-3}$Gy (in air)
Dose rate	D´	gray per second (Gy/s)	m^2s^{-3}	gamma radiation field. 1 μR/h=8.69 nGy/h in air.
Dose equivalent	H	Sievert (Sv)	m^2s^{-2}	biological effects of radiation. 1 rem=10^{-2} Sv
Photon dose equivalent rate	H'_x	Sievert per second (Sv/s)	m^2s^{-3}	dose equivalent per unit time
Equivalent dose	H_T	Sievert (Sv)	m^2s^{-2}	biological effects of radiation
Effective dose	E	Sievert (Sv)	m^2s^{-2}	biological effects of radiation to man

2.8.2. Ground radioelement concentration units and conversion constants

In geology and nuclear geophysics, radioelement concentrations in rocks, air and water are expressed in the following units:

mass concentration of K:	% K	(percent potassium)
mass concentration of U:	ppm U	(parts per million of uranium)

mass concentration of Th: ppm Th (parts per million of thorium)

1 ppm = 10^{-6} g/g = 1g/ton

activity concentration of Rn in soil gas and air: kBq/m^3, Bq/m^3

activity concentration of radioelements in groundwater: Bq/litre, Bq/m^3

The specific activity of K, U ad Th are given in Table 2.5.

TABLE 2.5. CONVERSION OF RADIOELEMENT CONCENTRATION TO SPECIFIC ACTIVITY (IAEA, 1989).

1% K in rock	= 313	Bq/kg	^{40}K
1 ppm U in rock	= 12.35	Bq/kg	^{238}U, or ^{226}Ra
1 ppm Th in rock	= 4.06	Bq/kg	^{232}Th

Contamination of the earth's surface by man-made radionuclides is expressed either in surface activity (activity per unit area, Bq/m^2), or by specific activity (activity per unit mass, Bq/kg). An important factor in the relationship between these two quantities is the vertical distribution of the radionuclide in the soil. This is given by the relaxation mass per unit area (g/m^2) (ICRU, 1994).

2.8.3. Conventional ground reporting units

The estimation of the potassium concentration in rocks and soils by gamma ray spectrometry is through the detection of 1461 keV gamma rays emitted by ^{40}K. ^{40}K occurs in nature as a fixed ratio to other, non-radioactive, isotopes of potassium. Thus, the estimation of K is direct, and results are reported in % K (percent potassium). The estimation of uranium is through detection of 1765 keV gamma rays of ^{214}Bi, a daughter product in the ^{238}U disintegration series. The estimation of U by gamma ray spectrometry is thus indirect, and the results are reported in ppm eU (parts per million of equivalent uranium). The 'equivalent' serves as a reminder that the estimate is based on the assumption of radioactive equilibrium in the ^{238}U decay series. Similarly, estimation of thorium is through detection of 2615 keV gamma rays of ^{208}Tl, a daughter product of ^{232}Th decay series, and estimates are reported in ppm eTh (parts per million of equivalent thorium).

The response of total count gamma ray instruments to radiation from K, U or Th sources depends on the concentration of the source, the detector volume and efficiency, and the energy threshold of the instrument. In 1976, the IAEA introduced the unit of radioelement concentration, denoted "ur" (IAEA, 1976), to allow the reporting of total count measurements that are independent of the source and source/detector geometry. This unit of measurement does not entirely eliminate the instrument response and should be considered as a compromise. More recently, total count measurements are converted to gamma dose rate or exposure rate. However, these conversions are also approximations.

2.9. Natural and man-made absorbed doses

The radiation environment is formed by a flux of elementary particles and energy. The radiation is either man-made, is generated by the decay of unstable, naturally-occurring elements, or is of extra-terrestrial origin. In geoscience, both natural and man-made sources of radiation are studied through their ability to cause ionization in matter. This ionizing radiation is due to alpha, beta, gamma and neutron radiation. Natural sources of radiation comprise that part of the natural radiation environment that has always accompanied life on Earth.

Cosmic radiation, consisting mainly of high-energy particles from the sun and outer space, interacts with the earth's atmosphere and gives rise to a secondary radiation of particles and gamma rays, which prevail at the earth's surface. Cosmic ray intensity increases with altitude, doubling about every 2000 m, and shows small changes with latitude. The cosmic radiation dose rate at sea level is about 32 nGy/h (Grasty et al., 1984). Cosmogenic radionuclides are produced through the interaction of cosmic rays with atoms in the atmosphere, and do not contribute significantly to radiation absorbed doses.

Terrestrial radiation results from the primordial radionuclides in rocks that were synthesised during the creation of the Earth. The most significant sources are potassium, uranium, and thorium and their decay products (Table 2.6). A typical range of terrestrial gamma dose rate is 20-100 nGy/h, with a global average of about 55 nGy/h (UNSCEAR, 1988). Isotopes of radon, a radioactive gas in the ^{238}U, ^{232}Th and ^{235}U decay series, and radon decay products, are the main sources of radioactivity in air. Radon gas originates in rocks and soils and emanates from the ground into the atmosphere or groundwater. Concentration of radon and its daughter products in air varies. Over land, a reasonable global estimate of the activity concentration of ^{222}Rn in the air at ground level is 5 Bq/m^3 (UNSCEAR, 1988). The concentration of natural radionuclides in groundwater is several orders of magnitude lower than in rocks. Further descriptions of the natural radiation environment can be found in Grasty et al. (1984), UNSCEAR (1988), Adams and Gasparini (1970), Kogan et al., (1971), and Adams and Lowder (1964).

TABLE 2.6. THEORETICAL GAMMA RAY EXPOSURE RATES AND GAMMA DOSE RATES 1 m ABOVE A PLANE AND INFINITE HOMOGENEOUS SOIL MEDIUM PER UNIT RADIOELEMENT CONCENTRATION ASSUMING RADIOACTIVE EQUILIBRIUM IN THE U AND Th DECAY SERIES (IAEA, 1989, IAEA, 1991, Lovborg, 1984).

Radioelement concentration	Exposure rate (μR/h)	Dose rate (nGy/h)
1% K	1.505	13.078
1 ppm U	0.653	5.675
1 ppm Th	0.287	2.494

Man-made sources of radiation imply natural radioactive materials concentrated or relocated by human activity, artificially generated radionuclides, nuclear reactors and various other instruments emitting radiation. Coal mining activities and the use of coal give rise to a concentration of naturally occurring radionuclides in coal ashes. High gamma dose rates (500 nGy/h) have been observed over coal ash heaps enriched by U to 1150 Bq/kg (ca 100 ppm U), and increasing ^{222}Rn activity concentration in the atmosphere to 13-95 Bq/m^3 (Mende, 1993). Uranium mining and associated processing and waste disposal can lead to large radioactive anomalies easily detected by ground or airborne surveys.

Potassium and phosphate fertilizers can increase soil radioactivity (Pfeister and Pauly, 1980). Medical diagnostic equipment that use radioactive sources contribute significantly to annual absorbed doses – typically increasing the annual absorbed dose to natural radiation with an additional 20-30%.

Nuclear bomb tests conducted in the atmosphere since 1945 have resulted in the introduction of artificial radionuclides into the environment. The most long-lived radionuclide from nuclear fallout is ^{137}Cs. The concentration of ^{137}Cs has a maximum concentration in the northern hemisphere between 40-50 degrees latitude and a mean surficial activity up to 2.9 kBq/m^2 (UNSCEAR, 1982). Other causes of nuclear fallout are accidents in the nuclear power industry followed by the release of radionuclides into the atmosphere. Short-lived fallout radionuclides decay rapidly – usually to negligible proportions within days or weeks. But high concentrations of ^{137}Cs, accumulated in the upper 10 cm of the soil can remain in the environment for many decades, with a surficial activity in the range of hundreds and thousands of Bq/m^2. This surpasses the effects of radiation due to the natural environment (Mundigl et al., 1994, Korun et al., 1993). Lost nuclear sources and nuclear power accidents may have local radiation consequences.

Natural and man-made sources of radiation cause external and internal irradiation to humans. Cosmic radiation, terrestrial radiation, building materials, nuclear fallout and man-made radiation are the sources of external radiation. Internal exposures result from the ingestion and inhalation of naturally occurring radioactive substances in food, water and air. Inhalation of radon contributes significantly to overall annual absorbed radiation doses. The biological effects of absorbed radiation are defined in terms of effective dose, and are expressed in sieverts (Sv).

The estimates of annual effective dose from natural radiation sources (Table 2.7) (UNSCEAR, 1988) shows that radon (mainly in indoor air) is the largest contributor to absorbed radiation dose. Contributions to annual effective dose from nuclear power plants, research reactors, global nuclear fallout and agricultural fertilizers are generally low, while average annual effective dose from medical irradiation is estimated 0.6-1.5 mSv (BfS, 1998, Novotna, 1986) and may reach higher values.

TABLE 2.7. THE GLOBAL AVERAGE ANNUAL EFFECTIVE DOSE FROM NATURAL RADIATION SOURCES (UNSCEAR, 1988)

Source of irradiation	External (mSv)	Internal (mSv)	Total (mSv)
Cosmic rays	0.410 (17)		0.410 (17)
Cosmogenic radionuclides		0.015 (1)	0.015 (1)
Natural sources:			
^{40}K	0.150 (6)	0.180 (7)	0.330 (13)
^{238}U - series	0.100 (4)	1.239 (51)	1.339 (55)
^{232}Th - series	0.160 (7)	0.176 (7)	0.336 (14)
Total	0.820 (34)	1.616 (66)	2.436 (100)

Note: relative values are given in brackets (%).

3. FUNDAMENTALS OF GAMMA RAY SPECTROMETRY

The gamma ray method is unusual in that it requires the consideration of many factors. The source intensity and the source-detector geometry affect observed gamma ray fluence rates. Environmental and other effects such as soil moisture, rainfall, vegetation, non-radioactive overburden, and the distribution of airborne sources of radiation all affect the measured fluence rates. This chapter reviews the fundamentals of gamma ray spectrometry and concludes with a brief discussion of simple analytical models that are used to obtain an insight into the physics of the method.

3.1. Sources of gamma radiation

Each gamma ray photon has a discreet energy, and this energy is characteristic of the source isotope. This forms the basis of gamma ray spectrometry – by measuring the energies of gamma ray photons, we can determine the source of the radiation.

Natural sources of radiation derive from radio-isotopes synthesised during the creation of the solar system. Because of their long half-lives, they still exist today. Of these, potassium (^{40}K), uranium (^{238}U and ^{235}U and their daughters), and thorium (^{232}Th and its daughters) are the only radio-isotopes that produce high-energy gamma rays of sufficient intensity to be used for gamma ray mapping.

The development of nuclear energy has resulted in the creation of artificial radio-isotopes. These are created during nuclear weapon test blasts and in research reactors for scientific and industrial uses. ^{137}Cs is the main gamma-emitting fall-out product from nuclear explosions and accidents. It has a single photopeak at 0.662 MeV and has a half-life of about 30 years.

Radiation not originating from the earth's surface is usually regarded as "background", and is removed during data processing. There are three main sources of background radiation: atmospheric radon, cosmic background, and instrument background.

Atmospheric radon (^{222}Rn) and its daughter products are the main source of background radiation. ^{222}Rn (radon gas) is mobile, and can escape from rocks and soils and accumulate in the lower atmosphere. Its daughter products (^{214}Bi and ^{214}Pb) attach to airborne aerosols and dust particles and emit gamma rays on decay.

High energy gamma rays and atomic particles of cosmic origin react with atoms and molecules in the upper atmosphere and generate a complex secondary radiation. This secondary radiation reacts with surrounding matter to produce a "cosmic" gamma ray background. Instrument background refers to radiation due to trace amounts of K, U and Th in the detector and surrounding equipment. This will include radiation from the aircraft or vehicle, in the case of airborne and car-borne surveys, respectively. This component of background is constant.

3.2. Properties of gamma ray spectra

Potassium and the uranium and thorium equilibrium decay series each have characteristic line spectra (Figure 3.1). These are theoretical abstractions that represent the energy distribution of emitted photons at the source. Each line spectrum (or "emission" spectrum) shows the energy and relative intensity of gamma ray emissions in the decay series.

However, the energies of these original photons are reduced by Compton scattering in the source, in the detector, and in matter between the source and the detector. The relative contribution of scattered and unscattered photons to the gamma ray fluence rate thus depends on the source-detector geometry and on the amount of attenuating material between the source and the detector. Figure 3.2 shows the simulated gamma ray flux due to each of K, U, and Th at 300 m height (Kirkegaard and Lovborg, 1974). Each radioelement generates a sharp peak representing the energy of directly transmitted photons. This is superimposed on the spectrum of Compton scattered photons which show a continuum of energies up to the maximum energy of the photons emitted by the isotope. This continuum is due to single and multiple scattering events between the source and the detector.

In practice, it is impossible to record the gamma ray flux spectra shown in Figure 3.2. This is because the shape of the measured spectrum, in addition to the factors mentioned above, is also a function of the detector response.

3.2.1. The detector response

Thallium-doped sodium-iodide scintillation crystals are the most common detectors used in natural radioelement mapping. These detectors modify the spectrum considerably. The main aspects of the detector response are detector efficiency, directional sensitivity, energy resolution and dead time.

Detector efficiency relates to how well the detector absorbs gamma rays. The detector energy resolution is a measure of a detector's ability to distinguish between two gamma rays of only slightly differing energy. Dead time refers to the finite time required for the spectrometer to process individual photons. Heath (1964) gives a good summary of other factors that affect the shape of the pulse amplitude spectrum, such as escape events, accidental summing, and the characteristic "Compton edge". Spectrum photopeaks have Gaussian shapes. This is mainly due to the limited energy resolution of NaI detectors.

3.2.2. Source-detector geometry

Source thickness has a significant effect on the shape of observed spectra. With increasing source thickness there is build-up of the Compton continuum due to scattering in the sources. The photopeaks are thus reduced relative to the Compton background. Since low-energy photons are more easily attenuated than high-energy photons, this effect is more pronounced at lower energies.

Terrestrial radiation is attenuated in the source and by material between the source and the detector. The shape of the observed spectrum depends on the amount of attenuating material between the source and the detector. With increasing attenuation, the photopeaks are reduced relative to the energy continuum. Measured spectra are thus functions of the concentration and geometry of the source, the height of the detector above the ground, the thickness of any non-radioactive overburden, and the response function of the detector.

Typical examples of airborne K, U, and Th spectra recorded with long integration times are shown in Figure 3.3. The effect of the detector response and the interaction of the gamma rays with matter is a smearing of the original theoretical line spectra shown in Figure 3.1. The spectra shown in Figure 3.3 were recorded on the ground using specially constructed radioactive sources. Wood was used to shield the detectors from the sources, thus simulating the attenuation of the gamma rays by air.

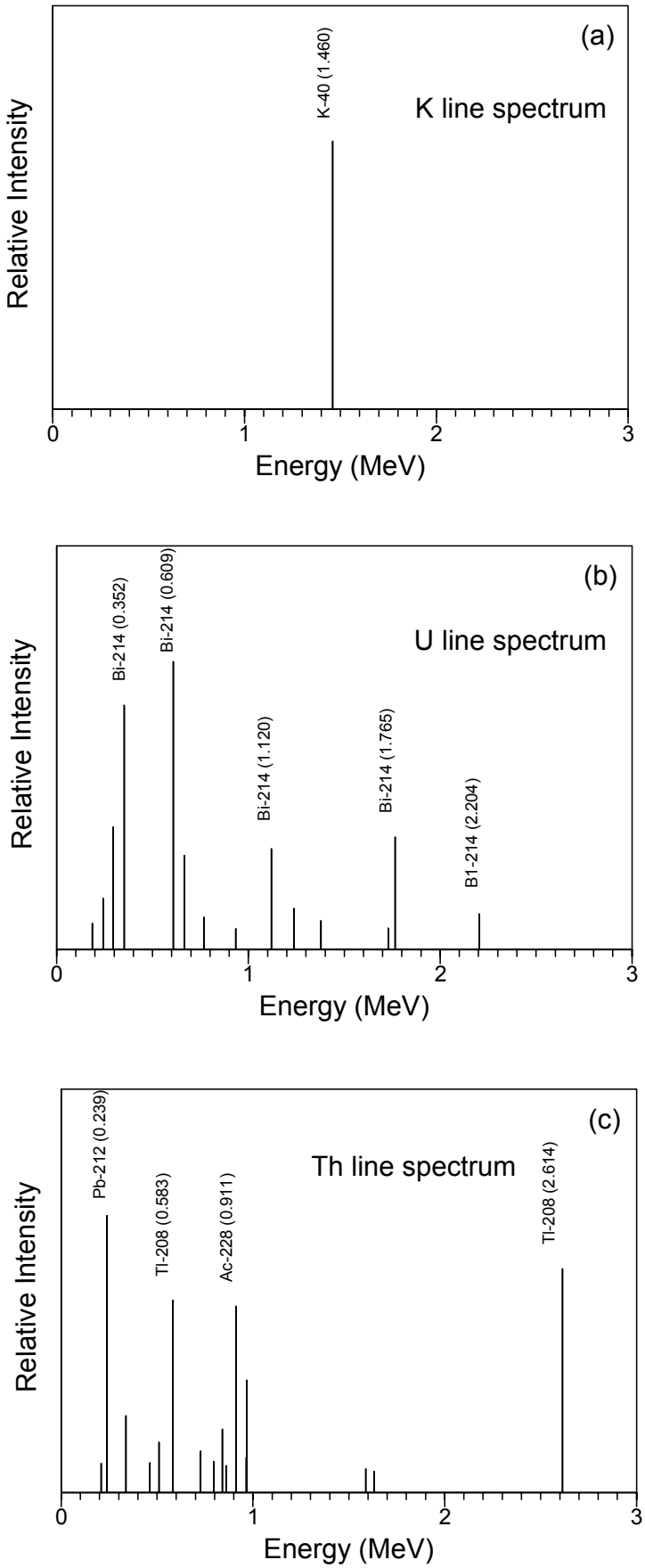

FIG. 3.1. Gamma ray emission line spectra of: a) potassium; b) uranium; c) thorium.

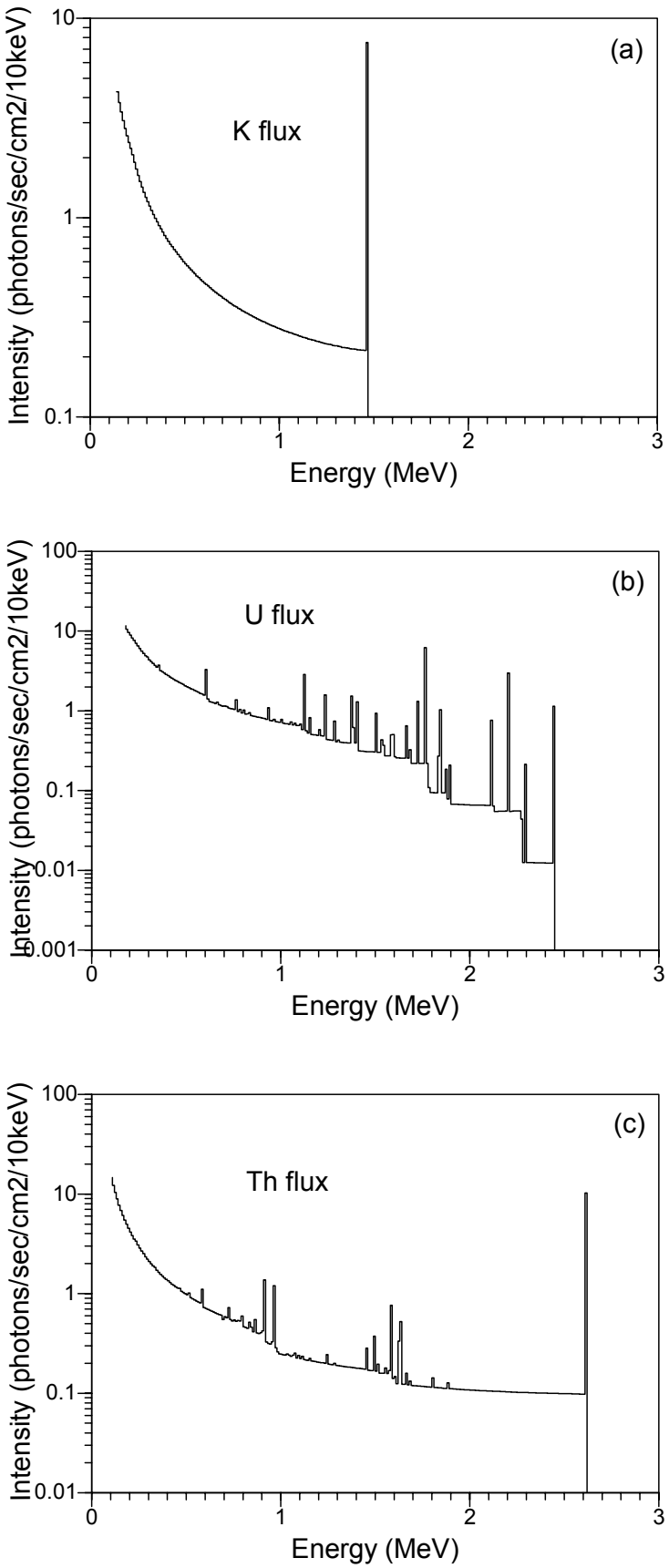

FIG. 3.2. Simulated potassium (a), uranium (b) and thorium (c) fluence rates at 300 meter height.

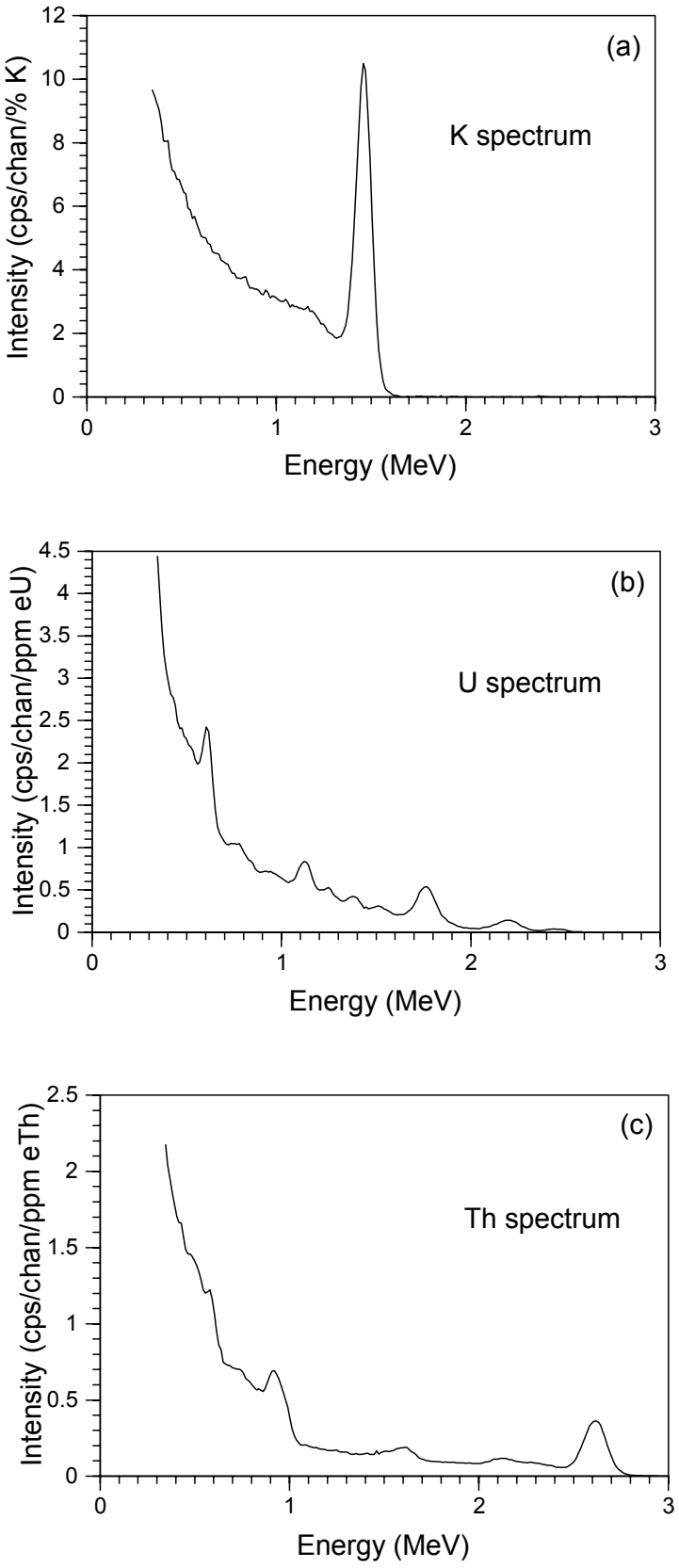

FIG. 3.3. Typical examples of potassium (a), uranium (b) and thorium (c) spectra recorded by a NaI(Tl) detector with long integration times. The specially constructed radioactive sources were shielded from the detectors by wood to simulate attenuation by air.

3.3. Measurement of gamma radiation

Modern gamma ray spectrometers typically record 256 (or 512) channels of information in the energy range 0-3.0 MeV. Each channel thus records all gamma rays absorbed by the detector that have energy within a 11.7 keV range. Count rates are usually low. An airborne gamma ray spectrometer with 32 litres of NaI detectors will record perhaps one or even zero counts in some high energy channels during a one-second counting period. A typical airborne gamma ray spectrum is shown in Figure 3.4.

The precision to which a spectrometer can measure the energy of a gamma ray is known as the spectrometer energy resolution. This is usually measured as the full width of a photopeak at half the maximum amplitude (FWHM) expressed as a percentage of the photopeak energy (Figure 3.5). Typical spectrometer resolutions for large-volume NaI detectors are 10% for ^{137}Cs at 0.662 MeV and 7% for ^{208}Tl at 2.61 MeV.

The conventional approach to the acquisition and processing of gamma ray spectrometric data is to monitor three or four relatively broad spectral windows (Figure 3.4, Table 3.1). The K energy window monitors the 1.46 MeV gamma rays emitted by ^{40}K. The U and Th energy windows monitor gamma ray emissions of decay products in the U and Th decay series. These windows are generally accepted as the most suitable for the measurement of K, U and Th. The total-count window gives a measure of total radioactivity.

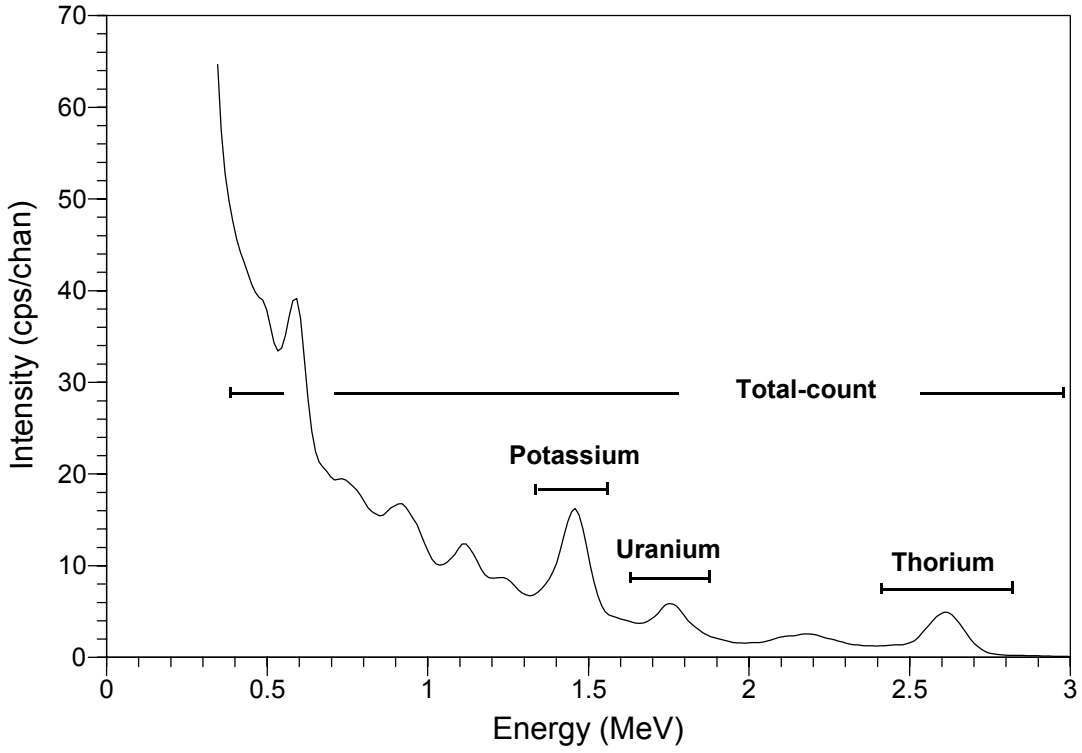

FIG 3.4. Typical airborne gamma ray spectrum showing the positions of the conventional energy windows.

3.4. Physical models

Two types of models are widely used in gamma ray spectrometry. Physical models provide an insight into the physics of the method. This insight is necessary for both effective survey design, and for the design of data processing and interpretation procedures. Statistical models are used for estimating or predicting errors.

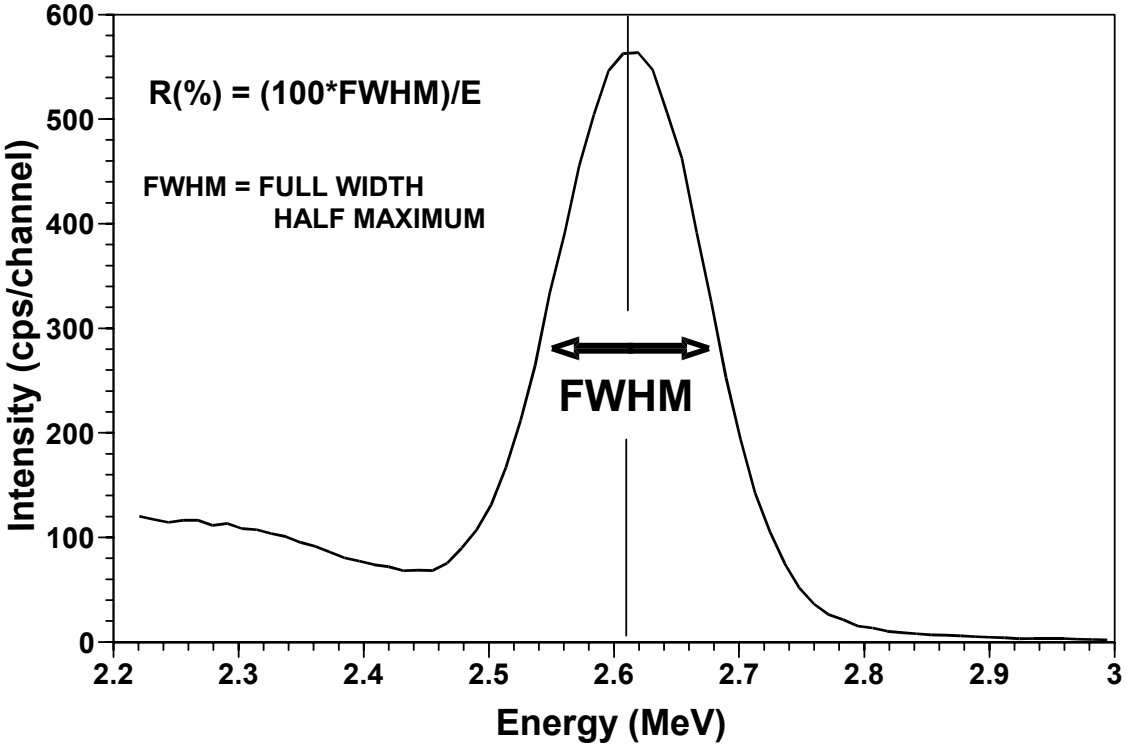

FIG. 3.5. Diagram illustrating the energy resolution of a gamma ray spectrometer. The spectrometer energy resolution is defined as the full width of a photopeak at half the maximum amplitude (FWHM) expressed as a percentage.

TABLE 3.1. STANDARD GAMMA RAY ENERGY WINDOWS RECOMMENDED FOR NATURAL RADIOELEMENT MAPPING (IAEA, 1991). THE ENERGY OF THE PHOTOPEAK BEING MONITORED IS SHOWN IN BRACKETS AFTER EACH NUCLIDE

Window	Nuclide	Energy Range (MeV)
Total Count	–	0.400 – 2.810
Potassium	^{40}K (1.460 MeV)	1.370 – 1.570
Uranium	^{214}Bi (1.765 MeV)	1.660 – 1.860
Thorium	^{208}Tl (2.614 MeV)	2.410 – 2.810

The simplest approach to the modelling of gamma ray fields is a semi-empirical one based on mono-energetic (unscattered) radiation. Clark et al. (1972) used a two-layer model with the earth as an infinite half-space with a constant density and radioelement concentration overlain by non-radioactive air of constant density (Figure 3.6). They showed that the mono-energetic radiation intensity, dI, due to a photopeak of intensity E_0 from gamma ray emissions by a volume element dV within the earth is given by

$$\mathrm{d}I = \frac{A\varepsilon}{4\pi R^2} e^{-\mu_e r_e} e^{-\mu_a r_a} N \,\mathrm{d}V \tag{3.1}$$

where $N\mathrm{d}V$ = number of gamma rays of energy E_0 emitted per second by the volume element dV;

A = effective cross-sectional area of a spherical detector;

ε = photopeak efficiency of the detector for gamma rays of energy E_0;

μ_e, μ_a = linear attenuation coefficients for the earth and air respectively;

r_e, r_a = the distances through the earth and air that the gamma rays travel ($R=r_a+r_e$).

Equation 3.1 can be integrated over various source geometries to obtain the photopeak response due to particular source types. For example, the radiation due to a thick circular source expressed as a percentage of the radiation due to an infinite source is given by (Grasty, 1987).

$$P = 100\left(\frac{E_2(\mu h) - \cos\varphi E_2\left(\frac{\mu h}{\cos\varphi}\right)}{E_2(\mu h)}\right) \tag{3.2}$$

where h is the detector height above ground level, μ is the linear attenuation coefficient of gamma rays in air, E_2 is the exponential integral of the second kind, and the circular source subtends an angle of 2φ at the detector.

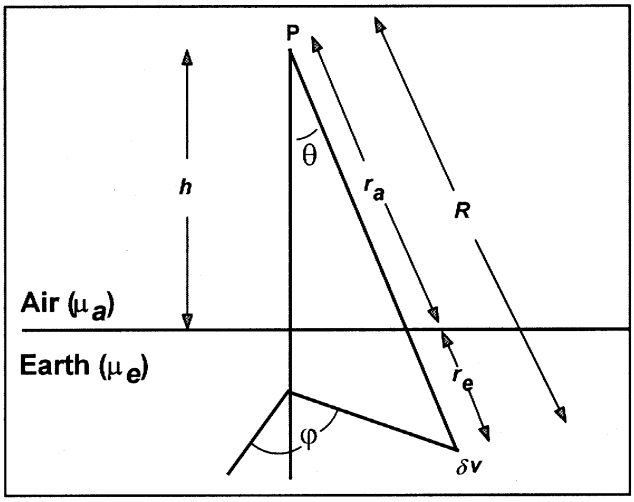

FIG. 3.6. Source-detector geometry for a two layer earth-air model.

Figure 3.7 shows the percentage of the "infinite source yield" (equation 3.2) for thorium gamma rays (^{208}Tl) at 2.61 MeV as a function of source radius. A linear attenuation coefficient for air of 0.00505 m^{-1} and a detector altitude of 100 m have been used. This shows that at 100 m height, less than 40% of the infinite source yield originates from a source with a radius of 100m, and over 20% of the measured photons for an infinite source originate at lateral distances greater than 300 m. The effective "field of view" contributing to a typical airborne sample is thus much larger than the 60 m interval over which samples are typically acquired.

As a second example, the radiation due to a broad source of thickness D expressed as a percentage of the radiation due to a broad source of infinite thickness is given by (Grasty, 1987)

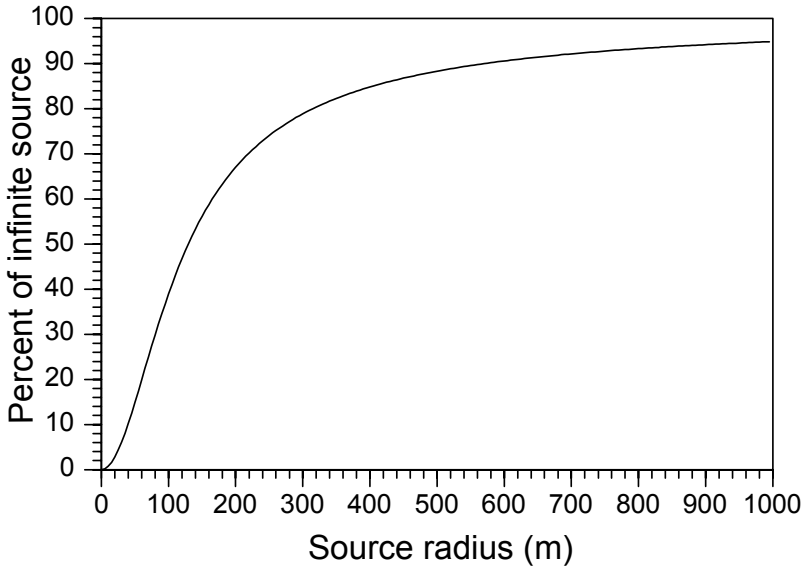

FIG. 3.7. Percentage of the infinite source radiation detected from thick circular sources of varying radius for thorium gamma rays of energy 2.62 MeV and a detector height of 100m.

$$P = 100\,(1 - E_2(\mu D)) \tag{3.3}$$

where μ is the linear attenuation coefficient of the source material, E_2 is the exponential integral of the second kind and the detector is at ground level. This relationship is illustrated in Figure 3.8 for thorium gamma rays (^{208}Tl) at 2.61 MeV. A source density of 2.2 gm/cm^3 and a mass attenuation coefficient of 0.0396 cm^2/gm (i.e. μ=0.0871 cm^{-1}) was used. This shows that over 98 percent of the radiation originate from the top 35 cm of the earth's crust. The airborne gamma ray spectrometric method can therefore only map the concentration of radioelements in a thin layer at the earth's surface.

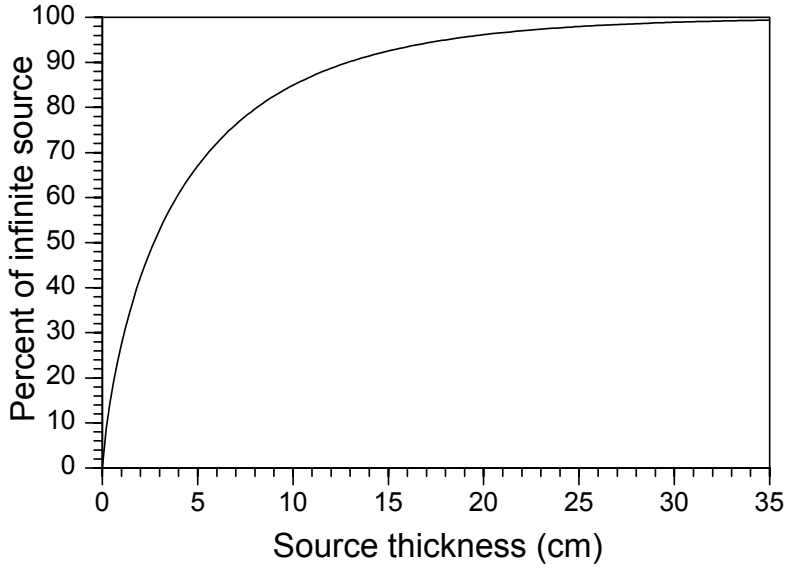

FIG. 3.8. Percentage of the infinite source radiation detected from broad sources of varying thickness for thorium gamma rays of energy 2.62 MeV and a source density of 2.2 g.cm^{-3}.

3.5. Environmental effects

The amount of attenuating material between the radioactive source and the gamma ray detector affects the measured radiation. In airborne gamma ray spectrometry the height of the detector above the ground has a large effect. Ten metres of air will affect the measured radiation by about 7%. Non-radioactive overburden can significantly reduce the radiation output from the earth's surface. For example, just 2 cm of cover can reduce by 35 percent the radiation penetrating to the ground surface. Dense vegetation will have the same effect. The trunks of trees in dense forests have a collimating affect on radiation from the ground. Snow cover can significantly attenuate radiation from the ground. 10 cm of fresh snow will attenuate gamma rays as effectively as 10 m of air.

Changing temperatures and pressures can lead to a change in air density by up to 30 percent. This effects the attenuation of gamma rays to the same extent. Atmospheric radon trapped in temperature inversion layers close to the ground can adversely affect estimates of background radiation in airborne surveying.

Soil moisture can be a significant source of error in gamma ray surveying. An increase in soil moisture of 10 percent will decrease the measured fluence rate by about the same amount. Precipitation can have a large effect on uranium estimation. Daughter products of airborne radon attach themselves to dust particles in the atmosphere. The radioactive precipitation of these particles by rain can lead to apparent increases of more than 2000 percent in uranium ground concentrations (Charbonneau & Darnley, 1970). Gamma ray surveying should therefore not be carried out during rainfall or shortly thereafter. About three hours is required for the anomalous surface activity to decay away.

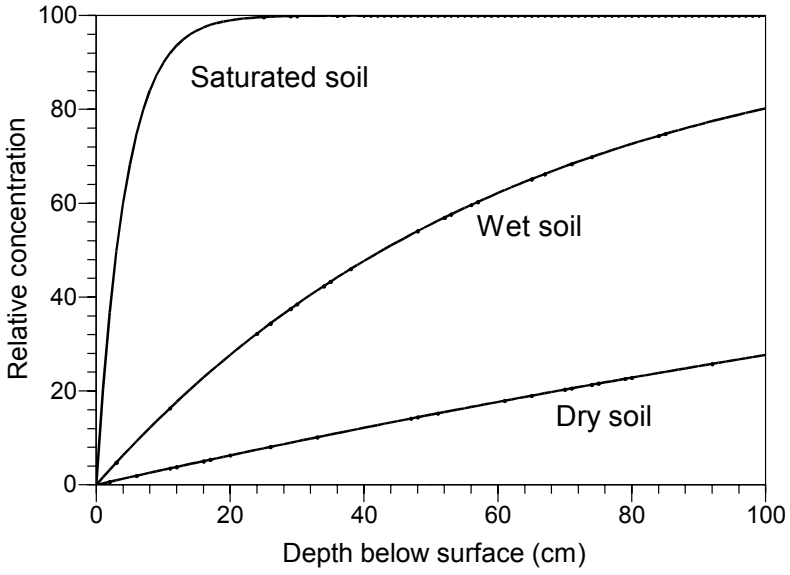

FIG. 3.9. Effect of soil moisture on radon concentration with depth.

Grasty (1997) showed that high soil moisture contents could actually lead to an increase in uranium radiation output. There are two components of ^{222}Rn in soils – an emanating fraction that finds its way into soil pores, and a non-emanating fraction that is trapped in the soil particles. The emanating fraction typically varies between 20% and 40% (Markkanen and Arvela, 1992) of the total ^{222}Rn concentration. The concentration of the emanating fraction with depth for a soil under three different soil moisture conditions is shown in Figure 3.9. The concentrations have been normalized to 100 arbitrary concentration units for effectively

infinite depths. The diffusion coefficients (0.05 cm^2/s for dry soil, 0.002 cm^2/s for wet soil and 0.00001 cm^2/s for water saturated soil) are the same as those used by Grasty (1997). Thus, radon escapes more freely from dry soil than from wet soil. High soil moisture concentrations can lead to a build-up of radon in the soil.

Topographic effects can be severe for both airborne and ground surveying. Both airborne and portable gamma ray spectrometers are calibrated for a 2π surface geometry. Field estimates of the concentrations of the radioelements are thus based on the assumption of a 2π source geometry. Where there are deviations from this assumption, concentration estimates will be in error. Portable spectrometer readings taken in creek beds where there are steep banks or in road cuttings will give completely erroneous results. Similarly, airborne readings in valleys or on the crests of ridges will be in error.

4. GROUND RADIOMETRIC METHODS

Portable and car-borne gamma ray spectrometry are used for both regional and detailed mapping surveys for estimating the surface concentrations of the radioelements. Borehole gamma ray spectrometry can be used to acquire information on lithology and mineralization in subsurface geological structures. Marine gamma ray spectrometry provides similar mapping capabilities of the seafloor.

4.1. Portable gamma ray spectrometry

Portable gamma ray spectrometry has been used since the 1960's for uranium exploration, geological mapping and environmental studies. There are well-established procedures for measurement, instrument calibration and data processing.

4.1.1. Instrumentation

Portable hand-held gamma ray spectrometers are widely used in field studies. Portable threshold spectrometers have up to 100 cm^3 of NaI(Tl) crystals as detectors, and several switch-operated energy thresholds. The threshold can be set to a low energy for total count measurement, and to energies slightly below 1.46 MeV, 1.76 MeV and 2.62 MeV for K, U, and Th measurement, respectively. A reference gamma ray emitting source is used for instrument gain adjustment. Threshold spectrometers with small crystal volumes are suitable for crude spot measurements of total count anomalies.

Most modern portable gamma ray spectrometers are differential spectrometers. These typically have at least 350 cm^3 of NaI(Tl) detectors, and record either 256 or 512 channel of data in the energy range 0-3 MeV. Automatic spectrum stabilization is by either a low-energy peak from a reference isotope (typically ^{137}Cs at 0.662 MeV), or one of the natural radionuclide peaks (either ^{40}K at 1.46 MeV or ^{208}Tl at 2.62 MeV). The instruments can record the full gamma ray spectrum as well as sum channels over broad energy windows for the in-situ estimation of K, U and Th radioelement concentrations. Calibration constants are stored in the instrument memory. Several thousands of field measurements or several hundreds of full energy spectra can be recorded in the instrument memory. The use of large volume scintillation crystals and sample intervals of several minutes give acceptable precision for quantitative analyses.

Germanium multichannel gamma ray spectrometers make use of the excellent gamma energy resolution of germanium detectors to distinguish between gamma ray emitters. A germanium detector for field use would have a volume of about 50 cm^3. A typical sampling time would be of the order of tens of minutes.

4.1.2. Field measurement

Portable gamma ray spectrometers used for natural radionuclide mapping monitor energy windows centred on the 1461 keV (^{40}K), 1765 keV (^{214}Bi) and 2615 keV (^{208}Tl) photopeaks for the estimation of K, U, and Th concentrations, respectively (IAEA, 1989). Nuclear fallout of ^{137}Cs and ^{134}Cs can be detected by monitoring two 100 keV wide windows centred on 662 keV and 796 keV, respectively. Several methods of estimating the concentration of nuclear fallout radionuclides have been developed (Grasty and Cox, 1996). Most methods use both a

low-energy and a high-energy window for each radioisotope. Multichannel methods have also been developed.

The field procedure for portable gamma ray spectrometry depends on the purpose of the survey and the geological or environmental problem being investigated. The type of spectrometer, detector volume, measurement times, and mode of measurement depend on the radiation environment and the type, size and distribution of radioactive sources.

The response of a portable gamma ray spectrometer is dependent on the size, location and geometry of radioactive sources. Meaningful measurements along a traverse can only be obtained if the source-detector geometry is constant for all observations. The detector should either be placed directly on the earth surface, or be kept at a low but constant height. This minimizes the effects of local variation in relief and radioelement distribution. For a detector placed on the ground, the effective rock sample has a thickness of approximately 25 cm, a radius of 1 m, and a mass exceeding 100 kg. If the height of the detector is raised, the effective source increases rapidly in diameter from several metres to tens of metres depending on the energy of gamma rays (Kogan et al., 1971, IAEA, 1979, IAEA 1989). The same source-detector geometry used to calibrate the spectrometer should be used in the field.

The sampling time required for a measurement depends on the radioactivity of the source and the precision of measurement required. Equations (2.9) and (2.11) can be used to estimate the number of counts required for a given relative error. However, the K, U, and Th spectra overlap, and the counting time required for a specified precision in the estimates of these radionuclides is more complicated. Lovborg and Mose (1987) derived equations giving the counting time for K, U, and Th assays with a 10% error in various K, U, and Th ratios in rocks (Figures 4.1, 4.2 and 4.3). But there is always a compromise between the precision of measured count rates and the economy of field measurements. For a 350 cm^3, NaI(Tl) detector, a sampling time of 2 min for highly radioactive rocks and 6 min for low radioactivity rocks is a reasonable compromise.

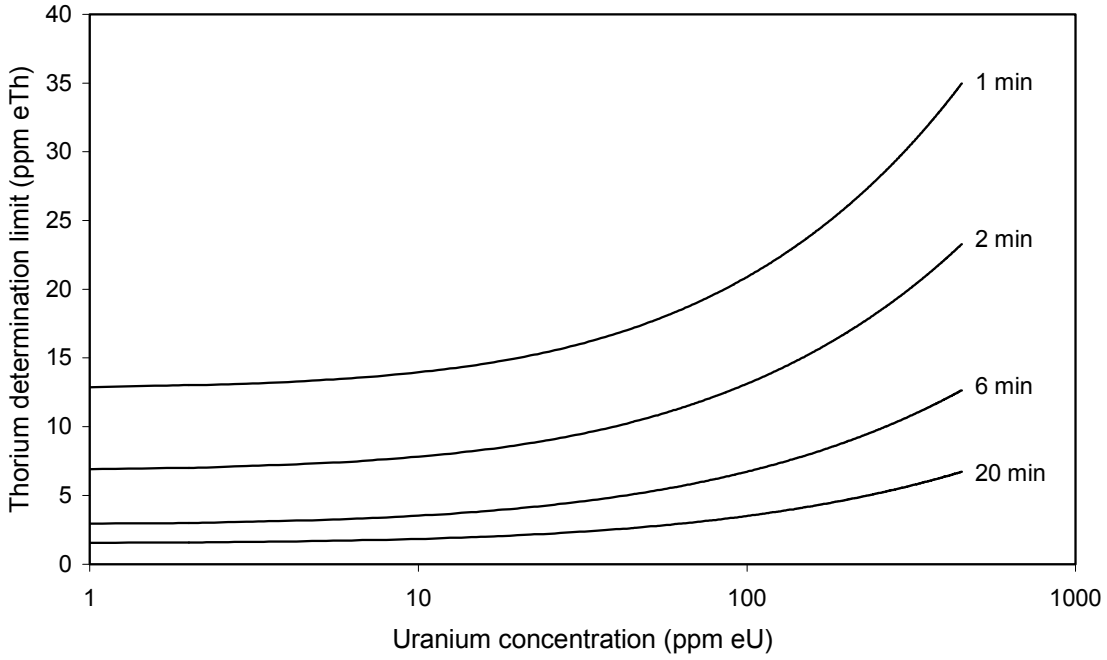

FIG. 4.1. Counting times for a GR320 spectrometer with a 0.35 litre NaI(Tl) detector required to estimate thorium concentration with 10% precision.

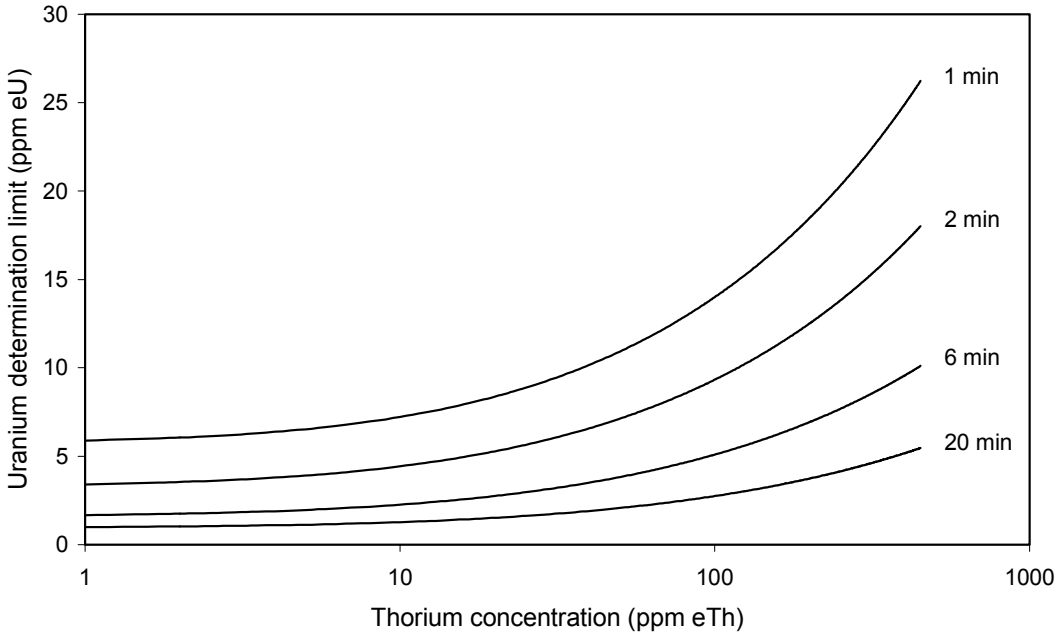

FIG. 4.2. Counting times for a GR320 spectrometer with a 0.35 litre NaI(Tl) detector required to estimate uranium concentration with 10% precision.

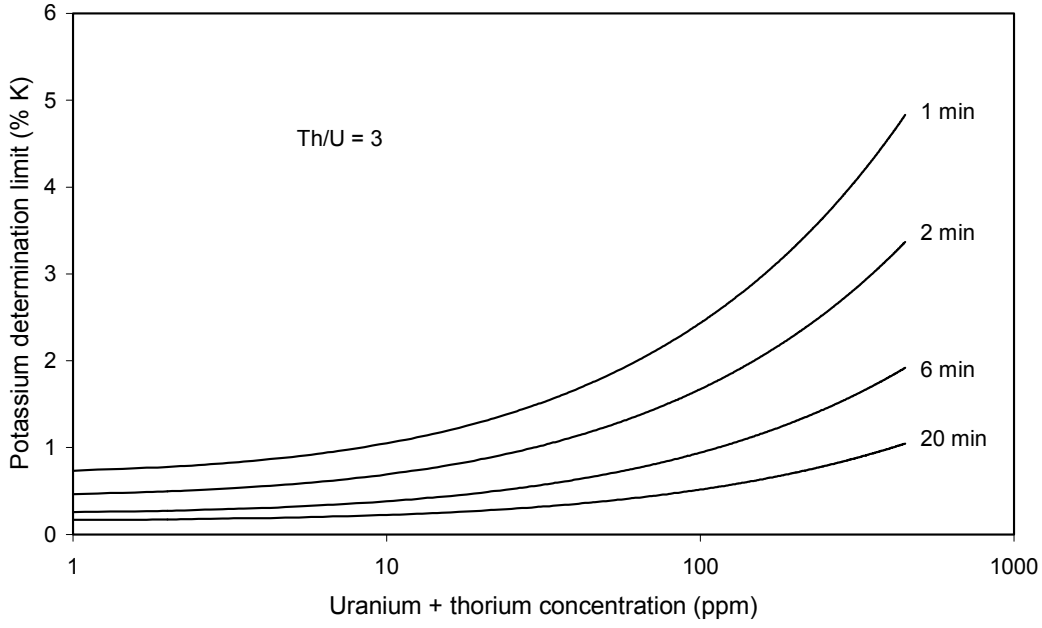

FIG. 4.3. Counting times for a GR320 spectrometer with a 0.35 litre NaI(Tl) detector required to estimate potassium concentration with 10% precision.

Survey grids and traverse spacings should reflect the expected strength, size and distribution of sources. For example, it is unlikely that small point sources will be detected on traverses tens of metres apart. On the other hand, regional traverses can give good estimates of the radioactivity of broad-scale lithological units. Systematic traversing is mainly used in mineral exploration and for the location of man-made sources. The traverses are preferably

perpendicular to the geological strike, and the traverse and station spacings depend on the height of the detector and the expected size of the targets. An initial traverse spacing can be 50-250 m, with detailed traverses at about 5-10 m and a station spacing 5 m. Thirty to sixty stations per day can be measured with one portable spectrometer. Both the spectrometer function and variations in background radioactivity should be checked daily at an established reference station in the survey area.

Field measurements can be carried out in either static or dynamic mode. In static mode, the radioactivity is measured at discrete points. In dynamic mode, the instrument is transported over fixed distances during measurement, and the accumulated counts reflect the average radioactivity of the traverse sector. The observed data, along with identifiers, are stored in internal memory. It is a good practice to note any geological, topographic, climatic and environmental features that may help with subsequent interpretation of the data.

4.1.3. Instrument calibration

The calibration of gamma ray spectrometers is the estimation of those constants that relate instrument count rates to either radionuclide concentration or environmental dose rate. This includes the estimation of background radiation, stripping ratios and sensitivity constants.

Background radiation is due to the internal radioactivity of the instrument, cosmic radiation, and atmospheric radon. The background is estimated by taking measurements from a small boat (preferably fibreglass) over a river or lake, and at least 200 m from the shore. The shoreline should be flat. Background count rates are recorded in all energy channels.

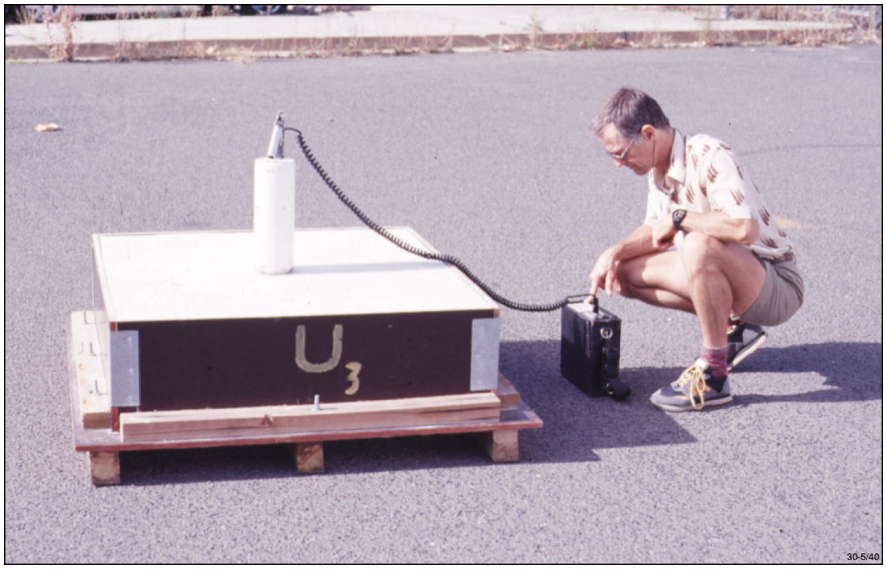

FIG. 4.4. Calibration of a portable spectrometer on a transportable calibration pad.

Portable gamma ray spectrometers used for assaying K, U and Th in rocks are calibrated by means of calibration pads. A calibration pad is a slab of concrete containing known concentrations of the radioelements (Figure 4.4). Ideally, calibration pads should simulate a geological source of radiation. The IAEA (IAEA, 1989) recommended four cylindrical concrete pads with dimensions: diameter - 3 m and thickness - 0.5 m. Each of the pads is enriched in either K, U or Th. Recommended concentrations (IAEA, 1989) are 8% K in the K-pad, 50 ppm U in the U-pad, and 125 ppm Th in the Th-pad. The fourth pad serves as a

background pad. Grasty et al. (1991) showed that smaller transportable pads (1×1×0.3 m) are also suitable for calibrating portable gamma ray spectrometers. Geometrical correction factors must be applied to the instrument sensitivities derived from these calibration experiments. These factors correct for the density and finite dimensions of the calibration pads.

The K, U and Th window count rates obtained over the pads are linearly related to the K, U and Th concentrations in the pads. Let n_i (i = 1, 3) be the count rate in the i-th energy window (either K, U or Th), and let s_{ij} (i = 1, 3; j = 1, 3) be the sensitivity of the i-th elemental count rate to the concentration of the j-th element (either K, U or Th), then

$$n_i = s_{iK}c_K + s_{iU}c_U + s_{iTh}c_{Th} + n_{iBG} \tag{4.1}$$

where n_i = count rate in the i-th energy window (i = 1, 2, 3), (c/s);
s_{ij} = sensitivity of the spectrometer for the detection of the j-th element in the i-th energy window, (c/s per unit concentration of the j-th element);
c_j = concentration of the j-th element, (% K, ppm U, ppm Th);
n_{iBG} = background count rate in the i-th energy window, (c/s).

Since the estimation of K, U, and Th is based on measurements in 3 energy windows, and the background count rates n_{iBG} can be subtracted, equation (4.1) may be written in matrix notation as follows:

$$\mathbf{N} = \mathbf{SC} \tag{4.2}$$

where $\mathbf{N}$ = column vector of background-corrected count rates (n_i-n_{iBG});
$\mathbf{S}$ = 3×3 matrix of sensitivities (s_{ij});
$\mathbf{C}$ = column vector of concentrations (c_K, c_U, c_{Th}).

The sensitivity constants, s_{ij}, are estimated from measurements on the four calibration pads. The detector is placed on the centre of a calibration pad and count rates, n_i, are measured in three energy windows (i = 1, 2, 3). Backgrounds are removed by subtracting the counts measured on the background pad, n_{iBG}, and subtracting the concentration of the background pad from the concentrations of the other three pads. Equation (4.1) is thus modified as follows:

$$n_i - n_{iBG} = s_{iK}\Delta c_K + s_{iU}\Delta c_U + s_{iTh}\Delta c_{Th} \tag{4.3}$$

where Δc_j = the difference between the concentrations of the j-th element in a calibration pad and the concentration of the j-th element in the background pad.

Or, in matrix notation

$$\mathbf{N} = \mathbf{S}\Delta\mathbf{C} \tag{4.4}$$

where $\mathbf{N}$ = 3×3 matrix of background-corrected count rates, (n_i - n_{iBG});
$\mathbf{S}$ = a 3×3 matrix of sensitivities (s_{ij});
$\Delta\mathbf{C}$ = 3×3 matrix of differential concentrations of K, U, and Th in the K, U, and Th pads minus the K, U, and Th in the background pad.

The sensitivity matrix may then be estimated as

$$\mathbf{S} = \mathbf{N}\Delta\mathbf{C}^{-1} \tag{4.5}$$

where $\Delta\mathbf{C}^{-1}$ is the inverse of $\Delta\mathbf{C}$. The sensitivities s_{ij} are in units of count rate (in a specific energy window) per unit concentration (1% K, 1 ppm U, 1 ppm Th) of the radioelements.

For the K, U and Th energy windows (i=1, 2 and 3), the "stripping ratios" α, β, γ, a, b and g (see §4.1.4) are defined by the ratios of sensitivities as follows

$$\alpha = \frac{s_{2Th}}{s_{3Th}} \qquad \beta = \frac{s_{1Th}}{s_{3Th}} \qquad \gamma = \frac{s_{1U}}{s_{2U}} \tag{4.6}$$

$$a = \frac{s_{3U}}{s_{2U}} \qquad b = \frac{s_{3K}}{s_{1K}} \qquad g = \frac{s_{2K}}{s_{1K}} \tag{4.6}$$

The stripping ratios define the ratios of count rates, caused by a single element in an energy window, to the count rate of the same element in its principal energy window. They are used during data processing to estimate the net count rate of a single element in an energy window. The stripping ratios α, β, γ, and a also give an indirect measure of the energy resolution of a detector system – the smaller their values, the better the energy resolution of the detector.

IAEA recommended concentrations of K, U, Th in calibration pads enable calibration of a portable gamma ray spectrometer, equipped with a NaI(Tl) 76×76 mm detector, to a relative precision of 1%, in a 10 min sampling time. Due to the finite dimensions of calibration pads, a geometrical correction, G, must be applied to the derived sensitivities. The correction depends on the pad dimensions, pad density, and the height of the centre of the scintillation crystal above the pad surface. The ratio, R, of gamma radiation from a cylindrical pad 0.5 m thick to that from an infinite source, with the detector placed on the centre of the pad, and $h/r < 0.2$, is

$$R = 1 - \frac{h}{r} \tag{4.8}$$

where h = height of the scintillation crystal centre above the surface of the pad (m);
r = radius of a cylindrical pad (m).

The geometrical correction can be applied by multiplying the derived sensitivities (equation (4.5) by $G = 1/R$. Note that equation 4.8 is based on the assumption that the pads are infinitely thick. For pads of finite thickness, the correction factor also depends on pad thickness and on the linear attenuation of gamma-radiation in the pads (and hence the density of the pads and the energy of the gamma rays). An example of the sensitivities and stripping ratios estimated for a portable gamma ray spectrometer are given in Table 4.1. Examples of geometric correction factors for cylindrical pads are given in Tables 4.2 and 4.3. These were calculated using the computer program of Lovborg et al., 1972. Examples of geometric correction factors for rectangular transportable pads are given in Table 4.4.

TABLE 4.1. TYPICAL ENERGY WINDOW SENSITIVITIES AND STRIPPING RATIOS FOR A PORTABLE GAMMA RAY SPECTROMETER WITH NaI(TL) 76×76 MM DETECTOR (IAEA, 1989)

Sensitivities	K window	U window	Th window
counts/s per 1% K	3.36	0	0
counts/s per 1 ppm eU	0.250	0.325	0.011
counts/s per 1 ppm eTh	0.062	0.075	0.128

Stripping ratios	Ratio of sensitivities	Stripping ratio
α	0.075/0.128	0.586
β	0.062/0.128	0.484
γ	0.250/0.325	0.769
a	0.011/0.325	0.034
$b = g$		0.000

TABLE 4.2. GEOMETRIC CORRECTION FACTORS FOR CYLINDRICAL PADS 2m IN DIAMETER AND 0.5m THICK

Cylindrical calibration pad (dimensions 2m diam × 0.5 m thick)	Energy (MeV)	Correction factor (detector height = 0.06 m)
K pad (density=2.24 g/cm^3)	1.46	1.068
U pad (density=2.24 g/cm^3)	1.76	1.070
Th pad (density=2.24 g/cm^3)	2.62	1.074

TABLE 4.3. GEOMETRIC CORRECTION FACTORS FOR CYLINDRICAL PADS 3m IN DIAMETER AND 0.5m THICK

Cylindrical calibration pad (dimensions 3 m diam × 0.5 m thick)	Energy (MeV)	Correction factor (detector height = 0.06 m)
K pad (density=2.24 g/cm^3)	1.46	1.042
U pad (density=2.24 g/cm^3)	1.76	1.043
Th pad (density=2.24 g/cm^3)	2.62	1.046

TABLE 4.4. GEOMETRIC CORRECTION FACTORS FOR TRANSPORTABLE CALIBRATION PADS (after Grasty et. al. 1991)

Transportable calibration pad (dimensions 1×1×0.3 m)	Energy (MeV)	Correction factor (detector height = 0.06 m)
K pad (density=2.23 g/cm^3)	1.46	1.156
U pad (density=2.24 g/cm^3)	1.76	1.165
Th pad (density=2.28 g/cm^3)	2.62	1.188

Note: Detector height is the height of the centre of the scintillation crystal above the pad.

Detailed descriptions of available calibration facilities are given in IAEA (1989). Variable moisture content in calibration pads can lead to a change in radiation output. Pads should therefore be kept dry.

The calibration of Ge semiconductor spectrometers for field use is based on experimentally estimating the instrument detection efficiencies for individual gamma ray energies (peak count rate per unit photon flux), and then converting these to isotope ground concentration. A series of point source standards, emitting various gamma energies, of known activity, should be available for calibration (ICRU, 1994). A simpler approach of calibrating Ge spectrometers by means of large concrete calibration pads for evaluating the specific activity (Bq/kg) of natural radionuclides has been suggested (IAEA, 1989).

4.1.4. Data processing procedure

Gamma ray field measurements yield a number of counts, N, registered in a particular energy window for a counting time, t. These can be converted to a count rate, $n = N/t$ (c/s). Modern portable gamma ray spectrometers automatically correct for instrument dead time by extending the counting time. For the estimation of K, U, and Th concentrations in rocks or soils, the recorded count rate is related to the concentrations of the radioelements by equation 4.1. The observed count rates, n_i, are corrected for background and the elemental concentrations can be estimated using either the matrix method or the stripping method.

The matrix method is based on equation 4.2. The concentrations of K, U, Th are estimated as follows:

$$\mathbf{C} = \mathbf{N}\mathbf{S}^{-1} \tag{4.9}$$

The stripping method uses the "stripping ratios" to estimate elemental count rates in each window before converting these to concentrations. Assuming that stripping ratios $b = g = 0$, the net count rates, $n_{ij,}$ of the j-th radioelement in a specific energy window, i, are given by

$$n_{3Th} = \frac{n_3 - n_{3BG} - a(n_2 - n_{2BG})}{1 - \alpha a} \tag{4.10}$$

$$n_{2U} = n_2 - n_{2BG} - \alpha n_{3Th} \tag{4.11}$$

$$n_{1K} = n_1 - n_{1BG} - \beta n_{3Th} - \gamma n_{2U} \tag{4.12}$$

and the concentrations are given by

$$c_K = \frac{n_{1K}}{s_{1K}} \tag{4.13}$$

$$c_U = \frac{n_{2U}}{s_{2U}} \tag{4.14}$$

$$c_{Th} = \frac{n_{3Th}}{s_{3Th}} \tag{4.15}$$

where s_{ij} are the instrument sensitivities. The concentration are in % K, ppm eU and ppm eTh.

Ratios between radioelement concentrations (Th/U, Th/K, U/K) are often used to reduce the effect of terrain geometry on the concentration estimates. Anomalous ratios are often indicative of mineralization and rock alteration.

Estimates of the radioelement concentrations may be converted to either the dose rate in air or the exposure rate. Conversion constants were given in Table 2.6. Modern portable gamma ray spectrometers can be calibrated to give an estimate of the terrestrial dose rate directly. Since the ratio of the attenuation coefficients of gamma rays in air, and in NaI(Tl) scintillation crystals has been found relatively constant for the energy interval 400-3000 keV, the energy deposited per unit distance in air and in the crystals should be proportional. Based on this assumption, a sum of products of count rate in each channel and its respective energy can be converted to dose rate by a calibration constant. A comparison of gamma dose rate values, estimated using an ionization chamber and a portable gamma ray spectrometer, show excellent agreement (Grasty and Lamarre, personal communication).

Spectral smoothing techniques (§5.5.2) may be applied to ground traverse data to reduce statistical noise. Grasty (2001) presents an example of data continuously sampled at a 5 s interval, where the noise was reduced by a factor of approximately 4.2 (equivalent to increasing the detector volume by a factor of 18).

4.1.5. Errors

A precision of about 0.1% K, 0.4 ppm eU and 0.6 ppm eTh can be expected from field assays with a scintillation gamma ray spectrometer using a sampling time of 4 minutes. The main factors that reduce assay precision are the statistical nature of radioactivity, variable background radiation due to atmospheric radon, and the variable water content in rocks.

The geometry of surrounding terrain can substantially affect the estimates of radioelement concentration. Due to the relatively long paths of gamma rays in air, an uneven earth surface due to hills and valleys, steep slopes, quarries and building excavations can change the observed count rates by several tens of percent. A careful record of field measurement conditions can help to exclude false anomalies.

4.2. Car-borne gamma ray spectrometry

Car-borne gamma ray spectrometry fills the gap between portable and airborne techniques. It has the advantage over portable systems in terms of much greater coverage for a given time and cost, and over airborne systems for quick mobilisation and improved resolution. These systems are more likely to be used for environmental applications (eg. mapping nuclear fallout, searching for lost radioactive sources). These systems are of course restricted to areas where vehicle access is possible, which is much less of an issue for portable or airborne systems.

4.2.1. Instrumentation

Historically, car-borne instrumentation has essentially consisted of airborne systems modified for use in a vehicle. In the last few years, instrument manufacturers have designed systems specifically for car-borne use, or adaptable to a variety of platforms (vehicle, helicopter or fixed wing). Car-borne systems use smaller crystal packs, typically 4 or 8 l. As with an airborne system, GPS navigation is standard. It may include a GIS-based navigation screen, with detailed road maps displayed, so that real-time decisions on survey routing are possible. Radiation levels and radioelement responses are also displayed, with an audible warning system for target location.

4.2.2. Field measurement

Field measurement depends on the application. Geological mapping requires “off-road” traverses, as paved roads, and many earthen roads as well, are severely contaminated by the material used to construct and maintain the roads themselves, and poorly reflect the geology of interest. Environmental applications, where background levels may already be available, are usually conducted “on-road” if the road network provides sufficient coverage. In these situations, the focus is usually on radionuclides from man-made sources that exceed the natural (or historical man-made) background by some appreciable amount. One must bear in mind that the background levels of a road may change over time due to natural wear, maintenance and reconstruction. For off-road surveys in winter conditions, these systems have been adapted to be towed behind snowmobiles, and can provide useful data despite attenuation by the snow.

The field of view of a car-borne system is much closer to that of a portable rather than airborne system. The speed of operation is on the order of 1/5 to 1/10 to that of an airborne system. Consequently, the resolution of the data along a car-borne traverse is much greater than that of an airborne flightline. However, the data are also much more susceptible to local variations that are likely considered to be “geological noise”, such as soil composition, soil moisture content, surface water (eg. puddles), transported versus in-situ material, weathering and outcrop exposure. Topographic effects in even moderate terrain may have a significant effect on car-borne data, particularly where road cuts expose fresh bedrock. Trees and buildings are other potential noise sources, depending on the survey objectives. Pockets of radon may also produce localized effects. Variations in the system background levels may be

higher than for an airborne system, due to collection of dust, mud, etc. inside and outside the vehicle. Grasty and Cox (1997) show that the efficiency of a car-borne detector at locating nearby sources is highly dependent on the geometry of the detector, and the shielding elements within the vehicle and the spectrometer system.

Detectors are mounted on a vehicle's roof if an increase in the field of view is required (Killeen, 1979). The shielding effect of the vehicle can be advantageous if sampling of the underlying road material is not desired. Lead shields can be utilized as well. The detectability of an anomaly is determined by the detector volume and the velocity of the vehicle, which govern the signal-to-noise and the spatial wavelength resolution respectively. Consequently, systems designed for geological mapping may be configured and deployed differently than those optimized for mapping fallout or locating lost sources. Audio and/or visual alarms are often built in to systems to signal the operator that a significant anomaly has been detected and immediate follow-up is possible.

Car-borne systems are quickly mobilized relative to airborne systems. Production levels on roads can approach those from the air as a car-borne system can be operated day and night, and through inclement weather. Car-borne systems are more suited to winter conditions, where roads are kept clear of snow. Should the vehicle become contaminated during response to nuclear fallout, it can quickly be exchanged for a clean one. Denser road networks in urban areas often provide sufficient coverage when quick mapping in an emergency is required.

4.2.3. Instrument calibration

Instrument calibration occurs on concrete pads using the same procedures as for airborne spectrometers (§5.3.2), with the detector removed from the vehicle. For determination of background count rates, Grasty and Cox (1997) suggest connecting the detector to a portable spectrometer and taking the measurements over a large body of water with a metal or fibreglass boat. System sensitivities can be determined by recording car-borne data centred over a 15-20 m diameter area where the ground concentrations have been averaged from a grid of calibrated ground spectrometer measurements. A test line to monitor the system should be established in a stable area off-road (e.g. grass field), and "driven" on a daily basis. In the case of a nuclear emergency response, a more elaborate calibration scheme is required to account for the deposition and decay of man-made radionuclides, particularly ^{134}Cs and ^{137}Cs (§10.1).

Karlsson et al. (2000) compare ^{137}Cs measurements from nine car-borne systems (eleven detectors) acquired over a 200 km traverse and at four specific calibration sites, all during the same day. Even though each system was calibrated, the levels of ^{137}Cs, reported as equivalent surface activity, varied by a factor of two. These differences were attributed mainly to different calibration procedures, but also possibly to geometry, shielding or displacement of the systems.

4.2.4. Data processing procedure

The following corrections should be applied. Where appropriate, the corresponding section for airborne gamma ray spectrometer data processing is provided for the details of the procedure.

1. Pre-processing (§5.5.1);
2. Live time correction (§5.5.3);

3. Energy calibration (§5.5.4);
4. Background correction (§5.5.5) - subtraction of background spectra determined from daily test line;
5. Stripping correction (§5.5.7) - applied using the stripping ratios α, β and γ, without any height correction;
6. Reduction to elemental count rates (§5.5.9) - utilises the sensitivity coefficients determined during calibration or by measuring the test line; and
7. Levelling (§5.5.10) – data can be levelled if frequent measurement stops at "perfect geometry fields" are taken (Mellander, 1995).

Road-based measurements will typically follow an irregular network. Preparing grid images from such data can be difficult, but the minimum curvature algorithm (Briggs, 1974) is suitable if the gridding parameters are well-chosen. The resultant images should be prepared with the road traverses superimposed so that the most reliable portions of the grid are easily determined. Profile presentation of the data, possibly incorporating manual contouring, may be more appropriate where the network is sparse.

4.3. Borehole gamma ray spectrometry

Gamma ray spectrometry forms one of many techniques used to acquire measurements in boreholes after drilling, to characterize the physical properties of the intersected geology. Borehole surveys typically involve multi-parameter measurements using a multitude of sensors, to provide complementary datasets. Gamma ray spectrometry is part of a broader range of nuclear techniques used in borehole logging, particularly for petroleum exploration. A density (or gamma-gamma) logging system uses a gamma ray source (e.g. ^{137}Cs) to generate back-scattered gamma rays, which reflect the density of electrons and provides a bulk density of the surrounding rock. Various types of neutron logging systems emit neutrons to characterize porosity, liquids (e.g. oil, gas, water, brine) and certain lithologies (e.g. calcium, silicon). Killeen (1997b) describes the use of nuclear sources (gamma ray, neutron) and measurement of the resultant emissions (gamma ray, neutron, X-ray) for mineral exploration applications, including density logging, heavy element detection, and particularly location of ore zones and determination of their grades. IAEA has produced several reports on applications of nuclear techniques to logging and assaying. This report concentrates on borehole systems that utilize gamma ray spectrometry to measure the natural content of radioactive elements.

4.3.1. Instrumentation

A borehole system typically comprises a probe (tool) incorporating detectors only (passive system) or sources and detectors (active system) that is lowered down a borehole (Killeen, 1997a). The probe is attached to a recording system on surface by a cable that is used to transmit power to the probe (unless batteries are installed in the probe), and data to the surface (unless recorded in memory in the probe). A winch and pulley assembly is used to lower/raise the probe at a predetermined speed for continuous logging, or held for stationary measurements, and incorporates a depth counter. Multi-parameter surveys may be conducted with probes that contain more than one set of instrumentation, and/or require multiple logging sessions with different probes.

Gamma ray spectrometer borehole probes typically use NaI(Tl) or CsI(Tl) detectors measuring 25 mm × 76 mm or smaller (Killeen, 1997b), roughly one-third the volume of hand-held detectors. In a borehole, the detector is surrounded by the source and provides the optimal 4π sampling geometry, and consequently does not suffer from topographic effects.

4.3.2. Field measurement

The gamma ray spectral probe measures the full gamma ray spectrum, from which the total count, K, U and Th windows are extracted, similar to ground and airborne systems. These have replaced the total count (scintillometer) systems. Measurements are undertaken continuously down/up the hole at a typical speed of 3 m/minute (Killeen, 1997b). The lateral penetration adjacent to a borehole is 10-30 cm, depending on the density of the rock.

Fullagar and Fallon (1997) describe the cost advantages of utilizing percussion or reverse circulation drilling combined with borehole logging over the considerably more costly diamond drilling, particularly to define ore zones in a mine environment. The information and accuracy provided by the logging compensates for the less competent drill core, and can define ore zone boundaries quite precisely to optimize blasting.

4.3.3. Instrument calibration

The Geological Survey of Canada established several borehole test sites for many techniques, and model calibration facilities specifically designed for gamma ray spectrometry (Killeen, 1986). The test site at Bells Corners, Ontario comprises six boreholes drilled to depths up to 300 m below surface, in an area where three sedimentary horizons overlie a granite-gneiss basement, which incorporates a weathered alteration zone. These lithologies, and subdivisions within them, are characterized by distinct K, U and Th signatures. The boreholes are well documented by the GSC for several techniques, and provide a site for testing probes and systems, and comparing results.

The model boreholes were constructed in 1977 to provide quantitative calibration facilities in Ottawa, Ontario. Nine cement columns, measuring 3.9 m high and 1.9 m in width, each contain a 1.5 m thick "ore zone". The single element ore zones contain nominal amounts of potassium (0.7%, 1.1% or 3%), uranium (15 ppm, 100 ppm or 950 ppm) or thorium (8 ppm, 35 ppm or 350 ppm). The columns contain three holes of different sizes (A-46 mm diameter, B-60 mm and N-75 mm). They are portable, and can be transported to other sites for comparative testing. Using the known concentrations of the ore zones, measured through laboratory analysis, the system's stripping factors and sensitivities can be determined similar to portable gamma ray spectrometers (§4.1.3).

Calibration facilities have been established in other locations (e.g. Colorado, South Australia, Sweden) using model boreholes similar to the GSC site. In the 1980s, IAEA sponsored a series of intercalibrations between these facilities to resolve discrepancies found when a system was calibrated at the various sites (Killeen, 1979). The Colorado site also includes models with thin (50 mm) ore beds dipping at 30˚, 45˚, 60˚ and 90˚ to the vertical borehole, to test the effects of their geometry on various systems. Wenk and Dickson (1981) describe the Australian calibration facility and suggest that the uranium-enriched model boreholes must be monitored over time for variation due to radon loss or water content.

4.3.4. Data processing procedure

Reduction and correction of borehole gamma ray spectrometer data can ignore certain effects characteristic of surface and airborne measurements, but must consider others peculiar to down hole measurements (Killeen, 1979). In a borehole, the detector is surrounded by the source and the background radiation is essentially non-existent. Cosmic effects are virtually

nil, as is the contribution of radiation from the air (none if the hole is liquid-filled). Some drilling muds incorporate potassium compounds, and obviously will contribute to background radiation if they are used instead of water or muds of other composition as a drilling fluid. Boreholes left dormant for long periods of time can have a build-up of radon. This is prevented by leaving the holes filled with water or flushing them prior to logging. The dead time of the system must be determined and accounted for (§5.5.3) if not done so automatically.

Killeen (1979) provides graphs showing corrections for the attenuation effects of water (if present), probe housing composition and drill hole casing thickness (if present). It may be necessary to determine these experimentally for a specific system and casing thickness at a calibration site. Some steel used for metal casing was manufactured with radioactive material (§10.4). Steps in the logs coincident with section breaks in the casing are an indication that some sections of casing are radioactive and thus contaminating the measurements.

Wahl (1983) undertook a comprehensive study of several conditions that may affect the borehole gamma ray spectrometer data, lateral penetration and interpretation. These include borehole fluid (mud) density and composition, borehole radius, formation density, formation energy levels, probe geometry (e.g. off-centre), vertical resolution and photoelectric effect. Numerous experiments show that many effects incorporate two or more inter-related conditions. Conaway et al. (1980) studied the effects of probe velocity, sampling interval and detector length.

The small size of the detectors in borehole probes and continuous measurement often lead to low count rates, and consequently low signal-to-noise. This may require low pass filtering to improve the coherence of the data. Conaway et al. (1980) suggest a sinc function tapered by a Blackman window. Where geological unit boundaries are well-defined by sharp changes in their radioelement responses, the spatial derivative computed along the borehole will more precisely locate the contact. Conaway and Killeen (1978) propose a simple inversion technique to deconvolve the borehole response to the "geologic impulse response", and provide an accurate determination of radioelement concentrations, particularly for determination of the grade-thickness product of a uranium ore interval. Direct comparison between estimated ore grade from a log and assayed ore grade from drill core should consider that the log has sampled over a wider radius, and of course has not sampled the core itself.

The standard presentation of borehole data of any sort is in chart form, with the vertical axis aligned with the trajectory of the borehole. Each measured parameter is scaled to show an increase in the horizontal plane to the right side of the chart. This type of presentation allows direct correlation between measured and derived parameters, to characterize the properties of specific intervals within the borehole for lithology, alteration and/or mineralization. 3-D visualization technology is revolutionizing the presentation of subsurface data of all kinds, and is helping popularize borehole techniques with the broader geoscientific population. Automated interpretation of multi-parameter logs utilize a variety of techniques including scatter plots, principal component analysis, discriminant analysis, neural networks and cluster analysis (Fullagar and Fallon, 1997).

The geological applications of borehole gamma ray spectrometry are similar to those of ground and airborne methods, but tend to be more focused on advanced mineral exploration projects. Direct detection of ore zones may be limited to radioactive minerals, but indirect detection (e.g. potassium-enriched sericitic or feldspathic alteration associated with gold mineralization) and characteristic of host rock (e.g. phases of kimberlite) are also important

applications. As with all borehole techniques, lithologies and horizons can be traced from hole-to-hole.

Løvborg et al. (1980) logged 23 boreholes that intersect a uranium-thorium deposit at Kvanefjeld, Greenland. They utilized nearly 2,000 individual assays to determine the sensitivities and stripping ratio for U and Th, separately for each borehole. The result was an estimate of the uranium ore tonnage that matched closely with the estimate determined from assay results. The Th concentrations computed from the logs matched closely with the assays, but the U data produced more of a scatter. It was found that radon emanating from the ore reduced the accuracy of the U logs, and it varied with the presence and composition of water, and porosity of the rock. Schmid and Olschewski (1986) determined experimentally that for uranium concentrations below 0.7% U, a linear relationship exists between eU determined from a borehole log and %U. Above this level, the linearity deteriorates.

4.4. Laboratory gamma ray spectrometry

The laboratory analysis of K, U, Th and Ra in rock samples is used to complement field surveys in uranium exploration, radiometric mapping and mineral prospecting. Lead is used to shield a NaI(Tl) scintillation detector from background radiation in a laboratory. A multichannel analyzer is used to detect, analyse and display gamma rays emitted by rock samples. Quantitative analysis is essentially comparative: the radiation from a rock sample is compared with the radiation from known standards. The accuracy and precision of the results depends on many factors: the size and energy resolution of the detector; the mass and geometry of the sample; the shielding of laboratory background; counting time; data processing procedures; and the quality of the radioactive standards.

High-resolution Ge laboratory spectrometers can be used for more sophisticated applications. These include the identification of environmental isotopic pollution, the identification of unknown gamma radiation sources, and detailed studies of radioactive equilibrium and the distribution of radionuclides in soil and rock samples.

4.4.1. Rock samples and laboratory equipment

Rock samples are crushed to a grain size 1 mm, and placed into sample containers. The containers are usually metal or plastic and are sealed so that no radon can escape. The size and shape of the containers depends on the radioactivity of the samples. Low radioactivity rock samples can be effectively measured in Marinelli-type containers or in cylindrical containers with a volume of several hundred cubic centimetres (Figure 4.5). U and Th ore-grade samples are measured in smaller cylindrical containers with volumes of several tens of cubic centimetres.

A typical laboratory scintillation gamma ray spectrometer consists of a NaI(Tl) scintillation detector with a minimum size of 76×76 mm NaI(Tl), a preamplifier, a multichannel analyzer (1024-4096 channels), a stabilized high voltage supply, a display unit, and a data recording unit. The sample and detector are enclosed within 6-10 cm of lead shielding to reduce the background radiation. A 5 mm thick brass plate is installed inside the lead shielding to minimize the effect of induced X-ray radiation in the lead shielding.

The performance characteristics of a particular laboratory spectrometer should be known, as this affects the selection of the best method of analysis. The energy resolution of the detector can be measured using the ^{137}Cs peak at 662 keV. This can be used to select an appropriate channel width setting. The noise level in the 10-30 keV energy range should be

experimentally determined and eliminated by correctly setting the instruments lower energy discriminator. The stability of the instrument may be tested by a series of repeat measurements of a reference source. The measured standard deviation should not be greater than that expected from a Poisson distribution due to the statistical nature of the radiation field. Very high count rates from ore grade samples can induce an energy spectrum shift in the output. The spectrum shift range at high count rates can be experimentally determined. A set of reference gamma-emitting sources is used to facilitate the instrument energy calibration.

FIG. 4.5. Marinelli type metal and cylindrical plastic containers for laboratory sample analyses.

4.4.2. Laboratory determination of natural radionuclides

Pulverized rock samples with a mass of 200-1000 g are sealed in containers for the accumulation of ^{222}Rn. Table 4.5 shows the accumulation of free radon with time once the containers are sealed.

TABLE 4.5. ACCUMULATION OF FREE ^{222}Rn IN SEALED CONTAINERS

Accumulation time (days)	10	14	18	22	30	38
Percent of equilibrium concentration	83.7	92.1	96.2	98.1	99.6	99.9

Note: the half-life of ^{222}Rn is 3.825 days.

Several gamma ray methods have been developed to estimate the concentration of K, U, Th and Ra in rock samples. The simplest technique is to monitor their specific gamma ray energies in four energy windows. Depending on the size and configuration of the NaI(Tl) detector, Ra and Th concentrations can be estimated using either high or low energy windows (Table 4.6). The high energy windows are used with large detector volumes. For 76×76 mm and 100×100 mm NaI(Tl) scintillation crystals, the low energy lines are preferable.

TABLE 4.6. RECOMMENDED ENERGY LINES FOR U, Th, Ra, AND K LABORATORY GAMMA RAY SPECTROMETRY ANALYSIS OF ROCK SAMPLES

Element	Isotope	Energy (keV)	Isotope	Energy (keV)
U	^{234}Th	92.6		
Th	^{212}Pb	238.6	^{208}Tl	2614.7
Ra	^{214}Pb	352.0	^{214}Bi	1764.7
K	^{40}K	1460.8		

The energy resolution of the detector and the operational stability of the equipment must be considered when choosing window energy widths. Window widths are usually in the range of tens up to hundreds of keV. The initial equipment gain, which is estimated using a reference energy source, determines the channel energy width and the energy range of an amplitude analyzer. The choice of sampling time depends on the level of radioactivity and the required precision of analyses. For medium to high radioactivity rock samples, a counting time of 2000 s per sample is adequate. For low radioactivity samples, such as limestones and basaltic rocks, a counting time of 4000 s would be appropriate. For practical and control reasons, the counting time is divided into two measurements with the same time intervals. Since the gamma radiation of a sample is related to its mass, recorded count rates must be normalized to unit mass.

A four component (U, Th, Ra, K) analysis is based on measurements in four specific energy windows (i = 1, 2, 3, 4), and the count rates per unit mass are related to the concentrations as follows:

$$n_i = s_{iU} c_U + s_{iTh} c_{Th} + s_{iRa} c_{Ra} + s_{iK} c_K , \tag{4.16}$$

where n_i = background-corrected count rate per unit mass in the i-th energy window, (c/s per g);
s_{ij} = sensitivity of a spectrometer for the detection of the j-th element in the i-th energy window, (counts/s per unit mass and unit concentration);
c_j = concentration of the j-th element.

This can be expressed in matrix notation as follows

$$\mathbf{N} = \mathbf{SC} , \tag{4.17}$$

Where **N** = column vector of background-corrected count rates of a sample per unit mass;
S = 4×4 matrix of sensitivities (s_{ij});
C = column vector of concentrations (c_j).

4.4.3. Instrument calibration

The sensitivity, s_{ij}, of a spectrometer to the detection of the *j*-th element in the *i*-th energy window is determined by instrument calibration. For a four-element laboratory gamma ray spectrometric analysis, U, Th, Ra and K standards are necessary. Standards should have identical containers and geometry to the samples being analysed. They should also have a similar matrix composition. The concentrations of the radioelements are reported in ppm U, ppm eTh, ppm eU for Ra concentration and %K. Ra concentration is expressed in equivalent equilibrium concentration of U, using the mass ratio:

$$U_{natural} : {}^{226}Ra = 1 : 3.376 \times 10^{-7}. \quad (4.18)$$

The IAEA introduced a RG-set of 3 geological reference materials for laboratory gamma ray spectrometry analysis (IAEA, 1987). RGU-1 is a U+Ra geological reference material with 400 ppm U and 392 ppm eU. RGTh-1 is a Th geological reference material with 800 ppm Th. RGK-1 is a geological reference material with 44.8% K. A pure uranium standard can be prepared from U chemical reagent, not containing Ra, mixed with a rock matrix. The pure U standard should be rich in U (about 1000 ppm U), and have very low concentrations of Th, Ra and K.

The calibration procedure is essentially the same as for portable gamma ray spectrometers, except we now have four radioelements and four energy windows. The determination of background count rates (n_{iBG}) in each energy window, and a series of repeat measurements of the four standards, expressed in count rates per unit mass, result in the following system of equations

$$\mathbf{N} = \mathbf{SC}, \quad (4.19)$$

where $\mathbf{N}$ = 4×4 matrix of background-corrected count rates per unit mass of the standards;
$\mathbf{S}$ = 4×4 matrix of sensitivities;
$\mathbf{C}$ = 4×4 matrix of U, Th, Ra, K concentrations of the standards.

The sensitivities (s_{ij}) may be calculated by means of inverse matrix of concentrations $\mathbf{C}^{-1}$,

$$\mathbf{S} = \mathbf{N}\mathbf{C}^{-1}. \quad (4.20)$$

The matrix of sensitivities, **S**, also serves as a measure of the instrument performance and the mode of analysis. The determinant of this matrix should be as small as possible.

4.4.4. Data processing procedure

The measured window count rates are corrected for equipment dead time and background radiation, and normalized to unit mass. Some instruments apply the dead time correction automatically. The concentrations of U, Th, Ra and K are estimated by:

$$\mathbf{C} = \mathbf{N}\mathbf{S}^{-1} \quad (4.21)$$

where **C** = column vector of concentrations (c_U, c_{Th}, c_{Ra}, c_K);
N = column vector of background-corrected count rates per unit mass of the sample;
$\mathbf{S}^{-1}$ = inverse of the 4×4 sensitivity matrix **S**.

The assay precision is a function of the equipment performance, the method of analysis, the activity of the samples, and the counting time. Typical errors for a single rock sample analysis are in the range 0.5-2 ppm U, 0.2-0.5 ppm eTh, 0.1-0.3 ppm eU for Ra, and 0.03-0.1% K. Relative errors are highest for U estimation at 92.6 keV (15-30% for low U abundances). This is due to interference from scattered gamma rays, induced X-ray fluorescence, and the absorption of low energy gamma rays by the particular rock matrix. The lower limit of detection for a given element may be estimated as a threefold of the mean error of analysis of a low radioactivity rock.

Modern computer techniques enable the full multichannel gamma ray processing of spectra. This eliminates spectrum drift by normalizing the data to reference gamma ray spectra. The relative concentrations of U and Ra in a sample can be used to estimate the radioactive equilibrium between these isotopes.

4.4.5. Laboratory determination of gamma ray sources

Semiconductor laboratory gamma ray spectrometers have the capacity to identify unknown isotopes in various materials and rock samples. Qualitative interpretation of gamma ray spectra with good energy resolution (Figure 4.6) is by comparison of the observed photopeaks to a library of known gamma emitting source energies. The net peak area is related to element activity or concentration. The possibility of detecting the 1001 keV energy line of ^{234m}Pa, the near decay product of ^{238}U, makes the direct determination of U reliable. Multi-element analysis of semiconductor gamma energy spectra can be used to estimate radioactive equilibrium in the U and Th decay series.

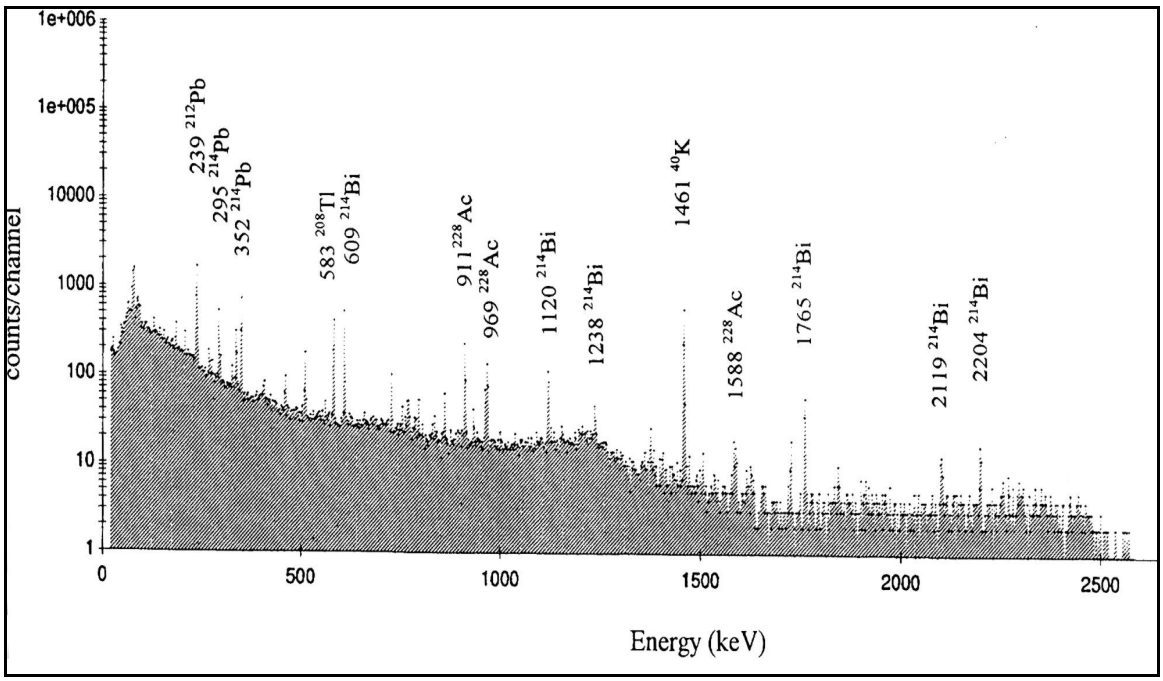

FIG. 4.6. Typical germanium detector gamma ray spectrum.

4.5. Marine gamma ray spectrometry

Marine gamma ray spectrometry is obviously limited by the attenuation of gamma rays in water. Nevertheless, innovative detector design allows gamma ray measurements to be undertaken in shallow and deep waters. Jones (1999) provides an overview of seabed exploration with radiometric methods.

Most of these studies have focused on geological mapping of outcrop on the seafloor, at depths up to 6 km. Surveys around active hydrothermal vents have also been undertaken.

4.5.1. Instrumentation

Two types of detectors may be used. In each case, they are attached to a ship (or submersible) by a cable. The data is passed up the cable where an on-board spectrometer analyses the pulses transmitted from the seafloor. One type of system consists of a detector housed in a pressure-resistant casing that is lowered onto the seafloor for spot measurements. The second type of system is dragged along the seafloor so that the detector is towed within cm of the seafloor. A pinger may be used to monitor the cable positioning relative to the bottom so that the detector remains at a consistent height. Innovative designs for housing the detector (eg. a hose assembly) are required to prevent snagging of the instrumentation on outcrop.

4.5.2. Field measurement

Table 4.5 shows the attenuation of gamma rays in water, air, mudstone and concrete. The attenuation in water is about 10^3 times that of air, but only half that of the solid materials. For a photon energy of 1.76 MeV, a seafloor clearance of 0.175 m would provide the equivalent to an aircraft terrain clearance of 150 m. Obviously, to be effective, marine measurements are best taken on the seafloor or very close to it (within 20 cm). The relatively slow ship speed in the range of 1.0 to 2.5 m/s and counting times between 100 and 500 s improves the signal despite the difficult operating conditions.

TABLE 4.7. ATTENUATION OF GAMMA RAYS (after Durrance, 1986 and Grasty, 1979)

Photon energy (MeV)	Half-thickness (m)			
	Air[a]	Water	Mudstone[b]	Concrete[c]
1.46	102	0.118	0.058	0.053
1.76	112	0.130	0.064	0.058
2.62	137	0.160	0.078	0.070

[a] 0°C, 760 mm Hg, density 0.001293 g/cm^3
[b] density 2.30 g/cm^3
[c] density 2.5 g/cm^3

Background measurements are taken several meters above the seafloor and/or in the water column at the beginning and end of a traverse, when the sensor is lowered or raised. The detector assembly itself contributes most of the background radiation (cosmic and gamma rays). In deep water, radon's contribution is usually minimal as the bottom waters sweep away any emanations from the seafloor, except in the vicinity of active hydrothermal vents or

gas and water seepages. Likewise, tides and currents in continental shelf waters are usually sufficient to remove nuclear fallout (tests, accidents or waste disposal). Seabed emissions may increase near waste disposal sites if the material has been absorbed by the near-shore sediments.

4.5.3. Instrument calibration

Instruments may be calibrated using a uniform seafloor with known radioelement concentrations. This is usually not practical. Typically, the spectrometer is calibrated on concrete pads using the same procedures as for airborne spectrometers (§5.3.2).

4.5.4. Data processing procedure

The following corrections should be applied. Where appropriate, the corresponding section for airborne gamma ray spectrometer data processing is provided for the details of the procedure.

1. Pre-processing (§5.5.1) – may include further averaging over time to improve signal;
2. Live time correction (§5.5.3) - likely of little consequence due to the long counting times;
3. Energy calibration (§5.5.4) - not required for self-calibrating spectrometers, and a small source of error otherwise;
4. Background correction (§5.5.5) - simple subtraction of averaged background spectra;
5. Stripping correction (§5.5.7) - applied using the stripping ratios α, β and γ, without any height correction;
6. Water attenuation - correct for water attenuation using the known or estimated height above sea floor (generally the largest source of error as the height and/or detector geometry is not well-known); and
7. Reduction to elemental count rates (§5.5.9) - utilises the sensitivity coefficients determined during calibration or by measuring a ground-based test line with the marine system.

Presentation of the data in profile form may be more suitable than gridded images unless the survey coverage follows a dense, regular pattern of lines.

5. AIRBORNE GAMMA RAY SPECTROMETRY FOR NATURAL RADIOELEMENT MAPPING

Airborne gamma ray spectrometry has been used for many years for the direct detection of ore bodies and as a lithological mapping tool. Environmental applications such as health risks associated with radon in houses, and the mapping of fallout from nuclear accidents have also been developed. In recent years, the scope of the method has expanded to include applications such as soil mapping, ground water discharge and salinity studies. Recent developments include multichannel processing methods and the use of statistical methods to reduce noise in multichannel spectra.

5.1. Instrumentation

Modern airborne spectrometer systems typically comprise a detector consisting of at least two 16.4 litre detector packages. Each detector package consists of four 10.2 cm × 10.2 cm × 40.6 cm thallium-doped NaI crystals in a thermally-insulated container. Older detectors were thermally-stabilized using an internal heating blanket and temperature monitoring circuitry. The modern systems continuously monitor the channel position of a prominent photopeak and automatically adjust the gain to individual crystal photomultiplier tubes to maintain spectral stability. Spectrometers record at least 256 contiguous channels of data in the energy range 0-3.0 MeV. An additional window (the "cosmic" window) monitors all radiation above 3.0 MeV. Measurements are made at least once every second, and the system live time is automatically logged and output with the data stream.

Airborne detector packages can also be configured with an additional NaI crystal mounted above the four main crystals. The main crystals then partially shield the additional crystal from radiation from the ground. The additional crystal (the "upward-looking" detector) gives the detector a directional sensitivity, and can be used to estimate the concentration of atmospheric radon.

Ancillary equipment usually includes GPS navigation (real-time differential), radar altimeter, barometer and thermometer. The radar altimeter, temperature and pressure are used to correct gamma ray data for the height of the detector above the ground. Gamma rays are attenuated by air. The density of the air, which is, in turn, affected by the prevailing temperature and pressure, affects the degree of attenuation. Real-time differential GPS navigation is accurate to within about 5 m. The radar altimeter is accurate to about 2%. The GPS navigation equipment and radar altimeter record the instantaneous position and height of the aircraft every second. Temperature and pressure are also recorded every second.

5.2. Survey methodology

Airborne geophysical surveys are normally flown on a regular grid along parallel lines ("flight lines"). The flight line spacing depends on the survey application. For detailed surveys, used for geological and environmental mapping, flight lines are usually between 50 m and 400 m apart. Regional geochemical baseline surveys may be flown with a flight line spacing of 1 km or greater.

Surveys are typically flown at a constant height above the ground of between 40 m and 100 m, with helicopters able to fly considerably lower than most fixed-wing aircraft. This is the "nominal" height of the aircraft above the ground, and the extent to which the aircraft deviates from this height depends on both the topography and the skill of the pilot. A complementary set of lines ("tie lines") are often flown perpendicular to the flight lines, and

with a line spacing about 5 times that of the flight line spacing. The flight line spacing is a compromise between the desired resolution of the data, and the cost of the survey. The flying height is usually related to the line spacing, but is limited by safety considerations. The speed of the aircraft is about 50-60 m/s for fixed-wing surveys, but can be appreciably slower for helicopter surveys (25-30 m/s). Airborne gamma ray spectrometric data are almost always collected along with other remotely sensed data - such as measurements of the earth's magnetic field. The survey design therefore is usually never optimized for a particular geophysical method, but is a compromise between the methods being used.

There is obviously a trade-off in data acquisition between the observed count rates, and hence the accuracy of the measurements, and sampling time, aircraft speed, and spatial resolution of the data. Gamma ray spectrometric data are usually acquired over a sample interval of 1 s. During this interval a fixed-wing aircraft traverses about 55 m along the line. This dense sampling along lines, with a complete absence of data between lines, is typical of airborne surveying. Some of the data reduction procedures may require that the gamma ray data be summed over longer time intervals ("integration intervals") to reduce the fractional errors associated with each channel count. However, the final processed data are invariably presented with a 1-s sample interval.

Airborne gamma ray spectrometric data can be severely distorted in rough terrain as follows:

1. the radiation signal decays at an approximately exponential rate with increasing distance to the source, thereby reducing the signal-to-noise ratio of the data;
2. the rate of decay of radiation signal with distance depends on the source geometry - eg. the signal from narrow sources attenuates more quickly than from broad sources. This limits the accuracy of the height correction of airborne data;
3. the field of view of an airborne spectrometer increases with aircraft height, thus reducing the resolution of discrete sources;
4. terrain clearance will vary from line to line depending on the direction of flight (i.e. climbs occur at a greater height above a slope than a descent);
5. the necessity for flight lines and control lines (tie lines) to intersect at the same height for magnetic levelling purposes, will result in a "loose drape" flight surface;
6. the source geometry varies from the 2π surface, depending on the aircraft height and the severity of the topography – e.g. increased signal in a narrow valley due to contributions from the valley sides; and
7. the geometry of the detector may have a directional bias – e.g. rectangular pad detectors are less sensitive to lateral sources than a spherical detector.

These problems can be mitigated by:

1. flying the survey in "drape mode" - i.e. tracking the topography at a constant height above the terrain;
2. using a helicopter rather than fixed wing platform, to improve adherence to a tight drape surface;
3. where valleys have steep walls, flying additional lines parallel to the valleys to allow lower terrain clearance;
4. increasing the spectrometer crystal volume (e.g. from 33 litre to 49 litre) to improve the signal-to-noise ratio;
5. using 256-channel data processing techniques to improve the signal-to-noise ratio;
6. applying deconvolution and height correction techniques (e.g. Gunn and Almond, 1997, Craig et al., 1999) to minimize the effect of topography.

Where the terrain is very rugged (e.g. the Andes), it is often impossible to safely maintain a reasonable flying height. In such cases, the data should be examined and a terrain clearance threshold set, above which the data should be considered unreliable and not displayed. The appropriate threshold depends on the sensitivity of the detector and the strength of the geological signal.

5.3. Calibration data requirements

The main corrections that must be applied to airborne gamma ray data are background correction, stripping correction, height correction, and sensitivity correction (reduction to elemental concentrations). For each of these corrections, the approach taken to calibration is empirical. For example, the response of the detector system to variations in survey height (to obtain height attenuation coefficients) or ground concentrations of the radioelements (to obtain sensitivity coefficients) are measured. There are four main procedures for acquiring calibration data: high altitude background calibration flights, ground calibrations over radioactive sources to determine stripping ratios, calibration flights over a calibration range to determine height attenuation coefficients and sensitivity coefficients, and flights to measure the radon spectrum. These are described briefly below. The actual calibration procedures are described in §5.5.

5.3.1. High-altitude aircraft/cosmic background flights

These are usually flown offshore in an area where there is low atmospheric radon. Spectra are measured at a range of heights – typically 1.0, 1.5, 2.0, 2.5, 3.0 and 3.5 km above the water. Fifteen minutes accumulation time at each height is sufficient for a 33 litre detector. The data are processed to estimate aircraft and cosmic background (§5.5.5).

5.3.2. Ground calibration using radioactive pads

Since K, U and Th spectra overlap, empirically derived stripping ratios are used to correct each elemental window count rate for the effects of the other elements. Measurements over concrete calibration pads with dimension 1 m × 1 m × 0.3 m and known concentrations of the radioelements are used to calculate the stripping ratios (§5.5.7). Four pads are required. Three of the pads have anomalous concentrations of K, U and Th respectively. The fourth pad acts as a background pad. About ten minutes sample accumulation time is required to affect the calibration. The calibration is best performed with the detector mounted in the aircraft and each pad placed, in turn, beneath the detector under the belly of the aircraft. If two detectors are present, the calibration should be performed for each detector and the results averaged.

In some instances it may be impractical to do the calibration with the detectors mounted in the aircraft. In this case the calibration can be performed by placing the detector package directly on the calibration pads. This approach results in a decrease in the ^{208}Tl photopeak count rate at 2.61 MeV due to accidental summing of some of these gamma rays with ^{208}Tl at 0.583 MeV. These summed gamma ray events end up being counted as part of the cosmic (>3.0 MeV) count rate. So an approximate correction for this effect can be made by noting the increase in the cosmic window count rate when the Th source is used, and adding this to the Th window count rate. The stripping ratios derived in this way should also be corrected for the thickness of attenuating material in the aircraft belly.

The composition and construction of calibration pads must be carefully planned. Grasty and Shives (1997) show that local variations within a 2 m diameter uranium pad from the Pelindaba, South Africa facility exceed +/- 30% from the mean throughout the pad. A three-

year experiment to measure the seasonal effects on a Danish uranium pad showed a range from 153 ppm to 242 ppm eU over the worst year. These variations are attributed to radon "frozen" in water when the pad was wet, and released when it dried out. A phosphate glass is a preferable material to concrete for constructing a pad as it will better retain the original radioelement concentrations.

5.3.3. Calibration range flights

A calibration range is an easily navigated strip of land that is used to measure the response of an airborne gamma ray spectrometer to changes in detector height (height attenuation coefficients) and to sources of known elemental concentrations (sensitivity coefficients). Guidelines for the establishment of a calibration range are given in IAEA (1991). The calibration range is flown at different heights – typically in the range 60 m to 240 m at 30 m intervals. Flights over a nearby body of water at the same height serve as estimates of background. The background-corrected and stripped window count rates are used to estimate the elemental attenuation coefficients (§5.5.8). The ground concentrations on the calibration range are measured using a portable gamma ray spectrometer at the same time as the airborne calibrations are flown. This enables the system "sensitivity coefficients", which are used to convert airborne count rates to elemental concentrations on the ground, to be estimated (§5.5.9).

5.3.4. Radon background calibration flights

The calibration requirements depend on the background estimation method being used. Calibration procedures are described in (§5.5.6). For the full-spectrum or spectral-ratio method, a radon spectrum can be measured by flying over water in the presence of radon and then subtracting the aircraft and cosmic components. For the upward-looking detector method, over-water flights in the presence of radon are also required. Flight lines traversing both land and water can also be used to calibrate the upward-looking detector method (§5.5.6).

5.3.5. Calibration frequency

Airborne gamma ray spectrometers should be fully calibrated every twelve months (Grasty and Minty, 1995). More frequent calibrations are only necessary if equipment modifications that affect system sensitivity or aircraft background have been made. Grasty and Minty (1995) recommend that a thorium source test be carried out before the commencement of each survey. If the background-corrected Th window count rate varies by more than 3% from that recorded at the time of the last calibration, then the system sensitivity has changed significantly and all calibrations should be repeated.

5.4. Survey monitoring procedures

Survey monitoring procedures are designed to ensure that the raw airborne gamma ray spectrometric data acquired during survey operations is of the highest quality. This requires that the airborne gamma ray spectrometer is both adequately calibrated and functioning correctly. It also requires that environmental conditions (such as soil moisture) are conducive to airborne operations.

5.4.1. Calibration integrity test

A thorium source test is conducted both before and after the spectrometer is calibrated. This test is used to ensure that the sensitivity of the spectrometer has not changed during the course of the calibration. Measurements are made with a Th source placed at least 40 cm from the centre of each detector package. This ensures that the crystals in the detector package are adequately irradiated. Background measurements are also made with the source removed. The live time and background corrected Th window count rates must not differ by more than 3%, otherwise the calibration must be repeated. The average of these Th window count rates can be used as a check on the system sensitivity before each subsequent survey.

The Th source test must be repeated prior to each survey. If the corrected/background-corrected Th window count rate differs by more than 3% from the mean count rate at the time of the last spectrometer calibration, then this is an indication that the system sensitivity has changed. In this case, the source of the problem should be found and corrected, or the complete spectrometer calibration procedure (height altitude flights, pad calibration, calibration range flights) should be repeated.

5.4.2. Daily thorium source tests

During the course of a survey, the Th sensitivity tests are conducted daily - both before and after each day's flying. These tests are used to ensure that the system sensitivity does not change appreciably during the course of the survey. The background-corrected Th window count rates from these tests must be within 5% of the average of all recent Th source tests. If this is not the case, flying is suspended until the source of the problem is diagnosed and rectified.

5.4.3. Daily system resolution test

The usual measure of the energy-resolution of a spectrometer system uses the "full width at half maximum (FWHM)" of a photopeak. This is the width of the peak at half the maximum amplitude divided by the energy of the photopeak (Figure 3.5). The resolution is defined as the ratio of the FWHM to the photopeak energy expressed as a percentage as follows:

$$Resolution = \frac{100 \times FWHM(energy)}{Peak\_position(energy)} \tag{5.1}$$

The FWHM and the photopeak energy can be expressed as either an energy or a channel number.

The overall system resolution based on the Th photopeak at 2.61 MeV should always be better than 7%. A Th resolution test should be conducted daily. If the resolution changes by more than 1% from that measured at the start of the survey, flying operations must cease until the source of the problem is found and rectified.

5.4.4. Monitoring spectral stability

Modern self-stabilising spectrometers generally maintain the position of photopeaks to within one channel (approx. 17 keV) of their correct positions. However, in older temperature-stabilized systems, the position of the Th photopeak at 2.61 MeV could drift by up to four

channels during the course of a day's flying. This can introduce significant errors into the processed gamma ray data.

Spectral stability is monitored by plotting average spectra for each line showing the actual positions of the K and Th photopeaks relative to their nominal positions in the spectrum. Accurate estimation of peak positions requires good quality average spectra. Where lines are less than 1000 s in length (for a 32 litre detector system), spectra are accumulated over more than one line for plotting.

5.4.5. Survey test line

A survey test line is an 8 km line flown at the start and at end of each day. The line serves two purposes. First, it serves as a final check on system sensitivity and the radioactivity of the aircraft. Second, it serves to monitor the effect of soil moisture in the survey area.

The survey test line should be easy to navigate, of uniform radioactivity, and should be typical of the survey area in terms of soil moisture content. After live time, background, and height correction, the average Th window count rate over the test line should be within 10% of the mean Th window count rate for all previous flights.

Failure to meet this requirement may be because of equipment malfunction, or a change in aircraft background. In these cases, the source of the problem should be found and corrected. If the change in Th window count rate is due to a uniform change in soil moisture in the survey area due to widespread precipitation, then flying should be temporarily suspended. If the change in Th window count rate is due to local precipitation only, then flying can proceed in those parts of the survey area unaffected by precipitation. In this case, a short section of a previously flown line in the unaffected area can be reflown to demonstrate system integrity.

5.5. Data processing and calibration procedures

The role of data processing is to correct the observed data for those influences that are not related to the geology, and then reduce the airborne count rates to estimates of the ground concentrations of the radioelements.

This section reviews data processing procedures for airborne gamma ray spectrometry. The corrections or procedures are described below in the same order in which they must be applied. The calibration requirements for each procedure are also described.

5.5.1. Pre-processing

Pre-processing is essentially part of the quality control procedure and should be carried out in the field. This usually includes such procedures as the merging of data from different sources (if this is a requirement of the particular data acquisition system), validating the recorded data (i.e. establishing that the recorded values are reasonable), and checking the data for missing or spurious values (spikes).

Some of the measured parameters should also be filtered as part of the pre-processing. The radar altimeter is usually lightly filtered (5-point average) to smooth out rapid changes that may occur in rugged terrain. The cosmic channel is usually quite heavily filtered (10-20 point average) to reduce statistical noise. However, the raw data must also be archived should reprocessing of the data be required.

5.5.2. Spectral smoothing techniques

Spectral methods for reducing noise in gamma ray spectra are a recent development in the processing of multichannel spectra that has dramatically improved the quality of processed data. The methods remove noise from raw gamma ray spectra, and the noise-reduced spectra are then processed in the normal way. There are two methods currently being used – the NASVD method (Noise Adjusted Singular Value Decomposition) and the MNF method (Maximum Noise Fraction). Both methods use a principal component (PC) type analysis to extract the dominant spectral shapes ("PC's" or "components") present in the raw spectra. The PC's are then used to reconstruct spectra that have most of the original signal but little of the noise. The NASVD and MNF methods differ mainly in how they normalize the input spectra for noise prior to spectral component analysis.

The NASVD method (Hovgaard and Grasty, 1997) transforms the observed spectra into orthogonal spectral components that are ordered according to the degree to which each component contributes to the shape of the observed spectra. Since the signal correlates between channels, this ends up in the lower-order components. The random noise, on the other hand, does not correlate from one channel to the next, and tends to be evenly represented in all of the components. The noise is removed by reconstructing the spectra using the lower-order (signal-rich) components only. The NASVD method differs from the principal component method in two important respects. First, the spectra are normalized to unit variance in each channel prior to analysis using an *a priori* model of the noise. Second, the singular value decomposition method is used to extract the spectral components.

The MNF method (Green et al., 1988; Lee et al., 1990) is a more general method for removing noise from multispectral data. The procedure involves two linear transformations of the data. The first transformation decorrelates and normalizes the noise to equal error variance in each channel. The second transformation is a standard PC transformation on the now "noise-whitened" data. The two transformations are combined into a single transformation and called the Maximum Noise Fraction (MNF) transform. The MNF transform orders data into new components by decreasing signal/noise ratio. The noise is removed by discarding the higher-order components before doing the inverse transform. The MNF method uses a sample of noise to calculate the noise-whitening transformation. In current implementations of the method as applied to gamma ray spectra, the noise sample is obtained from the survey data by forward-differencing of the spectra along each line. So the method actually used is the MAF (Minimum/Maximum Autocorrelation Factors) method of Switzer and Green (1984). However, these implementations are commonly referred to as the MNF method.

The implementation of both the NASVD and MNF methods can be improved by first sorting the raw spectra into clusters on the basis of similarity in spectral shape (Minty and McFadden, 1998). The NASVD or MNF method is then applied to each cluster of spectra in turn. This typically further reduces the statistical noise by a factor of two.

Minty (2000b) showed that the NASVD and MNF methods produced similar results when applied to airborne gamma ray spectra. Minty and Hovgaard (2001) used synthetic data to show that the methods produce almost identical results in terms of both the degree of noise reduction and the accuracy of the processed data. However they do caution that the NASVD and MNF methods may well remove real anomalies if the anomaly spectral shape is not well represented in a dataset. There is also some evidence that the methods can introduce false anomalies where a spectral shape is not well represented in a dataset (R.L. Grasty, personal communication). For example, in a dataset where the Th/U ratio is almost constant except for

a single, large Th anomaly, NASVD noise reduction has been found to introduce a small U anomaly at the position of the Th anomaly.

The spectral methods for removing noise should be applied with caution. The number of spectral components used to reconstruct the signal (typically eight) should be determined for each dataset being processed and after careful consideration. The eigenvectors (NASVD method) and eigenvalues (NASVD and MNF methods) give some indication as to which components represent signal and which represent noise. Eigenvectors (PC's) that represent signal should show some indication of coherent spectral shape. The eigenvalues are the variances of the eigenvectors and are a measure of the contribution that each PC makes to the survey spectra. Typically, the larger eigenvalues represent signal and the smaller eigenvalues represent noise. But the eigenvectors and eigenvalues should not be solely relied upon to estimate the number of components to use in the reconstruction of the signal. Possibly the best method for deciding whether a particular component represents signal is to grid the amplitude of the component. If the grid shows evidence of spatially coherent structure then the component represents signal and should be used in the spectral reconstruction.

5.5.3. Live time (or dead time) correction

Spectrometers require a finite time to process each pulse from the detector. While one pulse is being processed, all other incoming pulses are automatically rejected. The total counting time available is thus reduced by the time taken to process all pulses (the "dead time"). The time during which the spectrometer is receptive to incoming pulses is the "live time". The dead time is therefore the difference between the sample accumulation time and the live time. The correction is usually small, but can be significant in areas of high radioactivity. Most modern spectrometers automatically record the system dead time (or live time), which is output with the data stream for later processing. A typical dead time would be of the order of 5-15 μs/pulse, and can be corrected for as follows:

$$N = \frac{n}{1 - Ct} \tag{5.2}$$

where N = corrected count rate (counts/sec);
n = observed count rate (counts/sec);
C = total count rate over all channels(counts/sec);
t = the equipment dead time per pulse.

Dead time can be measured experimentally (IAEA, 1991) by connecting the spectrometer to two identical detector packages. The total-count count rates are measured with each of the detector packages connected to the spectrometer separately, and then with both packages connected to the spectrometer simultaneously. Clearly, the difference between the count rate measured with both packages connected, and the sum of the count rates due to the individual packages, gives an indirect measure of the equipment dead time. Usually the individual detector packages will yield approximately the same count rates, in which case the dead time is given by (IAEA, 1991).

$$t = \frac{2N - N_T}{NN_T} \tag{5.3}$$

where N = average total count rate from the individual detector packages;
N_T = total count rate measured with both detector packages connected;
t = dead time per pulse (seconds).

This calibration procedure is based on the assumption that the total dead time is *nt*, where *n* is the total number of counts recorded. This is not necessarily the case, and users should refer to the manufacturer's specifications for individual spectrometers.

5.5.4. Energy calibration

Spectrometers are affected by energy drift in the measured spectra. This drift is caused by changes in the gains of the photomultiplier tubes as a result of drift in the high-voltage supply and changes in temperature. Older spectrometers are capable of drifting up to 2-4 channels during the course of a day (1 channel=11.7 keV), and this is a significant source of error. Modern spectrometers have in-built self-stabilising features and the total drift with these instruments is less than one channel. Measured spectra can be corrected for energy drift as long as all of the crystals comprising the detector drift together.

The energy calibration procedure is based on the estimation of the positions of prominent photopeaks in the observed spectra. This requires well-defined spectra. The usual approach is to sum spectra along each line over at least 600 s, and determine the peak positions from this sum spectrum. The peak positions are then used to energy calibrate each of the individual 1-s spectra used in the summation. The energies of at least two prominent photopeaks are determined as the maximum value of a quadratic fitted in the vicinity of each photopeak. A linear function is then fitted to the photopeak positions (channel numbers versus energy) to estimate the energy at channel 1 and the gain (keV per channel). These parameters are then used to correct each 1-s spectrum within the sample accumulation period by re-sampling each channel to its correct energy range using linear interpolation.

5.5.5. Aircraft and cosmic background corrections

The aircraft spectrum is constant. The cosmic spectrum at each observation point is estimated by scaling a normalized cosmic spectrum by the cosmic window count rate. The aircraft and cosmic background spectra are then subtracted from the live time and energy-calibrated observed spectra.

The calibration procedure for estimating the aircraft spectrum and the normalized cosmic spectrum requires the acquisition of spectra over water at a number of different heights (say 1.0, 1.5, 2.0, ... 3.5 km above sea level) in an area where atmospheric radon is at a minimum. The measured spectra are each the sum of the aircraft component (constant) and the cosmic component. Also, the count rate in the 3-6 MeV cosmic window is linearly related to the count rate in the *i*'th energy channel. Thus, a linear regression of the cosmic window count rate on any other particular channel yields the cosmic sensitivity (slope of regression line) and aircraft background (zero intercept) for that channel as follows.

$$n_i = a_i + b_i n_{\cos} \tag{5.4}$$

where n_i = aircraft + cosmic background count rate in the *i*'th channel;
n_{cos} = cosmic window count rate;
a_i = aircraft background in the *i*'th channel;
b_i = cosmic background in the *i*'th channel normalized to unit counts in the cosmic window.

Aircraft and cosmic spectra are shown in Figures 5.1 and 5.2. This type of analysis can also be applied to energy window data. A typical regression is shown in Figure 5.3.

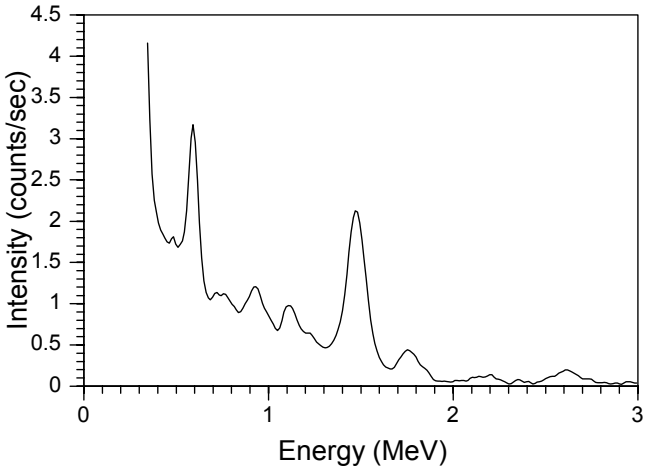

FIG. 5.1. The aircraft gamma-energy spectrum.

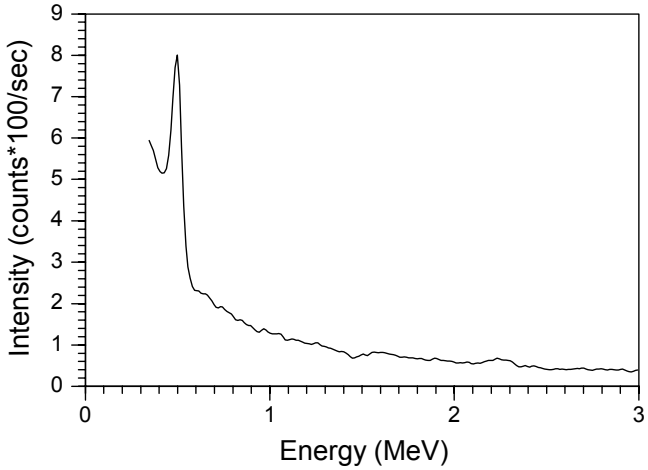

FIG. 5.2. The normalized cosmic gamma-energy spectrum.

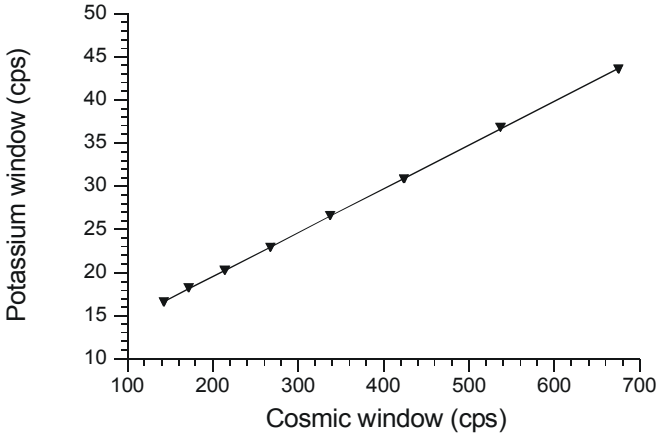

FIG. 5.3. High altitude regression plot for aircraft and cosmic background in the potassium window.

5.5.6. Radon background correction

There are three procedures that can be used for removing atmospheric radon background. The "spectral-ratio method" and the "full-spectrum" method use the shape of the gamma ray spectrum to estimate the atmospheric radon concentration. These methods cannot be used in the northern hemisphere where there is significant ^{137}Cs contamination. The alternative approach is through the use of upward-looking detectors. These detectors give the spectrometer a directional sensitivity capable of distinguishing between atmospheric radon and terrestrial sources of radiation.

All three methods require good quality spectra, and the radon concentration is estimated by summing spectra over large time intervals – typically 200-600 s, depending on the method. The spectral-ratio and full-spectrum methods operate on multichannel spectra. The upward-looking detector method requires window data. In this case the spectra are summed over the conventional windows prior to background estimation.

Spectral-Ratio Method

The low energy ^{214}Bi photopeak at 0.609 MeV from atmospheric radon suffers far less attenuation relative to the ^{214}Bi peak at 1.76 MeV than is the case for radiation from the ground. The spectral ratio method (Minty, 1998a) uses this fact to estimate the contributions of atmospheric radon to the observed spectrum.

The method calls for the monitoring of four windows (Figure 5.4) which are denoted by *L* (low energy), *K* (potassium), *U* (uranium) and *Th* (thorium). *L* represents counts above the Compton continuum in the 0.609 MeV photopeak, and *K*, *U*, and *Th* represent counts in the conventional K, U and Th windows (Table 3.1) respectively, after correcting the spectrum for aircraft and cosmic background. Then it can be shown (Minty, 1998a) that the radon contribution to the low energy photopeak (L_r) is given by

$$L_r = \frac{\left(L_{ob} - U_{ob}\left(c_2 - c_4\,\gamma\right) - Th\left(c_3 - c_2\,\alpha - c_4(\beta - \alpha\gamma)\right) - c_4 K_{ob}\right)}{\left(1 - c_2/c_1\right)} \qquad (5.5)$$

where α, β, and γ are the conventional stripping ratios, and c_1, c_2, c_3 and c_4 are calibration constants. L_r is used to scale a standard radon spectrum for multichannel background removal. At this stage of the processing the spectra are summed over the conventional energy windows.

The radon spectrum can be derived from calibration flights at survey height over water and in the presence of radon. The aircraft and cosmic contributions are subtracted from the observed spectrum to give the radon spectrum. c_1 is measured directly from the radon spectrum. The factors required to calculate the radon contributions to the K and Th windows for a fixed number of radon counts in the U window are also determined directly from the radon spectrum. The c_2, c_3, and c_4 coefficients can be estimated from simulated K, U and Th component spectra (Minty, 1998a).

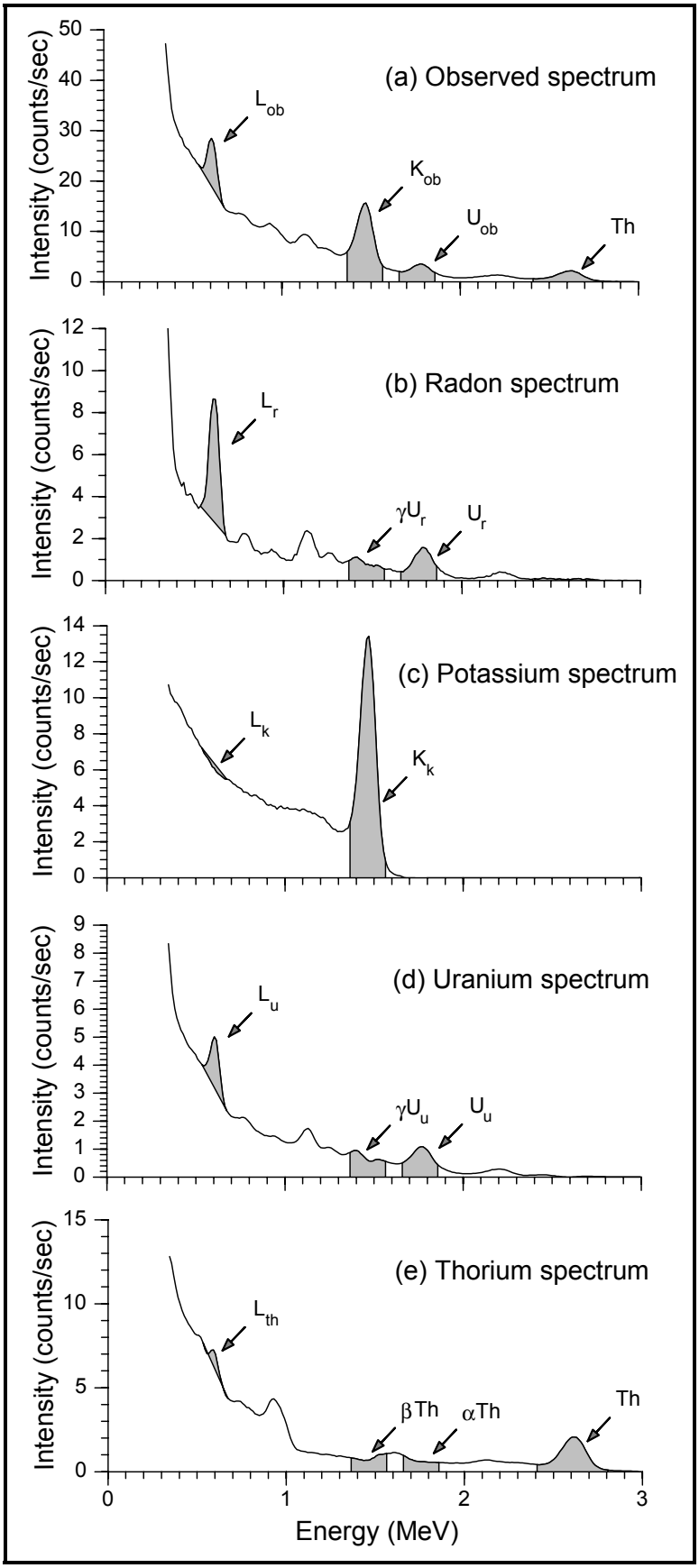

FIG. 5.4. Potassium, uranium, thorium and radon spectra relative to the windows used for the spectral-ratio method for estimating radon background.

Full-Spectrum Method

After removing aircraft and cosmic background, the observed spectrum can be expressed as a linear sum of four components due to each of K, U, Th and atmospheric radon as follows:

$$I_{obs} = |K| f_K + |U| f_U + |Th| f_{Th} + |R| f_{radon} \tag{5.6}$$

where I_{obs} is the observed spectrum, $|K|$, $|U|$, $|Th|$ and $|R|$ are the elemental count rates due to K, U, Th and atmospheric radon, respectively, and f_K, f_U, f_{Th}, and f_{radon} are the normalized component spectra due to each of K, U, Th and atmospheric radon. The elemental count rates in equation 5.6 can be estimated using the least-squares method. The K, U and Th component spectra can be simulated during calibration experiments on the ground (Minty, 1998a).

Upward-looking Detector Method

The upward-looking detector method uses an additional crystal pack that is partially shielded from radiation from below to give the system a directional sensitivity and the ability to discriminate between radiation from the atmosphere and from the ground.

The radon contribution to the uranium window of the main detector package (i.e. the "downward" U window) is given by (IAEA, 1991)

$$U_r = \frac{u - a_1 U - a_2 T + a_2 b_t - b_u}{a_u - a_1 - a_2 a_t} \tag{5.7}$$

where U_r = radon background in the "downward" U window;
u = count rate in the "upward" U window;
U = count rate in the "downward" U window;
T = count rate in the "downward" Th window;

and a_1, a_2, a_u, a_t, b_u and b_t are constants derived by suitable calibration.

Grasty (1975) showed that the total-count and potassium backgrounds are linearly related to the uranium background, and the background in these channels can be derived from the background in the uranium channel by suitable calibration.

The calibration requirements for the upward-looking detector method are comprehensively described in IAEA (1991), and will not be described fully here. There are several ways of affecting the calibration. a_u, a_t, b_u and b_t are regression coefficients that relate radon background in the upward uranium window to radon background in the downward uranium window ($u_r = a_u U_r + b_u$), and radon background in the downward thorium window to radon background in the downward uranium window ($T_r = a_t U_r + b_t$). These are determined by subtracting aircraft and cosmic background from over-water flights showing a range of radon concentrations. Linear regressions yield the calibration coefficients a_u, a_t, b_u and b_t. Similar regressions on this data yield the required constants for determining the radon contribution to the total-count and potassium windows from the radon background in the uranium window.

The second stage of the calibration is to relate measured count rates in the upward uranium window to those in the downward uranium window for radiation due to uranium in the ground. These components are related by the equation

$$u_g = a_1 U_g + a_2 T_g \tag{5.8}$$

where u_g, U_g and T_g are the ground components, and a_1 and a_2 are the calibration coefficients required. The easiest way to determine a_1 and a_2 is from background corrected data acquired from lines that both traverse and are adjacent to a large body of water. The over-water sections of the lines are used to remove the total background to yield a number of estimates of u_g, U_g, and T_g over a range of source concentrations. Estimates of a_1 and a_2 are obtained by solving the simultaneous equations (IAEA, 1991)

$$a_1 \sum (U_g)^2 + a_2 \sum U_g T_g = \sum u_g U_g \tag{5.9}$$

$$a_1 \sum U_g T_g + a_2 \sum (T_g)^2 = \sum u_g T_g \tag{5.10}$$

5.5.7. Stripping corrections

The stripping correction is used to correct each of the K, U and Th window count rates for those gamma rays not originating from their particular radioelement or decay series. For example, thorium series gamma rays appear in both the uranium and potassium windows, and uranium series gamma rays appear in the potassium window. The corrections are applied as follows:

$$\begin{aligned} n_{th(corr)} &= \frac{n_{th} - a n_u}{1 - a\alpha} \\ n_{u(corr)} &= \frac{n_u - \alpha n_{th}}{1 - a\alpha} \\ n_{k(corr)} &= n_k - \beta n_{th(corr)} - \gamma n_{u(corr)} \end{aligned} \tag{5.11}$$

α, β, γ and a are called "stripping ratios". α are the counts in the U window per unit count in the Th window for a pure Th source, β are the counts in the K window per unit count in the Th window for a pure Th source, γ are the counts in the K window per unit count in the U window for a pure U source, and a are the counts in the Th window per unit count in the U window for a pure U source (Figure 5.5).

The stripping ratios are calculated from calibration experiments over specially constructed radioactive pad sources (§5.3.2). The processing of the calibration data to estimate system stripping ratios is the same as for portable spectrometers (§4.1.3). However, for airborne surveying a correction must be applied to the stripping ratios for the survey height (IAEA, 1991). Correction factors are given in Table 5.1.

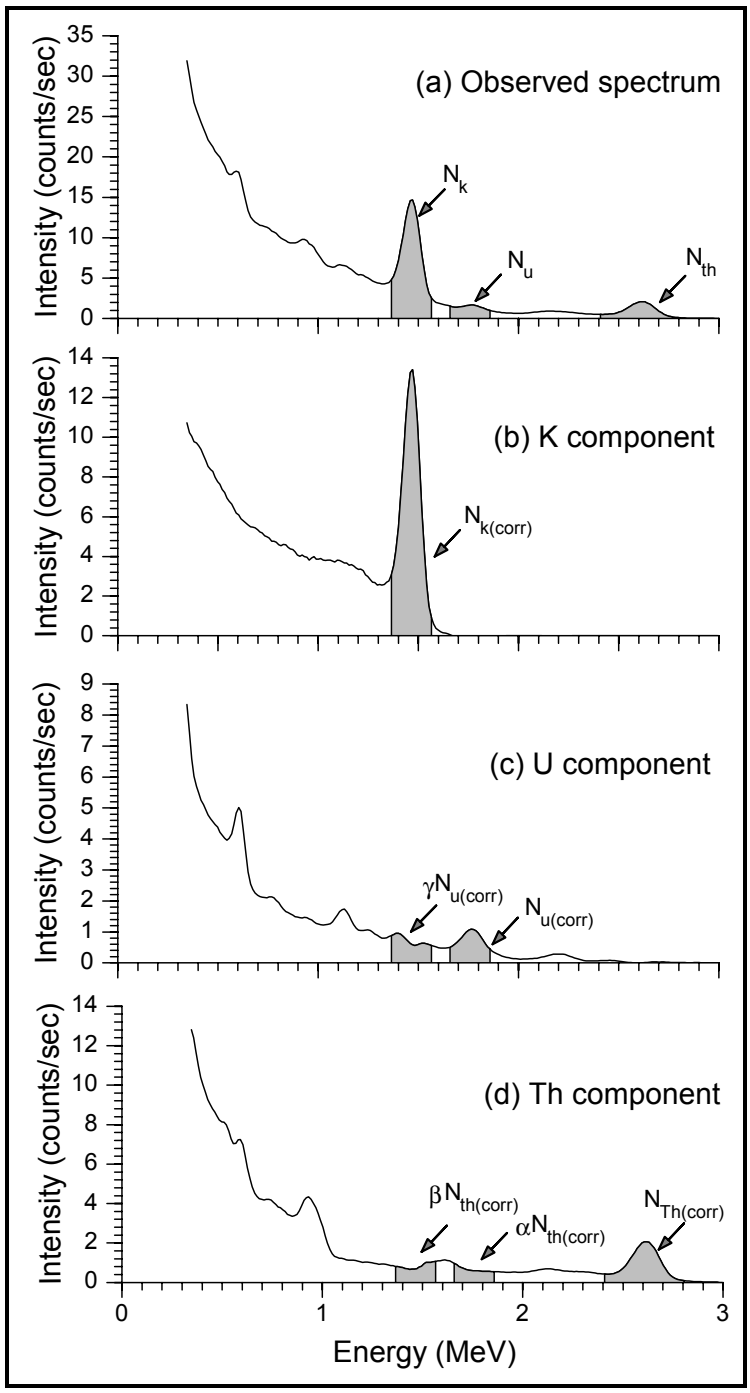

FIG. 5.5. Potassium, uranium, thorium spectra showing the positions of the conventional potassium, uranium and thorium windows and the parameters used for stripping.

TABLE 5.1. INCREASE IN STRIPPING RATIOS WITH ALTITUDE (after IAEA, 1991)

Stripping ratio	Increase per metre
α	0.00049
β	0.00065
γ	0.00069

5.5.8. Height correction

In airborne surveying the height of the detector changes continuously as the aircraft proceeds along a flight line, and the window data must be corrected to a nominal survey height. Window count rates vary approximately exponentially with height for the range of heights normally encountered in airborne surveying. An estimate of the count rate at the nominal survey height is given by

$$n = n_0 e^{-\mu(H-h)} \tag{5.12}$$

where μ = the window attenuation coefficient (per metre);
n_0 = the observed count rate at the STP height, h; and
n = the corrected count rate for the nominal survey terrain clearance H.

This algorithm is adequate for infinite sources and subdued topography and survey heights in the range 50-250 m. In mountainous areas, more accurate algorithms may be necessary. Schwarz et al. (1992) describe an improved method for handling height corrections in areas of rugged topography. The true fall-off of radiation with height for infinite sources more closely approximates that for an exponential integral rather than the simple exponential given in equation 5.12. But the difference between the two over the range of heights 50-250 m (Figure 5.6) is small.

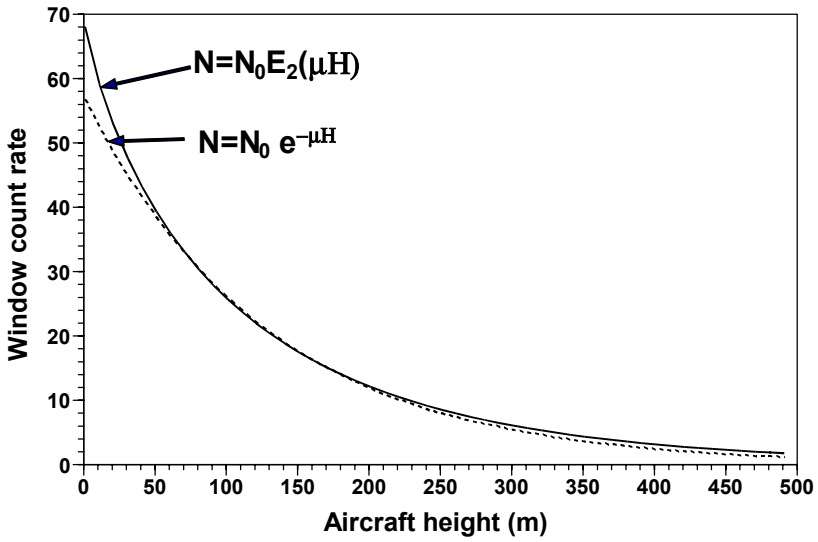

FIG 5.6. Exponential functions used to model the theoretical fall-off of gamma radiation with height.

The height used in equation 5.12 must be corrected for the ambient temperature and pressure, since both affect the density and thus the attenuating properties of the air. The equivalent height at standard temperature (273.15 °K) and pressure (101.325 kPa) - i.e. the STP height, is given by (IAEA, 1991)

$$h_{STP} = \frac{273.15 \times P \times h_{obs}}{(T + 273.15) \times (101.325)} \tag{5.13}$$

where h_{obs} = observed height above ground level (metres);
h_{STP} = equivalent height at STP (metres);
T = air temperature (°C);
P = barometric pressure (kPa).

The temperature, pressure and radio altimeter data can be lightly filtered prior to the application of the altitude correction.

Height attenuation coefficients for each window are calculated from data acquired over a calibration range. The calibration range is flown at a range of heights, and attenuation coefficients are derived from an exponential regression of each background corrected and stripped channel count rate against detector height. An example of this is given in Figure 5.7.

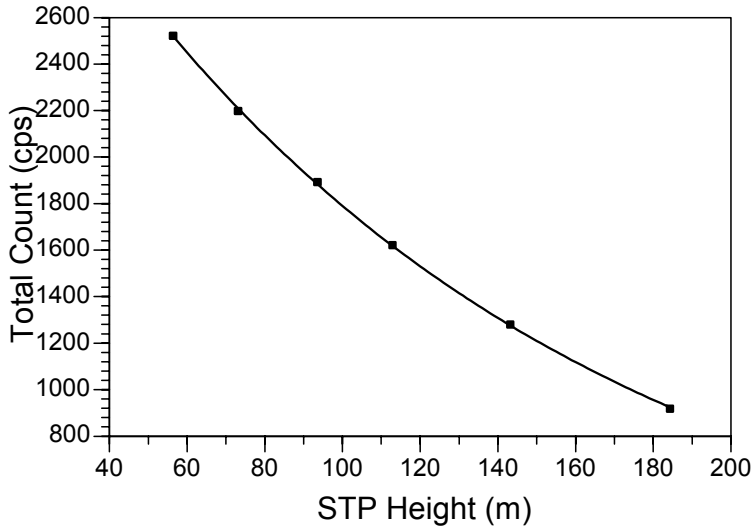

FIG. 5.7. Height attenuation regression plot for the total-count window.

5.5.9. Reduction to elemental concentrations

Measured count rates are dependent not only on the ground radioelement concentrations, but also on the equipment used, and on the nominal height of the survey. This is undesirable, as measuring units should have a direct geological significance and be independent of the instrumentation and survey parameters. Count rates should therefore be converted to ground concentrations of the radioelements. The simplest means of achieving this is to divide each of the corrected window count rates by a "sensitivity" coefficient. The coefficients for each window are estimated from data acquired from airborne flights over a calibration range. The concentrations of the radioelements along the calibration range are measured using a well-calibrated portable spectrometer at the same time as the airborne data are acquired. This allows changing radiation output from the ground due to soil moisture content and other environmental factors to be accommodated.

The coefficients are estimated by dividing the average background-corrected and stripped window count rates at the nominal survey height by the appropriate average ground concentration for the calibration range, i.e.

$$S = \frac{N}{C} \tag{5.14}$$

where N = average background-corrected and stripped count rate at the nominal survey height (c/s);
C = average ground concentration;
S = sensitivity coefficient.

This procedure provides only poor estimates to the true concentrations since it does not accommodate the penetrating nature of gamma radiation. For example, the airborne response due to even a point source is a broad anomaly spread over several observation points. Better estimates of the true ground concentrations of the source are obtained by deconvolving the source/detector response function with the elemental count rates. Gunn (1978) described the theory for performing a rigorous deconvolution of airborne gamma ray spectrometric data. Craig (1997) and Billings and Hovgaard (1999) describe the modelling of gamma ray detector response functions. Craig (1997) describes a method for the deconvolution of gridded airborne gamma ray spectrometric data. The data must be of a high quality as the method tends to amplify high frequency noise.

Equation 5.14 can also be used to calculate the sensitivity coefficient required to convert the total-count count rate to air-absorbed dose rate. Let N be the fully-corrected average total-count count rate over the calibration range. Let C be the average air-absorbed dose rate over the calibration range, calculated using the average elemental concentrations along the range and the conversion factors given in Table 2.6. Then S will convert total-count count rate to air-absorbed dose rate.

Alternatively, a less precise estimate of air-absorbed dose rate can be obtained directly from the estimated elemental concentrations using the conversion factors given in Table 2.6.

5.5.10. Levelling the data

Processed airborne gamma ray spectrometric data often have residual long wavelength "level shift" errors – particularly in the total-count and uranium windows. These are due to a combination of background estimation errors and soil moisture effects. One, or more, of three methods are used to correct the data:

(a) *Conventional levelling using cross-over ties*. Tie lines are flown perpendicular to the flight lines with a spacing of about 5 times the line spacing. These can be used to level the data by warping each line and tie (using low-order polynomials, for example) in order to minimize the differences in estimated radioelement concentrations at the tie/line intersection points.

(b) *Use of between channel correlation information*. The method removes residual background estimation errors from the uranium window using between-channel correlation information (Green, 1987). The method is based on the assumption that there is usually a good correlation between U and Th concentrations in nature.

(c) *Micro-levelling*. Residual errors can be removed from gridded data using directional grid filtering techniques. The filtered grids can then be used to correct the line data (Minty, 1991). These methods must be used selectively, as real elongate anomalies in the flight line direction are removed just as easily as levelling errors.

5.6. Sources of noise and error propagation

The greatest source of error in gamma ray spectrometry is statistical noise. The radioactive decay of nuclei in the source is a random process. The observed count rates in airborne gamma ray spectrometry are small, and this leads to large errors in the estimates of the

radioelements. An insight into the errors in gamma ray spectrometry can be obtained through an understanding the source of errors and how these affect the estimates of the K, U and Th concentrations.

For a function of two variables, $f(x,y)$, with known standard deviations (σ_x and σ_y, say) associated with the variables x and y, the standard deviation in $f(x,y)$ is given by:

$$\sigma_f = \sqrt{\left(\frac{\partial f}{\partial x}\right)^2 (\sigma_x)^2 + \left(\frac{\partial f}{\partial y}\right)^2 (\sigma_y)^2} \tag{5.15}$$

Examples of equation 5.15 evaluated for simple mathematical operations are as follows

$$f(x,y) = x + y \quad \Rightarrow \quad \sigma_f = \sqrt{(\sigma_x)^2 + (\sigma_y)^2} \tag{5.16}$$

$$f(x,y) = x - y \quad \Rightarrow \quad \sigma_f = \sqrt{(\sigma_x)^2 + (\sigma_y)^2}$$

$$f(x,y) = xy \quad \Rightarrow \quad \sigma_f = \sqrt{y^2(\sigma_x)^2 + x^2(\sigma_y)^2}$$

$$f(x) = ax \quad \Rightarrow \quad \sigma_f = \sqrt{a^2(\sigma_x)^2}$$

These equations can be used to estimate errors in processed gamma ray spectrometric data. Since counting errors in gamma ray spectrometry follow a Poisson distribution, the standard deviation is equal to the square root of the mean count rate. If the mean count rate in the raw data can be estimated, then equation 5.15 can be used to trace how the statistical errors are propagated by the data processing procedures into the estimates of K, U and Th elemental abundances.

Table 5.2 shows an example of this type of analysis for a 33 litre detector system at 100 m height. Assuming typical count rates due to average concentrations of the radioelements (2% K, 2.5 ppm eU, 9 ppm eTh) and moderate-high background levels (36 cps in the U window), Table 5.2 shows how the background and stripping corrections affect both the absolute and fractional standard deviations. This assumes that there are no errors associated with the estimation of background radiation or calibration constants.

Errors in the raw data are thus amplified by the data processing procedures. Even though the backgrounds are assumed to be estimated with no error, the correction increases the fractional errors in all windows, since the count rates in all windows are reduced. The stripping correction results in an increase in the absolute error in both the potassium and uranium channels, since thorium statistical errors are propagated into the uranium channel, and both thorium and uranium statistical errors are propagated into the potassium channel.

TABLE 5.2. Propagation of statistical errors by the data processing procedures for airborne count rates over typical crustal material (2% K, 2.5 ppm eU, 9 ppm eTh) at 100 m altitude and under conditions of high atmospheric radon concentrations. The fractional errors are shown in brackets and are the standard deviations expressed as percentages of the count rates.

	Window count rates and fractional errors		
	K	U	Th
observed	253.7 ± 15.9 (6.3)	66.3 ± 8.1 (12.3)	53.5 ± 7.3 (13.7)
background adjusted	212.1 ± 15.9 (7.5)	30.3 ± 8.1 (26.9)	45.5 ± 7.3 (16.1)
stripped	175.9 ± 18.3 (10.4)	14.7 ± 8.5 (58.0)	45.5 ± 7.3 (16.1)

The height correction procedure has not been included in this analysis since the procedure scales both signal and noise by the same factor, and the fractional errors thus remain the same. However, as the height of the aircraft increases, there is an exponential decrease in the measured count rates. This increases the fractional errors in each window. It is not unusual to see changes in the noise envelope in processed K, U and Th window data associated with changes in the height of the detector.

Dickson (2001) reviewed the calibration results from several recent surveys and described potential sources of error in estimating the parameters necessary to correct airborne gamma ray spectrometer data. He suggests guidelines for the expected parameter ranges. A few surveys exhibited abnormally high or low Compton stripping coefficients, and some omitted the use of the stripping coefficient *a* (U into the Th window) altogether. Some surveys showed high values for the cosmic stripping coefficients. Determination of the height attenuation coefficients over a test line may be adversely affected by variations in radon concentration within the air column. The height attenuation coefficients should be $\mu_K > \mu_U > \mu_{Th}$ and μ_{TC} within 5% of μ_{Th}. Radon may also affect the estimation of the sensitivity coefficients, particularly for U. Dickson (2001) suggests that the K/Th and K/U ratios be determined at various heights, and should show a slight but steady decrease with height. Deviations in K/U from this pattern would indicate a radon problem.

6. DATA STANDARDIZATION AND SURVEY BACK-CALIBRATION

Geological mapping and mineral exploration over the past four decades have yielded a large quantity of gamma ray data and maps that contain valuable geological and geochemical information. Unfortunately, much of the older data are in units of count rate. This renders these data unsuitable for defining the natural radiation environment and for estimating terrestrial and man-made radiation dose to the population. Data standardization and survey back-calibration is used to upgrade older databases so that these data may be merged with modern data and used in regional radiation assessment studies.

6.1. Motivation

Radiometric surveys for geological mapping and mineral exploration use a variety of different methods and instruments. Early measurements were often taken with uncalibrated equipment and the data were reported in units that are a relative measure of the radioactivity. Recent gamma ray spectrometric survey results, on the other hand, are reported as either dose rate or radioelement concentrations. Standardization is the procedure for unifying disparate data by converting them to either dose rate units or radioelement concentrations and ensuring the data are levelled. The general procedure includes the quality checking of the original radiometric data, and ensuring that the data are levelled. The data are then converted to gamma dose rate in air, or radioelement abundances in rocks, either directly, or through back-calibration. Back-calibration is the conversion of older data through comparison with ground measurements made with a calibrated portable gamma ray spectrometer.

Several effects can lead to the inconsistency found between survey datasets. For example, detector volume and efficiency, the discrimination threshold (TC instruments), and window boundaries all affect the response of gamma ray instruments. Estimated background values vary considerably according to altitude and the prevailing atmospheric radon concentration. Radiometric data from airborne and ground surveys often reflect the environmental conditions at the time of data acquisition. Airborne spectrometers are calibrated for the estimation of atmospheric radon under the assumption that the radon is evenly distributed through the lower atmosphere. However, radon can accumulate close to the ground under temperature inversion conditions, and this can lead to serious errors in the estimation of background radiation. Radon concentration close to the ground varies with time. Maximum gamma radiation has been observed between 4 am and 9 am. Rainfall can cause a temporary increase in measured radioactivity at the earth's surface due to the deposition of radon daughter products attached to aerosols onto the earth surface. Daily and seasonal precipitation results in variable attenuation of gamma rays by soil moisture and snow cover. Annual and long-term changes in vegetation may affect the observed radiation (Rubin et al., 1980). Lovborg (1984) showed that instrument instability, leading to spectral drift, contributes to data variations. A description and analysis of factors affecting errors in gamma ray spectrometry are found in other IAEA publications (IAEA, 1979, Matolin, 1997a).

Whereas mineral exploration tends to focus on the location of individual gamma ray anomalies, geological and environmental mapping applications require coherent coverage of large areas. This requires that older surveys be converted to modern units of radioactivity.

6.2. Recovery of older survey data

Data standardization requires knowledge of the survey parameters, and some insight into the quality of the survey data. An important prerequisite is an acceptable accuracy of the

geographical positioning of the survey data points. Adequate documentation of the field procedures and data processing procedures is important. This includes:

1. the scale, type and extent of the survey;
2. the recording instrument - its detector, volume and sensitivity;
3. reporting units;
4. calibration procedures and calibration source (if used);
5. the background estimation procedure; and
6. the data processing procedures.

Attention should be paid to topography, vegetation and any changes due to nuclear fallout in the area since the survey was conducted. The quoted errors of the original survey results are also important.

Individual airborne, car-borne or ground radiometric measurements reflect the conditions at the time of measurement. This can lead to level differences between data acquired at different times. Prior to any back-calibration, the data should be levelled. There are several approaches to radiometric data levelling (IAEA, 1990). Cross-over tie levelling is based on a warping of lines and ties to minimize the differences at tie/line intersection points. The correct location of these intersection points is thus critical. Ideally, the levelling of two airborne survey areas should be based on regional airborne gamma ray spectrometry tie-lines intersecting both survey areas (Darnley et al., 1995).

Data levelling and back-calibration are applied to digital data. For older analogue surveys, the choice is whether to digitize the original analogue records or the compiled map information. Analogue radiometric data is usually present in one of three formats:

1. the annotation of individual anomalies along flight lines, sometimes with annotated response levels;
2. stacked profiles (or profile maps) of total count and the three radioelements, plotted by chart recorder on the aircraft; and
3. contour maps of total count, and the K, U and Th window count rates.

Current digitising techniques rely on scanned images of the original hard copy. This facilitates the semi-automatic recovery of large volumes of analogue data. Typically, the process requires separate recovery of the flight path and gamma ray data. The flight lines are digitized in the local coordinate system of the maps. Where the data are archived on separate records (e.g. stacked profiles), some kind of common fiducial is needed so that the positional and radiometric data can be merged.

The accuracy of the flight path location on older surveys (i.e. pre-dating GPS navigation systems) is often poor. If the flight lines were originally plotted over a photomosaic, then their locations can be transcribed to a more accurate base (e.g. satellite image) prior to digitising.

Care must be taken in the digitising of profile data, so that all radioelement channels are positioned coincidentally. Slight offsets along a survey line can result in significant false anomalies in computed radioelement ratios.

The recovery of analogue data from contour maps is typically accomplished by digitising the contour values where they intersect the flight path. This strategy recognizes that the contours were originally prepared from an interpolated grid that usually best reproduces the original profile data along the flight lines. If the flight path is not known, the contours should be

digitized along a set of pseudo-flightlines rather than tracing out the contours. The latter procedure can introduce difficulties at the gridding stage.

6.3. Standardization and back-calibration methodology

Standardization and back-calibration methodology depends on the type of data. Where instruments were adequately calibrated and the data presented as radioelement concentrations, gamma dose rates can be calculated directly. Data presented as fully-corrected window count rates may be converted to radionuclide concentrations and dose rate through suitable back-calibration. Total count surveys expressed in specific or relative units (c/s) may be converted to gamma dose rate.

6.3.1. Gamma ray spectrometry surveys with calibrated instruments

Where survey results are reported as K, U, and Th concentrations, they can be converted to dose rate (nGy/h). If the source can be approximated by an infinite plane surface, then the constants given in Table 2.6 can be used to do the conversion. The contributions from K, U and Th are summed to map terrestrial gamma dose rate.

6.3.2. Gamma ray spectrometry surveys with uncalibrated instruments

Back-calibration of gamma ray spectrometric surveys is based on a comparison of the fully-corrected window count rates to the concentration of K, U, Th on the ground. The ground concentrations are estimated using a well-calibrated, portable gamma ray spectrometer. Comparisons are made over several large geological structures that are radioactively homogeneous but have different radiometric signatures. Ten or more measurements are taken at each site with the measurement stations 10-20 m apart. The conversion factors are estimated using a linear regression of the mean K, U and Th radioelement concentrations for the individual areas against the mapped count rates in the respective energy windows.

A similar procedure can be employed for the back-calibration of profile data. Several sections of line are chosen on the following basis:

a) each individual section should have uniform radioactivity;
b) line sections should be topographically flat;
c) the sections should span a range of radiometric signatures; and
d) each section should be about 1000 m long.

Each section is measured with a calibrated portable gamma ray spectrometer at sites separated by 25-50 m along the flight line. Local ground radioactivity variations and the width range of airborne measurements are compensated through ground measurements at several (five) stations at each site. Stations are situated on a profile perpendicular to the flight line. Conversion factors for uncalibrated airborne data are estimated from a linear regression between the mean values of fully-corrected airborne window count rates and the measured K, U, Th ground concentrations. After correcting the airborne data there should be a good correlation between airborne and ground measurements (Figures 6.1, 6.2 and 6.3).

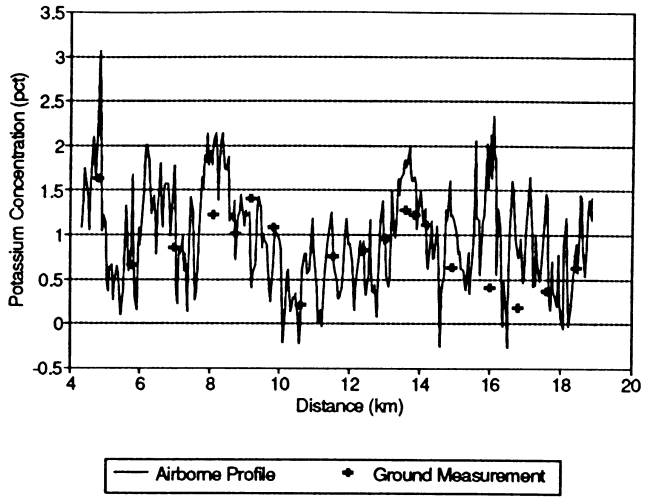

FIG. 6.1. The relationship between the potassium ground concentration and calibrated airborne measurements in Malaysia (after Grasty et al., 1995).

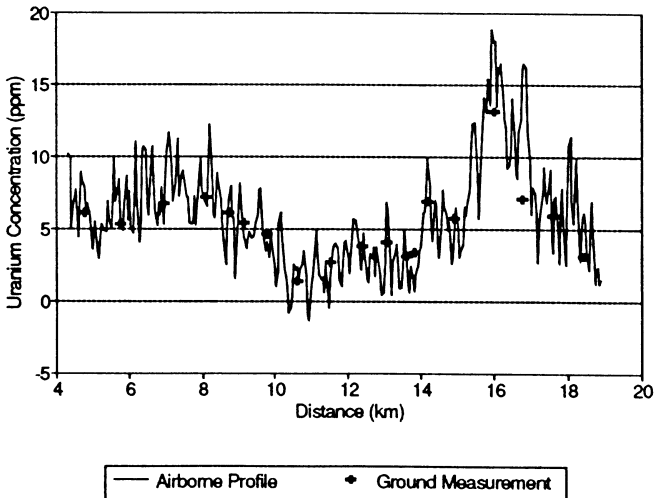

FIG. 6.2. The relationship between the uranium ground concentration and calibrated airborne measurements in Malaysia (after Grasty et al., 1995).

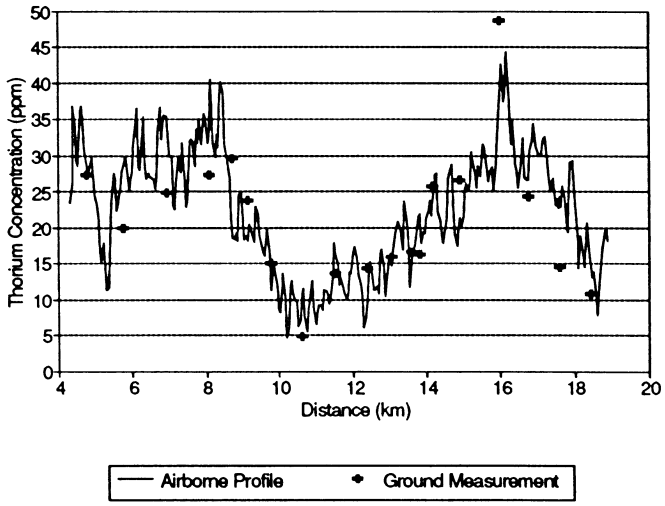

FIG. 6.3. The relationship between the thorium ground concentration and calibrated airborne measurements in Malaysia (after Grasty et al., 1995).

Car-borne surveys can be back-calibrated in the same way. Car-borne traverse segments of about 50 m length are selected for comparison with ground measurements. The segments should cover a range of signatures from low to high radioactivity. Segments are measured with a portable gamma ray spectrometer at sites separated 10 m along the traverse. At least three ground measurements are made along a line perpendicular to the traverse segment at each site. A regression of the fully-corrected K, U and Th count rate means for the car-borne and portable spectrometer gamma ray measurements is used to estimate the conversion constants.

Note that for ground-based surveys (i.e. including car-borne) where the survey data are reported as raw energy window count rates, back-calibration can be affected through the measurement of a minimum of four areas. If these areas have different radiometric signatures, then 3 measured count rates, n_i, at each of the four areas, and using equations (4.1), nine constants of sensitivities, s_{ij}, and three background count rates, $n_{iBG,}$ may be estimated.

6.3.3. Total count surveys with uncalibrated instruments

Specific features of TC instruments affect the standardising of total count surveys. The relationship between the background corrected count rate, n_{TC}, and the concentration of K, U, and Th in the ground is given by

$$n_{TC} = s_K c_K + s_U c_U + s_{Th} c_{Th} \tag{6.1}$$

where n_{TC} = background corrected total count rate (c/s);
s_K, s_U, s_{Th} = K, U and Th sensitivities of the TC instrument (c/s per unit concentration);
c_K, c_U, c_{Th} = K, U, and Th radioelement concentrations.

The sensitivities can be estimated by measuring the TC response over three geological sources that have different K, U, and Th concentrations.

The TC response of an instrument to gamma radiation reflects the properties of the detector and the instrument energy threshold. Due to differences between K, U, Th spectra, the sensitivities s_K, s_U, s_{Th} do not vary proportionally with changes in the instrument parameters. Equation (6.1) can be written in the form:

$$n_{TC} = s_U \left(\frac{s_K}{s_U} c_K + c_U + \frac{s_{Th}}{s_U} c_{Th} \right), \tag{6.2}$$

where s_K/s_U = uranium equivalent of potassium;
s_{Th}/s_U = uranium equivalent of thorium.

The term “uranium equivalent” refers to the concentration of uranium (ppm U), in an infinite homogeneous plane source, that gives the same total count measurement as 1% K or 1 ppm Th. The ratio s_K/s_U varies significantly with detector volume and discrimination threshold, typically from 1.5 to higher values. The ratio s_{Th}/s_U varies moderately in the range 0.37-0.45.

The air dose rates due to unit concentration of K, U and Th are given in Table 2.6. This shows that the gamma dose rate from 2.30 ppm U is equivalent to the dose rate from 1% K. The gamma dose rate from 0.44 ppm U is equivalent to the dose rate from 1 ppm Th. For

radiometric instruments with s_K/s_U = 2.30 and s_{Th}/s_U = 0.44, the count rate is proportional to gamma dose rate. For instruments with other uranium equivalents the measured count rates do not vary linearly with dose rate. Relative deviations between the true dose rate and that estimated from TC instruments vary by up to 25%, and depend on the K/U and Th/U radioelement ratios (IAEA, 1990).

Total count surveys reported in equivalent uranium concentration (ppm eU), calculated as n_{TC}/s_U, may be converted to dose rate by multiplication by 5.675 (Table 2.6). This does not eliminate deviations in the dose rate as discussed above.

Total count surveys with uncalibrated instruments (reported as count rate) provide only a relative measure of environmental radioactivity and must be standardized through back-calibration. The total count rates from selected areas are compared to the gamma dose rate estimated by a portable gamma ray spectrometer or ionization chamber. A linear regression of dose rate on count rate is used to estimate the appropriate conversion factor.

Total count instruments with low energy discrimination thresholds are sensitive to low-energy gamma rays. Much of this low energy radiation is from back-scattered gamma rays. These are gamma rays that originate at large distances from the detector and have been scattered back towards the detector by the atmosphere. Consequently, back-calibration of these data should be based on large areas of uniform radioactivity. Further description of radiometric data standardization procedures can be found in IAEA (1990).

6.4. Merging survey data

Automatic methods for the merging of airborne magnetic survey data use the differences between gridded survey data values in those areas where the surveys overlap to estimate the correction factors required to level one grid to another. A similar approach can be applied to the merging of airborne gamma ray spectrometric survey data. The overlap areas are used to estimate a base level shift and scaling factor which, when applied to one of the surveys, minimizes the differences in the overlap region. This can be used to merge an un-calibrated survey to a survey calibrated to elemental concentrations of the radioelements.

Grids are usually levelled one at a time to gradually assemble large blocks of data. But this sequential approach tends to introduce long-wavelength errors into the final levelled grid (Reford et al. 1990; Tarlowski et al. 1992; Barritt 1993; Black et al. 1995). As each new grid is added to the compilation, levelling errors are propagated and amplified. Minty (2000a) describes a technique that minimizes this long-wavelength problem. Rather than join grids sequentially, the levelling of all of the grids in the regional compilation is considered as a single inverse problem. The weighted least-squares method is used to determine the best correction factors for each survey.

Where the grids being joined are of different quality, the poor quality grids are best adjusted to fit the good quality grids. In areas where there is insufficient dynamic range in the grid overlap areas to affect reliable joins, the flying of tie lines to level old surveys may be a cost-effective option.

Levelled grids seldom match perfectly along their common borders. Cheesman et al. (1998) describes a final cosmetic procedure to near-seamlessly join the grid edges. They use a Fourier analysis of the residual differences between grids at their common edges to calculate corrections that are propagated smoothly into the grids by distances proportional to their wavelengths.

6.5. Application of back-calibration methodology

Back-calibration has been used in many parts of the world to upgrade the gamma ray data from older surveys to create regional compilations. In Malaysia, a regional airborne gamma ray spectrometric survey flown with uncalibrated equipment was back-calibrated using a 10 km section of a flight line. Nineteen ground measurement sites were chosen where the line intersected roads. Four ground measurements were made with a portable spectrometer at each site. Ground measurements were typically 10-20 m apart. A comparison of airborne count rates with K, U, Th concentrations yielded 19 separate sensitivities for each of K, U and Th. The means of these sensitivities were used to convert the airborne data to ground concentrations of K, U, Th and a dose rate map was compiled (Grasty et al., 1995).

A large part of Portugal was surveyed using a hand-held TC instrument and the results published as count rates. Fourteen sites with varying concentrations of K, U, and Th were investigated for back-calibration. Three measurements, several tens of metres apart, were made at each site using scintillometers and a calibrated portable gamma ray spectrometer. Eleven of the sites were selected for their uniform radioactivity. A linear regression of the estimated exposure rate on the original TC data was used to estimate the back-calibration conversion constant (Grasty et al., 1995).

Back-calibration was used in the Czech Republic to up-grade the radiometric map of the country and to convert the data to air dose rate. The original total count airborne contour maps (1:200,000 scale) were expressed in "exposure rate" based on calibration with a ^{226}Ra point source in the late 1950's. The first step in the standardization was to digitize the contour maps. A calibrated portable gamma ray spectrometer was used to survey 122 regional ground traverses, between 1 and 5 km long, that were evenly distributed over the Czech Republic. The traverses were chosen over low, medium and highly radioactive rocks, and the survey results were expressed in gamma dose rate (nGy/h). Regression analysis between these dose rate data and the airborne data resulted in a multiplication correction constant of 0.85 for the airborne data (Figure 6.4).

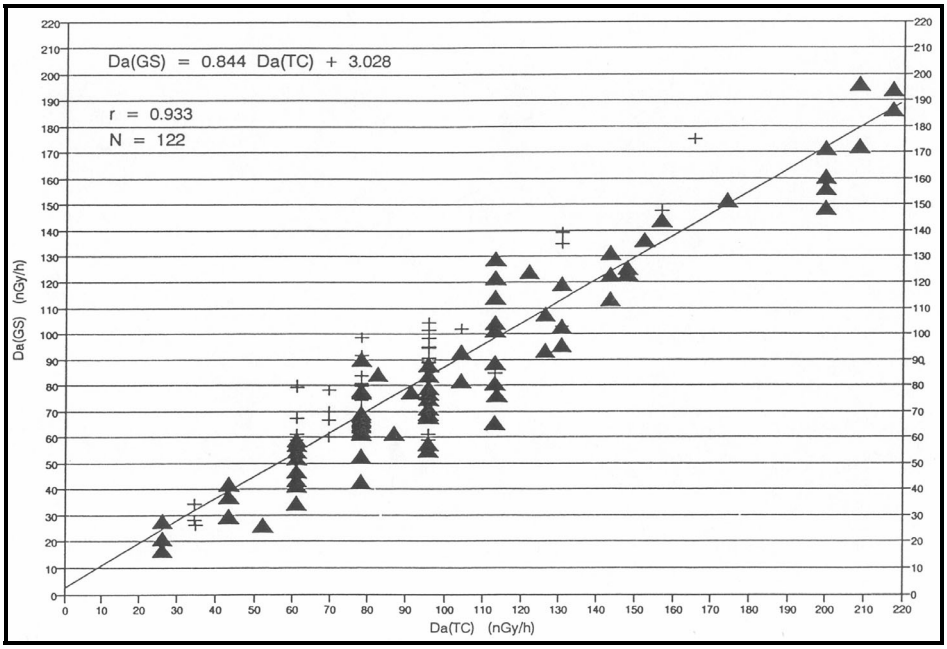

FIG. 6.4. Regression between gamma dose rate determined by ground gamma ray spectrometry (GS) and airborne total count measurement in the Czech Republic (TC). Δ-GS measurement on the earth surface, + GS measurement in hole 0.6 m deep (Matolin, 1997a).

The systematic error in the original airborne data was mainly due to the use of a point source for calibrating the original survey instrument (Matolin, 1997a, Manova and Matolin, 1995).

A total of 2.2 million line-km of radiometric data from 42 surveys in Brazil were recompiled to provide a unified database from most of the institutional data sets available in that country (PGW et al., 1997). Judicious review of the original data acquisition systems, compilation procedures, and survey parameters allowed preparation of radioelement concentrations for all of the data through the back-calibration of six surveys. After spike removal, and microlevelling of flightlines and blocks of flightlines, the surveys merged well once the new calibration constants were applied. Figures 6.5 and 6.6 show "before" and "after" images of the data. The resultant maps show remarkable correlation with the published regional geology, and also serve to delineate areas where the radiometric data and geological mapping require reconciliation. The radiometric compilation in Brazil is a powerful complement to earlier magnetic and gravity compilations. A calibration facility was established in Brazil as part of this project, so that new surveys can be merged with the existing database.

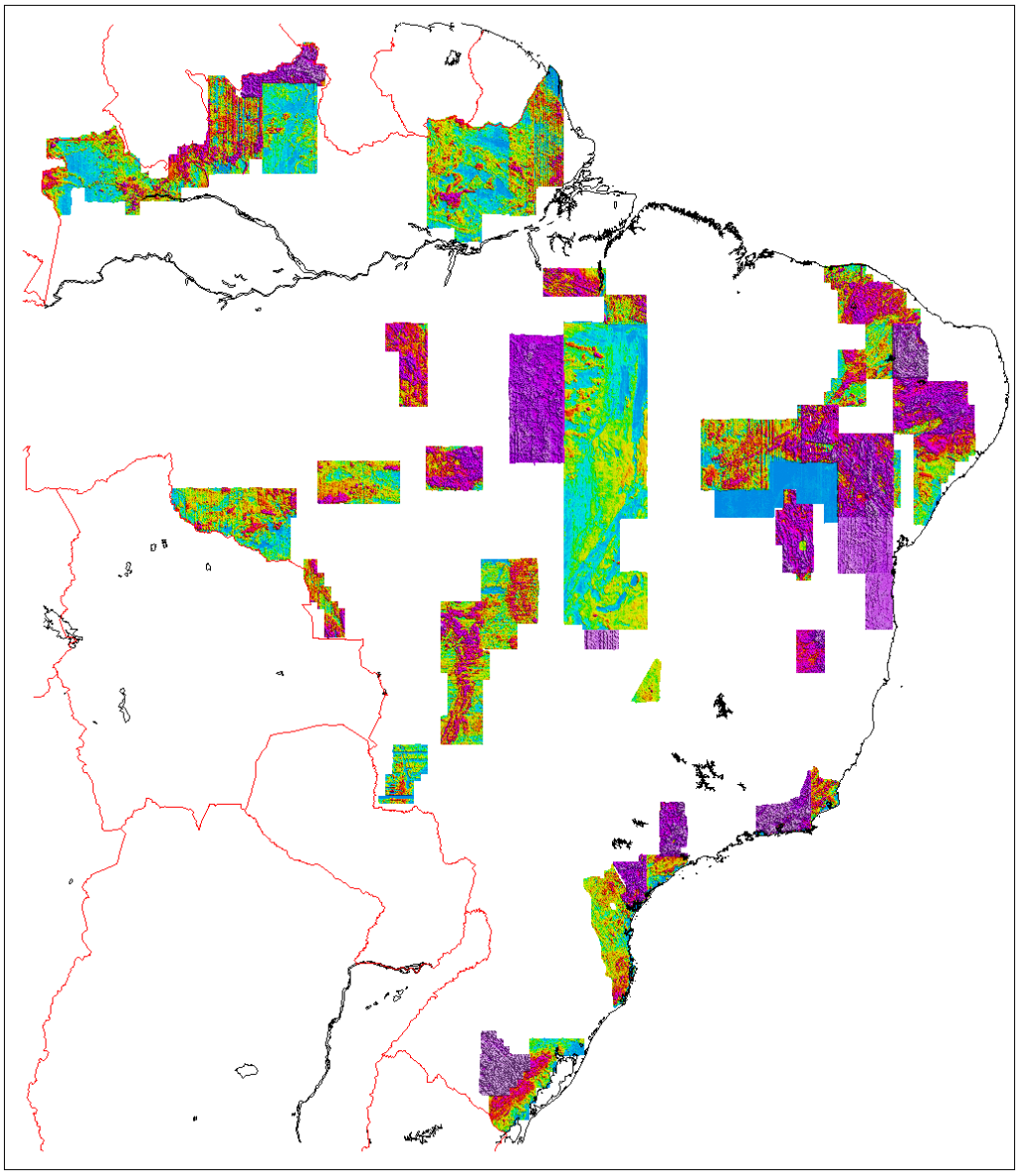

FIG. 6.5 Thorium grids before correction and back calibration, Brazil (PGW et al., 1997).

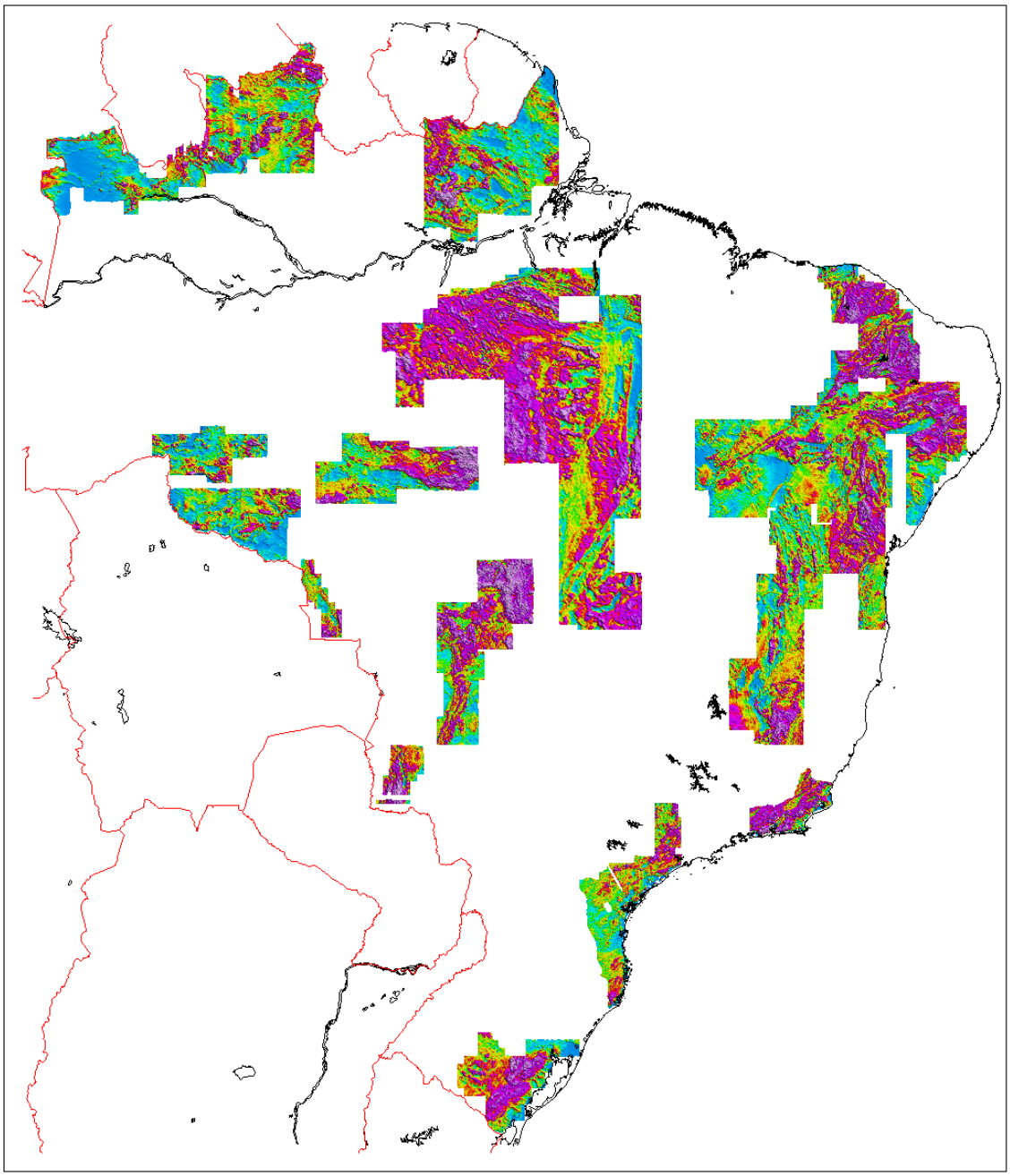

FIG. 6.6. Thorium grids after correction and back calibration, Brazil (PGW et al., 1997).

7. DATA PRESENTATION AND INTEGRATION

Fully-processed gamma ray survey data can be presented in a variety of ways to enable interpretation of radioelement profiles and grids. Since the 1980's, the enhancement of gamma ray spectrometric data has benefited from digital image processing techniques. Nevertheless, the traditional presentation methods, such as profiles and contour maps, have their advantages, and are still in common use today. Although some visualization methods can be considered as routine in the presentation of gamma ray spectrometry data, none of the individual methods are universally applicable to all gamma ray mapping applications. In general, one should experiment with different methods to find those that are optimally suited for a particular interpretation.

7.1. Georeferencing and map projections

Prior to presenting gamma ray spectrometric data, it may be necessary to transform the data to another coordinate system, map projection or map datum. This may be required to register the survey data to other data sets, such as base maps or remotely sensed data or to merge surveys registered on different map projections and datums. Datum conversions became increasingly important when geophysical surveys started using GPS receivers for navigation. Ground positioning systems use a geocentric datum, such as the World Geodetic System 1984, where the centre of the Earth is defined at the true centre of gravity. Cartographic projections, on the other hand, employ ellipsoids chosen for a particular region, each having its own estimate for the axes of the ellipsoid and the location of the centre of the earth. This has resulted in the definition of a large number of local datums. Fortunately, modern image processing and geographic information systems are equipped with functions to transform the point-located survey data from one datum to another.

Before the introduction of GPS, gamma ray spectrometric surveys were registered with reference to aerial photographs. These surveys have poor positional accuracy when compared to modern surveys. Mismatches between poorly positioned surveys may become apparent when field checks are conducted or when seams appear after gridded surveys are merged together. In the fortunate situation where topographic features, such as river bends and lakes can be recognized, it may be possible to register these data to a more accurately positioned grid or image data set. This grid-to-grid registration procedure proceeds by identifying a number of common control points and estimating the transformation between grid positions using least squares techniques. The poorly registered grid is then resampled to new grid coordinates on the basis of the transformation between the control points. Similar registration techniques may be used to co-register gamma ray spectrometry data with other remotely sensed data sets for their integrated analysis in a geographic information system (GIS).

7.2. Scatter plots

Scatter plots are useful for analyzing the inter-relationships between radioelements and for identifying trends and clusters. Anomalous radioelement signatures, for example, can often be recognized as distinct clusters. Interpreters should be aware, however, that there is always greater scatter at higher concentrations of the radioelements. This is because the errors in raw counts are Poisson distributed, such that their amplitude increases with the square root of the detected count rate. Characteristic radioelement signatures can be annotated on the basis of ground spectrometry and detailed lithological surveys. Shives et al. (1995) presented annotated scatter plots for analysing the associations of radioelement patterns with mineralization. Examples are given in Figures 9.8 and 9.10.

7.3. Profile data presentations

Airborne gamma ray spectrometric surveys are frequently presented as profiles, multiple profile plots, or stacked profile maps. An obvious advantage of profile over grid presentations is that the data can be displayed at their full spatial resolution. In grid presentations the data is low-pass filtered along the flight lines before interpolation to a grid interval that is inevitably larger than the sampling interval to eliminate aliasing problems (Horsfall, 1997).

One-dimensional filters or arithmetic combinations of the TC, K, U, and Th channels may be used to enhance anomalous features or reduce noise in profile presentations. Some of the frequently applied enhancements include low-pass and median filters, scaling the data in standard deviations from the mean and ratios between the radioelement channels. Figure 7.1 shows an example of an airborne Th profile together with profiles derived from high-pass, low-pass and a non-linear spike removal filter.

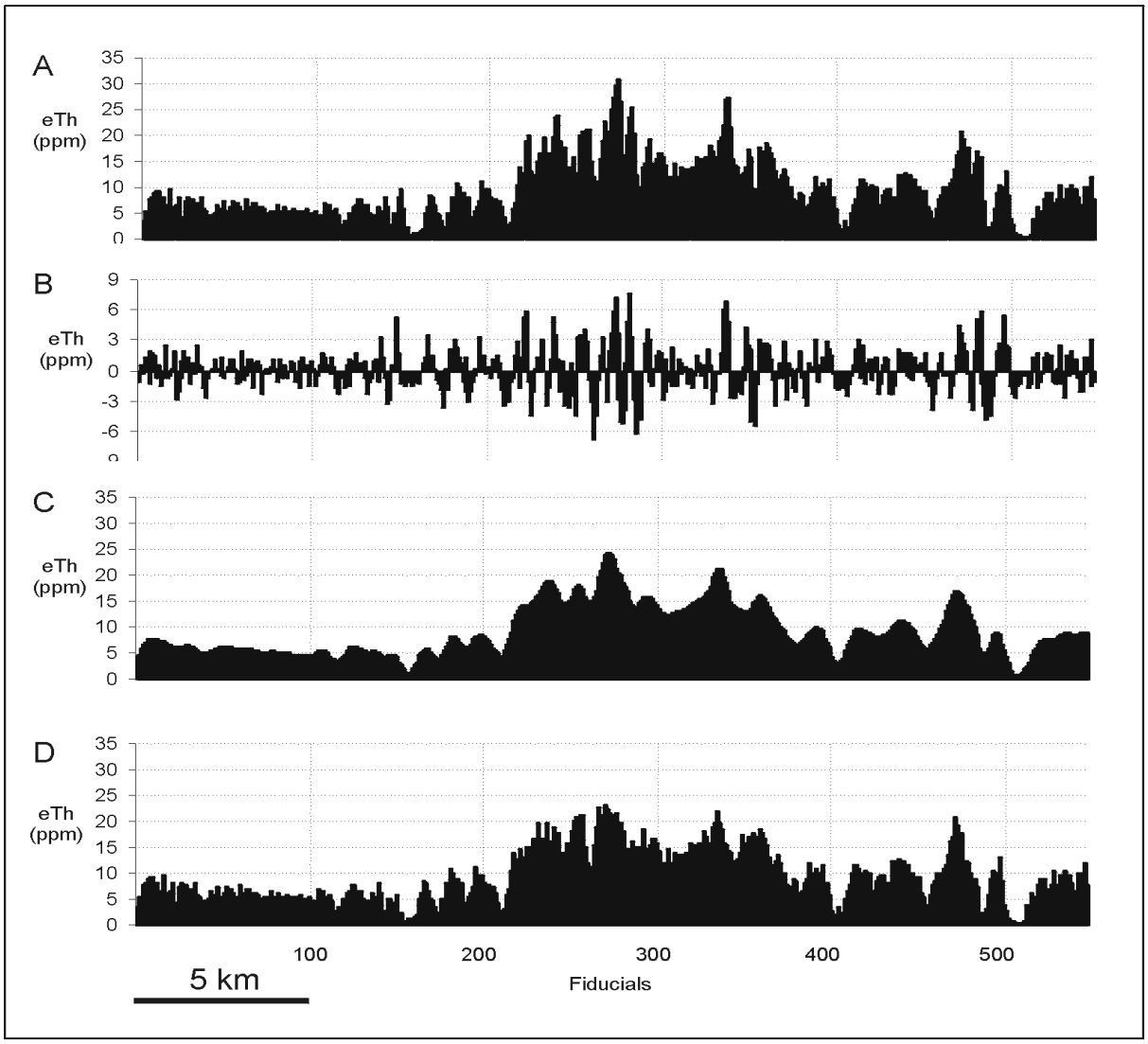

FIG. 7.1. Airborne gamma ray spectrometer profiles of equivalent thorium (eTh) and filtered derivatives: (a) eTh profile; (b) eTh profile after applying a high-pass filter with a cutt-off of 20 fiducials; (c); after applying a low-pass filter with a cutt-off of 20 fiducials; (d) after applying a non-linear filter that removes spikes.

Stacked profile plots (Figure 7.2) provide useful visualizations for interpreting the inter-relationships between the TC, K, U, Th, ratios, and other data channels. Stacked profiles are often represented together with a profile representing lithological units. Such integrated visualizations make it easier to reconcile the gamma ray response with mapped lithology, and also permits the identification of anomalous responses within lithological units that may represent mineralization.

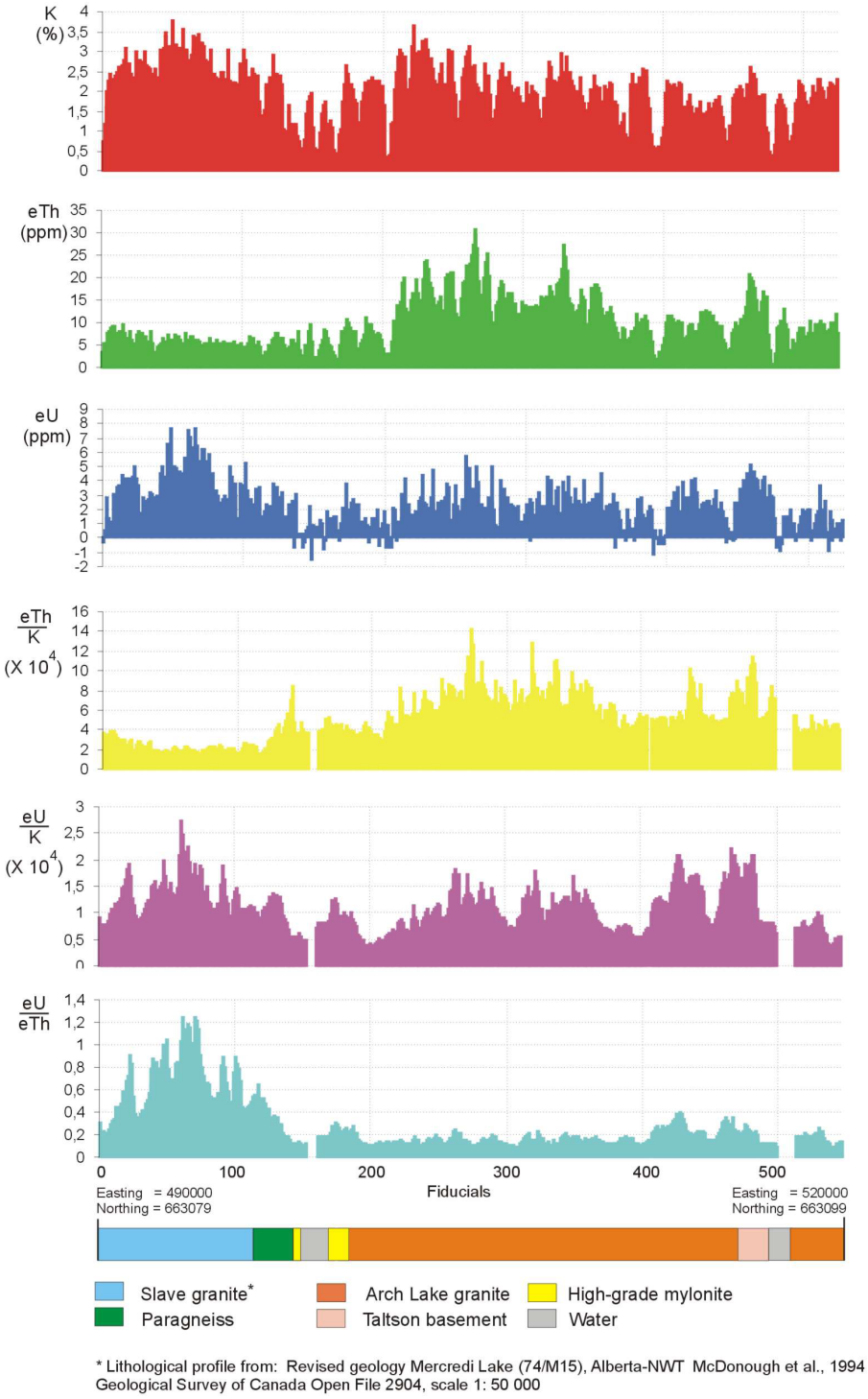

* Lithological profile from: Revised geology Mercredi Lake (74/M15), Alberta-NWT McDonough et al., 1994 Geological Survey of Canada Open File 2904, scale 1: 50 000

FIG. 7.2. Typical example of stacked airborne gamma ray spectrometer profiles showing K, eTh, eU, eTh/K, eU/K, eU/eTh and bedrock lithology. Airborne geophysical survey northeast Alberta, open file 2807 Geological Survey of Canada, Ottawa.

Profile maps show the flight line profiles with reference to the (x, y) co-ordinates of the survey (Figure 7.3). An appropriate base level and vertical scale factor must be chosen so as to avoid interference between profiles from adjacent flight lines. The main advantage of profile maps is that similarities in anomaly shapes on adjacent flight lines are easily recognized. Thus, irrespective of their wavelength, anomalous features can be traced from one flight line to the next.

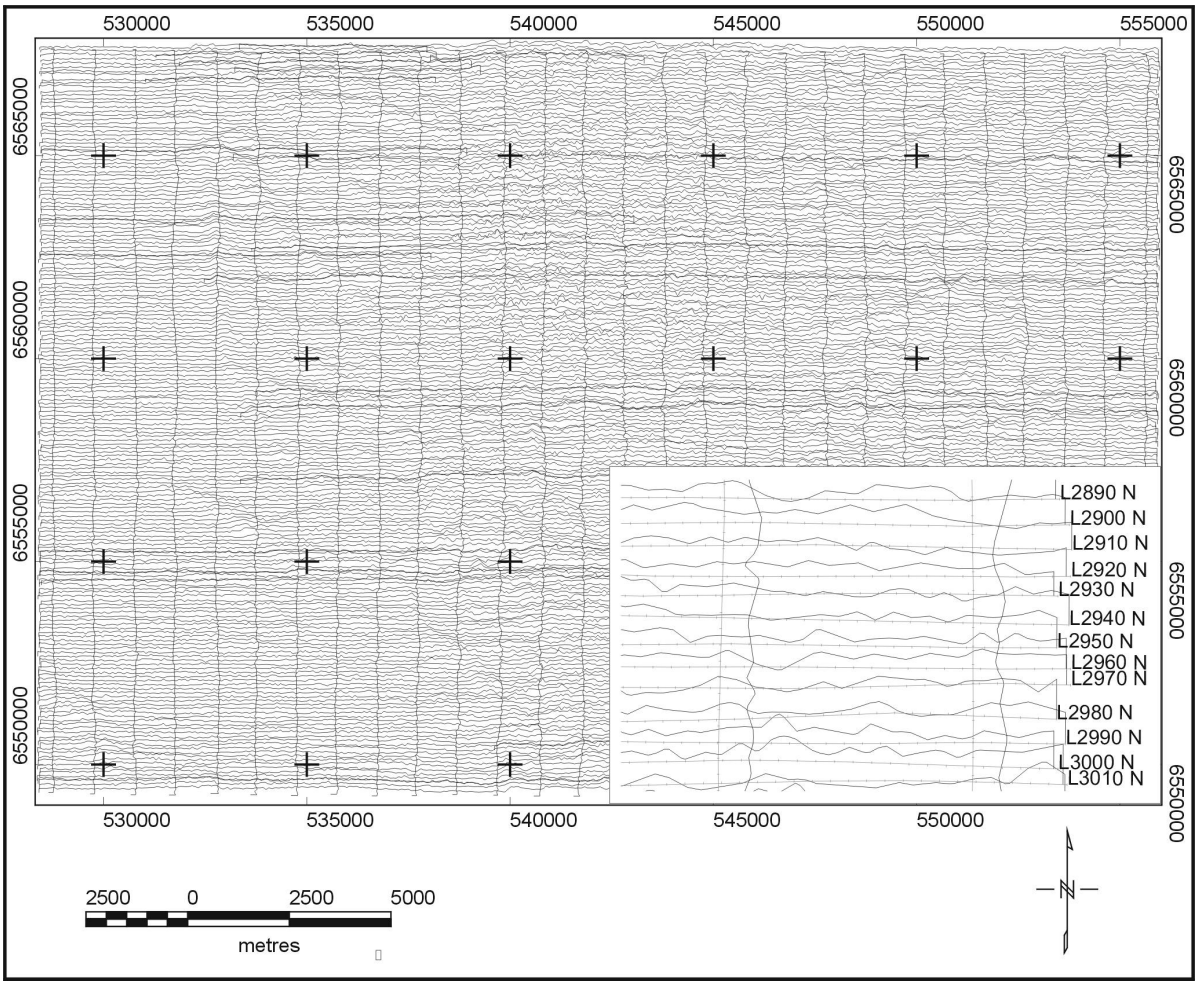

FIG. 7.3. Example of potassium profile map from a small part (< 5%) of the Broken Hill geophysical survey. The nominal flight line spacing is ca. 100 meters, the spacing between tie lines is ca. 1000 m. Inset shows detail of the profile map with flight lines and fiducials (Data courtesy of Geoscience Australia).

7.4. Contour maps

Traditionally, airborne geophysical data were contoured by hand. This was the task of an experienced draftsman with a "feel" for the shapes of the anomalies. The quality of hand-contoured maps was therefore largely dependent on the skill and experience of the draftsman, sometimes incorporating existing geological knowledge to trace particular trends. Automated computer-based contouring was initially developed in the 1960's for generating structural contour maps in the petroleum industry (Merriam, 1969), and has now completely replaced hand contouring. Although image presentations of airborne geophysical data, including gamma ray spectrometric data, are today by far the most popular, contour maps are sometimes

preferred for the extraction of amplitude values and undistorted presentation of anomaly shapes (Gunn et al., 1997). An additional advantage of contour maps is that their digital storage requirements are an order of magnitude smaller than those required for grid presentations.

Contouring proceeds by: (1) gridding the flight line data (see §7.5), (2) interpolating between grid values at a user-defined contour interval, and (3) threading of the contour lines by connecting the interpolated values by straight or curved line segments. Contour lines appear smooth if the segments are short with respect to the map scale and the line thickness used for plotting. Applying this criterion usually results in a smaller cell size than that considered optimal for direct grid presentation. Figure 7.4 shows an example of a contour map of potassium.

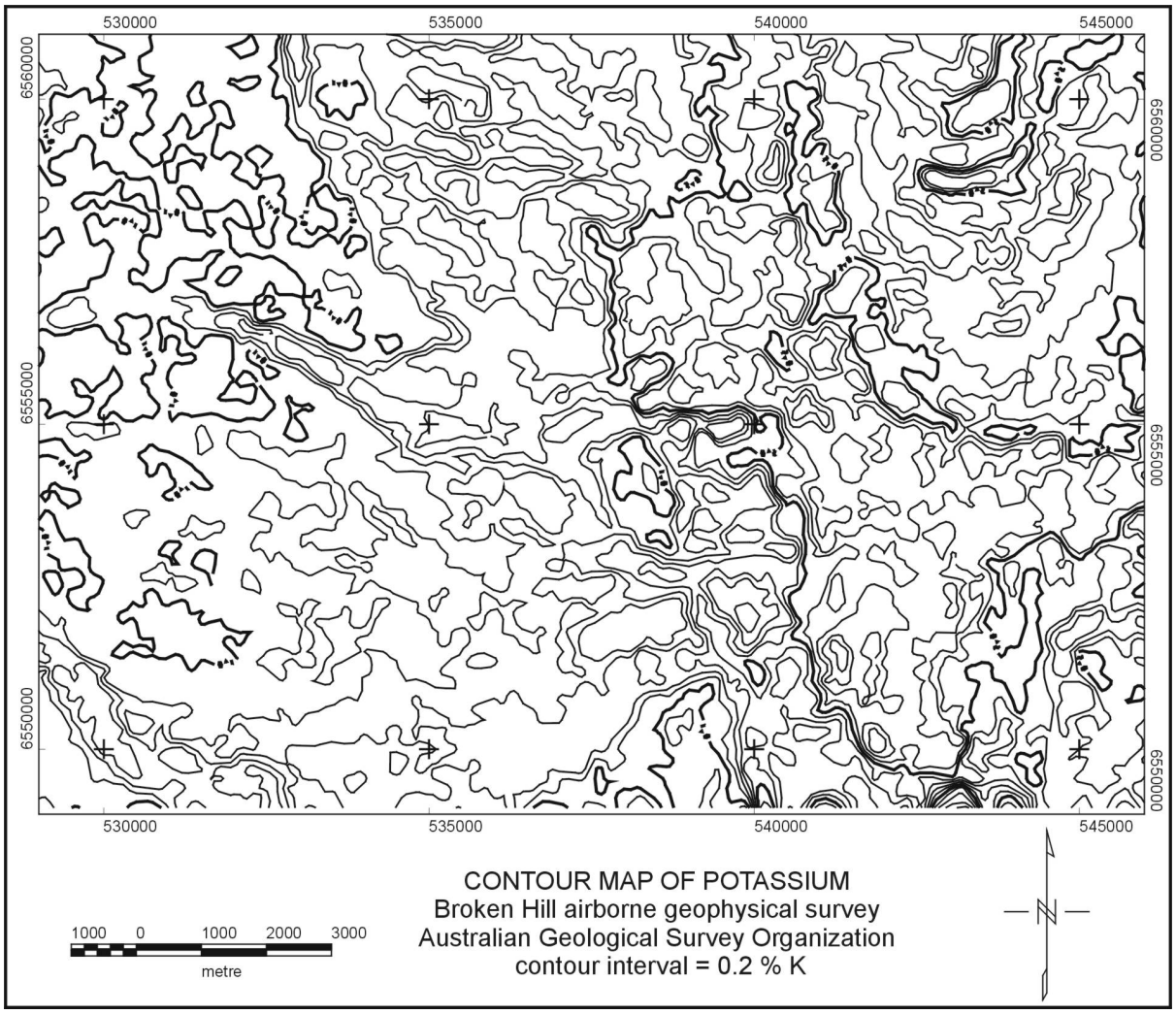

FIG. 7.4. Example of potassium contour map from the Broken Hill airborne geophysical survey. Area depicted coincides with the area shown in Figure 7.3. (Data courtesy of Geoscience Australia).

7.5. Gridding

Contour maps and image renditions of data require that the data be gridded – i.e. the interpolation of the original data onto a mesh of values at regularly spaced intervals (the grid nodes). Once a value has been assigned to each grid node, contours can be generated by interpolation between the grid nodes (see §7.4), or the grid can be directly rendered as an image on a display device. A variety of gridding algorithms are available, but not all the algorithms are suited to the inherent anisotropy in the sample distribution of airborne surveys. A suitable gridding algorithm should honour the original data points while giving a continuous and smooth surface. Because the sampling density along the flight lines is typically four to ten times greater then the sampling density across the flight lines, anti-aliasing filters are usually applied along the flight lines to obtain a comparable spatial frequency content in both directions (Luyendyk, 1997). The most frequently used algorithms for airborne surveys are (1) bi-directional gridding and (2) minimum curvature (Briggs, 1974).

7.5.1. Bi-directional gridding

Bi-directional gridding is an efficient algorithm that exploits the line-to-line correlation of airborne survey data by applying spline interpolation both along and across the flight lines. The data are first interpolated along the flight lines at an interval equal to the pre-defined grid cell size. A low-pass filter is applied to remove spikes and prevent aliasing. Next, these interpolated values are interpolated across the lines, again at a spacing equal to the grid resolution.

Bi-directional gridding is particularly useful in situations where the lines are flown perpendicular to a relatively constant and predominant geological strike. If the survey is flown oblique to the general strike, so called trend-enforced bi-directional gridding can be applied. Here the data are interpolated along the flight lines and then along a user-defined trend (i.e. strike direction). Bi-directional gridding should only be used where flight lines are approximately parallel.

7.5.2. Minimum curvature gridding

Minimum-curvature gridding uses two-dimensional splines to fit the flight line data to a grid surface. Using an iterative procedure, weights are adapted such that the curvature of the surface is minimized according to the conditions formulated by Briggs (1974). A search radius is specified that defines the distance around a grid node, within which flight line samples are included in the interpolation. As with moving average interpolation, an inverse distance function is used to compute a distance-weighted average from the surrounding grid nodes. The curvature of the interpolated surface is compared with the curvature of the interpolated surface in the previous step, resulting in an adaptation of the weight function. The interpolation is complete after a specified number of iterations have been reached, or when the flight line samples are within a specified tolerance from the surface. For airborne surveys, the search distance should be larger then the flight line spacing to include two adjacent flight lines in the computation of the distance weighted average.

Although computationally very demanding, the minimum curvature algorithm produces high quality results, and should be preferred over bi-directional gridding if there is no dominant geological trend perpendicular to the line direction. Minimum curvature gridding is also a suitable technique for randomly distributed data.

7.5.3. Moving average gridding

Moving average gridding applies a specified weighting scheme to the data surrounding a grid node. The weighting is usually based on an inverse distance function that favours the data nearest the grid node. The trade-off between honouring the original data and the smoothness of the grid (i.e. reducing the inherent statistical noise) is controlled by the type of weighting function and its radius of influence. A gamma ray spectrometric grid produced using a moving average algorithm tends to have a more aesthetically pleasing appearance than grids.

7.5.4. Kriging

Kriging is an interpolation technique that should be well suited to gamma ray spectrometric data. Due to the stochastic nature of radioactive decay, gamma ray data have an inherent (non-spatial) randomly distributed component (noise) that is superimposed on the spatially dependent signal in the data. Kriging explicitly takes this non-spatial variation into account by decomposing a regionalized variable into three components: (1) a trend, (2) a spatially dependent or autocorrelated component, and (3) a noise component. The last two components are modelled from the semivariances computed from the data at different distance intervals (or "lags"). The semivariance, γ, is a measure of the correlation of a variable with itself as a function of lag distance and is defined as:

$$\gamma = \frac{1}{2n}\sum_{i=1}^{i=n}(z_i(x) - z_i(x+h))^2 \qquad (7.1)$$

where $z_i(x)$ and $z_i(x+h)$ are a pair of observations at distance h, and n is the total number of observations.

Figure 7.5 shows an example of a semivariogram scatter plot. The semivariogram is modelled by fitting three parameters: (1) the nugget, (2) the sill and (3) the range to the computed semivariance values. The nugget (C_0) is the intercept with the abscissa and reflects the non-spatial variation in the data due to noise. The sill (C_1) is the constant level in semivariance reached at a particular distance called the range (a). Observations beyond the range are not spatially dependent. The essential part of the semivariogram to be modelled is where the semivariogram rises from the nugget value to the sill.

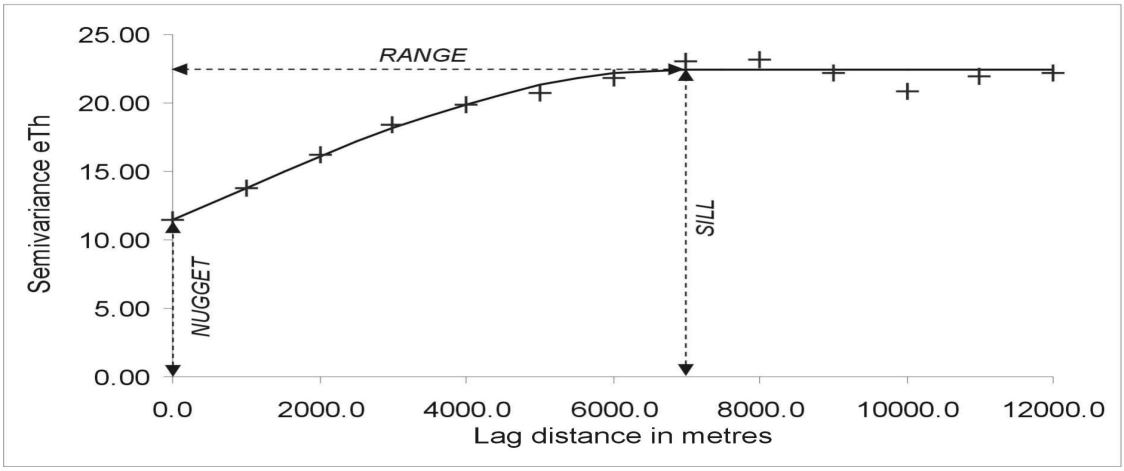

FIG. 7.5. Semivariogram plot of airborne eTh data fitted to a spherical model (nugget = 11.5, sill = 22.5 and range = 7000 metres).

In the example shown in Figure 7.5, a spherical model has been fitted to the semivariogram plot. Other models include linear, power-law, exponential, and circular functions.

The weights used in the gridding are contrary to the arbitrarily defined weight functions of the moving average interpolation (see § 7.5.2) derived from the model semivariogram. Like minimum curvature gridding, kriging is computationally demanding. Kriging has not been widely used for the gridding of airborne gamma ray spectrometric data, as it is difficult to account for the anisotropy in flight line sample density when modelling the semivariogram.

7.5.5. Integrated interpolation schemes

Billings and FitzGerald (1998) studied a number of gridding algorithms, focusing on their application to airborne gamma ray spectrometric data. They propose a scheme whereby a number of gridding algorithms are formulated within a common mathematical framework that allows both exact and smooth interpolations. Their approach also generates a continuous model of the data. This allows the rapid resampling (regridding) of the data at different sampling intervals. The grids can also be made to inherit specific desirable characteristics such as smoothness or minimum variance. They reviewed several alternative gridding techniques such as kriging, radial basis functions, tension splines and smoothing splines.

7.6. Image presentation techniques

Image presentations of airborne gamma ray spectrometric and potential field data have gained enormous popularity since the late 1980's with the development of low-cost image processing systems. Image presentations of the data are far easier to visualize than the conventional contour and profile maps, although they lack the absolute quantitative value of the older methods. The image format also enables the interpreter to benefit from a variety of digital image processing techniques. These include image enhancement and the automated extraction of specific features. This section gives an overview of image display and enhancement techniques applicable to gamma ray spectrometric data. Lillesand and Kiefer (1994) give a good general overview of digital image processing.

7.6.1. Grey scale images

Gridded gamma ray spectrometric data (TC, K, U and Th) can be rendered directly on a computer monitor by scaling the values of the grids to the dynamic range (typically 256 grey-scale levels between 0 and 255) of the display device. The grid values modulate the brightness of the elementary units of the display device, i.e. the picture elements, or pixels, and yield a grey-scale image.

There are several ways in which the dynamic range of a radioelement channel can be scaled to the dynamic output range of a display device. An image histogram (Figure 7.7) shows the frequency distribution of the grid values. This is a useful presentation of the data for the purpose of image enhancement. An analysis of the shape of the image histogram allows the identification of outliers, skewness, and the occurrence of multiple peaks. The histogram can be used to control the enhancement of contrast over the full dynamic range of data, or only over certain intervals of interest. This is called "contrast stretching". To illustrate the effect of contrast stretching, it is convenient to represent the transformation in graph form by the so called "transfer function", which shows how the input data are scaled to the output range of the display device. Examples of contrast-enhanced grey-scale presentations of a Th grid are shown in Figure 7.6. The transfer functions used in these enhancements and the image histogram of the Th grid are shown in Figure 7.7.

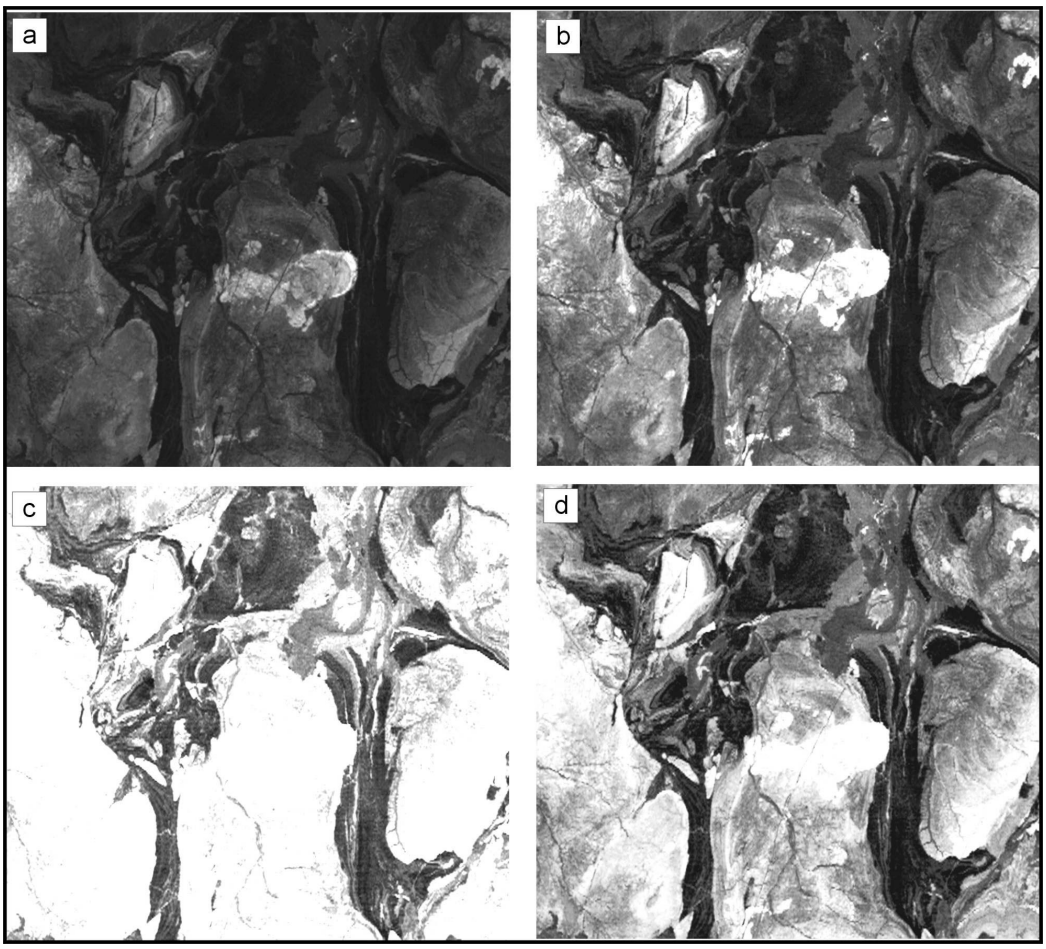

FIG. 7.6. Grey scale images of contrast enhanced Th grids. (a) Linear stretch of the full dynamic range; (b) Linear stretch using a two-sided 2.5% cut-off percentage; (c) Piece-wise linear stretch of the 0-5 ppm range; (d) Histogram equalization (Data courtesy of Geoscience Australia).

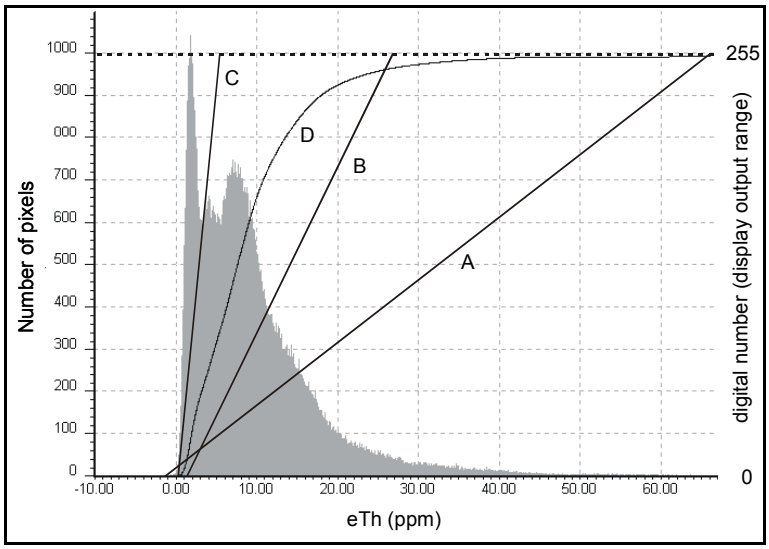

FIG. 7.7. Image histogram and transfer functions for contrast enhanced Th grids shown in Figure 7.6. The transfer functions are: a linear stretch of the full dynamic range (a); linear stretch with two-sided cut-off of 2.5% (b); a piece-wise linear stretch on the 0-5 ppm interval (c); and histogram equalization (d).

The simplest form of contrast stretching is a linear stretch, where the full dynamic range of the grid values is mapped linearly onto the full output range of the display device (Figure 7.6a). Because outliers are common in gamma ray spectrometry data, this linear stretch generally leads to a display that is poorly optimized. Nevertheless, subtle differences may become apparent that are not shown on other contrast-enhanced displays. Note for example that the Th-rich rim on the Th-rich intrusion in the centre (Figure 7.6a) is not apparent on the other contrast-enhanced presentations shown in Figure 7.6.

A better enhancement of the overall dynamic range is obtained by excluding the extremes of the data from the contrast-enhanced range. This can be achieved by specifying either cut-off percentages or a range in standard deviation (Figure 7.6b). Alternatively, if a particular range of interest in radioelement concentrations needs to be enhanced, the user can interactively define a piecewise linear stretch (Figure 7.6c). Here the slope and offset of the transfer function can be interactively edited and the results directly evaluated on the screen. Multiple piecewise or non-linear transformations can also be applied by defining additional break points.

Histogram equalization is a non-linear contrast enhancement technique that is commonly employed for the display of airborne geophysical grids. The input range is mapped to the output range in such a way that the magnitude of the output range is proportional to the frequency of occurrence of the grid values. This is achieved by using the cumulative frequency distribution of the grid as the transfer function (Figure 7.7). Histogram equalization results in an image with optimal contrast for the most frequently occurring radioelement concentrations. However, less frequent occurrences (anomalies) may be subdued to the extent that they cannot be identified. For example, the internal zoning in the Th-rich pluton in Figure 7.6a, and the lower Th ranges in Figure 7.6b, are not visible in Figure 7.6d. Clearly, the contrast enhancement method used must depend on the application. Anomalous radioelement concentrations can be effectively enhanced using a piecewise linear enhancement. However, if the main purpose of enhancement were to map the regional distribution of the radioelements or to map the main lithological assemblages in an area, histogram equalization or linear contrast enhancement would be preferred.

7.6.2. Band ratios

Any arithmetic combination of radioelement grids can be represented as grey-scale images. One of the more useful arithmetic combinations is the ratio of two radioelement grids. The ratio of the K and Th grids, for example, is computed as

$$r_{[K/Th]} = C\frac{K}{Th} \tag{7.1}$$

where C is an optional scaling.

The effect of environmental factors on radiometric response, such as soil moisture, vegetation, and topography, are less evident on band ratios. The ratios therefore often correlate more highly with geological units. Also, since there is usually a high correlation between bands, the ratios often show subtle features that are not apparent on the original grids.

In theory, the ratio values range from zero to infinity. A more uniform scaling can be achieved by computing the ratio as

$$r_{[K/Th]} = C \tan^{-1} \frac{K}{Th} \tag{7.2}$$

The ratios given by equation 7.2 range from 0 to 90 degrees, with a symmetric scaling around 45 degrees (e.g. % K = ppm Th). The obvious advantage is that the range is more uniformly scaled when rendered as grey-scale or pseudo-colour images. If C is chosen to be 2.83, the values range from 0 to 255, facilitating direct display across the full dynamic range of the display device.

Grant (1998) recommends a method to compute ratios above a pre-defined minimum noise level for both radioelement profiles and grids. The technique was motivated by the observation that low count rates in either the numerator or denominator yield large fluctuations in the computed ratios. Adjacent samples are summed until numerator and denominator thresholds are reached. The thresholds depend on the precision of the concentration estimates. Negative concentrations are excluded, and over-water samples are masked using a threshold on the K channel. Examples of ratio profiles and ratio grids are shown in Figures 7.2 and 7.13, respectively.

7.6.3. Colour coding techniques

While human vision can distinguish approximately 32 grey-scale levels, the human eye can easily distinguish millions of colours (Drury, 1992). This colour perception capability can in various ways be exploited in the presentation of gamma ray spectrometric data. Single radioelement channels can be mapped in pseudo-colour, which enables the interpreter to better recognize the regional distribution of radioelement concentrations. Radioelement channels can be combined in a colour composite image, commonly referred to as a ternary radioelement map. The following sections give insights into the underlying principles of colour coding techniques, the concepts related to colour perception, and to colour spaces.

7.6.4. Colour spaces

A colour space is a model that facilitates the specification and visualization of colour. Colour space models have been designed for specific applications such as display or printing devices, or to enhance an intuitive understanding of colour. One way of representing the range of colours displayable on a computer monitor is the RGB colour space shown in Figure 7.8. The three primary colours (red, green and blue) are defined by the emission characteristics of the computer monitor phosphors, and arbitrary colours can be displayed through combinations of the three primaries. If the phosphors are all off, the screen remains dark and is perceived as black. If the phosphors are put to their maximum voltage, the resulting colour is perceived as white.

Yellow is generated by equal intensity of the red and green phosphors, while blue is off. Equal amounts of red, green and blue give achromatic (grey scale) colours ranging from black to white. RGB colour coding is termed “additive”.

The Cyan-Magenta-Yellow (CMY) colour space is based on the “subtractive” system of colours used in printing and painting. The starting point is an object that reflects over the entire wavelength range of visible light, such as white paper. A dye used in colour prints, or paint, absorbs certain wavelengths of the visible spectrum – i.e. these wavelengths are

"subtracted" from white. This leads to the perception of a colour that is complementary to the absorbed wavelength range.

A major drawback of the RGB and CMY colour space models is that they do not relate intuitively to the attributes of human colour perception. For example, if the saturation of a colour needs to be increased, the associated changes in RGB values are not intuitively obvious. This limitation of the RGB space largely explains the popularity of perceptual colour spaces, such as the intensity-hue-saturation (IHS) space. The IHS colour space is based on the human colour perception of hue, saturation and intensity. Hue is the predominant wavelength of a colour, saturation is the purity or total amount of white white light in a colour, and intensity relates to the total amount of light that reaches the eye.

The IHS colour space can be represented as a cone (Figure 7.9a) defined by one vector and two angles (spherical coordinates). Intensity defines the vertical axis, saturation the co-latitude, and hue the circumferential angle of the cone. Because saturation is defined as an angle, the ratio between this distance and intensity defines its magnitude and surfaces of constant saturation will therefore lie on a cone with the intensity line as its central axis. The equations for the transformation from RGB to IHS space are given in Appendix I.

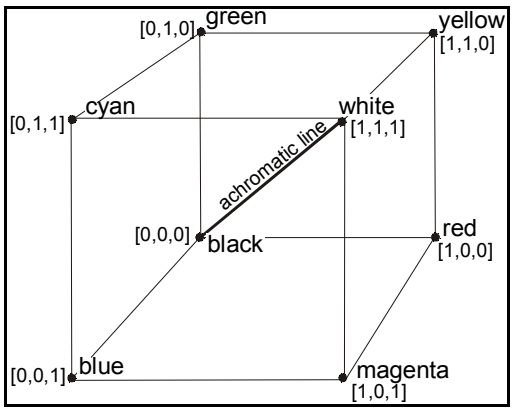

FIG. 7.8. RGB colour cube.

A commonly used alternative to the spherical IHS space is a cylindrical colour space (Figure 7.9b) where the saturation (S) coordinate is defined by the radial distance between a colour vector and the intensity axis. This is a convenient means of defining a hue-invariant transformation by addition or subtraction of white light. Such a transformation has been compared with the sun-illumination of a natural scene, in which the saturation of the sunlit parts of the scene decreases and appears "washed out" (Milligan and Gunn, 1997).

The IHS colour space provides only a crude approximation of a perceptually uniform colour space. In a strictly uniform colour space the Euclidean distance between the colours approximates a perceptual difference between two colours (Niblack, 1986; Robertson and O'Callaghan, 1988). Since the sensitivity of the eye to hue and saturation changes is dependent on wavelength, a uniform change in hue and saturation (of a geometrically defined colour space) of two colours are not perceived as equal changes in hue and saturation. Perceptually uniform colour spaces, such as CIEluv, can be used to overcome this problem (Robertson and O'Callaghan, 1988). The disadvantage of perceptually uniform colour spaces is that they can not be universally applied as the transformations between the red, green and blue phosphors and CIEluv coordinates are dependent on the display device and need to be obtained by calibration. Fortunately, for most colour image display applications, the precise properties of such colour spaces are not required (Niblack, 1986).

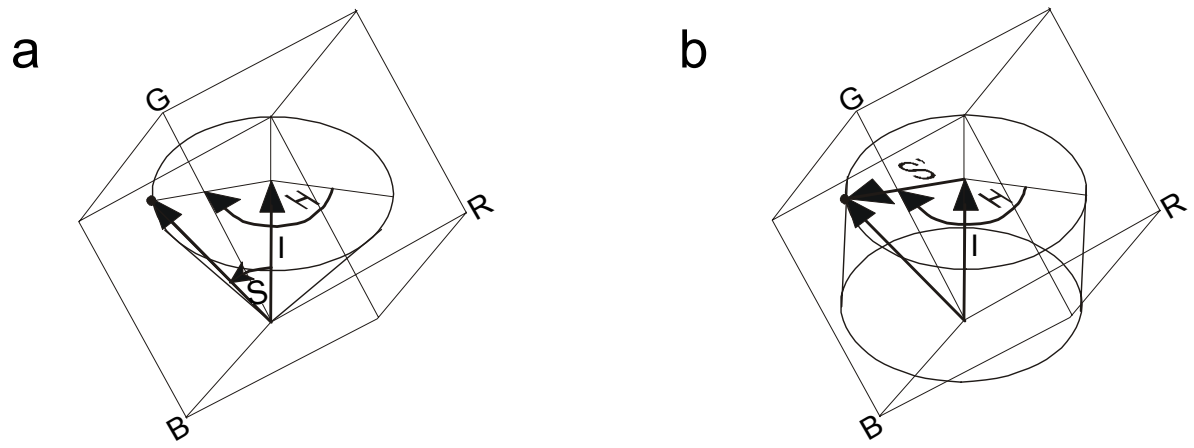

FIG. 7.9. Geometrical representation of IHS colour space: (a) spherical; and (b) cylindrical.

7.6.5. Pseudo-colour and shaded relief images

Pseudo-colour, through the use of colour look-up tables, can be used as an alternative to grey-scale presentations. A colour look-up table (Figure 7.10) assigns additive combinations of red, green and blue primaries to create individual colours. The colour lookup table should preferably be designed so that the perceived variations in colour can be intuitively related to variations of the radioelement concentrations. An obvious choice is to vary the values for red, green and blue, such that the intensity and saturation are held constant, while the hue varies proportionally. This colour coding technique is called pseudo-colour mapping. Pseudo-colour coding can be combined with relief-shaded presentations of grids.

DIGITAL NUMBER	RED	GREEN	BLUE
0	0	0	0
1	100	0	100
2	75	0	125
..			
..			
255	255	255	255

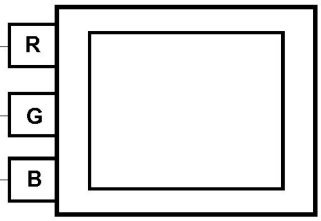

FIG. 7.10. Colour lookup table.

Figure 7.11a shows the ideal pseudo-colour mapping in the RGB cube, on a circle in a plane of constant intensity. Figure 7.11b shows the corresponding transfer functions for the red, green and blue primaries. These are sine functions with 120 degrees phase shifts. Figure 7.12 shows an approximation of the ideal pseudo-colour functions. This maps the data on a hexagon instead of a circle. Although the saturation is not held constant, the maximum possible saturation levels of the colours are adapted to the limiting surfaces of the RGB cube.

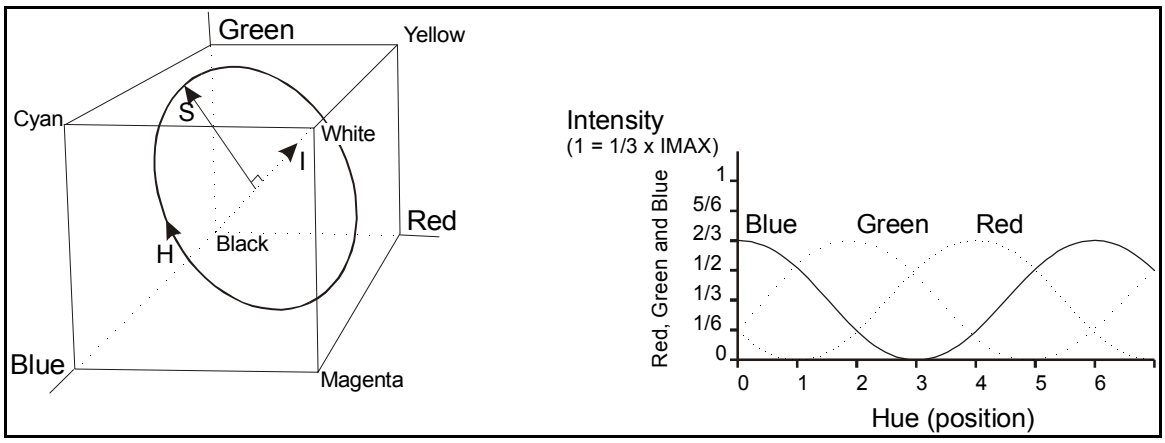

FIG. 7.11. (a) Pseudo-colour mapping in RGB space; (b) lookup table functions for R, G, B.

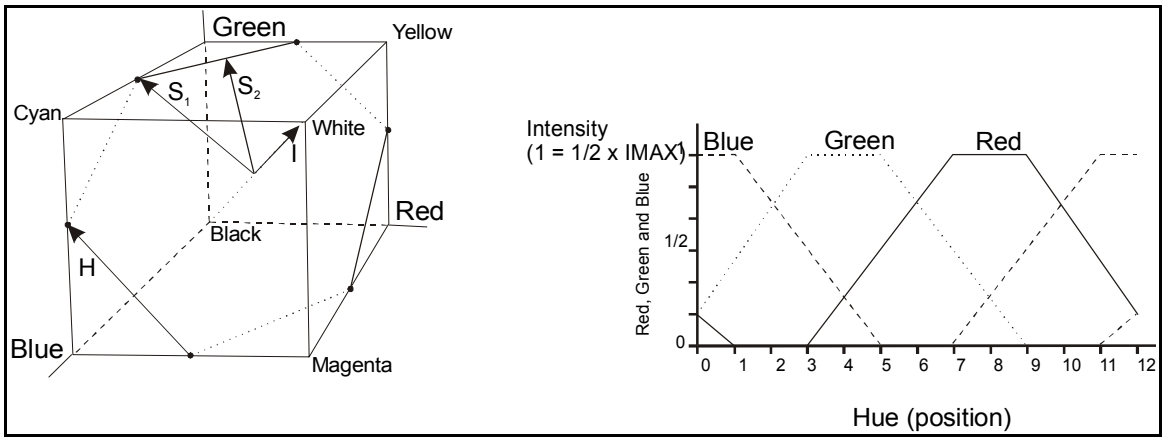

FIG. 7.12. (a) Hexagonal pseudo-colour mapping in RGB space; (b) Transfer functions for R, G, B phosphors of the display. Note that the saturation levels vary along the hexagon.

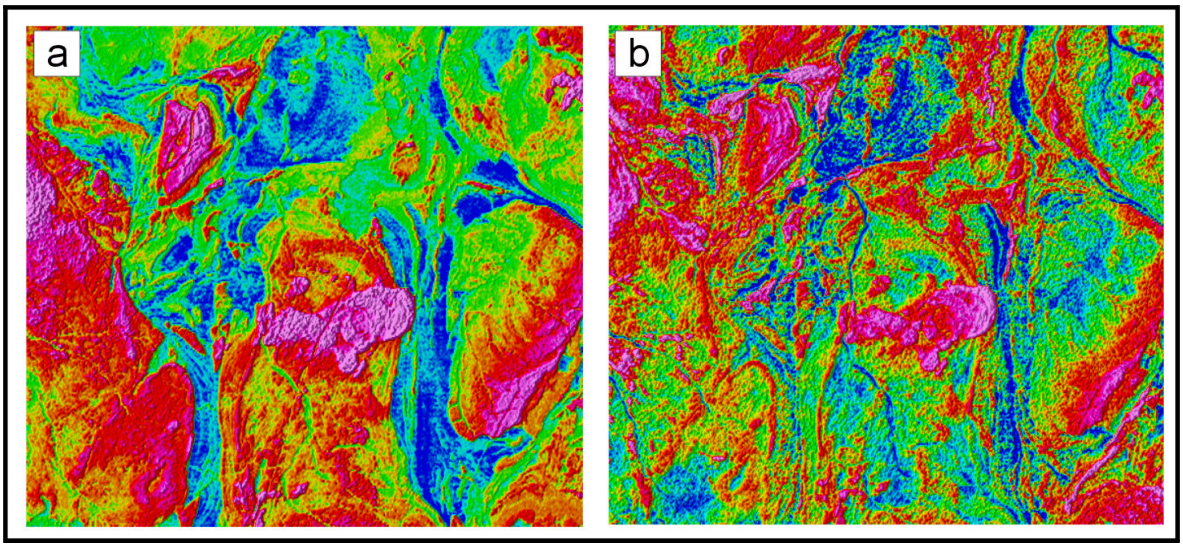

FIG. 7.13. Pseudo-colour presentations of gridded gamma ray spectrometry data: (a) Th grid; (b) Th/K ratio grid (data courtesy of Geoscience Australia).

Look-up tables need not necessarily maintain constant intensity. For example, variations in the data are perceived in more discrete intervals by changing the intensity with a sine function. This provides better definition of overall variations in the radioelement concentrations when the data are not gradient enhanced (Milligan and Gunn, 1997). Alternatively, user-defined intervals may be assigned a discrete colour. This is known as density slicing and may be useful to classify or mask certain data intervals. Figure 7.13 shows examples of pseudo-colour presentations.

Shaded relief (or gradient enhancement) incorporates a sunshading algorithm to artificially illuminate the image from a specific direction. This has the effect of adding spatial resolution to a colour image, and highlighting anomalies oriented quasi-perpendicular to the illumination vector. It is also an effective tool for quality control of gridded data, whether for line-to-line and flight-to-flight shifts, or general high-frequency noise. Milligan and Gunn (1997) outline a technique whereby a shaded colour image is prepared in IHS space, using the original colour image to modulate hue, the darker portion of the shaded relief to modulate intensity and the lighter portion of the shaded relief to modulate saturation. Shaded relief images may also be presented directly in grey-scale, to focus on the short wavelength information.

7.6.6. Ternary radioelement maps

A ternary radioelement map is a colour composite image generated by modulating the red, green and blue phosphors of the display device or yellow, magenta and cyan dyes of a printer in proportion to the radioelement concentration values of the K, Th, U and TC grids. The use of red, green and blue for K, Th and U, respectively, is standard for displaying gamma ray spectrometric data. Blue is used to display the U channel, since this is the noisiest channel and the human eye is least sensitive to variations in blue intensity. Areas of low radioactivity, and consequently low signal to noise ratios, can be masked by setting a threshold on the total count grid. This reserves more colour space and ensures a better colour enhancement for the remaining data. Figure 7.14a shows a ternary radioelement map from a high-resolution gamma ray spectrometry survey acquired over the Pilbara region, Western Australia.

Sum-normalization can be used to compute relative concentrations of K, Th and U prior to imaging as follows:

$$K_n = \frac{K}{K + U + Th} \tag{7.3}$$

$$U_n = \frac{U}{K + U + Th}$$

$$Th_n = \frac{Th}{K + U + Th}$$

This converts the radioelement concentrations to relative abundance. Sum-normalization can be useful to reduce the effects of the attenuation of gamma rays by vegetation or soil moisture. Provided the sum-normalized channels are linearly stretched, the chromatic colour variations (hue and saturation) are in proportion to the relative radioelement abundance of K, U and Th over the survey area, and can be quantitatively related to the ternary legend (Figure7.15a). Fully saturated yellow, for example, signifies equal proportions of Th and K relative to their full concentration range. The total count channel can be combined with the sum-normalized channels by using colour space transformation techniques (§ 7.5.7).

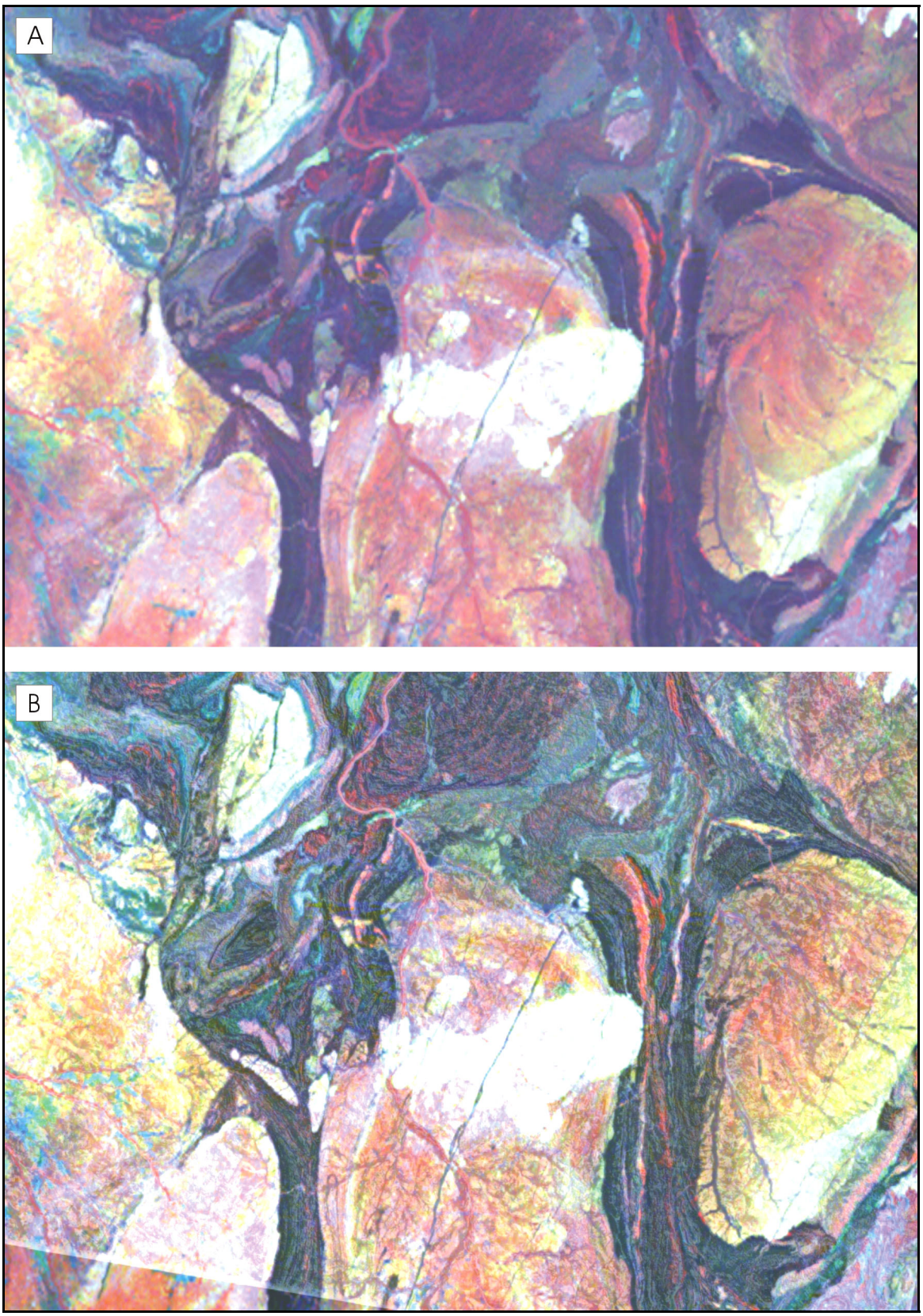

FIG. 7.14. (a) Colour composite image red = K, green = Th and blue = U; (b) Image sharpening of colour composite, shown in (a) by pixel addition of high-pass filtered Landsat band TM5 to the radioelement channels (data courtesy of Geoscience Australia).

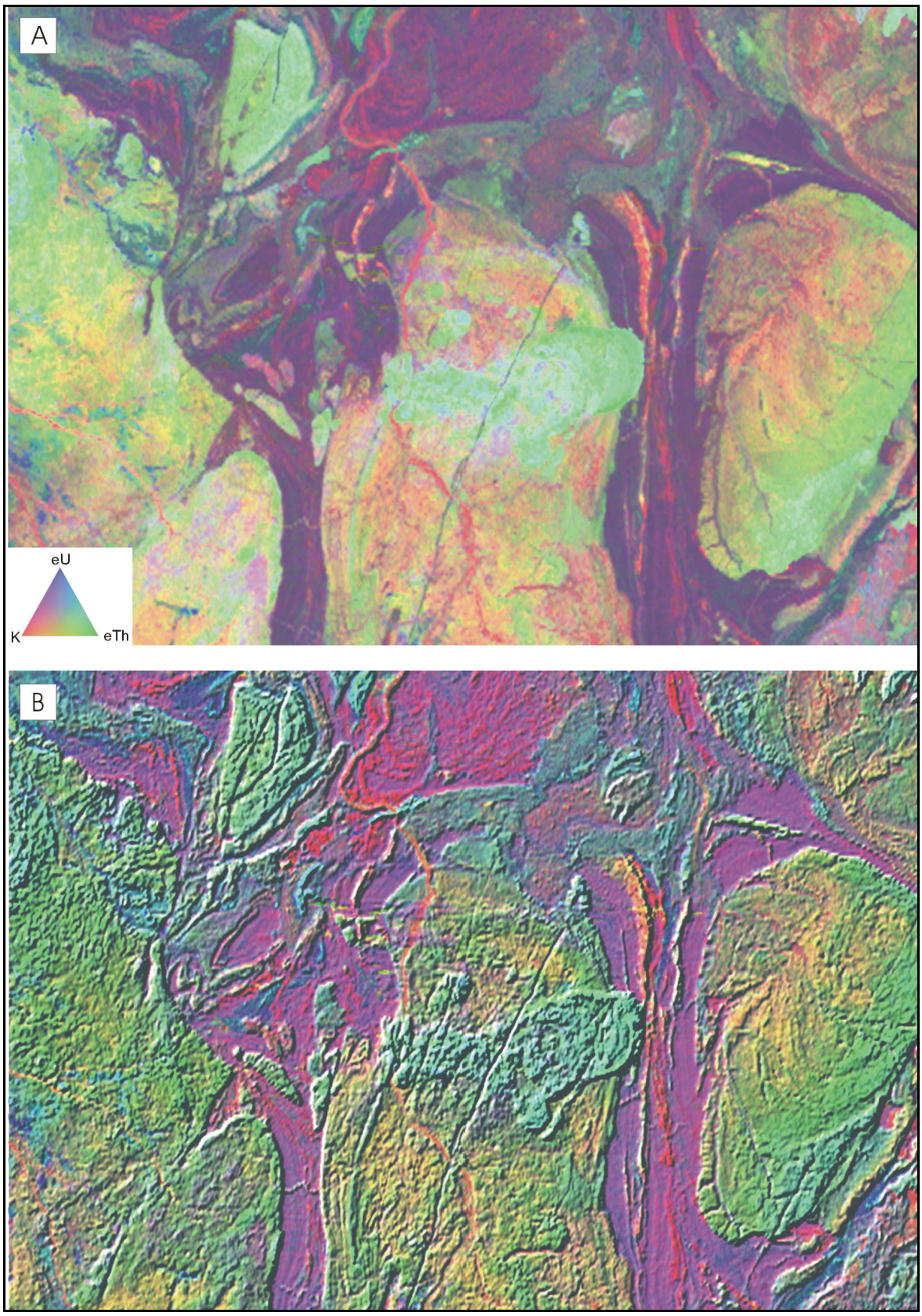

FIG. 7.15. (a) Ternary radioelement map H and S modulate relative radioelement abundance (K = red, Th =green, U =blue), I modulates total count channel; (b) IHS composite image, H and S modulate relative radioelement abundance, I modulates relief shaded total count channel (data courtesy of Geoscience Australia).

A similar normalization technique was used by Broome et al. (1987) for printing ternary radioelement maps in the CMY colour space. The radioelement channels are scaled as follows:

$$K_n = \frac{K}{K + U + Th/4} \tag{7.4}$$

$$U_n = \frac{U}{K + U + Th/4}$$

$$Th_n = \frac{Th/4}{K + U + Th/4}$$

For average crustal abundances of the radioelements, this normalization technique scales the radioelement channels to approximately equal range.

The proportional representation of the radioelements in this way does have the disadvantage that the data cannot be optimally stretched without changing the ratios between the radioelements. For example, compared to Figure 7.14a the range of the sum-normalized U channel in Figure 7.15a is small relative to the sum-normalized K and Th channels. This limits the U contrast enhancement.

7.6.7. Integrated image presentations

The sum-normalized K, Th and U channels can be combined with the total count (exposure rate) channel to produce a relief-shaded style presentation. With careful processing it is possible to retain the chromatic colours of such composite images in proportion to the relative abundance of the radioelements (Schetselaar, 2001). The IHS colour space, can be used to render four grids into a single image. A popular technique is to map the radioelement concentrations on hue, and a gradient-enhanced total count on intensity (Figure 7.15b). This has the advantage of enhancing gradients in total radioactivity, which may represent unit boundaries and structure, while maintaining hue and saturation in proportion to the radioelement abundances.

Ideally, the applied transformations should map the data uniformly on the perceptual colour attributes while using the available colour space of the RGB cube as much as possible. This requires considerable care in processing the data from the input grid to the final RGB image. Individual scaling of the RGB image channels within the RGB cube, for example, distorts the colour balance, and therefore the proportionality of the relative abundance of the radioelements (Schetselaar, 2001). An algorithm for generating IHS composite images without such distortions is given in Appendix II. A fast method of integrating the four gamma ray spectrometric channels is to multiply the sum-normalized radioelement channels with the TC or gradient enhanced TC channel. These are then mapped in RGB space with a uniform linear scaling.

There are several alternative colour-coding schemes in use. The Geological Survey of Canada commonly uses a technique where the TC channel is modulated by saturation while retaining a constant intensity level. This representation avoids extremes of dark and bright in the image,

while still accommodating TC. Geoscience Australia use a spherical IHS model to modulate intensity for the lower half range of a gradient enhanced TC grid, while the upper half range is modulated by saturation (Milligan and Gunn, 1997). The intensity of very dark and saturation of very bright areas are interactively adapted to improve the perception of hue in the ternary map. Although only half of the full range of possible intensity values is used, this technique tends to produce an effect similar to sun-illuminated natural scenes. This is because gradients facing the illumination source appear as undersaturated colours, and the slopes facing away from the illumination source are reduced in intensity.

Intensity substitution can also be employed to integrate the four gamma ray spectrometric grids with ancillary data such as satellite images, rasterized thematic maps, or other geophysical data sets. The transformation required is given in Appendix III. The integration of radioelement grids with images that have high spatial resolution adds spatial detail and provides a sharpened rendition of the otherwise fuzzy ternary image map (Wilford et al., 1997). Several data combinations have proved useful for geological mapping and interpretation, including those with radar data (Harris et al., 1990; Paradella et al., 1997) and Landsat TM data (Wilford et al., 1997; Schetselaar, 1998). An advantage of this approach is that geochemical information (the radiometric data) can be interpreted in a structural geologic or geomorphologic context. Also, natural and man-made features such as lakes, topography, and roads are easily recognized. Figure 7.14b shows a high-pass filtered TM band 7 integrated with the three radioelement channels using the cylindrical IHS transform.

Single radioelement grids can also be combined with ancillary data (Paradella et al., 1997). This is similar to the combined presentation of shaded relief and colour described earlier, and can be implemented with the algorithm given in Appendix II.

7.6.8. Perspective views

A digital elevation model (DEM) is a digital representation of the terrain elevation modelled as a regular grid. High quality models are now routinely derived from airborne geophysical surveys that use the Global Positioning System (GPS) for navigation. The DEM's are derived from a combination of the GPS position of the aircraft (which includes height above the geoid) and the ground clearance of the aircraft measured using a radar altimeter (Richardson, 2000). DEM's can also be derived through photogrammetric methods, the interpolation of elevation contours digitized from topographic maps, or the automatic analysis of stereo pairs acquired by orbital optical or radar sensors.

Three-dimensional perspective views of the gamma ray images draped over a DEM are a powerful visualization tool for the interpretation of gamma ray spectrometric data. These presentations are particularly useful for studying the relationships between gamma ray response and geomorphic variables, such as elevation, slope, aspect, and relief. Software for generating perspective views allows specification of the viewing position and distance. The vertical exaggeration and rotation can be interactively adjusted.

Both the individual and ternary radioelement grids may be draped onto relief-shaded DEM's. These presentations of gamma ray spectrometric data add further realism to the rendition of the "radioelement landscape". Examples of 2-D and 3-D relief-shaded DEM's and gamma ray spectrometric data presentations are shown in Figure 7.16 and Figure 7.17, respectively.

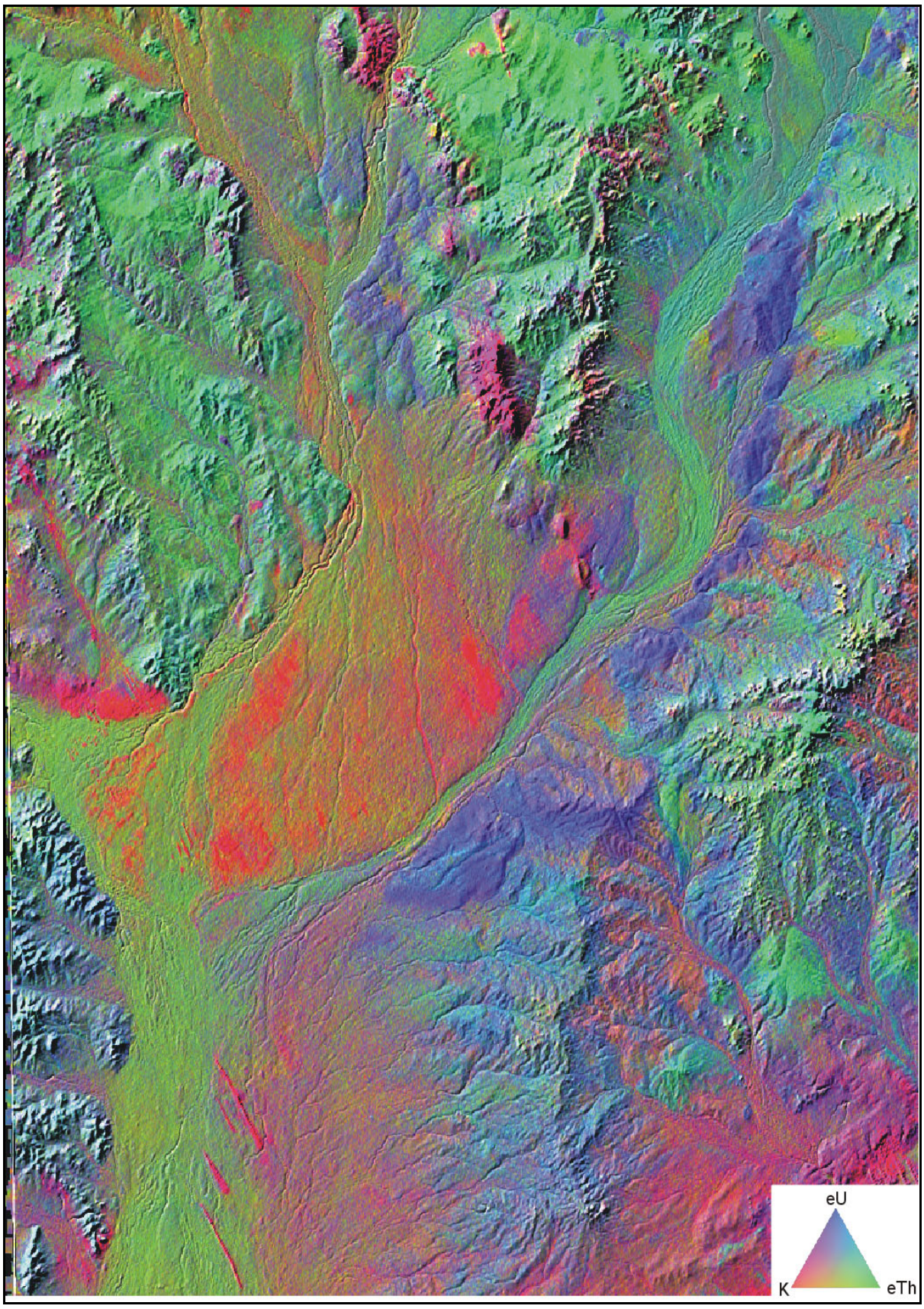

FIG. 7.16. IHS composite image of relief shaded digital elevation model and gamma ray spectrometry data (data courtesy of Geoscience Australia).

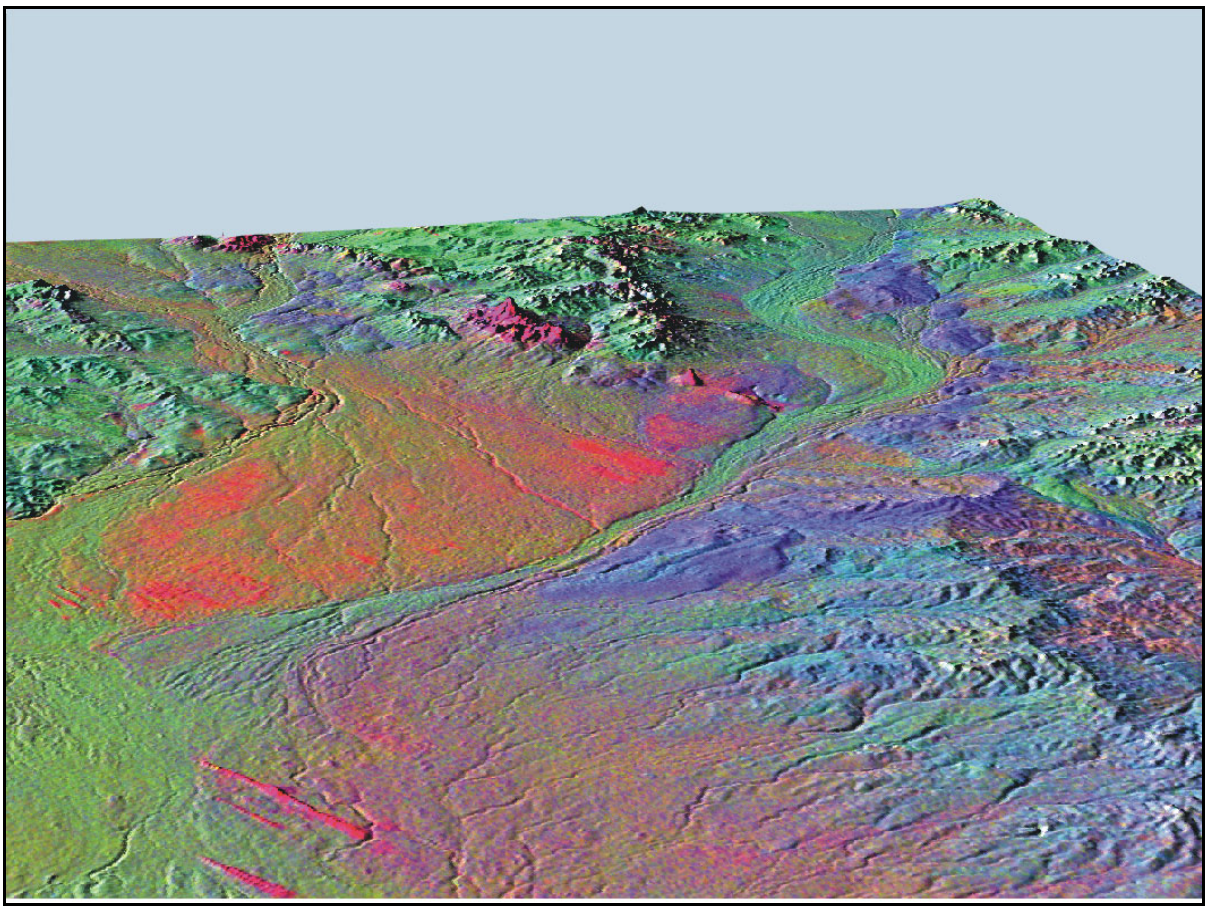

FIG. 7.17. 3-D perspective views of IHS composite image shown in Figure 7.16 (data courtesy of Geoscience Australia).

8. DATA ANALYSIS AND INTERPRETATION

The interpretation of gamma ray surveys should be directed towards applying knowledge on the processes that control the distribution of radioelements in rocks and soils to the enhancement and processing of the data. This interpretation process is now supported by the use of geographic information systems with image processing capabilities. Such hybrid systems are ideally suited for this purpose as they allow integrating digital processing of gamma ray spectrometry data with the integration of field and ancillary remotely sensed data. Besides the enhancement techniques intended to assist visual interpretation (reviewed in Chapter 7) a number of digital processing techniques are useful to support the analysis of gamma ray spectrometry data. Statistical methods, such as mean differencing, regression and principle component analysis can be used to enhance subtle variations in the data that otherwise would remain unnoticed. Pattern recognition techniques, such as edge detection, classification and cluster analyses can be applied for the automated identification of radioelement units and anomalies complementing the visual interpretation of enhanced radioelement grids.

8.1. Annotation of unit boundaries

Once gridded gamma ray spectrometric data have been adequately enhanced, a GIS system can be used to display the raster images and manually annotate the boundaries of discrete units directly on the computer screen as vector polygons. This requires the interpretation and delineation of units of similar radiometric character – i.e. similar concentrations of K, U, and Th, and similar spatial texture. Classification and clustering techniques (§8.5) can be used to guide the interpretation. Standard edge-enhancing methods may also be useful in guiding the interpretation. The unit boundaries are saved as vector polygons, and the polygons are used for sub-sectioning the data for subsequent statistical analyses.

8.2. Mean differencing

Statistical analysis of K, U and Th concentrations within each interpreted unit is useful for extracting subtle information from the data that is not immediately visible. The simplest analysis is to look at deviations from the unit means. The mean K, U and Th concentrations are calculated for each interpreted unit. These means are subtracted, and the residuals are imaged. Kovarch et al. (1994) called this “mean differencing”. Large deviations from the mean could be due to errors in the mapping of the unit boundaries. Alternatively, deviations could indicate alteration/mineralization or other geological processes such as magma differentiation or weathering.

8.3. Regression analysis

Single or multiple linear regression between the estimated radioelement concentrations can be used to model and remove the effects of geological processes within interpreted units. Again, the regression model is subtracted from the data within each unit and the residuals are imaged. The method is useful for removing gross systematic changes in radioelement concentration within an interpreted unit. Wellman (1998) gives a good example of this type of analysis.

8.4. Principal component analysis

Principle component analysis (PCA) is a mathematical procedure that can be applied to multi-band images. The result is a new set of images (principal components) that are uncorrelated.

Each of the principal components (PC's) is a linear combination of the original images. The PC's are ordered according to the proportion of total variance in the original dataset that they accommodate. The first image contains the majority of the variance in the multiband dataset. Higher order components contain less of the dataset variance.

PCA can offer an effective method for noise removal. Since there is a high level of correlation between TC, K, U and Th, these end up in the lower order components. The noise, on the other hand, does not correlate between channels and can be partially removed by spatially filtering (low-pass filtering) the higher order components before doing the inverse PCA transform.

Principle component images are frequently used to produce colour composites. This gives colourful images, as the data have been de-correlated. But the composite image has no physical meaning and cannot be directly interpreted with respect to radioelement concentrations. A more useful colour enhancement is decorrelation stretching (Gillespie et al., 1986), where the lower variance components (PC2 and PC3) are stretched before rotating the components back to the original radioelement channels. This produces an effect similar to saturation enhancement (Appendix III).

Instead of using the entire grid in a PCA analysis, it may be useful to sample the grids for features of interest to improve the interpretability of the results (Donker and Mulder, 1976). Others have selectively applied PCA on pairs of bands from multispectral image data (Chavez and Kwarteng, 1989). This allows transforming the pair in a component of radioelement signatures common (or different) among the channel pair. This is similar to regression analysis, and can be used to separate anomalies from background lithological variations. The difference between principal component analysis and regression analysis is shown in Figure 8.1. Unlike regression analysis, there are no dependent or independent variables. Instead of computing the best-fit line by least squares on one of the variables, the optimal fit is based on minimising the squared deviations of the two variables combined. This minimizes the deviations perpendicular to the line defined as the first principal component.

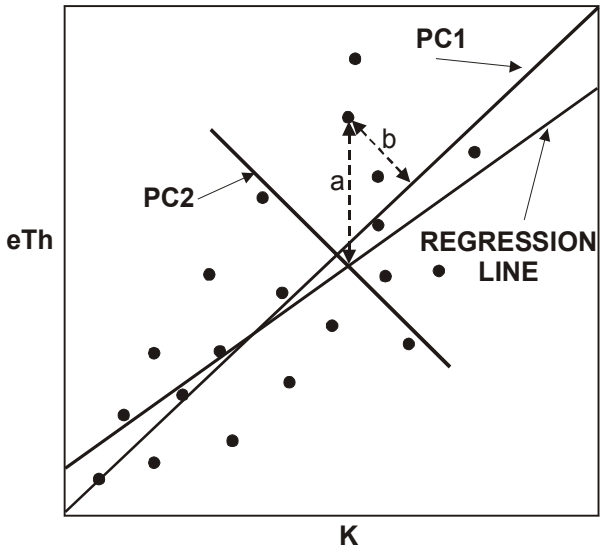

FIG. 8.1. K-eTh Scatter plot showing the difference between regression and pair-wise principle component analysis. In regression analysis the squared deviations of the dependent variable eTh (a) are minimized whereas in principle component analysis the squared deviations of eTh and K combined are minimized.

8.5. Clustering and classification

Clustering and classification are useful interpretation tools for analysing large multivariate datasets. These methods are used for the automatic identification of samples (pixels) that have a similar radiometric signature.

8.5.1. Clustering (unsupervised classification)

Clustering, or unsupervised classification, is a spectral pattern recognition technique used for finding naturally occurring groupings (i.e. classes or clusters) in a multiband dataset. The class allocation rules are based on some measure of distance in the data space spanned by the multispectral bands. Because classes are identified on the basis of gamma ray signature, their origin is still open to interpretation. The resulting map pattern must therefore be interpreted with respect to some reference source, such as a geological map. The advantage of unsupervised classification is that it has the potential to identify all clusters. It provides an unbiased map generalization with sharp boundaries between clusters.

The K-means algorithm (Niblack, 1986) is an iterative clustering method. The user specifies the number of classes, and initial class centres (means) are determined. Each sample is then allocated to the closest class centre (using Euclidean distance). The class means are recalculated, and the process repeated for a specified number of iterations or until a convergence criterion is met. The radioelement grids should be standardized to zero mean and equal variance before applying to clustering algorithm. This is to avoid dominance of the largest concentration range of the eTh grid.

Harris (1989) applied a minimum "distance-to-mean" clustering of gamma ray data acquired over Nova Scotia, Canada. The most informative clusters were derived from 6-dimensional (K, Th, U, U/Th, Th/K, U/K) and 4-dimensional (K, Th, U, U/Th) data sets. Spatially continuous clusters with distinct boundaries showed good correlation with the mapped geology. These mainly corresponded with mapped granitoid plutons. Some of the clusters were related to anomalous Th content within some of the plutons. However, in some cases the sensitivity of the clustering algorithm was not sufficient to identify geologically significant, yet subtle, colour variations in the ternary radioelement map (Harris, 1989). This suggests that clustering should be used to complement, rather than replace, visual interpretation.

Graham and Bonham-Carter (1993) applied the K-means algorithm to airborne gamma ray spectrometric data from the Marathon area, Ontario, Canada. They analyzed the correlation between clusters and mapped geology using GIS overlay techniques. They found a moderate to strong spatial association between bedrock units and radioelement clusters. Areas where the cluster and geological maps differed were identified for further field verification.

Figure 8.2 shows an example of the application of cluster analysis to the mapping of compositional variations within a granite batholith in northeastern Alberta, Canada. The cluster analysis yielded four classes with distinct radioelement signatures. The clusters were interpreted as Th-rich and Th-poor intrusive phases, which were both subdivided into relatively U-poor and U-rich classes. A comparison with the major element geochemistry indicated that the trend in U in the Th-rich cluster follows a trend in SiO_2. The increase of U with SiO_2 suggests a magmatic differentiation trend, the most evolved stages of which represent hydrothermal U-enrichment of the country rock envelope (Schetselaar, 2002).

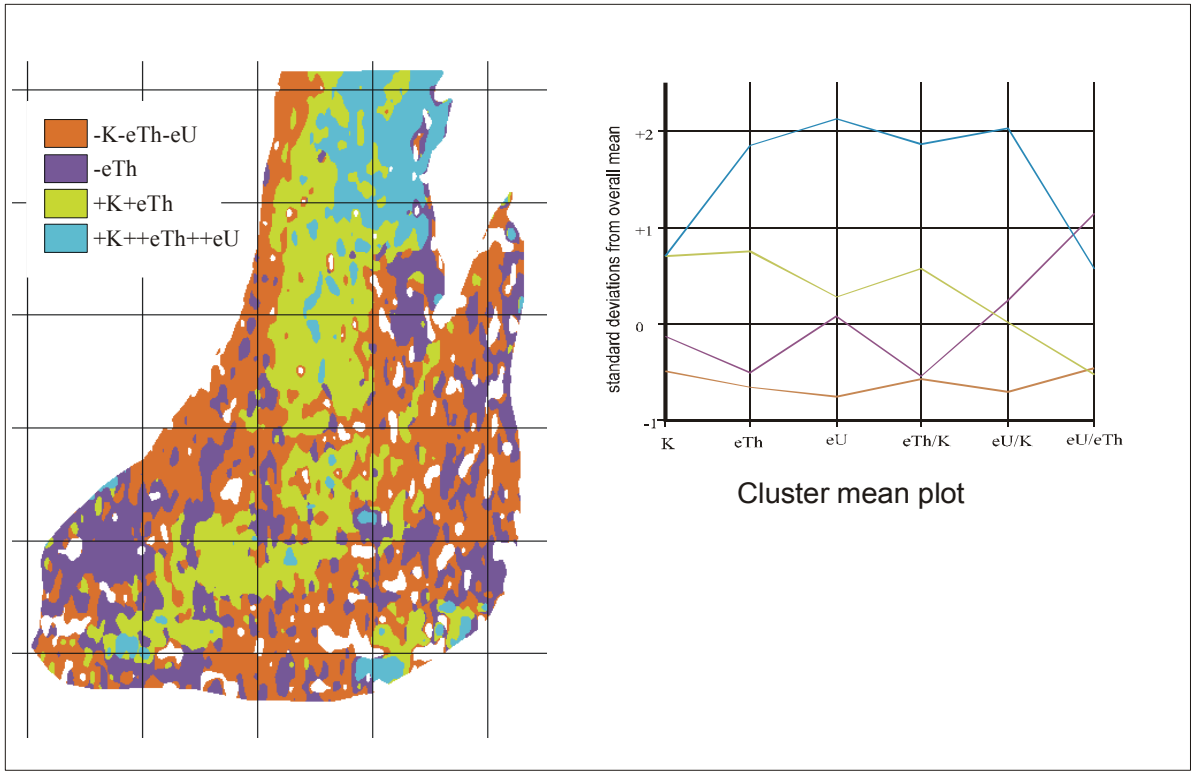

FIG. 8.2. Cluster analysis on the basis of K, U/Th, U/K grids, Arch Lake granite, northeastern Alberta, Canada. The cluster mean plot shows the deviations from the mean of each cluster for each of the six variables (Data from Geological Survey of Canada, Open File 2807, Charbonneau et al., 1994).

8.5.2. Supervised classification

Supervised classification methods are based on classes that have been pre-defined as meaningful with respect to ground observations. The decision rules for class allocation are based on sample sites considered representative for these classes. This sampling procedure, known as the training stage, distinguishes supervised classification from clustering routines. The decision rules are used to allocate samples to particular classes in the subsequent classification stage.

Supervised classification has been widely applied in the analysis of multispectral image data acquired by earth orbiting satellites for land cover mapping. The technique has also been applied to the classification of lithological units using gamma ray spectrometric data in combination with Landsat TM data and other airborne geophysical data, such as magnetic and electromagnetic data (Lanne, 1986; Eberle, 1993; An et al., 1995; Schetselaar et al., 2000).

The probability that a pixel belongs to a class depends on the ratios between the probability density functions of that particular class and the other classes. The available classification algorithms differ in the way the probability density functions for each class are modelled and estimated from the training data (McLachlan, 1992). The classification algorithms can be broadly categorised in: (1) parametric classifiers that model the class probability density functions with the estimated parameters of a multivariate normal distribution or (2) non-parametric classifiers that directly estimate the class probability density functions from the data. A recommended practice is to experiment with a number of algorithms. These are best applied to an area where the geology is well known to evaluate the performance of the different algorithms.

8.5.3. Case study

Schetselaar et al. (2000) used supervised classification of airborne magnetic and gamma ray spectrometric data to map lithological units in the Canadian Shield of northeastern Alberta, Canada. The geology is composed of a Paleoproterozoic granite gneiss basement complex with enclaves of metasedimentary rocks intruded by numerous Paleoproterozoic granitoid plutons. The plutonic suites have distinct gamma ray responses as a result of their distinct accessory mineral content (Charbonneau et al., 1997). Internal lithological variations in the basement complex can be seen in the magnetic data, but are poorly resolved in the gamma ray data.

A flow chart of the supervised classification procedure is shown in Figure 8.3. The analysis first focused on a training area consisting of 2795 field stations (step 1 in Figure 8.3). The resolving power of different combinations of images was then evaluated (step 2 in Figure 8.3). This analysis showed that a 5-channel data set consisting of the three radioelement channels, plus the total and residual magnetic field were best suited to outlining the ten lithological units. Multi-box whisker plots showing the distributions of the grid channels per lithological unit (Figure 8.4) give insight into the discriminating power of the grid channels for the different lithological units.

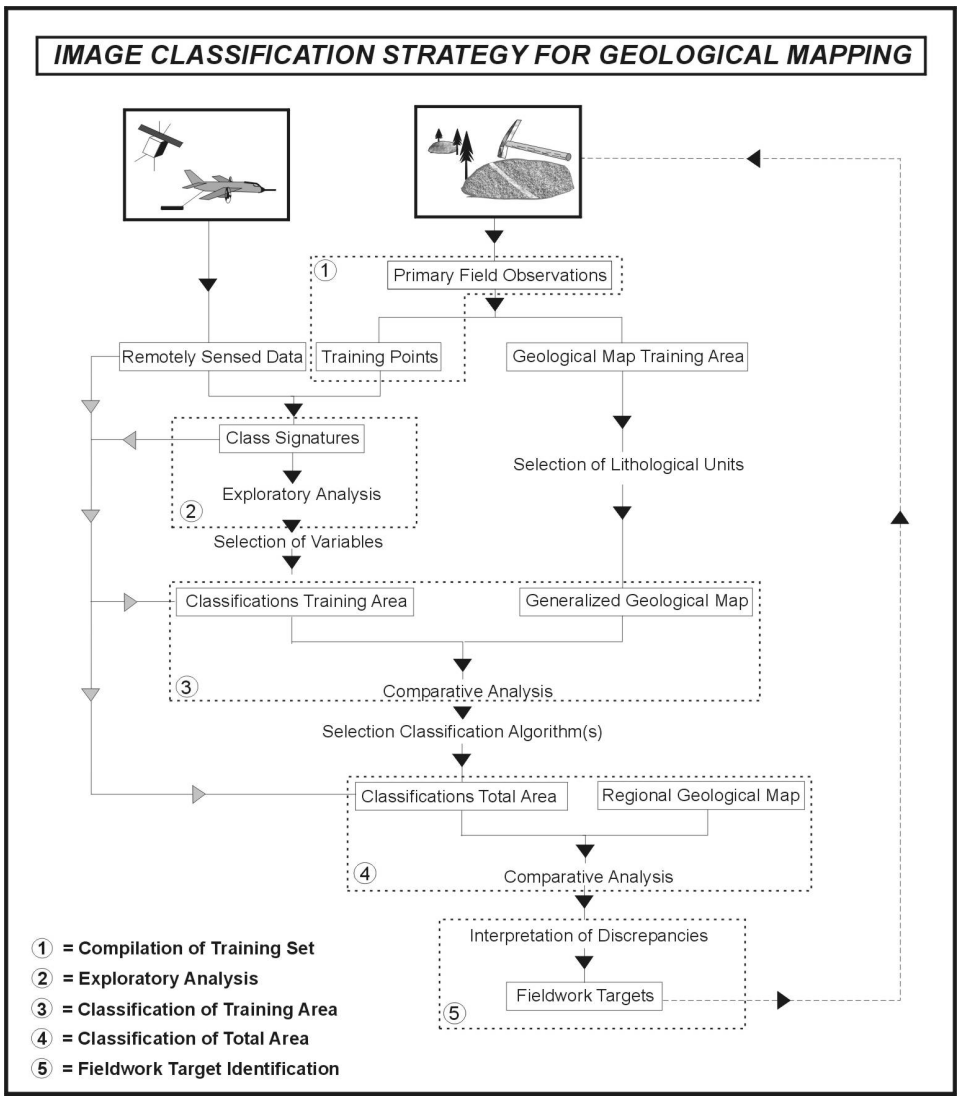

FIG. 8.3. Flow chart of supervised classification methodology.

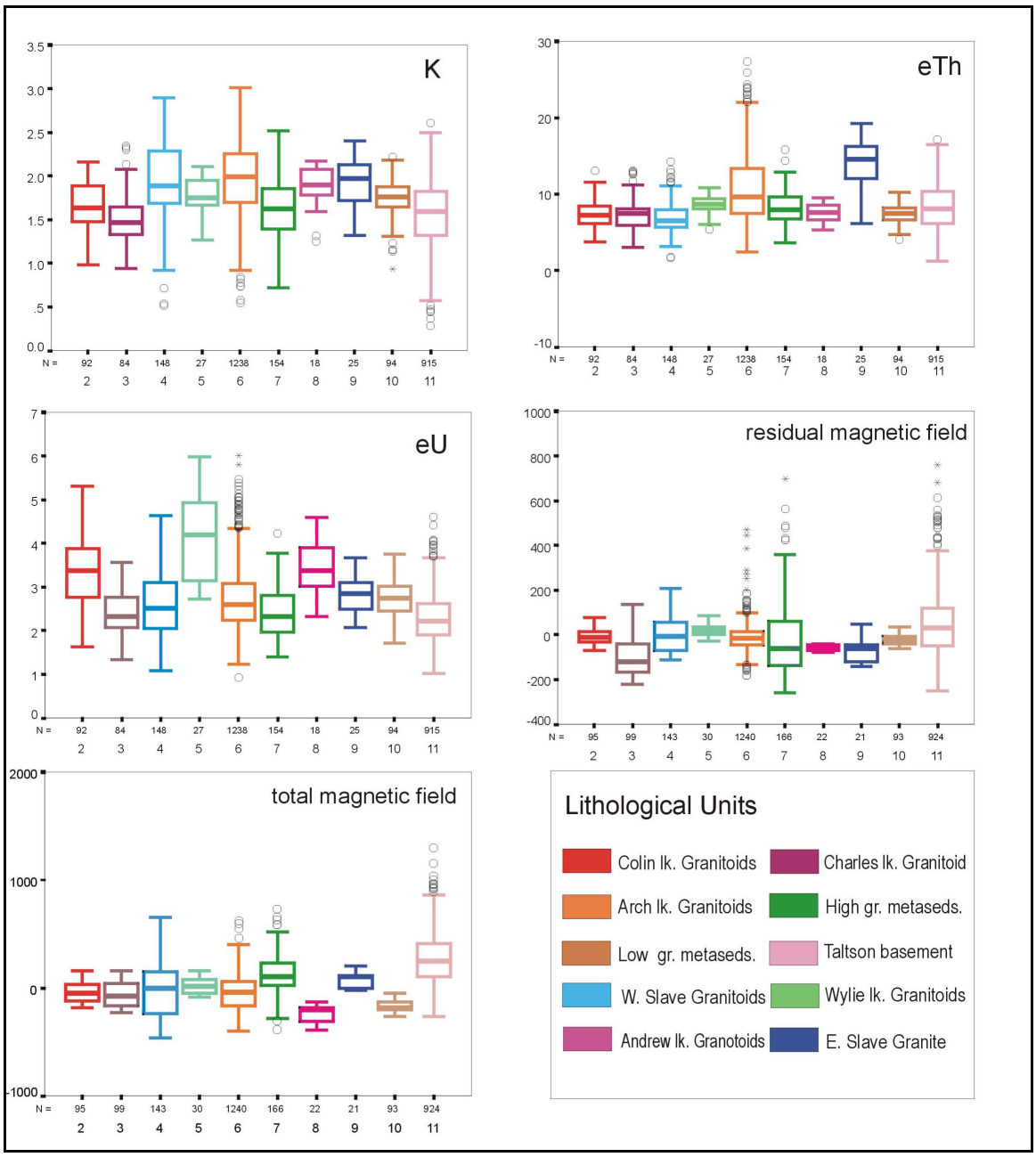

FIG. 8.4. Multi box-whisker plots for K, Th, U, total and residual field magnetic data lithological units.

Maximum likelihood, predictive and artificial neural network classifiers were used to predict the ten lithological units in the training area (step 3). The resulting classification patterns are shown in Figure 8.5. The classification yielded 65-70% correlation with the mapped geological units in the training area. The classification was then extended to the total study area (step 4), and compared with the regional geological map (Figure 8.6). The discrepancies between the classified patterns and the regional geological map were used to identifying targets for refinement of the geological map or as potential exploration targets (step 5). Some of the targets included internal zonations in granitoid plutons, uranium anomalies, and magnetic intrusive units in the near subsurface. As with the cluster analysis discussed earlier this study suggests that supervised classification is a useful method to assist geologists in fieldwork planning and in identifying targets for map refinement and exploration.

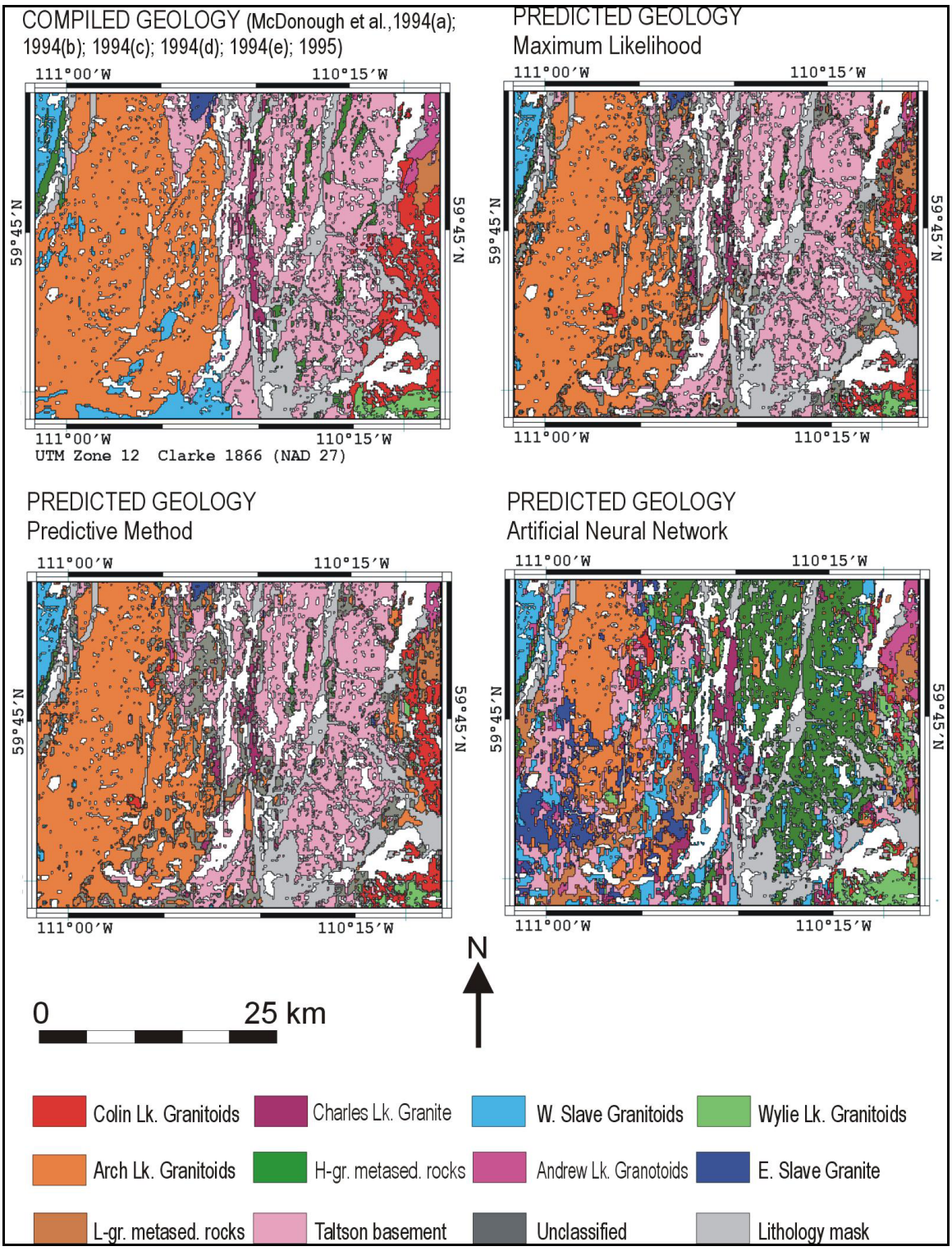

FIG. 8.5. Classification results from the training area, Canadian Shield of northeastern Alberta.

8.6. Integration with complementary data sets

The interpretation of gamma ray spectrometric data is rarely carried out in isolation. The integrated interpretation of gamma ray data with complementary data sets, such as airborne magnetics, satellite imagery and aerial photographs, provides a wealth of additional geological information.

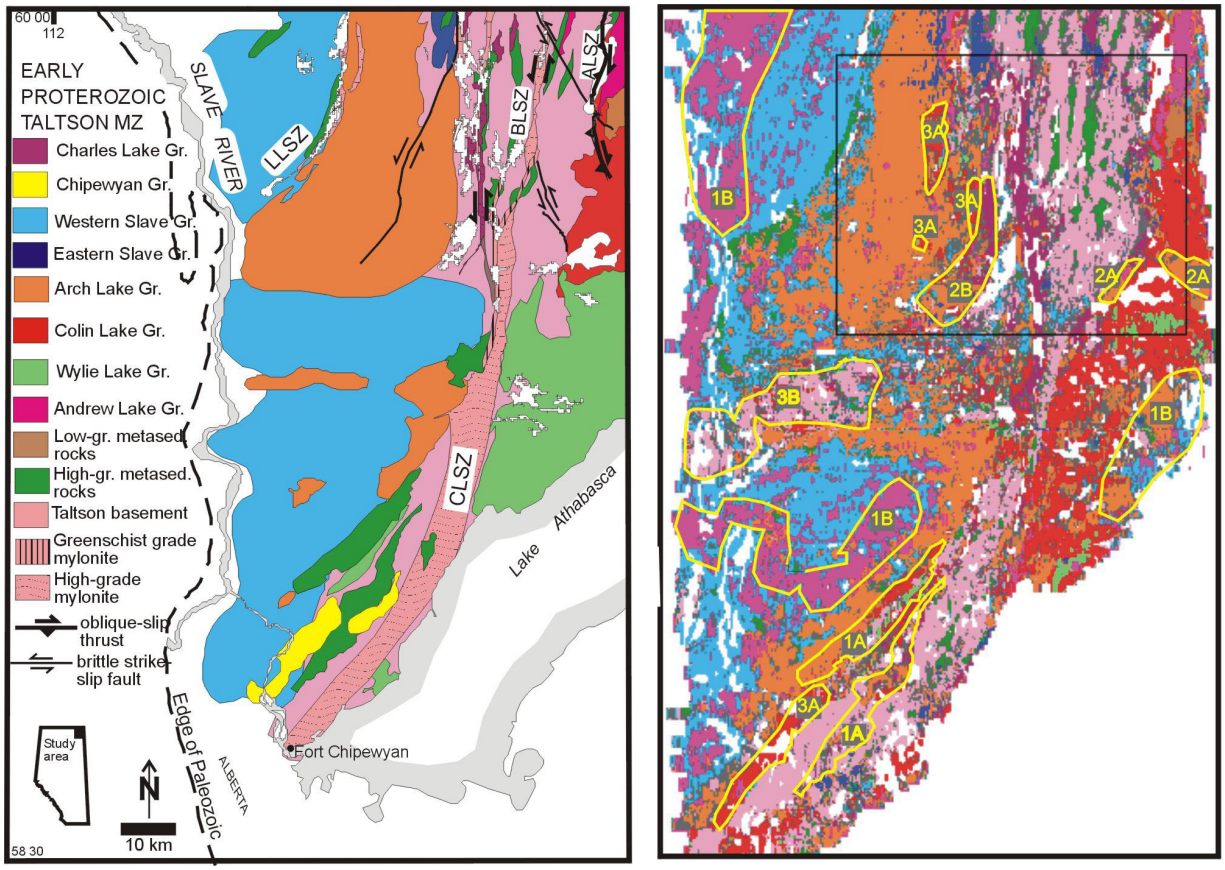

FIG. 8.6. Classification results of the Western Canadian Shield in northeastern Alberta. Yellow polygons demarcate discrepancies between the regional geological map and the classification providing follow-up targets for field exploration campaigns.

8.6.1. Magnetic data

The residual magnetic anomaly field reflects magnetic sources from the near surface to depths of 10 km or more. These data do thus not necessarily reflect surface geology. The magnetic anomaly pattern is also complicated by the orientation of the inducing magnetic field and the presence of remanent magnetization. Magnetic anomalies are thus not normally coincident with their sources. However, in areas of outcropping crystalline basement with near-vertical rock contacts (e.g. Archaean basement terranes) and induced magnetization, reduced-to-pole magnetic anomalies closely match the outlines of bedrock units. Also, enhancements such as downward continuation and vertical derivatives can be used to emphasise the effects of near-surface magnetic sources (Telford, 1990).

The extent to which the shape of magnetic anomalies is diagnostic in a pixel-by-pixel classification is dependent on the direction of induced magnetization, and the distribution of magnetic susceptibility contrasts at various distances from the plane of observation. The most favourable settings are those of vertical contacts in a steeply inclined field. The extent to which the magnetic anomaly field reflects surface geology is of fundamental importance for combining these data with gamma ray spectrometric data in an automated classification scheme. Such insight can be obtained by comparing the magnetic data with generalized geological map patterns, and evaluating the changes in the classification success rates when the magnetic data are included.

Derived products, such as pole-reduced, residual and vertical derivative fields are useful to enhance near-surface magnetic sources, but their limitations depend on the quality of the data and additional factors such as magnetic inclination. Further research is needed to test the applicability of other enhancement procedures to automated classification. The interpreter should always be aware that the magnetic signatures of deep sources could influence the classification. It is not uncommon to see the magnetic data reflecting basement rocks that may have little in common with the geology and structure of the overlying units mapped by the radiometric data.

8.6.2. Electromagnetic data

Airborne electromagnetic surveys respond to conductive material in the geological section, with a maximum depth penetration of 100-300 m, depending on the system used and the resistivity of the rocks. The greatest correlation with radiometric data is obtained from the data measured at the highest frequency (frequency-domain survey) or during the on-time/early off-time (time-domain survey), which should reflect near-surface conductivity. An apparent resistivity image derived from this portion of the electromagnetic data will be the most useful for comparison with the radiometrics. The composition and thickness of the overburden, the nature and degree of weathering, surface water and groundwater, the geomorphology and bedrock exposure all affect the resistivity. Under the right geological conditions, the radiometric and apparent resistivity can complement one another in characterization of the near surface geology. There may be less correlation between the radiometrics and deeper electromagnetic sources (including bedrock conductors) depending on the nature and geometry of the underlying geology.

8.6.3. Multispectral imagery

Multispectral sensors (e.g. Landsat TM, hyperspectral data) acquire image data in distinct wavebands in the visible and infrared ranges of the electromagnetic spectrum. They provide information on how electromagnetic radiation interacts with matter at the Earth's surface. Of interest to geological and soils mapping, wavelength-specific absorption features may appear in the measured reflectance spectra that are diagnostic for iron-oxides, carbonates, silicates and minerals with hydroxyl groups.

In a broad sense, patterns on multispectral imagery (e.g. Landsat TM, hyperspectral data) can be expected to correlate well with radiometric data in areas of sparse vegetation as both methods respond to the material exposed on the Earth's surface. At the level of mapping individual units, however, gamma ray spectrometry and Landsat TM image data obviously yield complementary lithological information (Anderson and Nash, 1997).

The spatial resolution of the multispectral data is typically better than airborne radiometric surveys. The multispectral images also display illumination of the terrain relief, as with other types of remotely sensed data (e.g. radar), and consequently can be combined with radiometric images to enhance structure and texture. Geological units may be well delineated by both types of data. Potential uses of the data include the interpretation of lithology, weathering, alteration, and regolith and soil profiles.

8.6.4. Digital elevation models

The geomorphology of an area plays an important role in the exposure of outcrop, the distribution of transported sediments, and the control of weathering processes. Geomorphology is usually critical to the interpretation of radiometric data. Drainage features are often laden with sediments derived from upstream sources. Topographic control of the downhill transport of eroded sediments is typically evident. This is an important factor in

determining what surface material is transported (reflecting sources upstream), and what has remained in-situ (reflecting bedrock). The sources of gamma ray spectrometric anomalies also often have a topographic expression. A composite view of the radiometric data with the digital elevation data, as either a 2-D or 3-D perspective view (§7.6.8), is a useful interpretation aid. This presentation of the data also helps in the interpretation of surficial structure.

8.6.5. Geochemistry

Gamma ray spectrometry is essentially a radioelement geochemistry technique. The efficiency of the data collection provides a spatial sample resolution that far exceeds conventional geochemistry. Where there is some correlation between the distribution of the radioelements and other measured elements, radiometric data can be used to tie geochemical data together into a more coherent interpretation. Where mineral exploration targets located by geochemistry have radiometric signatures (the host rocks, mineralization, or associated alteration), this can be used to guide further exploration. The radiometric data can also provide an excellent guide as to the provenance of surface material. This can be used in planning geochemical surveys or interpreting the results of geochemical surveys.

8.7. Interpretation methodology

Gamma ray interpretation methodology depends on the quality of the data, the survey area, and the scope and purpose of the interpretation. In practice, it is thus not possible to define a universal set of guidelines to enhance and interpret gamma ray spectrometry data. The various enhancement and feature extraction techniques discussed earlier contribute in a complementary fashion to the interpretation and analysis of the data. Figure 8.7 shows a flow chart of a proposed processing strategy applicable to the interpretation of gamma ray spectrometric data. Obviously, there are many alternatives to this strategy.

The first step in the interpretation process is the enhancement of the data to emphasize the overall variations in radioelement concentrations. Contrast stretching, pseudo-colour coding, gradient enhancement, and ternary mapping are techniques that contribute to this objective. Arithmetic combinations between the radioelement grids, such as sum-normalized data and ratios, are particularly relevant in survey areas where environmental factors related to water and land cover mask the gamma ray response from rocks and soil. Stacked profile and profile map presentations, their ratios, and the total count channels are used to analyze individual anomalies in detail. Interpretations should be based on several enhancements of the data, as no single enhancement can show all the relevant features in the data.

The second step in the interpretation is the outlining of spatially continuous radioelement domains and anomalies. The interpretation and annotation of radioelement domains can be supplemented by the identification of gradients in the total count grid that may associate with the boundaries of lithological and soil units, or geological structures. The annotation of these features can be carried out semi-automatically with the aid of automatic edge-detection methods.

Mean-differencing, regression, or principle component analyses can be applied within each outlined unit to locally enhance subtle gamma ray responses against the background variations and to identify anomalies. The results of these analyses can be used to refine the annotation of unit boundaries. Alternatively, the identification of units and anomalies can be extracted with automated pattern recognition techniques, such as clustering and supervised classification.

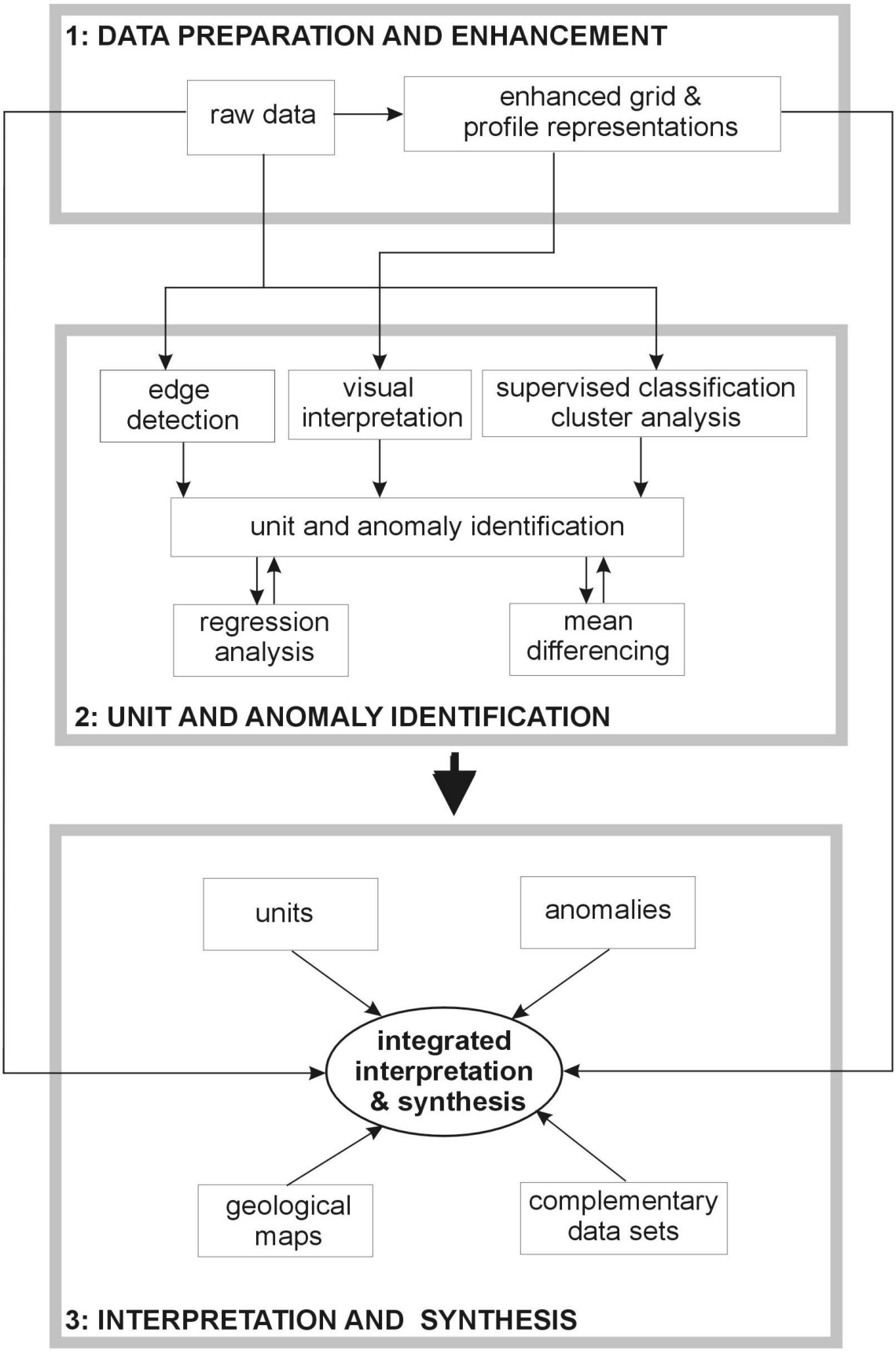

FIG. 8.7. Flow chart showing methodology for the interpretation of gamma ray spectrometry data.

The final step in the interpretation is to integrate all the available geological and other information into the gamma ray interpretation. Enhanced grid presentations with overlays of unit boundaries, tagged anomalies, and digitized geology can be displayed using the basic cartographic and overlay capabilities of geographic information systems. Such displays can be dynamically linked to the raw data using spatial query functions in support of the final synthesis and definition of follow-up targets.

Particular attention should be paid to the geomorphology and topography, and how these control the surface distribution of the radioelements. The response due to bedrock must be separated from that due to transported materials. Interpreters should be aware that factors such as vegetation, alluvium, soil moisture content, and variations in exposure to weathering could affect the signal from an otherwise homogeneous geological unit.

The noise levels are not the same in each radioelement channel (Table 5.2). The noise levels also depend on the concentrations of the radioelements. In areas where concentrations are low, local variations may simply reflect noise rather than signal. A thorough understanding of the factors that affect the quality of gamma ray spectrometric data, such as soil moisture variations, atmospheric radon variations, the effects of topography and so on, is an essential prerequisite for a satisfactory interpretation.

Ground truthing forms a critical component of any geophysical interpretation. This is particularly the case with radioelement mapping as the anomaly sources are always exposed. Any element of an interpretation that is considered important, but whose source is questionable, should be checked on the ground. The source of airborne anomalies can be checked on the ground using a calibrated portable gamma ray spectrometer.

What might appear to be a relatively homogeneous unit from an airborne survey may show significant variation on the ground. Ground truthing also provides an opportunity to measure other physical properties (e.g. magnetic susceptibility, mineral spectra, and conductivity).

The interpretation of gamma ray spectrometry data in terms of lithology can be difficult. With the exception of some granites and types of alteration, rock classification schemes do not typically accommodate radioelement content. The interpreter must therefore rely on a correlation with known geology and ground truthing to develop the lithological framework. Units mapped as homogeneous on geological maps often exhibit zoning in the radiometric data. This is particularly true of igneous units. Closer examination of the rocks should explain the differences and lead to a classification of geological subunits within the larger unit. Similar problems exist in magnetic interpretation, where the magnetic mineral content is usually not a critical element of rock classification schemes.

Ground truthing can be hindered in weathered terrains by a lack of fresh outcrop. Geological mapping under these conditions must rely heavily on full sample analyses. Gamma ray spectrometric surveying can be very useful in these circumstances for delineating lithologic units. Interpreters may have to rely on the characteristic radiometric signatures of various rock types to interpret lithology. Radioelement concentrations in weathered products (in-situ soils, laterite) can vary considerably. This can significantly hamper the interpretation of the bedrock geology unless the local weathering processes are well-understood.

Interpreters of airborne geophysical data typically depend on magnetic data for structural interpretation, with contributions from electromagnetic and gravity data where applicable. However, not all structure produces anomalous magnetic responses. Where structure plays a role in controlling the surficial geology, radiometric data can supplement the structural interpretation of the magnetic data.

9. MAPPING NATURAL SOURCES OF RADIATION

Darnley (1996) noted that the absence of quantitative geochemical data to map the surface composition of the earth is one of the major information gaps in present day environmental and earth science. Gamma ray spectrometric data is a vital sub-component of the geochemical data required for environmental mapping. High quality geochemical databases are pertinent to a wide range of investigations in the earth and life sciences, and should be considered as an essential component of environmental knowledge. The international geochemical mapping project studied the global inventory of geochemical data and endorsed the significance of radioelement mapping (Darnley et al., 1995).

9.1. Mapping fundamentals

Gamma ray spectrometry is widely used in geological mapping, soil surveying, mineral exploration, and regolith studies. The use of the method as a mapping tool requires an understanding of the geochemistry of the radioelements in rocks and soils, and the processes that effect their distribution and mobility. Mineralogical and geochemical studies of rocks and soils play a fundamental role in corroborating the interpretation of gamma ray spectrometry surveys, as they provide insight in the mode of occurrence of the radioelements and their petrogenetic or pedogenetic associations.

Gamma ray spectrometric mapping applications typically rely on an integrated approach. The gamma ray data are interpreted in combination with other airborne survey data such as magnetic and electromagnetic surveys, satellite images, and geological and soil maps. Geographic information systems (GIS) are ideal for this integration task, because they provide image processing and enhancement functionality with dynamic map overlay, and cartographic functionality.

9.1.1. Theoretical considerations

While gamma rays in the energy range used for the mapping of natural sources of radiation can penetrate several hundred metres of air, they are completely attenuated by about 50 cm of rock or soil. This has several implications for the mapping of natural sources of radiation.

The gamma ray method is a surface mapping method. Most of the gamma rays emanating from the earth's surface originate in the top 30 cm of the earth. This means that the interpretation of these data require an understanding of surface processes such as weathering, and the relationship between surficial materials and bedrock geology.

Gamma rays can penetrate appreciable thicknesses of air. This has implications for the "field of view" of airborne gamma ray spectrometers. A terrestrial point source, for example, can influence the measured fluence rate at large lateral distances from the detector. Conversely, the measured fluence rate at an observation point, say 100 m above the ground, reflects the average concentration of the radioelements over a large area of many thousands of square metres.

Disequilibrium in the U decay series is a serious source of error. Estimates of U concentrations are based on the assumption of equilibrium conditions, and this is not necessarily the case.

Finally, the environment affects measured fluence rates. Gamma rays attenuate exponentially with distance from the source. Vegetation and soil moisture can adversely affect the estimates of the surface concentrations of the radioelements.

9.1.2. Geochemistry of the radioelements

Potassium

Potassium is a volatile lithophile element and is monovalent under natural conditions. The abundance of potassium in the Earth's upper crust is 2.33 wt. % K. Most K occurs as alkali-feldspar and micas in felsic rocks, mainly granitoids, which contain 3.5 wt. % K on average. Mafic and ultramafic rocks contain much lower concentrations, with average K content ranging from 0.58 to 0.75 wt. %. The feldspar mineral series, the feldspathoids leucite and nepheline, and the micas biotite and muscovite, together contain virtually all the potassium in metamorphic and magmatic rocks. Some amphiboles contain up to 1 wt. % K. Table 9.1 lists the common minerals of which K is an essential constituent and some other common K-bearing minerals (Mittlefehldt, 1999).

TABLE 9.1. POTASSIUM MINERALS.

Potassium Minerals	**Chemical Formula**	**% K**
Rock forming silicate minerals		
Feldspars	$(K,Na)AlSi_3O_8;(Na_x,Ca_{1-x})Al_2\text{-}xSi_2+xO_{8(x=0-1)}$	
Alkali-feldspar	$(K,Na)AlSi_3O_8$	13
Microcline	$KAlSi_3O_8$	13
Orthoclase	$KAlSi_3O_8$	13
Sanidine	$KAlSi_3O_8$	13
Leucite	$KAlSi_2O_6$	17
Nepheline	$(Na,K)AlSiO_4$	23
Biotite	$K(Mg,Fe)_3AlSi_3O_{10}(OH)_2$	8
Muscovite	$KAl_2AlSi_3O_{10}(OH)_2$	8
Phlogopite	$KMg_3AlSi_3O_{10}(OH)_2$	8
Hornblende	$(K,Na)_{0\text{-}1}(Na,Ca)_2(Fe,Mn,Mg,Ti,Al)_5(Si,Al)_8O_{22}(OH,F)_2$	1
Other K-minerals		
Alunite	$KAl_3(SO_4)_2(OH)_6$	
Glauconite	$(K,Ca,Na)_{<1}(Al,Fe^{3+},Fe^{2+},Mg)_2[(OH)_2/Al_{0.35}Si_{3.65}O_{10}]$	
Sylvite	KCl	

Thorium

Thorium is an actinide element with a valence state of Th^{4+} in solution with evidence for lower valence states in solid state. It forms with the anions fluoride, oxalate, iodate and phosphate insoluble precipitates (Krishnaswami, 1999). Th can be dissolved in acid solutions and its solubility is enhanced by humic acids (Chopin, 1988). The abundance of Th in the Earth's crust is low, typically in the range of ppb to ppm with an average of about 12 ppm (Dickson and Scott, 1997).

Th is a constituent of the accessory minerals zircon, monazite, allanite and xenotime, apatite and sphene. Table 9.2 lists these with their average Th content, along with other minerals that have Th as a major constituent. Th is the parent of a decay series of which the highest energetic gamma rays (2.62 MeV) are emitted by the daughter isotope ^{208}Tl. In general, about 60 years is required to establish radioactive equilibrium in the Th series, and gamma ray

activity is thus a good measure of Th concentration. Chemical fractionation among the members of the U and Th series occurs during magmatic processes. This results in radioactive disequilibrium between ^{238}U and ^{230}Th, and ^{230}Th and ^{226}Ra in the ^{238}U decay series in volcanic rocks (Krishnaswami, 1999).

TABLE 9.2. THORIUM MINERALS.

Thorium Minerals	**Chemical Formula**	**% ThO_2**
Minerals with Th as major constituent		
Huttonite	$ThSiO_4$	80
Thorite, Uranothorite	$ThSiO_4$, $(Th,U)SiO_4$	50, < 50
Cheralite	$(Th,Ce,Ca)(SiO_4PO_4)$	30
Thorianite, Uranothorianite	ThO_2, $(Th,U)O_2$	80, < 80
Common accessory minerals		
Monazite	$(REE,Th)PO_4$	10
Xenotime	YPO_4	0.4-1
Zircon	$ZrSiO_4$	0.01-1
Allanite	(Ca,Al,Fe,Mg) silicate	0.1-1
Apatite	$Ca_5(PO_4)_3(F,Cl,OH)$	0.001-0.1
Sphene	$CaTiSiO_5$	0.001-0.1
Epidote	$CaFe^{3+}Al_2O.OH(Si_2O_7)(Si_2O_4)$	0.005-0.05

Uranium

Uranium is a reactive metal with an average abundance of about 3 ppm in the Earth's crust. U appears in the valence state U^{4+} in igneous rocks with crystallochemical properties close to Th^{4+} and the Light Rare Earth Elements (LREE), which explains the coherent geochemistry of U, Th and LREE in igneous rocks (Bea, 1999). This coherence is lost in hydrothermal and supergene conditions, where uranium is partially or totally oxidized to U^{6+}, which forms soluble complexes with the anions: CO_3^{2-}, SO_4^{2-} and PO^{3-} (Langmuir and Hermans, 1980).

The most abundant uranium minerals are listed in Table 9.3. Uraninite is common as minute inclusions in the rock forming minerals in granites or as large grains in mineralized granites and pegmatites. Uraninite also occurs in hydrothermal veins and sedimentary rocks. The accessory minerals zircon, monazite, apatite, allanite and sphene are common in igneous and metamorphic rocks, of which zircon and monazite are the most resistant to weathering. As U becomes mobile under supergene conditions, a large variety of U^{6+} minerals may form. This explains the variety of minerals found in uranium deposits, including silicates, phosphates, carbonates, sulphates, vanadates, molybdates, niobates, tantalates and titanates (Bea, 1999).

9.1.3. Distribution of the radioelements in rocks and soils

Scott and Dickson (1990) analyzed the radioelement content of Australian rocks and soils by laboratory gamma ray spectrometry. Their results are given in Table 9.4. The radioelement concentrations show an increase in average radioelement concentration with an increase of SiO_2 (Figure 9.1). For thorium and uranium this is due to the high charge and radius of the Th^{4+} and U^{4+} ions, which excludes them in the substitutions of major ions in the crystallization of early rock forming minerals. They are therefore accommodated in accessory minerals, such as zircon, allanite and monazite. Potassium is also highly incompatible during crystallization of magma. Earlier studies by the Geological Survey of Canada (Killeen, 1979) concentrated mainly on igneous rocks. The results are summarised in Table 9.5.

TABLE 9.3. URANIUM MINERALS

Uranium Minerals	Chemical Formula	% UO_2/ppm U
Minerals with U as major constituent		
Uraninite, (Pitchblende)	UO_2	
Betafite	$(U,Ca)(Nb,Ta,Ti)_3O_9.nH_2O$	
Huttonite	$ThSiO_4$	100-20000 ppm
Uranospherite	$(BiO)(UO_2)(OH)_3$	
Thorite, Uranothorite	ThSiO4, $(Th,U)SiO_4$	1-35%
Thorianite, Uranothorianite	ThO_2 $(Th,U)O_2$	5%
Common accessory rock forming minerals		
Zircon	$ZrSiO_4$	5%
Xenotime	YPO_4	5%
Monazite	$(REE,Th)PO_4$	100-20000 ppm
Allanite	(Ca,Al,Fe,Mg) silicate	10-2000 ppm
Apatite	$Ca_5(PO_4)_3(F,Cl,OH)$	5-200 ppm
Sphene	$CaTiSiO_5$	10-500 ppm

TABLE 9.4. RADIOELEMENT CONTENT OF AUSTRALIAN ROCKS AND SOILS (AVERAGE VALUES IN BRACKETS) AFTER DICKSON AND SCOTT (1997)

Rock type	Rock			Soil		
	K(%)	U(ppm)	Th(ppm)	K%	U(ppm)	Th(ppm)
Intrusives						
Granitoids	0.3-4.5 (2.4)	0.4-7.8 (3.3)	2.3-45 (16)	0.4-3.9 (2.1)	0.5-7.8 (2.7)	2-37 (13)
Gneissic rock	2.4-3.8 (2.4)	2.1-3.6 (2.5)	18-55 (15)	0.7-1.9 (1.3)	1.6-3.8 (2.2)	6-19 (12)
Pegmatite	2.6-5.5 (3.7)	0.3-1 (0.7)	0.3-9.6 (2)			
Aplites	0.6-4 (2.4)	1-8 (3.3)	3-20 (7)			
Quartz-feldspar porphyry	1-5 (2.9)	1.3-2.9 (1.7)	6-14 (13)			
Intermediate intrusives	0.7-5.6(2.7)	0.1-1.2 (0.8)	0.8-6.1 (2.4)	0.7-3.4 (1.6)	1.5-2.3 (1.9)	2.9-8.4 (5.6)
Mafic intrusives	0.1-0.8 (0.4)	0.0-1.1 (0.3)	0.0-3.1 (1.2)			
Extrusives						
Felsic volcanics	2.0-4.4 (3.7)	1.4-13 (2.4)	13-28 (17)	1.8-3.2 (2.4)	1.3-2.4 (2.1)	10-18 (13)
Intermediate volcanics	1.8-4.1 (2.7)	0.9-5.6 (2.3)	1.5-15 (9)	1.0-2.7 (1.9)	1.2-3.6 (2.1)	4-17 (10)
Low-K andesites	0.7-0.9 (0.8)	1.0-2.5 (1.6)	3-8 (5)	0.8-1.5 (1.1)	1.2-1.5 (1.3)	4-6 (5)
Mafic volcanics	0.3-1.3 (0.9)	0.3-1.3 (0.7)	2.0-5.0 (3.0)	0.2-1.4 (0.7)	0.6-2.5 (1.6)	3.3-13 (7.9)
Ultramafic volcanics	0.2-0.9 (0.4)	0.3-0.9 (0.6)	0.0-4.0 (1.2)	0.6	2.0	6
Sedimentary rocks						
Archean shales	0.4-1.6 (0.9)	0.3-1.3 (0.9)	1-5 (2.7)	0.8	1.2	3
Other shales	0.1-4.0 (2.6)	1.6-3.8 (2.6)	10-55 (19)	0.7-3.0 (1.5)	1.2-5 (2.3)	6-19 (13)
Arenites	0.0-5.5 (1.8)	0.7-5.1 (2.3)	4-22 (12)	0.1-2.4 (1.3)	1.2-4.4 (2.1)	7-18 (11)
Carbonates	0.0-0.5 (0.2)	0.4-2.9 (1.6)	0-2.9 (1.4)			

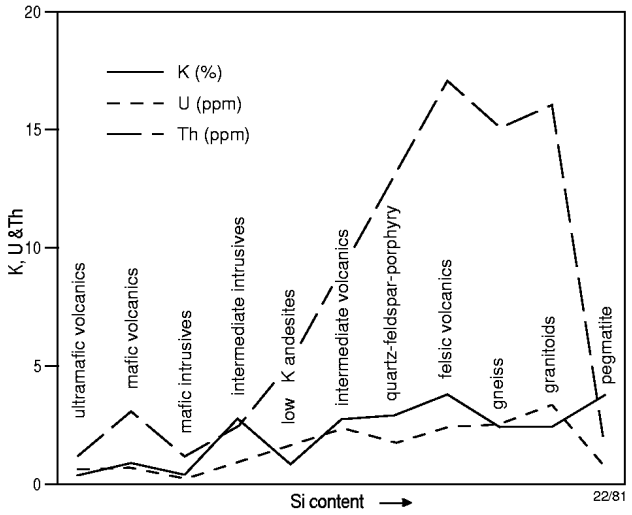

FIG. 9.1. Variation in average K, U and Th content for igneous rocks with increasing acidity (Si content)(From Dickson and Scott (1997).

TABLE 9.5. RADIOELEMENT CONCENTRATIONS IN DIFFERENT CLASSES OF ROCKS (after Killeen, 1979)

Rock Type	**Potassium (%)**		**Uranium (ppm)**		**Thorium (ppm)**	
	Mean	Range	Mean	Range	Mean	Range
Acid Extrusives	3.1	1.0 – 6.2	4.1	0.8 – 16.4	11.9	1.1 – 41.0
Acid Intrusives	3.4	0.1 – 7.6	4.5	0.1 – 30.0	25.7	0.1 – 253.1
Intermediate Extrusives	1.1	0.01 – 2.5	1.1	0.2 – 2.6	2.4	0.4 – 6.4
Intermediate Intrusives	2.1	0.1 – 6.2	3.2	0.1 – 23.4	12.2	0.4 – 106.0
Basic Extrusives	0.7	0.06 – 2.4	0.8	0.03 – 3.3	2.2	0.05 – 8.8
Basic Intrusives	0.8	0.01 – 2.6	0.8	0.01 – 5.7	2.3	0.03 – 15.0
Ultrabasic	0.3	0 – 0.8	0.3	0 – 1.6	1.4	0 – 7.5
Alkali Feldspathoidal Intermediate Extrusives	6.5	2.0 – 9.0	29.7	1.9 – 62.0	133.9	9.5 – 265.0
Alkali Feldspathoidal Intermediate Intrusives	4.2	1.0 – 9.9	55.8	0.3 – 720.0	132.6	0.4 – 880.0
Alkali Feldspathoidal Basic Extrusives	1.9	0.2 – 6.9	2.4	0.5 – 12.0	8.2	2.1 – 60.0
Alkali Feldspathoidal Basic Intrusives	1.8	0.3 – 4.8	2.3	0.4 – 5.4	8.4	2.8 – 19.6
Chemical Sedimentary Rocks	0.6	0.02 – 8.4	3.6	0.03 – 26.7	14.9	0.03 – 132.0
Carbonates	0.3	0.01 – 3.5	2.0	0.03 – 18.0	1.3	0.03 – 10.8
Detrital Sedimentary Rocks	1.5	0.01 – 9.7	4.8	0.1 – 80.0	12.4	0.2 – 362.0
Metamorphosed Igneous Rocks	2.5	0.1 – 6.1	4.0	0.1 – 148.5	14.8	0.1 – 104.2
Metamorphosed Sedimentary Rocks	2.1	0.01 – 5.3	3.0	0.1 – 53.4	12.0	0.1 – 91.4

The ranges derived from the average values of the individual units show substantial overlap. This suggests that no global classification based on radioelement content is possible. Thorium generally shows a much larger increase in comparison to U, and the Th/U ratio can be used as an indication of the degree of differentiation (Dickson and Scott, 1997). The tendency for the radioelement concentrations to increase with increasing Si content in igneous rocks breaks down at high concentrations of Si (> 70 wt. % SiO_2), particularly for U. In peraluminous S-type granites, two trends have been observed above 70 wt. % SiO_2. The normal evolution produces leucocratic differentiates, extremely depleted in U, Th, Y and LREE due to

monazite, +xenotime +zircon fractionation (Bea et al., 1994). In other cases, the U concentration increases in the residual melt due either to complexation with Cl or CO_2 or to the above-mentioned partial oxidation of U^{4+} to U^{6+}.

9.1.4. Geomorphologic and weathering processes

The geomorphology and weathering in a given area play a critical role in the distribution of radioelement concentrations at the earth's surface. Dickson and Scott (1997) studied the variations in radioelement concentrations in the upper few meters of the soil profile in moderately to highly weathered terrains of eastern Australia. Where the surface material has been weathered in-situ, and is derived from the underlying bedrock, the radioelement concentrations in relative and absolute terms may vary significantly through the profile. This is evident to some extent in Table 9.4. Several factors affect the variation between surficial and bedrock responses, including:

1. deposition of radium (e.g. at groundwater seepage sites) produces disequilibrium in the uranium and thorium decay series;
2. radon loss, which depends on soil particle size and moisture content, reduces the measured uranium signal;
3. general loss of K during pedogenesis;
4. weathered felsic rocks show loss of U and Th;
5. weathered intermediate to mafic/ultramafic rocks show increased U and Th, more so with increasing basicity;
6. removal of easily weathered minerals from granites (e.g. potassium enrichment through K-feldspar alteration);
7. kaolinization of granites results in preferential K-depletion;
8. K-depletion and U and Th-concentration in iron oxides for mafic volcanics (similar for intermediate intrusives);
9. K-depletion through pedogenesis of shales; and
10. K and Th-enrichment through silicification of shales.

This list is by no means complete. However, it illustrates that the interpretation of the radioelement concentrations of soils requires a thorough understanding of the local weathering processes. The interpreter needs to understand the effect of weathering of rocks and soils on the distribution of the radioelements in order to produce a geological map or determine the provenance of the soils.

Other factors that affect the radioelement concentration in soils (Dickson and Scott, 1997) include:

1. clay eluviation (i.e. clay filling fractures) results in U and Th build-up;
2. colluvial and aeolian transport overprint soil signatures of the source material; and
3. local soil movement will obscure or shift the apparent location of geological unit boundaries.

The surficial products of weathering in the regolith may have substantially different radiometric signatures than the underlying bedrock from which they were derived. For example (Dickson and Scott, 1997):

1. calcrete will generally have low radioelement concentrations relative to the bedrock;
2. ferricrete and iron-rich pisoliths concentrate Th, and to some extent U, but are low to severely depleted in K; and
3. gossan signatures depend on the source rocks (e.g. U-enrichment over sediments and felsic rocks, U-depletion over mafic/ultramafic rocks).

Geomorphology combines with weathering, erosion and the source rocks to control the radioelement distribution in the surficial material. There is a trade-off in the effects on the radioelement concentrations between weathering and deposition, depending on the erosional activity at a specific location. In active depositional regimes, the radioelement concentrations in the surface material are more likely to resemble those of the source rocks, although these sediments may have been transported over significant distances.

Wilford et al. (1997) have undertaken extensive studies for three areas in Australia, which provide a wealth of radiometric responses due to different geomorphologic and weathering processes. Some of their important conclusions are:

1. topographic relief affects the degree of erosion versus in-situ weathering;
2. topographic relief affects the types of clay and other weathering products developed;
3. topographic relief affects the composition, sorting and thickness of soil deposits;
4. soil composition is affected by types of water transport (e.g. river channels, flood plains); and
5. mobilization of the radioelements by groundwater flow and leaching varies (e.g. K is typically far more mobile that U or Th).

Gamma ray spectrometry thus provides an important tool for soil mapping, particularly the style of weathering, degree of leaching, acidity, texture, nutrient status, thickness and geomorphic activity. Areas of groundwater discharge and recharge, and its effect (e.g. soil salinity), can also be identified. In highly weathered terrains, it may be necessary for ground truth studies to incorporate measurements in augur holes or trenches.

9.2. Geological mapping

Gamma ray spectrometric data have been applied with variable degrees of success to the mapping of lithological units. The degree to which bedrock units can be delineated depends on many factors. The most important factors are:

1. the contrasts in radioelement content between lithological assemblages;
2. the extent of bedrock exposure and soil cover;
3. the relative distribution of transported and in-situ soils;
4. the nature and type of weathering;
5. the soil moisture content; and
6. the vegetation cover.

Unlike U, the average K and Th content of soils reflect the average K and Th content of the rocks from which they are derived. But the differences in soil radioelement concentrations are relatively small (Table 9.4; Dickson and Scott, 1997).

In general, a useful strategy for geological mapping is to first outline the major lithological units and than enhance the radioelement patterns within the individual units. A regional geological mapping example from the Pilbara, Australia, with outlines of major batholiths and greenstone belts, is shown in Figure 9.2. The ternary maps presented in Chapter 7 (Figures 7.14 and 7.15) show detailed views of the Pilbara and illustrate the richness in additional lithological details that can be extracted from these broad assemblages.

Enhanced products of gamma ray spectrometry data have often assisted in detailed mapping or further subdivision of lithological units. In some cases units with distinct radioelement signatures (mostly volcanic in origin) were identified that could be used as lithological markers in unravelling the geological map pattern in complex areas (Jaques et al., 1997). Integrated interpretation with aerial photograph, satellite imagery and other airborne geophysical data sets allows exploiting the complementary geological information and enables the radioelement distributions to be studied in a structural geologic and geomorphologic context.

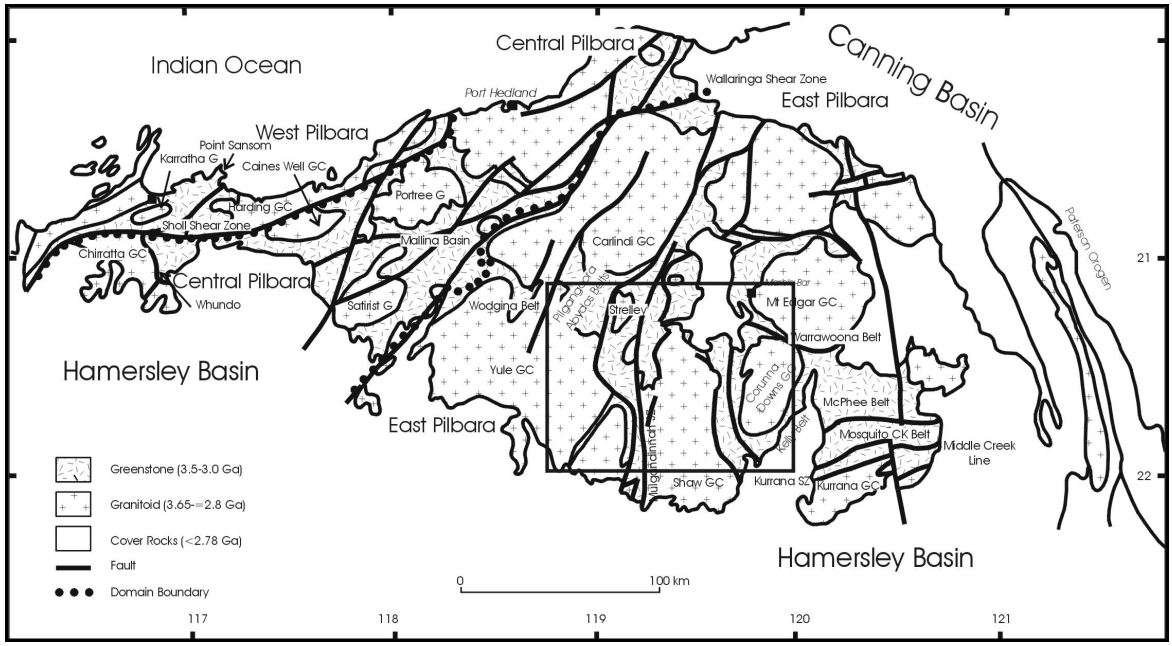

FIG. 9.2. Geological mapping example from the Pilbara, Australia. Outline indicates the area imaged in the ternary radioelement maps shown in Figures 7.14 and 7.15.

Gamma ray spectrometric data have shown to be uniquely applicable for mapping subtle compositional variations within igneous suites, particularly granitoid plutons and batholiths (Broome et al., 1987; Charbonneau, 1991; Goossens, 1992; Jaques et al., 1997; Wellman, 1998; Schetselaar, 2002). Zonation patterns in granites have been commonly recognized in gamma ray spectrometry surveys, many of which were not recognized by conventional field mapping (Broome et al., 1987; Schetselaar, 2002). This is because the bulk of the radioelements in igneous rocks occur within accessory minerals, such as monazite, xenotime, zircon, allanite, sphene and apatite. Subtle (but diagnostic) variations in the concentrations of these accessory phases are difficult to recognize in bedrock exposures. Also, late-stage magmatic and hydrothermal processes may control regional radioelement distributions in granitoids, particularly U.

Normal zoning in granitoid plutons formed by fractional crystallization, show a gradual increase in K and Th (and Th/U) from the margin to the centre. Along this path the SiO_2 content gradually increases and the mafic index decreases with the lithological composition ranging from quartz diorite through granodiorite to granite.

The positive correlation between SiO_2 and the radioelements breaks down in the last stages of magmatic differentiation when highly felsic pegmatites and aplites (with potentially high U concentrations) are emplaced. However, these late magmatic phases may be too small (aerially) to be detected by gamma ray surveys (Dickson and Scott, 1997).

Zoned granitoid plutons formed as a result of magmatic fractionation within a single magmatic pulse are relatively rare in nature. Many of the compositional variations in granitoid plutons are actually composed of distinct intrusive phases with relatively discrete boundaries. Such composite plutons were formed in multiple magmatic pulses that can both resemble normal or inverse zoning (Pitcher, 1993).

Thin section studies are useful to establish the mode of occurrence and textural associations of K, Th and U-bearing minerals, which in combination with trace element analyses shed light on the petrogenetic associations of the radioelements. Charbonneau (1991) and Charbonneau et al. (1997), for example, observed in the study of several peraluminous granites of the Canadian Shield that monazite and zircon are commonly spatially associated to biotite and Ti-Fe oxides (Figure 9.3). This spatial association between radioactive accessory minerals and early crystallising phases, particularly biotite, has important implications for the interpretation of gamma ray spectrometry surveys over granitoids. This association may be interpreted as restite (in which clusters of biotite with radioactive minerals, such as zircon and monazite are solid state residues) or to result from the nucleation of accessory minerals by the local saturation of slowly diffusing rare earth elements, (including Th, U) rejected from the hosting crystal/liquid interface of phenocrysts (Bacon, 1989). Variations in the distribution in U and Th over granitoid plutons may therefore, in addition to magmatic differentiation and hydrothermal processes, also reflect differentiation related to the separation of restite from the source rocks.

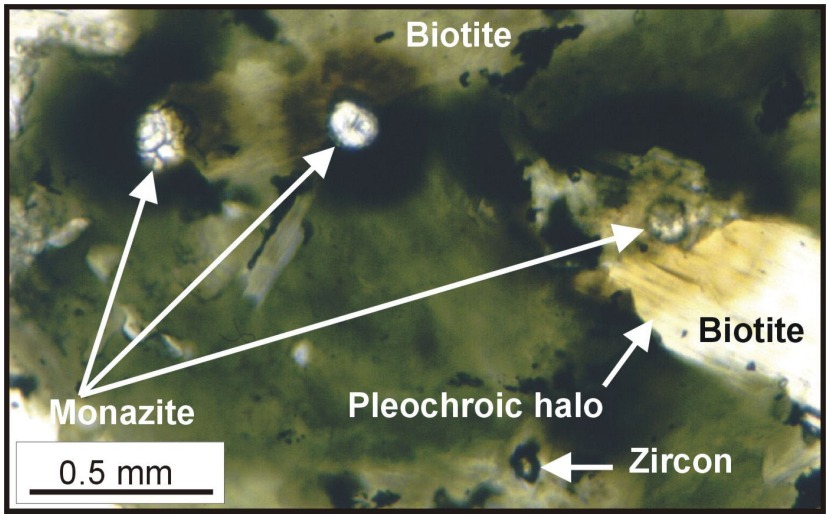

FIG. 9.3. Photo-micrograph of biotite crystals with inclusions of monazite and zircon in peraluminous granite. Pleochroic halos around monazite indicate damage of the crystal lattice of biotite by alpha radiation from Th and/or U decay.

Quantitative approaches to the estimation of the radioelement concentration within accessory minerals are based on radiometric methods, whole rock trace element analysis, and microprobe and fission track analysis. Barritt (1983), for example, used mass-balance equations to compute the contributions of accessory phases to whole rock Th and U concentrations for estimating radiogenic heat production of granite plutons in the Scottish Highlands.

Gamma ray spectrometry surveying also offers a promising tool for lithofacies mapping of sedimentary basins as evaporites, carbonates, sandstones and shales can usually be differentiated on their radioelement content and because clastic sediments often reflect the radioelement compositions of the provenance source materials (Dickson and Scott, 1997).

9.3. Regolith and soil mapping

Billings (1998) and Wilford et al. (1997) recently reviewed the application of airborne gamma ray spectrometry to regolith and soil mapping. The interpretation of aerial photography and satellite imagery has been the traditional means for the rapid mapping of soil types over large areas. The soil properties are inferred from differences in vegetation and from differences in landforms. But these features are easily obscured by the impact of land use by humans, cultural features, and the effect of bush fires. However, the gamma ray spectrometric response is unaffected by these disturbances. Also, the distribution of K, U and Th in the natural environment is controlled by many of the same factors that control the distribution of soil types. The method is thus being increasingly used for soil and regolith mapping.

In general, the gamma ray method appears to be most useful for soil and regolith mapping when it is interpreted in conjunction with other sources of information such as topography, aerial photography and satellite imagery (Cook et al., 1996; Bierwirth, 1996; Wilford, 1992 and 1995; Wilford et al., 1997).

The gamma ray spectrometric response of rocks and soils varies with the climate to which the area surveyed has been subjected. This is because the response due to fresh bedrock, weathered rocks and transported material differ. Figure 9.4 (after Dickson & Scott, 1997) shows variations in radioelement concentration of basalt with depth due to weathering.

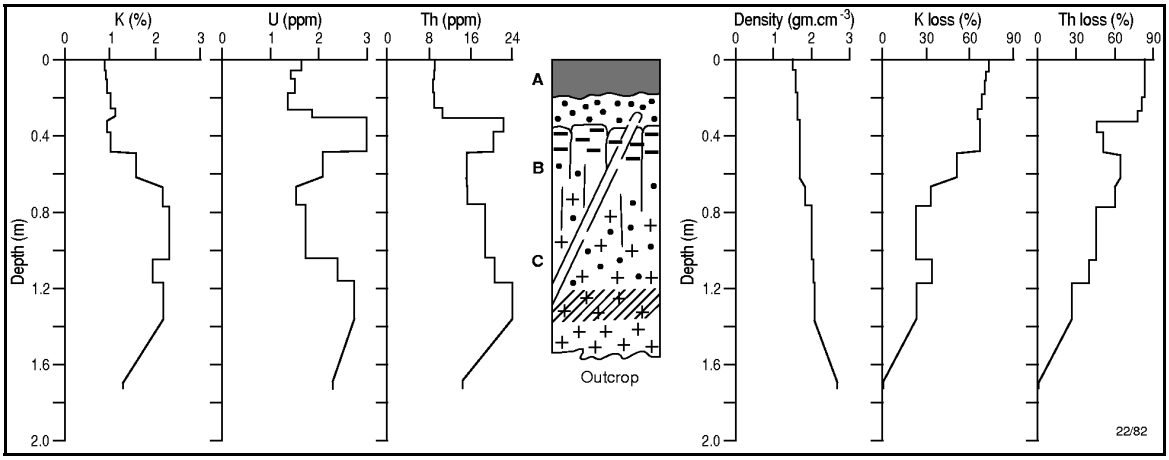

FIG. 9.4. Distribution of K, U and Th in a soil profile over adamellite, Sutton, New South Wales, illustrating the effects of clay elevation in the upper section of the profile (from Dickson and Scott, 1997).

Thus, weathering modifies the concentration and distribution of the radioelements relative to that of fresh bedrock. The gamma ray method can therefore provide information on geomorphic processes and soil/regolith properties (Wilford et al., 1997). The gamma ray data can be used to distinguish between areas of active weathering and erosion as opposed to deposition. Since the gamma ray response to weathering is often specific to the local geology, interpretations are best confined to particular geological groups or units.

9.4. Direct detection of mineralization

The most direct application of gamma ray spectrometry surveys during the 1970's and 1980's was the search for U and Th deposits (e.g. Dickson and Scott, 1997). U and Th anomalies may be identified on profile and grid presentations of the data. Ratioing and statistical image processing techniques (Chapters 7 and 8) can enhance subtle anomalies. Anomalies can be

followed up on the ground using portable gamma ray spectrometers. Geochemical analysis and microscopic studies of samples from rock or sediments are needed to fully identify the mineral phases that constitute the radioelements (see for example Charbonneau et al., 1997).

The character of radiometric anomalies associated with subsurface and outcropping U mineralization depends on the forms of U mineralization, the host rock, and the geological setting (Krasnov et al., 1975, Krasnov et al., 1980). Typical features of U mineralization detected at the earth's surface are:

1. elliptical dispersion halos with dimensions from 70 × 80 m up to 80 × 350 m;
2. anomalous U concentrations in the range 4-20 ppm eU;
3. associated Th anomalies in the range 5-40 ppm eTh;
4. ratios between the radioelement of Th/U<1, U/K>5-10, Th/K in the range 4-5; and
5. increasing gamma radiation with depth.

Due to relatively low penetration of gamma rays through rock and soil, the probability of discovery of uranium mineralization is dependent on the U concentration in the source, its surface dimensions, and the positions of the measured profiles. A small outcrop of high-grade U mineralization is a more difficult target for U exploration than low-grade mineralization with extensive surface outcrop. For example, in a high radioactivity granitic environment, a U anomaly at the 3σ confidence level would be detected by an 8.4 litre NaI(Tl) detector at 80 m height for circular outcropping sources with: 4 m diameter and 4860 ppm eU; 36 m diameter and 53 ppm eU; or 100 m diameter and 9 ppm eU (Matolin, 1980).

Several 4-12 ppm eU anomalies were mapped in airborne survey of the Urt mineral zone in Janchivlan region, 60 km southeast of Ulan Bator, Mongolia. The anomalies are within a coarse-grained porphyric biotite granite of Mesozoic age with U concentration of about 4 ppm. Ground follow-up using a portable spectrometer and radon soil gas measurement verified the presence of U mineralization. K, U and Th concentrations and their ratios mapped the mineralized zone (Figure 9.5). The high ^{222}Rn activity concentration illustrates the utility of emanometric methods for the exploration of subsurface U mineralization.

Systematic uranium exploration, based mainly on radiometric methods, was carried out in the Czech Republic between 1946 and 1990. This led to the discovery of 16846 U occurrences and 164 U deposits and U ore objects. Table 9.6 shows the radiometric methods and their efficiency in discovery of these U deposits (Suran, 1998). The most effective methods were radon surveys to a depth of 1 m, radiometric surveying of old mine and exploration sites, car-borne methods, and drilling in sedimentary basins. Airborne gamma ray spectrometry was applied after intensive ground exploration for U at the beginning of the 1960's. Airborne surveys mapped the regional radioactivity of the country, and led to the discovery of U deposits in the Sokolov Tertiary sedimentary basin, northwest Bohemia.

U ore reserves estimated by gamma ray spectrometry should be corrected for possible disequilibrium between ^{238}U and ^{226}Ra. Several methods of directly estimating U were developed and tested for borehole measurements in the 1970's. These make use of radiation originating directly from U atoms. X-ray fluorescence for the direct determination of U focuses on detection of the U-$K_{\alpha 1}$ 98.428 keV line (Lubecki and Wolf, 1978). Neutron methods are based upon the detection of prompt fission neutrons (Smith, 1977), or delayed fission neutrons (Steinman et al., 1976; Givens et al, 1976), originating from the interaction of neutrons with ^{235}U atoms.

Dickson and Scott (1997) provide an up-to-date review of the effect of hydrothermal processes, alteration and weathering on radioelement distribution. These processes do not only have implications for the direct detection of U and Th from gamma ray spectrometry surveys, but also for detecting a number of metal deposits. These include granophile deposits

of Sn, W and Mo, porphyry Cu-Au mineralization, gold mineralization and stratabound polymetallic mineralization. The relationships between radioelement distribution and each of these deposit types are varied and complex. A thorough understanding of the effects of silicification, K-alteration, weathering processes and local lithological variations is required to evaluate the mineralization potential associated with radioelement anomalies.

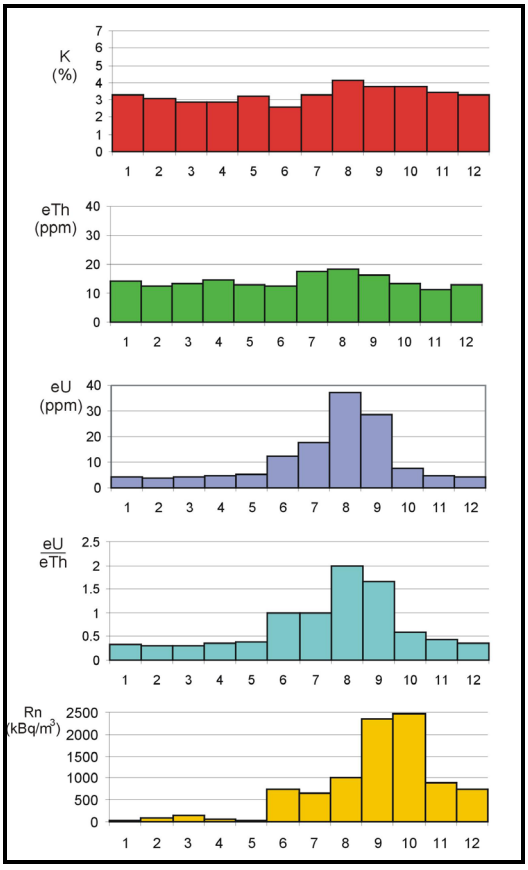

FIG. 9.5. K, U, Th concentrations and ^{222}Rn activity concentration oven U mineralization in the Urt mineral zone, Mongolia (Matolin, 1994).

TABLE 9.6. EFFECTIVENESS OF RADIOMETRIC METHODS IN U EXPLORATION IN THE CZECH REPUBLIC IN THE PERIOD 1946 - 1990 (Suran, 1998)

Method	Number of U ore occurrences discovered	Percentage of discovered U occurrences (%)
Radiometric revision of mining activities	37	23
Airborne gamma survey	4	3
Car-borne gamma survey	14	9
Radon survey to the depth 1 m	66	40
Radon (and gamma) survey to the depth 2 m	5	3
Surficial gamma survey	12	7
Gamma survey in shallow holes	2	1
Gamma survey to the depth 15 m	7	4
Combination of radiometric methods	2	1
Gamma survey in boreholes	15	9

The detection of K-alteration by gamma ray spectrometry surveys has received particular attention, as it has resulted in several mineral discoveries (Dickson and Scott, 1997; Shives et al., 1997). K alteration halos can be repeatedly distinguished from normal K variations by their characteristic low Th/K ratios (Shives et al., 1997).

A high-resolution magnetic/radiometric survey, undertaken by the Geological Survey of Canada in 1994, delineated a large hydrothermal system in the Lou Lake area, Northwest Territories, Canada (Shives et al., 1997). Figure 9.6 shows that the hydrothermal system is characterized by enrichment of potassium and magnetite within a volcano-plutonic magmatic zone. The potassium enrichment is evident as a potassium high, and confirmed by a low in the ratio of Th/K (i.e. preferential enrichment of potassium relative to thorium). The magnetite enrichment produces a significant magnetic anomaly. The Sue-Dianne polymetallic (Au-Co-Cu-Bi-W-As) deposit is located 20 km north of this hydrothermal system. It was originally discovered by exploring for the source of a uranium and U/Th ratio anomaly measured during a regional survey in 1974. A uranium halo around the edges of the hydrothermal system (high values in the ratio of U/Th) correlates with several veins of pitchblende. The geophysical responses to the alteration and uranium mineralization are clearly seen in profile form (Figure 9.7). Mapping the alteration system leads directly to the polymetallic deposits (Figure 9.8). Ground truth studies show that the effects of hydrothermal potassium enrichment within each lithologic unit are easily measured using gamma ray spectrometry (Figure 9.9).

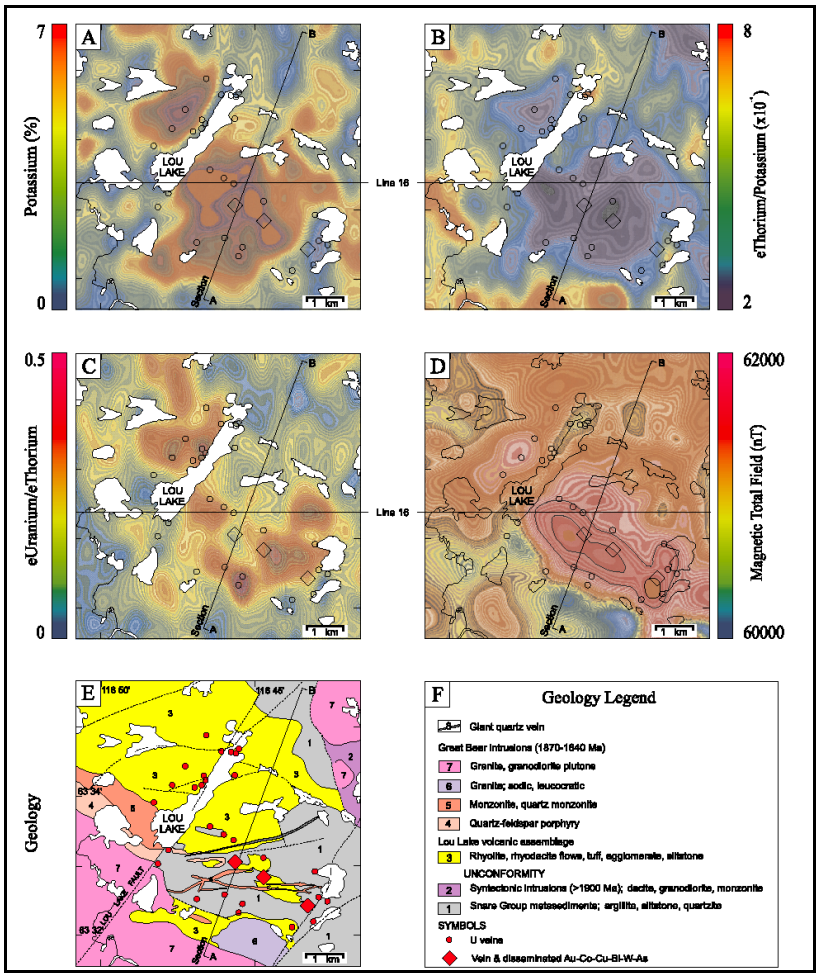

FIG. 9.6. Radiometric responses, magnetic response and the geology of the Lou Lake area, Northwest Territories, Canada. Polymetallic mineralization associated with potassium and magnetite-enriched hydrothermal system. Uranium enrichment occurs on the margins of the hydrothermal system (after Shives et al., 1997).

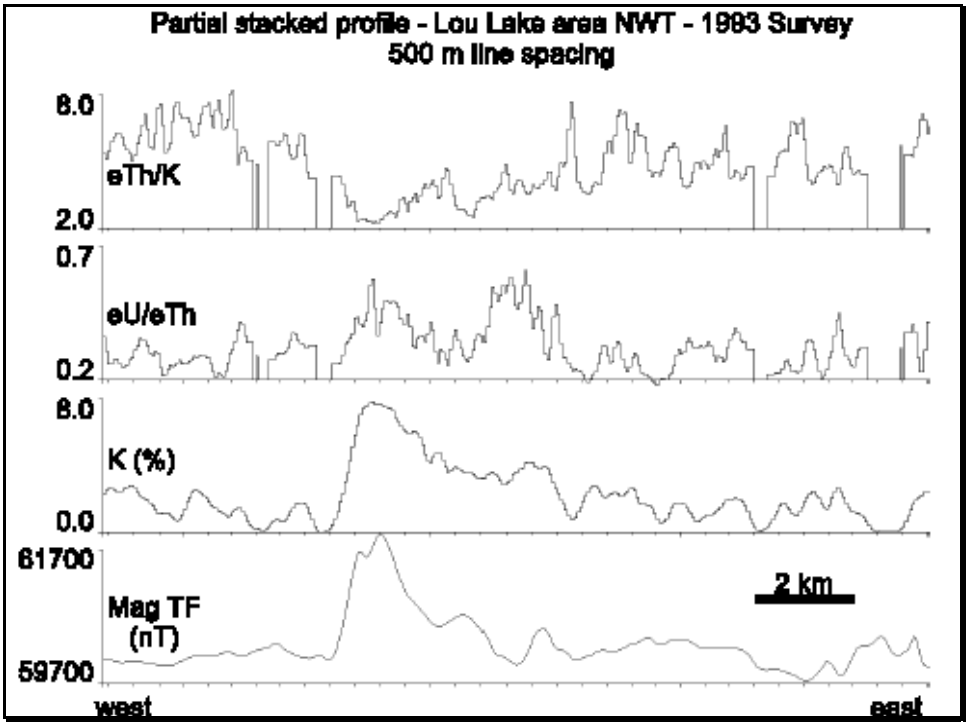

FIG. 9.7. Radiometric responses and magnetic response for flight line 16 (see FIG. 9.6) of the Lou Lake area, Northwest Territories, Canada. The hydrothermal system is evident in the high potassium and magnetic responses, and the coincident low in eTh/K. The high responses in eU/eTh reflect uranium mineralisation (after Shives et al., 1997).

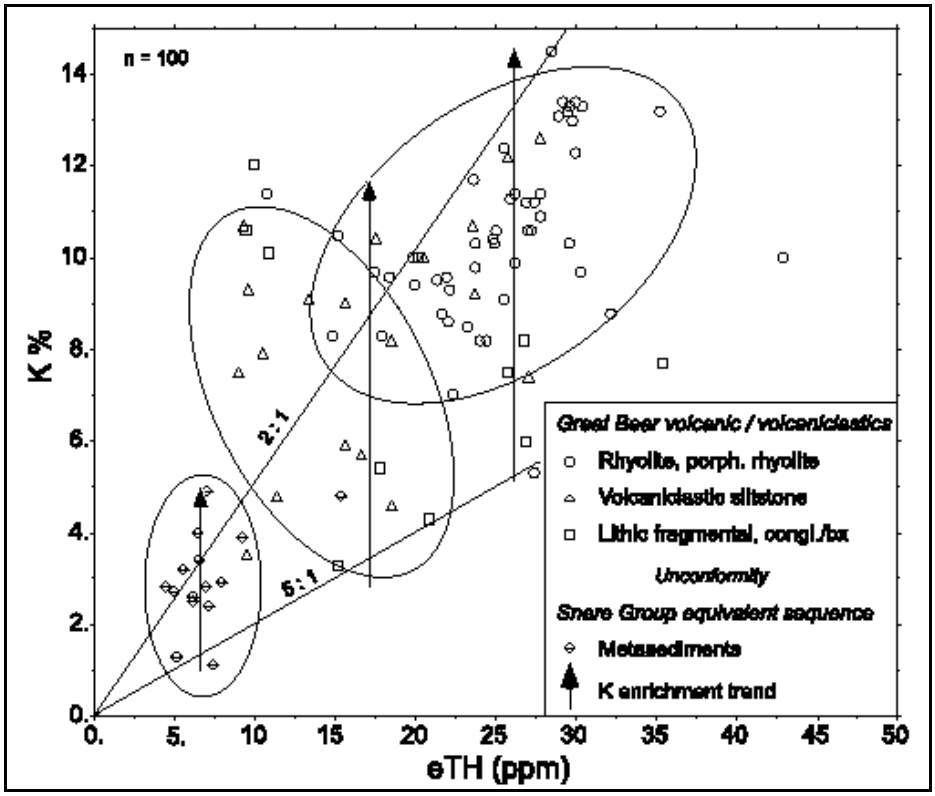

FIG. 9.8. Potassium versus thorium concentrations determined by in-situ gamma ray spectrometry, from the Lou Lake area, Northwest Territories, Canada. Increasing potassium within a lithologic unit reflects the hydrothermal potassium enrichment (after Shives et al., 1997).

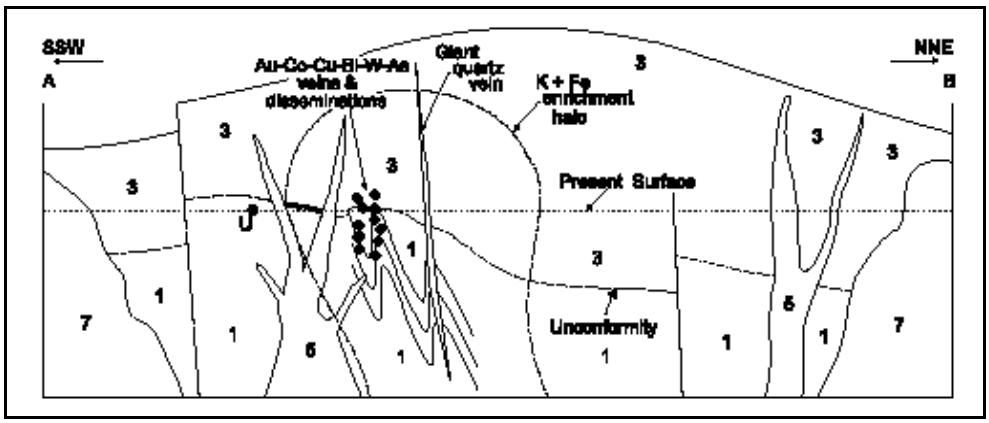

FIG. 9.9. Geological cross-section for line A-B (see FIG. 9.6) of the Lou Lake area, Northwest Territories, Canada, showing the mineralization relative to the halo of potassium and magnetite hydrothermal enrichment (after Shives et al., 1997).

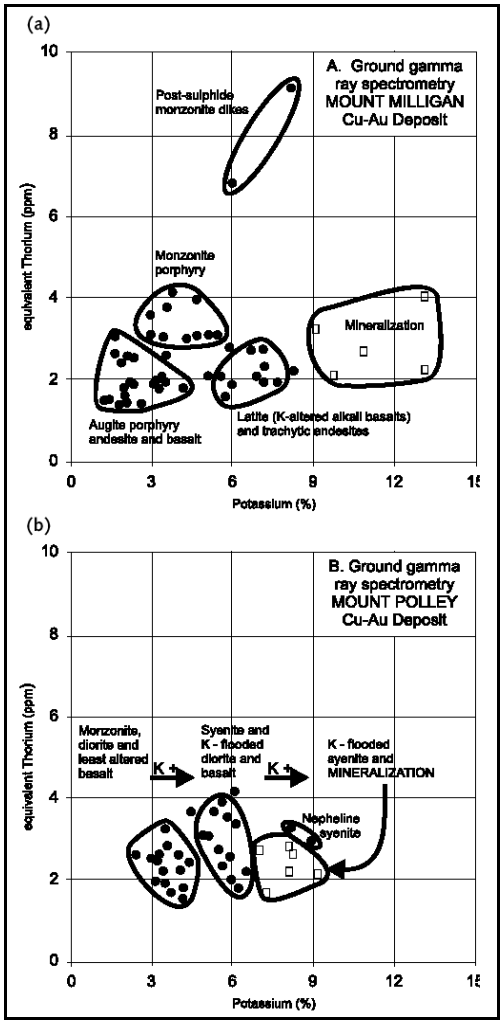

FIG. 9.10. Potassium versus thorium concentrations determined by in-situ gamma ray spectrometry, over the Mount Milligan (a) and Mount Polley (b) porphyry copper-gold deposits, British Columbia, Canada. Increasing potassium within a lithologic unit reflects the potassium enrichment associated with the mineralization (after Shives et al., 1997).

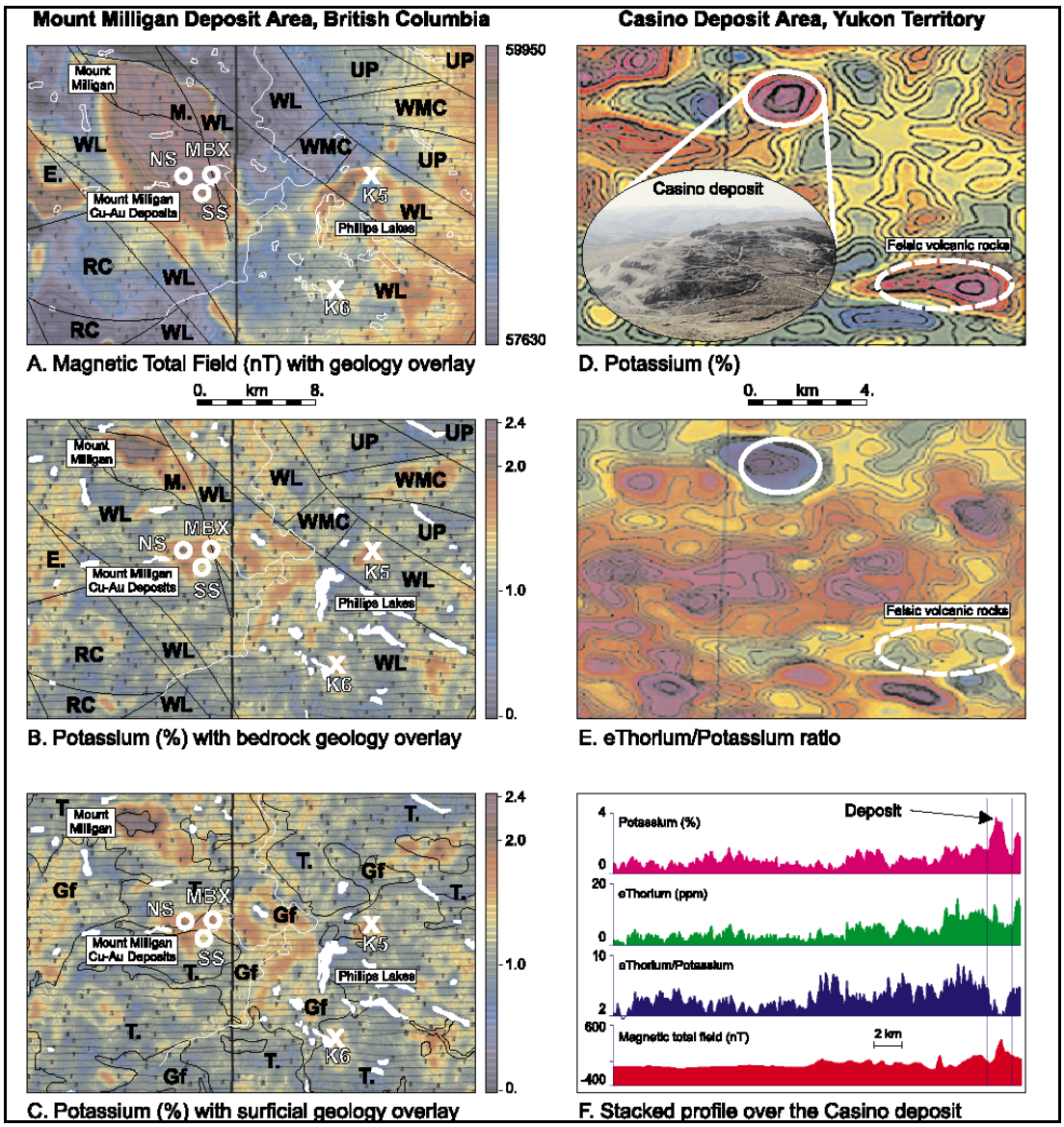

FIG. 9.11. A-B-C: Potassium response, magnetic response and geology over the Mount Milligan porphyry copper-gold deposit, British Columbia, Canada. Mount Milligan intrusive complex shows high magnetic and potassium responses, whereas the mineralised zones show more discrete, lower amplitude potassium anomalies. D-E-F: Radiometric responses over the Casino porphyry gold-copper-molybdenum deposit, Yukon Territory, Canada. Deposit distinguished by potassium enrichment (potassium high and coincident eTh/K low) (after Shives et al., 1997).

The radiometric signatures of several porphyry systems in the Canadian Cordillera have been studied (Figures 9.10 and 9.11). They demonstrate the need to process the data, to differentiate between lithologic and alteration signatures (e.g. preferential enrichment of potassium versus thorium).

More than thirty Canadian examples of geological mapping and mineral deposit characterization are provided in Shives et al. (1995), using airborne gamma ray spectrometry and systematic ground truthing. The deposit types covered include:

1. volcanic-hosted massive sulphides with associated potassium enrichment;
2. volcanic-hosted epithermal base and precious metals with associated potassium enrichment;

3. granite-hosted gold associated with illite alteration (potassium enrichment);
4. metavolcanic/metasediment-hosted gold with hydrothermal alteration (potassium enrichment);
5. metasediment-hosted skarn mineralization (Au-U-W-Mo-Co);
6. porphyry-hosted gold-uranium and copper–gold (molybdenum) with hydrothermal alteration (potassium enrichment);
7. metasediment-hosted polymetallic (Bi-Cu-Co-Au-As) with hydrothermal alteration (potassium enrichment);
8. carbonatite-hosted rare earth elements;
9. syenite-hosted rare metal/rare earth elements associated uranium enrichment;
10. dolomite-hosted epigenetic uranium-copper;
11. limestone-hosted uranium;
12. uraniferous pegmatites; and
13. metasediment-hosted pitchblende.

The Ashanti Belt in Ghana is a prolific producer of gold, and a high-resolution magnetic/radiometric survey has been flown over the area. The mineralization is hosted in two settings: Birimian metavolcanics and Tarkwaian conglomerate. Lo and Pitcher (1996) shows that the Birimian deposits are associated with sericite alteration, with a potassium enrichment signature. The Tarkwaian conglomerate can be mapped through its association with a potassium-rich phyllite marker horizon.

The physical properties of diamondiferous kimberlite sills in the Guaniamo area of Venezuela were studied and compared to neighbouring igneous rocks, which include granite, gabbro and volcanics (Versteeg and Paterson, 1997). The magnetic susceptibilities range widely and there is a significant overlap between rock types. The degree and depth of weathering makes geological mapping difficult and minimizes the effectiveness of electromagnetic surveys. Measurement of the radioelement concentrations from fresh rock samples and drill core clearly showed that the kimberlite could be distinguished from most other igneous rocks (altered and foliated granites, granodiorites, gabbros, rhyolites, lamprophyre dykes, altered mafic dykes) and metasediments through anomalously high levels of K, U and Th. The unaltered granites show similar levels of these radioelements, but the kimberlite is differentiated through higher Th/K and lower U/K ratios.

Gold mineralization within the La Libertad region, Nicaragua, is dispersed in epithermal quartz veins within Tertiary basaltic lavas. There are five alteration zones (I-V) characterized by secondary mineral assemblages (Darce, 1990). A regional, 30 km long, portable gamma ray spectrometer profile of the region showed an increase in K concentration and of the Th/K and KU/Th ratios (Table 9.7) toward the Au mineralized veins (Matolin, 1991).

TABLE 9.7. MEAN K, U AND Th CONCENTRATION DETERMINED BY GROUND GAMMA RAY SPECTROMETRY IN VOLCANIC ROCKS ON THE REGIONAL PROFILE JUIGALPA - LA LIBERTAD, AND AT GOLD BEARING QUARTZ VEIN STA ELENA, LA LIBERTAD, NICARAGUA

Alteration zone	K (%)	U (ppm eU)	Th (ppm eTh)	Th/K	KU/Th
I	0.3	0.2	0.8	1.3	0.1
II	0.7	0.5	1.0	1.5	0.3
III	0.8	0.9	2.1	3.0	0.3
Sta Elena	1.7	0.5	0.9	0.5	1.4

An airborne gamma ray spectrometry potassium anomaly (5% K in a background of 1.5-2%) with an associated Th/K ratio anomaly (Th/K=1 in a 4-6 background) led to the discovery of Zn-sulphidic mineralization in a belt of Devonian and Lower Carboniferous volcanites and sediments in Northern Moravia, Czech Republic. The distribution of natural radionuclides in an alteration zone was used to site drill holes that intersected the Zn mineralization (Gnojek and Prichystal, 1985).

Jayawardhana and Sheard (1997) presented a study of radiometric data over the Mount Isa Inlier, Australia. The area is host to more than eighty base and precious metal deposits. Over 700,000 line-km of airborne gamma ray spectrometric data were acquired in the province. The data provided critical contributions to mapping both lithology and regolith. GIS techniques were used to localize zones of radioelement enrichment or depletion, and correlated well with various types of base and precious metal deposits. The radiometric signatures in these areas were used to explore for similar deposits in the region.

9.5. Petroleum exploration

Sedimentary units typically associated with petroleum-producing provinces can be differentiated by their radioelement signatures (e.g. Table 9.8). Consequently, gamma ray spectrometry provides an additional tool for the geological mapping of sedimentary basins. The method can also delineate surface structure that may have implications for hydrocarbon entrapment.

TABLE 9.8. TYPICAL RADIOELEMENT CONCENTRATIONS OVER GEOLOGICAL UNITS OF PETROLEUM EXPLORATION INTEREST (after Saunders et al., 1994)

Rock type	K (%)	U (ppm)	Th (ppm)
evaporite	0.1	0.1	0.4
carbonate	0.3	1.6	1.5
sandstone	1.2	1.9	5.7
shale	2.7	3.7	11.2

Gamma ray spectrometry has historically been seen as a “fringe” technique for petroleum exploration. However, considerable efforts in recent years have demonstrated economic accumulations of hydrocarbons, perhaps at several kilometres depth, result in measurable geochemical anomalies at surface (Schumacher, 2000). Gamma ray spectrometry has a definite role to play as a reconnaissance tool and precursor to seismic surveys.

Indirect detection of economic hydrocarbon fields using gamma ray spectrometry can be ascribed to two alteration effects (Figure 9.12):

1. hydrocarbon microseepage; and
2. redox (reduction-oxidation) electrochemical cells.

Saunders et al. (1994) studied the radiometric response over several producing and prospective fields in Australia. This work was conducted as a follow-on to earlier work in the United States. They found that radioelement anomalies over hydrocarbon microseepages have the following characteristics:

1. thorium remains relatively constant;
2. potassium is significantly diminished; and
3. uranium is somewhat diminished.

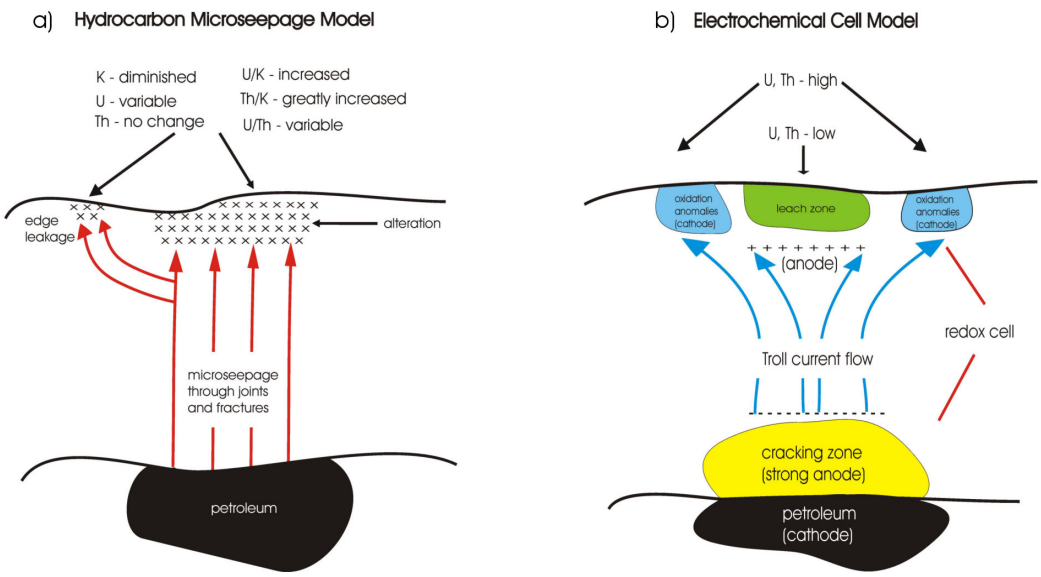

FIG. 9.12. Models for radioelement detection over hydrocarbon deposits for (a) microseepage (after Saunders et al., 1999) and (b) electrochemical cells (after Tompkins et al., 2000).

Their approach is to normalize the potassium and uranium to the thorium, as well as compare the relative abundances of the uranium and potassium. The primary technique is to look for low responses in the normalized potassium, supplemented by a high response in uranium relative to potassium.

Saunders et al. (1999) describe the mechanism that produces hydrocarbon microseepages as follows. Micro-sized bubbles of gas seep near-vertically through a network of groundwater-filled joints and bedding planes immediately above a hydrocarbon deposit. Carbonic and organic acids destroy the clay minerals, primarily illite that contain the much of the potassium and uranium in the system (Saunders et al., 1993). These radioelements are consequently released and leached away by groundwater. The uranium may not leach away entirely, but be chemically reduced to uraninite and precipitate, resulting in some build-up of uranium in the surface sediments. This explains the muted loss of uranium relative to potassium in the system. Thorium appears to be immune to these processes. The chemical reduction process can also result in the development of magnetic minerals, resulting in coincident "micromagnetic" anomalies.

LeSchack (1998) applied this methodology in the Western Canada Basin, using both airborne and ground gamma ray spectrometry. Economic discoveries, in areas where seismic discrimination of the productive channel sands is difficult, were directly attributed to the delineation of anomalous potassium depletion. Elsewhere, limestone pinnacle reefs produce a halo-shaped anomaly around the edge of the producing field. It was suggested that differential compaction resulted in the microseepage occurring along faults at the margins of the reef.

An alternative source of alteration, the redox electrochemical cell, is the basis for enzyme leach geochemical surveys being applied to petroleum exploration (Tompkins et al., 2000), as well as a wide variety of mineral deposits. A very high contrast in the "oxidation suite" of minerals, which includes uranium and thorium, can occur where these electrochemical cells develop above reduced bodies. Apical anomalies are prevalent, located over faults that act as a conduit for these minerals. However, halo anomalies are also found above the edges of the reducing body (cathodes), with a central low over the centre of the body (anode). The strength of the cell reduces with depth, with a consequent diminishing of the geochemical response.

The two types of alteration described above produce low radioelement responses over the petroleum field and/or high radioelement responses around the edges. Thus, acquisition of high-resolution gamma ray spectrometer data, and careful data processing and enhancement to discriminate alteration effects from the host lithologies, can provide a viable exploration technique. Magnetic data can provide a powerful complement to locate these subtle alteration signatures.

9.6. Radon risk mapping

An editorial in the Toronto Globe and Mail newspaper (November, 1998) stated that the lifetime risk of dying from cancer caused by background radiation in nature was 1 in 700. This is the same rate for cancer caused by an average number of X-rays. However, the risk of dying from disease caused by indoor radon is 1 in 440. This illustrates the importance of radon risk mapping.

Gamma ray spectrometry contributes to the mapping of radon prone areas. Radon is a colourless inert gas. Isotopes of radon originate in rocks by the decay of U and Th. ^{222}Rn is a daughter product in the ^{238}U series and has a half-life of 3.82 days. ^{220}Rn is a daughter product in the ^{232}Th decay series and has a half-life of 55.6 seconds. Finally, ^{219}Rn is a daughter product in the in the ^{235}U decay series and has a half-life of 3.92 seconds. ^{222}Rn is the only isotope of radon with a sufficiently long half-life to migrate through rocks and soils to effectively penetrate dwellings. ^{222}Rn migrates by diffusion and convection over distances of tens of meters through rocks and soils. Its activity concentration in rocks is in the range 0-100 kBq/m^3, depending on the geological and structural setting. Radon risk mapping is carried out by radon detection in soil gas and the determination of soil permeability.

^{222}Rn decays to ^{218}Po, ^{214}Pb and ^{214}Bi. The ^{214}Bi photopeak at 1765 keV is used in field gamma ray spectrometry and the method can thus contribute indirectly to the assessment of regional radon potential. However, experimental data show low correlation between U concentration in rocks estimated by gamma ray spectrometry, and radon gas concentration. Gamma ray spectrometry measures radioelement concentrations to a depth of about 0.25 m. But the radon concentration in this layer is highly variable due to variable moisture content and gas permeability of soils. Radon gas activity concentration, on the other hand, is based on soil gas sampling from a depth of 0.8-1.0 m, where the concentration of radon is more stable. Despite local disagreements between gamma radiation and radon in soil, in regional studies the average rock radioactivity and soil gas radon are approximately proportional. Gamma ray maps are thus widely used for the delineation of radon risk areas.

Gamma ray spectrometry has been applied to radon risk appraisal in several countries. In Israel, Vulkan and Shirav (1997) found an excellent correlation between U mapped by airborne gamma ray spectrometry, and ^{222}Rn activity concentration (Bq/m^3) in arid areas where there was little soil. However, in semi-arid, humid areas the correlation was poor. Low correlation was attributable to the gamma-shielding effect of several metres of thick rock and soil cover. In Sweden, Akerblom and Lindgren (1997) found a relationship between radon in water and elevated gamma radiation of bedrock. Airborne gamma ray spectrometry was used for radon risk mapping in Sweden, where an exposure rate of 30 μR/h is considered as a potential radon risk in dwellings (Akerblom, 1995). In Canada, Shives et al. (1995) found a direct correlation between predicted high levels of radon for homes in native communities, based on an analysis of the gamma ray spectrometry, geochemistry and geology, and directly measured levels.

Gamma ray spectrometry data was used to predict the radon risk over a carbonatite near Oka, Quebec, and prevent a large housing development located in an area that proved to be of quite high risk (Ford et al., 2000). Figure 9.13 shows a definite correlation between high radon levels measured in homes and high concentrations of equivalent uranium measured by airborne gamma ray spectrometry. The survey filled the gaps in information provided by geological mapping and radon measurements, to allow public health officials to develop a risk profile for the area, and undertake mitigating for existing homeowners and future municipal planning.

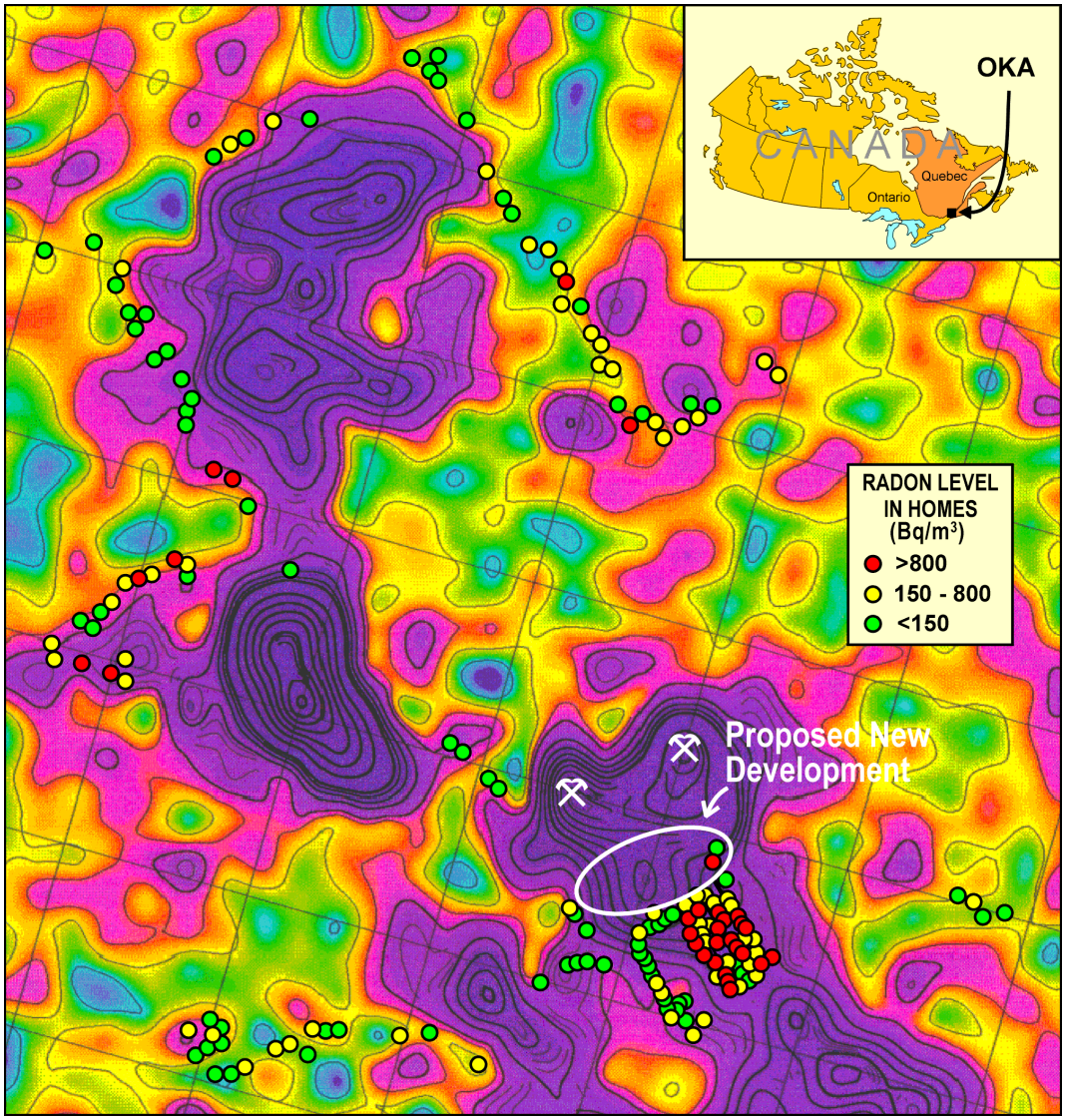

FIG. 9.13. Equivalent uranium map (grid lines spaced 1 km apart) derived from airborne gamma ray spectrometer survey (200 m line spacing) and in-home radon levels, Oka, Quebec (Ford et al., 2000).

Despite its limitations, the gamma ray method is still considered an important source of information on distribution of uranium rich rocks and soils that create radon hazards (Otton et al., 1995). The radon risk map of the Czech Republic (Figure 9.14) is based upon soil radon measurements at 7300 sites, soil permeability measurements and other geological and geophysical information (Barnet et al., 1998). This map retains the features of the airborne map of terrestrial gamma dose rate (Manova and Matolin, 1995), demonstrating the correlation between radon risk and regional radioactivity.

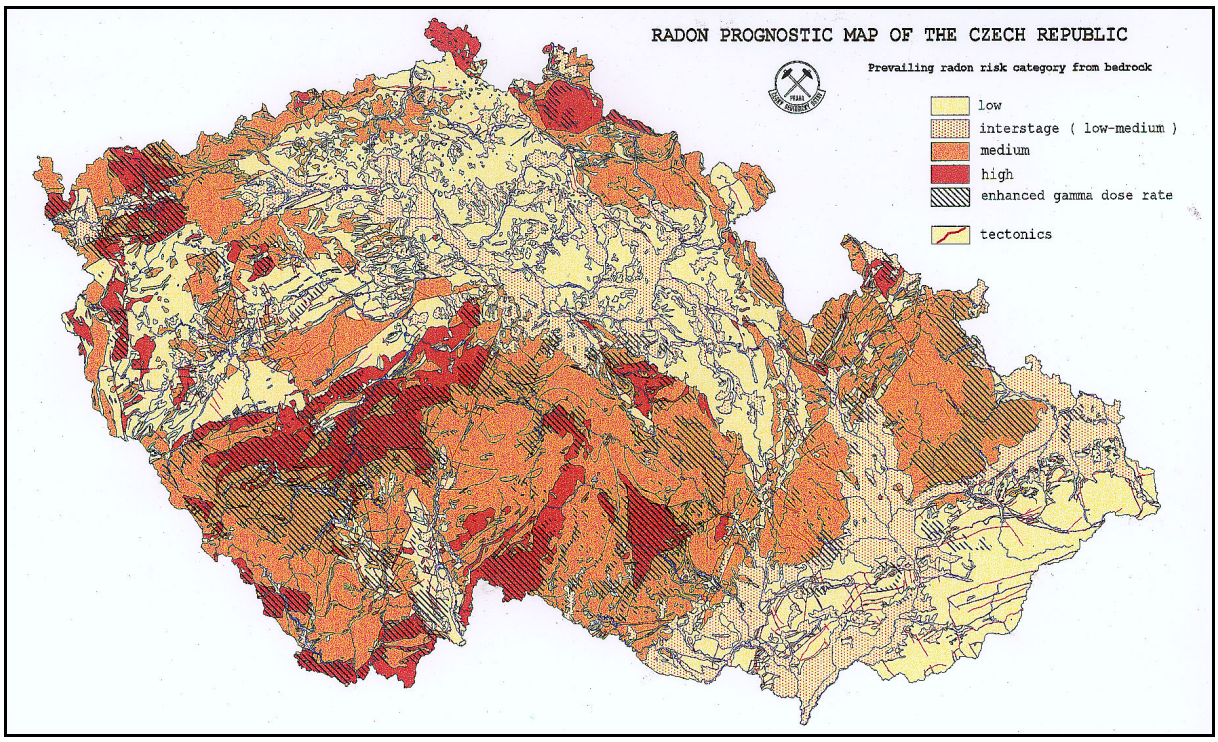

FIG. 9.14. Prognostic radon risk map of the Czech Republic based on field radon measurements, airborne radiometric data and lithology of the territory (Compiled by the Czech Geological Survey, Prague, 1998).

9.7. Other applications

Airborne gamma ray surveys have been used for biomass estimation. The shape of airborne gamma ray spectra depends not only on the relative concentrations of the radioelements, but also on the amount of attenuating material between the source and the detector. Through suitable calibration, the amount of attenuating material, and hence biomass, can be estimated. A method for direct determination of snow-water equivalent by airborne gamma ray spectrometry was developed and tested by Grasty (1982). The method is based on the change in shape of the gamma ray spectrum due to attenuation of gamma rays in snow mass and a build-up of low energy photons by Compton scattering. A ratio of Compton scattered gamma rays, measured in a low-energy window (0.72–1.36 MeV), to gamma rays measured in a high-energy window (1.36–1.56 MeV), can be used to estimate the thickness of the snow-water equivalent absorption layer. This can be useful for predicting water resources and for flood control when the snow melts.

Estimates of K, U and Th concentrations from gamma ray spectrometry can be used to estimate the heat generated by rocks. Disintegration of the natural radionuclides in the earth is accompanied by the release of thermal energy, and most of this is produced by the decay of K, U and Th. The heat production (*HP*) of rocks is related to the concentration of the radioelements c_K (% K), c_U (ppm U), c_{Th} (ppm Th), and density of rock by (Rybach, 1976)

$$HP = \rho\,(3.48\,c_K + 9.52\,c_U + 2.56\,c_{Th}).10^{-5} \quad (\mu W/m^3) \tag{9.1}$$

where ρ is the density of rock (kg/m^3).

Gamma ray spectrometry and the mapping of radioelement distributions have several other applications. The method has application to the planning of geochemical surveys. Radioelement distributions can be used to map drainage systems and catchment areas. They can also be used to interpret the presence of weathering profiles and transported overburden. This information can be used for locating the optimum positions for geochemical sample sites.

Inconsistency between natural geochemical databases can be a serious problem for continental and global studies; regional airborne gamma ray spectrometric traverses can be used to correct for systematic differences between regional geochemical databases. In particular, Th and K concentrations estimated from airborne gamma ray measurements can be used to correct the conventional Th and K geochemical data. However, due to the complexities of the corrections required for airborne gamma ray spectrometric estimates of terrestrial U concentrations, the use of U data for this purpose is not recommended.

Airborne gamma ray spectrometric surveys are increasingly being used for geochemical baseline studies. Surveys are flown in areas where there is a perceived potential environmental risk – for example around nuclear power stations or in areas where land degradation is a problem. Subsequent surveys serve to monitor any environmental changes.

10. MAPPING MAN-MADE SOURCES OF RADIATION

Man-made sources of radiation contribute to the radiation dose absorbed by the population. The mapping of the location and activity of these sources is thus necessary. Nuclear technologies are now widely used in research and industry, energy power plants, health services, and in the military. There is generally strict control on the installation and use of radioactive sources. But accidents do happen. Significant contributions to terrestrial gamma radiation were caused by reactor accidents at Windscale, UK (1958), and Chernobyl, USSR (1986), the loss of isotope sources in Mexico (1985) and Brazil (1987), and the re-entry of a nuclear-powered satellite in Canada (1978). Airborne and ground gamma ray methods are used for the location of lost sources and the mapping of areas contaminated by nuclear fallout.

Natural sources of radiation may also be concentrated in the environment by human activities. Mining activities, including uranium, and thorium (mineral sands), redistribute and concentrate the radioelements. Coal and peat power plants (and associated ashes) redistribute radioactive materials, as does the use of phosphate and potassium fertilizers in cultivated land.

10.1. Mapping nuclear fallout

Nuclear fallout is the contamination of the earth's surface by man-made radionuclides. The nuclides are transported in the air over considerable distances and deposited on the earth's surface by rain. Nuclear fallout can be due to the release of man-made radionuclides from nuclear bomb tests, nuclear power stations and nuclear research reactors. The most important gamma ray emitting nuclides of nuclear fallout that are detectable at the earth's surface are given in Table 10.1. Their half-lives vary considerably, and determine their longevity after deposition. The most important fallout radionuclides with long half-lives are ^{137}Cs, ^{134}Cs and ^{106}Ru. Note that most of the fallout nuclides emit gamma rays of lower energy than the diagnostic photopeak of naturally-occurring K, U and Th at 1461 keV, 1765 keV and 2615 keV, respectively. An exception is the gamma rays from ^{140}La gamma rays at 1596 keV. However, because of its short half-life, ^{140}La gamma-radiation decreases to low levels within 3-4 months after contamination.

TABLE 10.1. SIGNIFICANT NUCLEAR FALLOUT RADIONUCLIDES EMITTING GAMMA RAYS

Isotope	Half-life	Energy of gamma rays (keV)
^{95}Nb	35.15 d	766
^{95}Z	65.5 d	724, 757
^{103}Ru	9.5 d	497, 610
^{106}Ru	368.2 d	512
^{131}I	8.05 d	364
^{132}I	2.38 h	668, 773
^{132}Te	78.33 h	228
^{134}Cs	2.06 y	605, 796
^{137}Cs	30.12 y	662
^{140}Ba/La	12.78 d	487, 1596

Since the fluence rate at the earth's surface of primary photons from gamma sources in soil is strongly related to the vertical distribution of the sources in the soil, the migration of nuclear fallout in various soil types over time is important. Nuclear fallout isotopes are generally present in a thin (10-15 cm) layer at the earth's surface. The distribution can be described by the relaxation mass per unit area, β (g cm^{-2}), which is defined by the relationship (ICRU, 1994):

$$A_a = \beta A_{m,0} \tag{10.1}$$

where A_a = integrated activity per unit area, (Bq/cm^2),
β = relaxation mass of radionuclide per unit area, (g/cm^2),
$A_{m,0}$ = activity per unit mass at the surface of the soil, (Bq/g).

For a radiation source evenly distributed in soil, the relaxation mass per unit area approaches infinity, and for a source accumulated on the surface it approaches zero. An exponential model of the vertical distribution of fallout nuclides is often used, and is also characterized by the β parameter. The depth penetration of fallout nuclides is small in wooded areas, varies in meadows and noncultivated land, and is large in cultivated fields. Arid climatic conditions are favourable for surface accumulation, while humid climatic conditions support the infiltration of fallout sources into soils. The values of β also relate to the age of the nuclear fallout, with minima recorded for recent depositions. Typical values are 0.1-3.0 g/cm^2 for recent deposits, 1.0-7.0 g/cm^2 for nuclear fallout after several years, and 2-20 g/cm^2 for aged fallout (ICRU, 1994). Matolin et al. (1993) reported Cs gamma dose rates in the Teplice region on the Czech-German border of 10.9 nGy/h in woods, 6.1 nGy/h on meadows, and 2.9 nGy/h on cultivated fields.

Several methods can be used for the detection of nuclear fallout. Most artificial radioactive sources emit a higher proportion of low-energy gamma rays when compared with the naturally-occurring radioelements. Thus, the ratio of count rates in low (*L*) and high (*H*) energy windows of the spectrum is indicative of the presence of man-made (*M*) nuclides. An energy of 1400 keV is often used as the nominal upper threshold of nuclear fallout radiation. The man-made component can be calculated using the expression:

$$M = L - AH \tag{10.2}$$

where *A* is the low-to-high energy region count rate ratio for natural radiation ($A = L_{nat}/H_{nat}$).

The dose rate due to nuclear fallout may be estimated by monitoring a total-count window with a lower discrimination threshold of 200-300 keV. The fallout dose rate is calculated as the total dose rate minus the dose rate due to the natural radionuclides. The dose rate from nuclear fallout may also be calculated from the estimated activities per unit area - provided the vertical distribution of the sources is known.

Multichannel spectrometers can be used to identify and distinguish between different man-made isotopes. Spectral deconvolution can be used separate the components. This method is complex, and requires knowledge of the spectral shapes of each of the contributing sources.

Semiconductor Ge multichannel analyzers are currently used for multi-element fallout analyses on the ground and, under certain conditions, in the air. Scintillation airborne detector volumes should be reduced in highly contaminated areas to avoid instrument problems associated with very high count rates. The sampling time for Ge detectors can be shortened in these circumstances.

The calibration of gamma ray spectrometers for nuclear fallout mapping requires the estimation of the response (net count rate) of the instrument in a specific energy interval to unit concentration of the fallout nuclide contamination. Fallout is expressed in units of Bq/kg, Bq/m^2, or nuclear fallout dose rate in nGy/h. Existing fallout areas, where the concentrations are well known, can be used to calibrate field instruments. Grasty and Cox (1997) conducted and described calibration and field experiments in Finland over areas with a reported ^{137}Cs surface activity of 50 kBq/m^2.

The net count rate for the estimation of ^{137}Cs is the registered count rate in the ^{137}Cs window (Table 10.1) corrected for terrestrial K, U, Th contributions and gamma ray background. To remove the K, U, Th contributions, the sensitivity of the ^{137}Cs window count rate to K, U, and Th concentrations must be known. These 3 sensitivity constants can be estimated for portable ground spectrometers using 4 calibration pads (K, U, Th and background). The net count rate n_{Cs} of ^{137}Cs in the ^{137}Cs energy window is

$$n_{Cs} = n - n_{BG} - s_K c_K - s_U c_U - s_{Th} c_{Th} \qquad (10.3)$$

where n = count rate in the ^{137}Cs energy window , (c/s);
n_{BG} = background count rate in the Cs window, (c/s);
s_K, s_U, s_{Th} = K, U, and Th sensitivities in Cs window, (c/s per unit concentration);
c_K, c_U, c_{Th} = K, U, and Th concentrations (% K, ppm eU, ppm eTh).

Airborne spectrometer sensitivities and stripping ratios are height dependent, and airborne measurements over three test strips at various heights are required. Alternatively, the attenuation of gamma rays in air can be simulated by using wood, or a similar material, to shield the airborne detector during ground calibration experiments (IAEA, 1991).

The net count rate n_{Cs} in the ^{137}Cs window can be normalized to known surface activity (Bq/m^2). For a recent contamination, determination of both ^{137}Cs and ^{134}Cs isotopes is recommended, as there is some spectral interference between these isotopes (Table 10.1). Illustrative calibration constants for a portable gamma ray spectrometer are given in Table 10.2. Grasty and Cox (1997) described car-borne gamma ray spectrometer sensitivities and stripping ratios for ^{137}Cs assays. The calibration requirements for a full spectrum analysis for major fallout radionuclides are more complex. Detailed descriptions of the calibration and data processing procedures for airborne gamma ray spectrometry, focused specifically on nuclear fallout monitoring, are given in IAEA (1991).

TABLE 10.2. SENSITIVITIES AND STRIPPING RATIOS OF A PORTABLE GAMMA RAY SPECTROMETER WITH A NaI(TL) 76×76 mm DETECTOR FOR ^{137}Cs AND ^{134}Cs CALIBRATION

	Energy window (keV)		Stripping ratio
	618 - 705	743 - 843	
^{137}Cs sensitivity (c/s per 1 kBq/m^2)	1.067	0.003	0.003/1.067 = 0.003
^{134}Cs sensitivity (c/s per 1 kBq/m^2)	0.699	1.317	0.699/1.317 = 0.531

The nuclear fallout dose rate calibration is done through a comparison between instrument fallout net count rate and ground fallout dose rate. A test strip in a contaminated area is measured with a pressurized ionization chamber and the dose rate is estimated. The K, U and Th concentrations in the ground can be used to estimate the natural radionuclide dose rate (Table 2.6). This is subtracted from the total dose rate to give the fallout dose rate.

Fallout contamination measurements are mainly reported in kBq/m^2. Conversion of the activity per unit area to dose rate depends on the vertical distribution of the nuclides in the soil (defined by the relaxation mass per unit area, β). A detailed table of kerma rates for individual radionuclides (μGy/h), per unit activity per unit area (kBq/m^2), as a function of relaxation mass per unit area β, has been published by Jacobs et al. (ICRU, 1994). For ^{137}Cs with a vertical distribution defined by β = 0.1, 0.3, 1.0, 5.0, the corresponding values are 2.42, 2.15, 1.73 and 1.05 nGy/h per 1 kBq/m^2.

The errors and limits of detection in nuclear fallout estimates depend on the background radiation (including terrestrial K, U and Th), and the calibration and data processing procedures. Typically, for measurement with portable gamma ray spectrometer, a 10% relative error in ^{137}Cs estimation, and counting time of 4 min in an area with 3.3% K, 3.5 ppm eU and 18 ppm eTh, the limit of detection will be about 3.3 kBq/m^2. The minimum detectable ^{137}Cs activity per unit area, measured with a Ge detector using a 30 minute sampling time and typical background radiation is reported as 0.06 kBq/m^2 (ICRU, 1994). Since the vertical distribution of fallout nuclides in soil is mostly unknown, the data from nuclear fallout surveys are biased, and are based on the vertical fallout distribution at the calibration site.

Table 10.3 shows the general decrease in Cs contamination with time in Prague after the Chernobyl accident. The decrease is due to both natural decay and infiltration of the radionuclide into the ground. The data were acquired with a portable spectrometer, and the recorded spectra show the specific temporal decay of the ^{137}Cs and ^{134}Cs peaks (Figure 10.1).

A valuable contribution on the practical aspects of nuclear fallout mapping, based on experiences in Sweden, has been published by Mellander (1989).

TABLE 10.3. TEMPORAL CHANGE OF ^{137}Cs AND ^{134}Cs CONTAMINATION DETERMINED BY PORTABLE GAMMA RAY SPECTROMETER ON A GRASS AREA, PRAGUE

Date	Surface activity (kBq/m^2)	
	^{137}Cs	^{134}Cs
1986.10.07	26.3	11.4
1986.11.13	23.5	9.8
1986.12.17	23.1	9.0
1987.03.20	21.7	7.9
1987.09.23	17.3	5.4
1990.01.15	10.1	1.6
1997.05.06	4.7	0.6

10.2. Searching for lost radioactive sources

Airborne, car-borne and portable gamma ray spectrometer systems all have an important role to play in locating lost radioactive sources. Fortunately, few incidents have been reported in the last decade. Two cases of locating cobalt sources in the United States are reported in IAEA (1991), one lost in transit on the ground and the other due to a crashed missile. They were located using an airborne system developed by the Unites States Atomic Energy Commission. Surveys were flown over the trajectories of the sources until appropriate

anomalies were found in the air and locations confirmed on the ground. In the second case, the system had been calibrated using a cobalt source and the measured window (20 keV in width) centred on the ^{57}Co photopeak (122 keV).

Man-made sources generally have much lower energy than the K, U and Th typically measured for geological mapping purposes. Therefore, some knowledge of the lost source is desirable to optimise the spectrometer system configuration (e.g. detector size) and the survey design (e.g. detector altitude and line spacing). The detectability of a source can be determined using

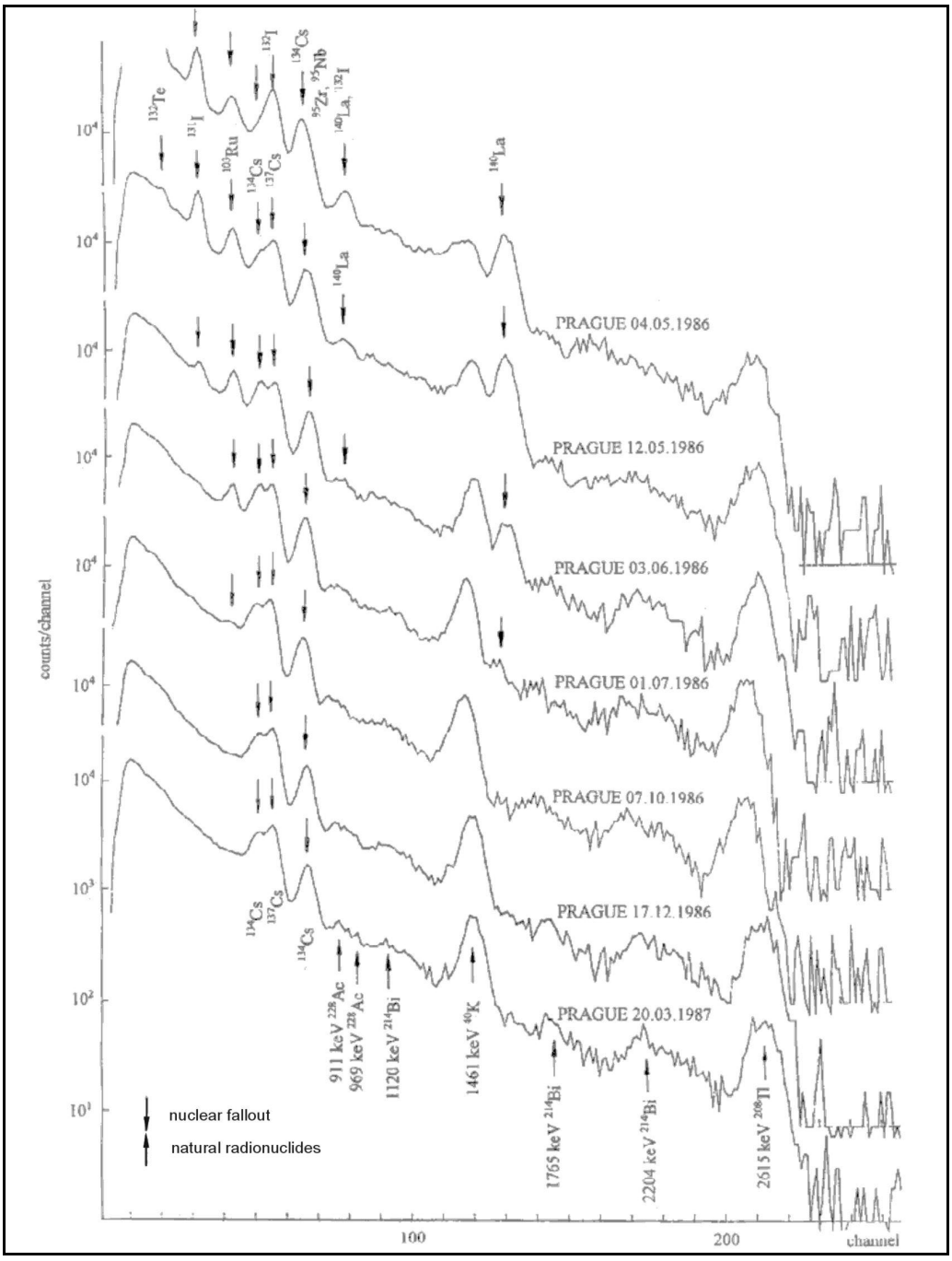

FIG. 10.1. Energy gamma ray spectra measured sequentially after 1986 nuclear fallout contamination on the Earth's surface at open grass area in Prague with portable multichannel gamma ray spectrometer, detector NaI(Tl) 76 x 76 mm, counting time 10 min (Matolin, 1995).

$$N = \frac{BfA\exp(-\mu\sqrt{D^2+H^2})}{4\pi(\sqrt{D^2+H^2})^3} \tag{10.4}$$

where N = number of gamma rays detected (c/s);
B = activity of the source, (Bq);
f = fraction of disintegrations producing gamma rays;
A = cross-section area of the detector (m^2);
μ = linear attenuation in the air of the gamma ray energies (m^{-1});
D = horizontal distance from the source (m);
H = altitude of the detector above the ground (m).

The equation does not consider detection efficiency of the detector, which is inferior to 1, hence, the registered rate N will be lower than given by eq. (10.4).

The search strategy should incorporate the following considerations:

1. optimise the detector size and spectral windows for the target source;
2. optimise the survey line spacing and height for the target source, distribution of multiple sources and system sensitivity to the source;
3. optimise the search area and flight direction for the probable source location and distribution;
4. prioritise the search over populated areas to minimise public risk;
5. real-time processing and data display to identify anomalies; and
6. communication with ground-based teams for immediate anomaly follow-up.

10.3. Nuclear satellite re-entry

Cosmos 954, a nuclear powered Russian satellite suffered orbital decay after only a few months in orbit and re-entered the earth's atmosphere on 24 January 1978. The satellite broke up on re-entry, scattering debris over thousands of square kilometres of Canada's Northwest Territories. The incident sparked a massive search to locate and dispose of this debris. Most of the recovered fragments were radioactive. A few pieces were found to be extremely radioactive – sufficient to have potentially serious effects on human health in certain circumstances (Grumer et al., 1980). Airborne gamma ray spectrometry was instrumental in the location of the radioactive debris (Bristow, 1978).

The debris from Cosmos 954 contained both fission and activation products. The significant gamma ray emissions in the 0.3-3.0 MeV range from these products were at energies less than 1.0 MeV. The ratio of a low-energy window (0.3-0.9 MeV) to a high-energy window (0.9-1.5 MeV) was used to map the radioactive debris. The initial search consisted of airborne traverses along widely spaced traverses (1 km spacing) perpendicular to the entry path of the satellite. As the debris footprint became better defined, the search grid was refined. Individual radioactive pieces were ultimately located on the ground with portable instruments.

Many countries now have emergency management plans in place in the event of nuclear satellite re-entry. Many older satellites are equipped with small nuclear reactors as a source of power. Satellites re-entering the earth's atmosphere do so at a low angle, and the likely impact area for debris is a footprint up to 1000 km long and 40 km wide. While a reactor would be unlikely to withstand re-entry, it is also unlikely that the nuclear fuel would be completely vaporized. Consequently, as in the Cosmos 954 incident, a great number of fuel particles containing fission products could reach the ground. The debris could range in size from

microscopic particles to large pieces. Such debris could pose a significant hazard to local populations.

Airborne gamma ray spectrometry using large NaI(Tl) detectors is the primary survey method for locating the radioactive debris footprint on satellite re-entry. Widely spaced lines are initially flown to locate the impact area. Line spacing is progressively decreased to locate as many particles as possible. Follow-up surveying is by helicopter-borne spectrometry and ground spectrometry using portable gamma ray spectrometers. The search strategy would be to find the most radioactive sources first, as these pose the greatest threat to individuals. Subsequent priorities will depend on factors such as the population density/distribution, topography and remoteness of the impact area.

10.4. Environmental monitoring

Monitoring of the environment using gamma ray spectrometry in the last decade has made tremendous strides. Northern and central European countries in particular were galvanized by the 1986 Chernobyl accident. Programs to monitor the background radiation due to natural and man-made sources have been implemented. Field exercises to test and modify monitoring techniques for nuclear emergency preparedness are undertaken regularly. Many advances in instrumentation and data processing have been driven by the requirements of the environmental scientists rather than mineral explorationists. IAEA (1995) and IAEA (1997) provide 68 papers devoted mainly to environmental applications of gamma ray spectrometry.

Baseline measurements on a country-wide scale are typically carried out by systematic airborne survey. A primary application is of course geological mapping. However, modern surveys also provide the background levels of both the natural radionuclides and the man-made sources with a longer half-life, particularly ^{137}Cs (Table 10.1). On a local level, baseline surveys flown around man-made facilities such as nuclear power plants and mines, preferably prior to construction, allow periodic monitoring for contamination and emergency response to leaks. Figure 10.2 shows results of a detailed airborne survey adjacent to a nuclear generating station in Bulgaria (Shives et al., 1995).

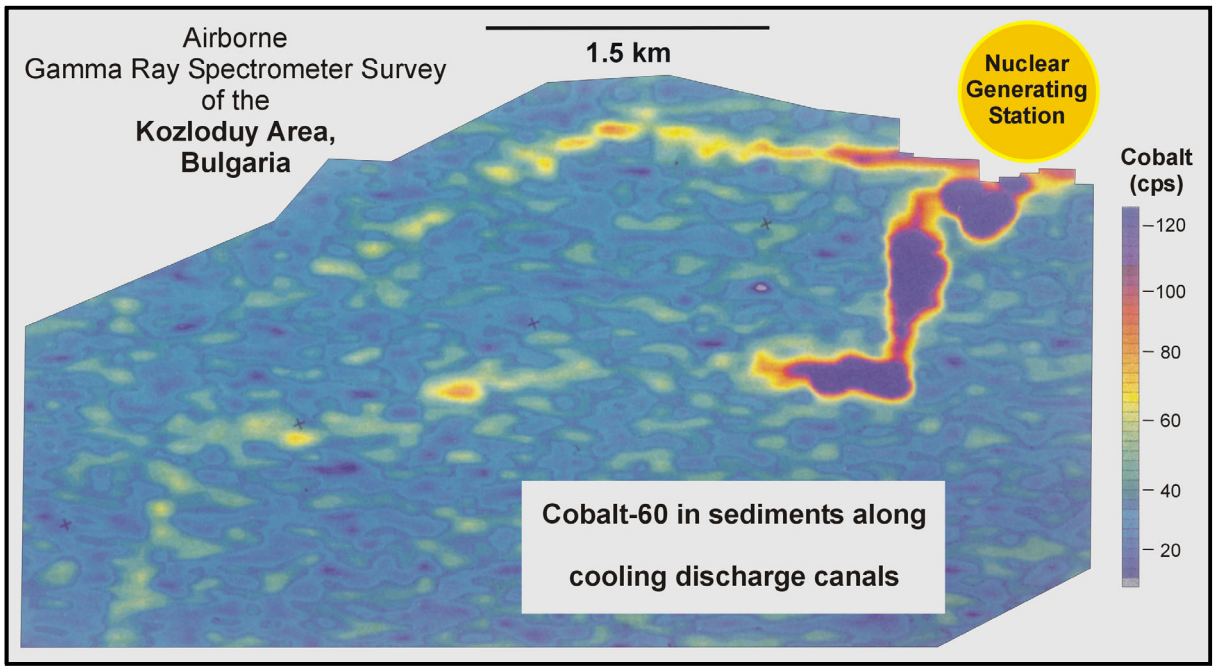

FIG. 10.2. ^{60}Co response from an airborne gamma ray survey around a nuclear generating station, Kozloduy, Bulgaria, showing elevated levels in soils adjacent to discharge canals (Shives et al., 1995).

High levels of ^{60}Co are evident in the soils adjacent to the cooling discharge canals for 2 km or so downstream. Elevated levels are seen for at least another 10 km. A 1996 survey in Latvia found high levels of ^{137}Cs concentrated in peat bogs and one unexplained anomaly. It was later found to result from a sawmill where the needles in pine and spruce tree branches stored there contain low levels of ^{137}Cs (Korsbech, personal communication).

There are now airborne systems available that will utilise an air to ground algorithm for real-time or post-processed models of the natural elements and deposits of man-made radioactive substances (Pavlik et al., 1997). To do so requires ground clearance of 10 m or less, and must be mounted in a helicopter. Flight patterns to trace stolen or lost radioactive sources, and to track radioactive plumes, have been developed. In the latter case, the local weather patterns are also monitored in real-time to minimise contamination of the system itself. These types of systems are particularly suited to emergency response. Real-time monitoring of radionuclides during a nuclear emergency also provides a warning system so that flight personnel can avoid dangerous levels of exposure.

The Nordic Nuclear Safety Research Secretariat (NKS), incorporating agencies from Denmark, Finland, Iceland, Norway and Sweden, has implemented a nuclear emergency preparedness project to deal with the consequences of radioactive release into the environment. It focuses on radioactivity monitoring and modelling the consequences of nuclear accidents, including emergency exercises, so as to improve response to nuclear accidents. The RESUME (rapid environmental surveying using mobile equipment) exercises in 1995 and 1999 utilised a variety of in-situ (portable and laboratory samples), car-borne and airborne systems to test methods for mapping contamination levels and searching for lost radioactive sources. Agencies from several countries outside NKS also participated. The results are documented in NKS (1997) and Karlsson et al. (2000) respectively. The RESUME 95 exercise involved ten airborne and seven car-borne teams from eight countries, as well as in-situ analysis. Three areas were surveyed near Lahti, Finland: a calibration site at an airfield, an area contaminated by ^{137}Cs from the Chernobyl accident, and an area containing ten hidden sources (^{60}Co, ^{137}Cs, ^{192}Ir and ^{99}Tc) of varying activity. Good quality maps of ^{137}Cs were prepared within hours of the survey from most airborne systems. Car-borne systems generally mapped the same spatial features, but absolute levels varied due to system geometry and calibration methods. Success in locating the hidden sources was variable; between one and six were detected depending on the system. Toivonen (1997) found that the NaI detectors were better suited to locating the hidden sources, but the HPGe detectors were superior at identifying them and measuring their levels of activity, and recommends that both types be employed in such a situation.

The RESUME 99 exercise involved nine car-borne systems and eleven detectors (nine NaI and two HPGe), as well as seven teams taking in-situ measurements, in the Gävle region of Sweden where ^{137}Cs contamination from Chernobyl varies significantly. A 1998 high-resolution airborne survey was available for comparison. The first day was devoted to a 200 km traverse, which included four calibration sites and two “lost” sources. The second day consisted of complementary quadrant mapping by the various teams. The data were delivered and processed in near real-time to simulate a nuclear emergency, and demonstrated that deliverable products could be produced in one or two hours after measurements were completed. Once system and calibration differences were accounted for, a composite map of ^{137}Cs activity compared favourably with its airborne counterpart.

Sanderson and Ferguson (1997) describe a parallel project sponsored by the European Community, involving agencies from Austria, Denmark, Finland, France, Germany, Norway,

Sweden, Switzerland and the United Kingdom. It focuses on the capabilities and applications of airborne gamma ray spectrometry for these agencies to respond in emergencies. Most of the participants are now able to deploy airborne systems within hours to commence fallout mapping and monitoring, although the approaches vary. The systems are otherwise deployed for geological mapping and environmental surveys. Some systems combine NaI and Ge detectors, to take advantage of the short integration time of the former and spectral resolution of the latter. The cooperative research and joint exercises have demonstrated the critical role of airborne gamma ray spectrometry in public health and safety immediately following an accident. Upgrades to airborne detector systems are necessary to locate and define the various man-made radionuclides. Calibration methodology and data processing techniques will require additional refinement to produce consistent measures of dose rate and radionuclide activity.

A magnetic/gamma ray spectrometer/electromagnetic high resolution survey was carried out over the English Midlands in 1998, with a more detailed follow-up survey in 1999 and ground truthing. Lee et al. (2001) describe the challenges of surveying in urbanised areas (e.g. restrictions on aircraft terrain clearance, cultural noise), but also the benefits of environmental baseline data. Lahti et al. (2001) note a number of man-made radioactive sources located in the region by the airborne surveys, including colliery spoil heaps, iron ore mines and processing centres, fly ash adjacent to coal-fired power station sites, Chernobyl fallout, nuclear reprocessing plant discharges and a ^{60}Co source. They describe the results of a similar survey in southeast Germany. It located uranium anomalies associated with waste adjacent to uranium mines and processing plants, and the drainage from these areas. Roads and houses constructed from uranium mine wastes also showed elevated levels of radioactivity. Other anomalies include high potassium over fields fertilised with phosphates, and Chernobyl fallout in forested areas. Both the English and German surveys provide a geological mapping component as well, including assessment of resultant radon activity.

Tyapkin et al. (2001) have undertaken a predictive study of the radiological load in a region of southeast Ukraine by combining the effects of geological sources (e.g. granites, faults), soil characteristics, manmade sources (Chernobyl accident, nuclear power plants, nuclear waste sites, mining activity, radioactive road-metal) and hydrogeology (surface and underground). They then adjust the effects of man-made sources to make various short and long-term predictions of the radiological environment under normal development circumstances and nuclear emergencies.

Helicopter gamma ray spectrometer surveys were undertaken over two operating Canadian nuclear power plants in 1999, and a nuclear waste disposal research facility slated for decommissioning in 2000 (Grasty and Sander, 2001). The objectives were to examine the radiation signatures of the facilities, and determine the background radiation levels in the surrounding areas. The data processing was configured to determine the levels of ^{137}Cs, ^{60}Co, ^{16}N and ^{41}Ar, in addition to K, U and Th. Normal levels for all elements were found within and outside the facilities, and particular signatures for each site explained by known sources. The survey results provide a baseline for the nuclear facilities and surrounding region, should any accident occur. The results were also provided to the communities proximal to the nuclear power plants, to familiarize the public with the existing levels of both natural and man-made radiation from all sources.

Stationary monitoring systems are located on the perimeter of nuclear facilities to provide real-time notification of airborne leaks. Similarly, vehicles entering landfill and waste disposal sites are monitored to ensure that radioactive sources are not deposited. The steel and

scrap metal industries utilise comprehensive systems to test metals at various stages for radioactive contamination, as do rail and shipping companies transporting these materials. Cox (1995) documents numerous examples where radioactive sources have inadvertently been melted with scrap steel, contaminating the new steel products, and resulting in millions of dollars in costs to decontaminate structures when the radioactive material was discovered months or years later.

Handheld gamma ray spectrometers are available that measure more than two dozen medical isotopes. This allows monitoring of medical facilities for general radiation levels, identification of specific isotopes, mapping spills, checking waste and determining patient radiotherapy dose rates.

11. ECONOMIC ASPECTS

Airborne radiometric surveys are typically one of the most cost-effective forms of exploration geophysics. They are usually flown in conjunction with a magnetometer survey. On a fixed wing platform, radiometrics adds a premium of 15% to 25% over the cost of a standalone aeromagnetic survey. For fixed wing electromagnetic systems and helicopter systems, the added weight of the gamma ray spectrometer, particularly the crystal packs, may reduce the fuel payload and consequently the length of a survey flight. The absolute cost of a survey depends heavily on the size of the survey, the logistical aspects (e.g. access, terrain), the weather, the stringency of the survey specifications, the data processing and survey products, etc. In recent years, costs have fluctuated considerably, depending on the global and local competition in the airborne survey contracting business and the cyclical nature of mineral exploration and commodity prices. The cost of larger fixed wing surveys (20,000 line-km or more) have been in the US$6 to $12 per line-km range during the late 90's, and somewhat lower for the very large surveys (>75,000 line-km).

Combined airborne magnetic/radiometric surveys have formed a critical component in several jurisdictions worldwide, as a means of stimulating mineral exploration. This accelerated through the 90's, as the cost/benefit of such initiatives were analyzed (e.g. Robson, 1998). It has been demonstrated that the tax or aid dollars spent on the acquisition of magnetic/radiometric surveys, and complementary geoscience data, are returned manifold through the exploration work that is stimulated. This is particularly evident where the terrains are prospective but under-explored. There are other benefits that accrue, including the provision of baseline data for environmental and land use studies, and stimulation to improve the technology (hardware, software and interpretation) of gamma ray spectrometry.

12. CONCLUDING REMARKS

This report brings together a wealth of material from diverse fields to provide a complete coverage, for the first time, of the application of gamma ray spectrometry to environmental mapping. The report covers the fundamentals of radioactivity and gamma ray spectrometry, instrumentation, data processing and interpretation methods, and reviews each of the main applications of the method. The uniform description of the fundamentals of the method, including a comprehensive coverage of SI and conventional quantities and units, will be useful to both new and existing users of the method. The report provides a complete reference for experienced users and will also be found useful as a training guide for new users.

The use of principal component-type analyses for the reduction of noise in raw gamma ray spectra has become an integral part of the processing procedure for airborne gamma ray spectrometric data. This methodology provides a compelling reason for the routine acquisition of multichannel spectra for all gamma ray mapping applications. Further reductions in statistical noise are likely as this methodology is developed, but further research is required to better understand the advantages and limitations of these spectral smoothing methods.

A fundamental aim in the development of the gamma ray spectrometric method is to increase the signal-to-noise ratio. The use of spectral noise-reduction methods represents a significant step in this direction. For airborne and car-borne surveying the trend towards using greater detector volumes will continue. Fifty litres of NaI(Tl) detectors is now the standard for airborne surveys. Lower flying heights, and the flying of closely draped surfaces with performance fixed-wing aircraft, will further improve the signal-to-noise ratio and reduce processing errors. This will enable downward continuation or the deconvolution of airborne data to equivalent surfaces to become part of mainstream data processing methodology.

Government agencies in many countries now have car-borne gamma ray systems that will be used during environmental emergencies such as nuclear accidents or for the location of lost radioactive sources. A significant effort is being put into the development of these systems. This is likely to lead to innovative new methods for searching for radioactive sources and for the real-time processing of survey data from these systems.

Borehole gamma ray spectrometry has a much greater role to play as a mapping tool. More physical property measurements are required to increase the utility of gamma ray data as an interpretation tool. Further work is required before the gamma ray method can be fully utilized in the area of soil and regolith mapping. A better understanding of the geological processes and mechanisms that control the distribution of the radioelements will greatly assist in the interpretation of gamma ray data.

As national databases grow, many agencies have embarked on the back-calibration of older survey data to enable the assembly of large regional compilations. This has focussed attention on the benefits of standardising acquisition, calibration and data processing procedures. The IAEA has been at the forefront of efforts to standardize gamma ray mapping methodologies. Those agencies that standardized early, now have the benefit of coherent database coverages. The new spectral smoothing methods (§5.5.2) is one area of recent development that could benefit from the introduction of standards for their implementation. If these methods are incorrectly applied, there is a very real danger that signal can be corrupted and real anomalies removed along with the noise. In some applications, such as searching for discrete mineralization occurrences or lost radioactive sources, this may be crucial.

APPENDIX I. MAPPING RADIOELEMENT CHANNELS IN IHS COLOUR SPACE

This appendix describes how the K, eTh and eU radioelement channels can be mapped to perceptual colour attributes, such as those defined by the IHS colour space. The radioelement channels are first scaled to equal range (0-1) to distribute the ranges of the radioelement channels equally in RGB colour space. Sum-normalization projects the data on the triangular RGB plane normal to the intensity axis (Figure A1):

$$K_n = \frac{K_{[0-1]}}{K_{[0-1]} + eTh_{[0-1]} + eU_{[0-1]}} \tag{I.1}$$

$$eTh_n = \frac{eTh_{[0-1]}}{K_{[0-1]} + eTh_{[0-1]} + eU_{[0-1]}}$$

$$eU_n = \frac{eU_{[0-1]}}{K_{[0-1]} + eTh_{[0-1]} + eU_{[0-1]}}$$

(Note that the colours defined by a full spread in H and S in this triangular plane produces the triangular colour legends that accompany ternary radioelement maps).

The sum-normalized radioelement channels are mapped on the Cartesian equivalent (Iv_1v_2) of the IHS colour space (Schettigara, 1992). This transformation is illustrated in Figure A1(a). The origin of the Iv1v2 space is defined as the intersection between the v1 and v2 axes with the intensity line in the triangular RGB plane. v1 connect the origin with maximum red r, v2 is perpendicular to v1 within the triangular plane. After vector-normalization, the transformation is written as:

$$[A] = \begin{bmatrix} \frac{2}{\sqrt{6}} & -\frac{1}{\sqrt{6}} & -\frac{1}{\sqrt{6}} \\ 0 & \frac{1}{\sqrt{2}} & -\frac{1}{\sqrt{2}} \\ \frac{1}{\sqrt{3}} & \frac{1}{\sqrt{3}} & \frac{1}{\sqrt{3}} \end{bmatrix} \tag{I.2}$$

If A is applied without normalising with i, (x_1, x_2, x_3) is mapped in cylindrical coordinates. Saturation and hue, as shown in Figure A1 are derived from v_1 and v_2 by:

$$s = \sqrt{v_1^2 + v_2^2} \qquad \text{[A1.5]} \tag{I.3}$$

$$h = \tan^{-1}\left(\frac{v_2}{v_1}\right) \qquad \text{[A1.6]}$$

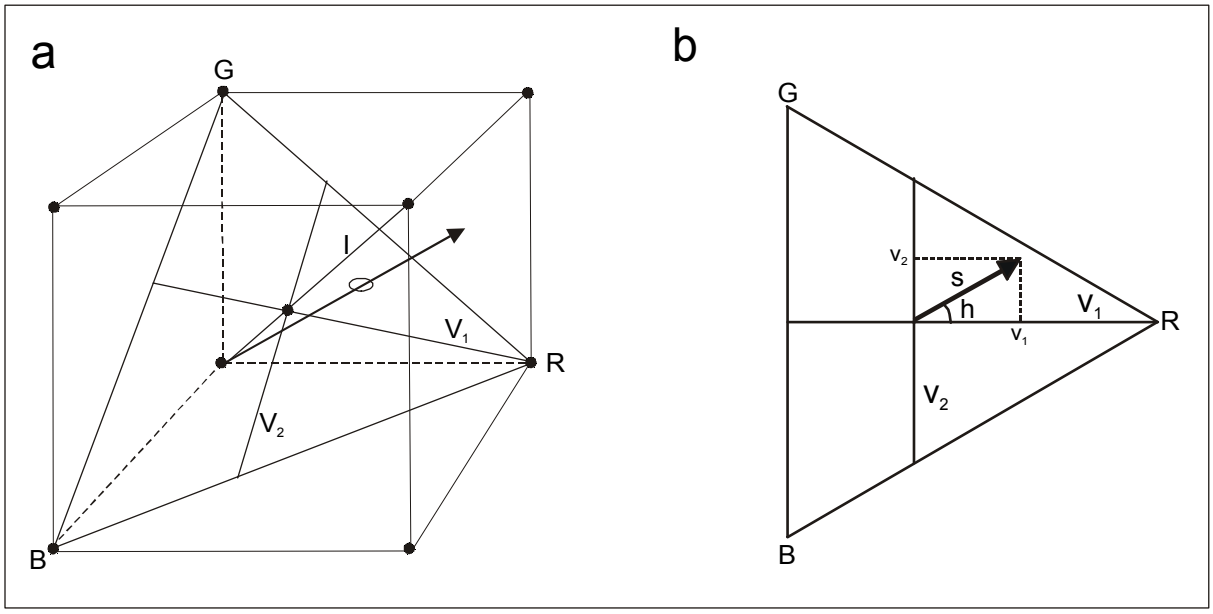

FIG. A1. Transformation from RGB to IHS space.

APPENDIX II. PSEUDO-COLOUR CODING USING THE IHS TRANSFORM

The IHS colour space transformation can be applied to integrate two or three images from different sensors, such as combinations of optical, radar and geophysical images (Harris et al., 1994; Paradella et al., 1997). Two or three image channels are mapped in IHS space after which the H and S channels are transformed to the v_1 and v_2 channels of Iv_1v_2 space:

$$v_1 = s\ cos(h) \tag{II.1}$$

$$v_2 = s\ sin(h)$$

The inverse matrix, $\mathbf{A}^{-1}$, is used to transform the image data set from V_1V_2I space to RGB space:

$$\begin{pmatrix} r \\ g \\ b \end{pmatrix} = \begin{pmatrix} \frac{2}{\sqrt{6}} & 0 & \frac{1}{\sqrt{3}} \\ -\frac{1}{\sqrt{6}} & \frac{1}{\sqrt{2}} & \frac{1}{\sqrt{3}} \\ -\frac{1}{\sqrt{6}} & -\frac{1}{\sqrt{2}} & \frac{1}{\sqrt{3}} \end{pmatrix} \begin{pmatrix} v_1 \\ v_2 \\ I \end{pmatrix} \tag{II.2}$$

Optimal results are obtained when the image dominated by low wave numbers is mapped on hue, and the image of high spatial resolution, or wave number content, is mapped on intensity (Mussakowski et al., 1991). The saturation channel can be used to modulate a third channel or can be set at a constant level. Harris et al., (1994) showed that the saturation level can be adapted to balance the hue and intensity contrasts. If the saturation level is low with respect to the maximum saturation level, the data mapped on the intensity channel is highlighted. If instead a high saturation level is used, the enhanced saturation provides a better perception of hue variation at cost of intensity contrast.

APPENDIX III. INTENSITY SUBSTITUTION TECHNIQUES

Intensity substitution techniques can be expressed in three equations that relates the concentration vector to equal range scaled components ($K_{[0-1]}$ $Th_{[0-1]}$ $U_{[0-1]}$) of a particular grid cell by a transformation T to a (RGB) vector in RGB space. In general form:

$$\begin{pmatrix} r \\ g \\ b \end{pmatrix} = T \begin{pmatrix} K_{[0-1]} \\ eTh_{[[0-1]} \\ eU_{[0-1]} \end{pmatrix} \qquad \text{(III.1)}$$

T is a non-linear transformation that can be decomposed into three matrices and the sum-normalization and de-normalization with the intensity I and replacement intensity I', respectively, modulated by the total count, relief shaded total count or other image data:

$$T = I'[A]^{-1}[E][A]I^{-1} \qquad \text{(III.2)}$$

$$I = \frac{1}{\sqrt{3}}(K_{[0-1]} + eTh_{[0-1]} + eU_{[0-1]})$$

The matrix **A** is the transformation from RGB space to the Cartesian equivalent of IHS space (equation III.3) and A^{-1} is its inverse. The matrix E is a diagonal scale matrix that defines a hue-invariant saturation enhancement:

$$[E] = \begin{bmatrix} e & 0 & 0 \\ 0 & e & 0 \\ 0 & 0 & 1 \end{bmatrix} \qquad \text{(III.3)}$$

The complete transformation is derived by substitution of A, A^{-1} and E in equation III.1:

$$\begin{pmatrix} r \\ g \\ b \end{pmatrix} = \begin{pmatrix} I' \\ I \end{pmatrix} \begin{bmatrix} \frac{1}{3}+\frac{2}{3}e & \frac{1}{3}-\frac{1}{3}e & \frac{1}{3}-\frac{1}{3}e \\ \frac{1}{3}-\frac{1}{3}e & \frac{1}{3}+\frac{2}{3}e & \frac{1}{3}-\frac{1}{3}e \\ \frac{1}{3}-\frac{1}{3}e & \frac{1}{3}-\frac{1}{3}e & \frac{1}{3}+\frac{2}{3}e \end{bmatrix} \begin{pmatrix} K_{[0-1]} \\ eTh_{[[0-1]} \\ eU_{[0-1]} \end{pmatrix} \qquad \text{(III.4)}$$

Equation III.4 directly maps a radioelement data vector ($K_{[0-1]}Th_{[0-1]}$ $U_{[0-1]}$) and replacement intensity I' to a (RGB) vector and involves a user-defined saturation enhancement (e). This transformation provides a method for hue-invariant intensity substitution, at reduced computational costs and includes uniform saturation enhancement. An appropriate value of e may be found by trial and error or by computing the percentage of RGB vectors outside the RGB cube. Note that if there is no saturation enhancement (eg. e =1), the transformation matrix becomes the unity matrix. If saturation enhancement is not necessary, this provides an easy method for substituting gradient enhanced total count or other image data for the intensity of the three radioelement grids.

BIBLIOGRAPHY

ADAMS, J.A.S., LOWDER, W.M. (editors), 1964. The Natural Radiation Environment. University of Chicago Press, Illinois.

ADAMS, J.A., GASPARINI, P., 1970. Gamma ray Spectrometry of Rocks. Elsevier, Amsterdam.

AKERBLOM, G., 1995. "The use of airborne radiometric and exploration survey data and technique in radon risk mapping in Sweden," Application of Uranium Exploration Data and Techniques in Environmental Studies, IAEA-TECDOC-827, IAEA,Vienna, 159-180.

AKERBLOM, G., LINDGREN, J., 1997. "Mapping of groundwater radon potential," Uranium Exploration Data and Techniques Applied to the Preparation of Radioelement Maps, IAEA-TECDOC-980, IAEA, Vienna, 237-255.

AN, P., CHUNG, C.F., RENCZ, A.N., 1995. Digital lithology mapping from airborne geophysical and remote sensing data in the Melville Peninsula, northern Canada using a neural network approach. Remote Sensing of. Environment, v. 53, 76-84.

ANDERSON, H., NASH, C., 1997. Integrated lithostructural mapping of the Rossing area, Namibia using high resolution aeromagnetic, radiometric, Landsat data and aerial photographs. Exploration Geophysics, v. 28, 185-191.

BACON, C.R., 1989, Crystallization of accessory phases in magmas by local saturation adjacent to phenocrysts. Geochimica et Cosmochimica Acta, v. 53, 1055-1066.

BARNET, I., 1995. " The role of airborne gamma spectrometric data in the radon programme of the Czech Republic." Application of Uranium Exploration Data and Techniques in Environmental Studies. IAEA-TECDOC-827, IAEA, Vienna, 151-158.

BARNET, I., MIKSOVA, J., PROCHAZKA, J., 1998. Radon database and radon risk map 1:500000 of the Czech Republic. Radon Investigations in the Czech Republic VII, Czech Geol. Survey, Radon Corp., Prague, 1-5.

BARRITT, S.D., 1983. The controls of radioelement distribution in the Etive and Cairngorm granites: implications for heat production. Unpublished PhD thesis, The Open University, Milton Keynes, England, 320 p.

BARRITT, S.D., 1993. The African magnetic mapping project. ITC Journal, 1993-2, 122-131.

BEA, F., PEREIRA, M.D., CORRETGÉ, L.G. and FERSHTATER, G.B., 1994. Differentiation of strongly peraluminous , perphosphorous granites. The Pedobernardo pluton, central Spain. Geochimica et Cosmochimica Acta, v. 58, 2609-2628.

BEA, F., 1999, Uranium. *In* Encyclopedia of Geochemistry, Marshall, C.P and Fairbridge, R.W. (editors), Kluwer Academic Publishers, London, 712 p.

BIERWIRTH, P., 1996. Investigation of airborne gamma ray images as a rapid mapping tool for soil and land degradation: Wagga Wagga, NSW. Australian Geological Survey Organisation, Record 1996/22.

BILLINGS, S.D., 1998. Geophysical aspects of soil mapping using airborne gamma ray spectrometry. PhD thesis (unpublished), University of Sydney, 1998.

BILLINGS, S.D., HOVGAARD, J., 1999. Modeling detector response in airborne gamma ray spectrometry. Geophysics, v. 64, 1378-1392.

BILLINGS, S.D., FITZGERALD, D.J., 1998. An integrated framework for interpolating airborne geophysical data with special reference to radiometrics. Exploration Geophysics, v. 29, 284-289.

BLACK, P.A., GREEN, C.M., REFORD, S.W., 1995. A pragmatic approach to continental magnetic compilations. Annual Meeting Expanded Abstracts, Society of Exploration Geophysicists, 773-774.

BRIGGS, I.C., 1974. Machine contouring using minimum curvature. Geophysics, v. 45, n.5, 39-48.

BRISTOW, Q., 1978. The application of airborne gamma ray spectrometry in the search for radioactive debris from the Russian satellite COSMOS 954 (Operation "Morning Light"). Geological Survey of Canada, Papers No. 78-1B, 151-162.

BROOME, H.J., CARSON, J.M., GRANT, J.A., FORD, K.L., 1987. A modified ternary radioelement mapping technique and its application to the south coast of Newfoundland. Geological Survey of Canada, Paper 87-14.

BUNDESAMT FÜR STRAHLESCHUTZ (Bfs), 1998. Strahlung und Strahlenschutz, Salzgitter (1998).

CHARBONNEAU, B.W., 1991. Geochemical evolution and radioactive mineralogy of the Fort Smith radioactive belt, Northwest Territories, Canada. *In* Primary Radioactive Minerals (The textural patterns of radioactive mineral paragenetic associations). Theophrastus Publications, Athens, Greece, 21-48.

CHARBONNEAU, B.W., & DARNLEY, A.G., 1970. Radioactive precipitation and its significance to high sensitivity gamma ray spectrometer surveys. Geological Survey of Canada, Paper 70–1, part B, 32–36.

CHARBONNEAU, B.W., HOLMAN, P.B., HETU, R.J., 1994. Airborne geophysical survey, Northeast Alberta. Open file 2807. Geological Survey of Canada, Ottawa.

CHARBONNEAU, B.W., HOLMAN, P.B., HETU, R.J., 1997. Airborne gamma spectrometer magnetic-VLF survey of northeastern Alberta. *In* Exploring for minerals in Alberta: Geological Survey of Canada Geoscience contributions, edited by MacQueen, Canada-Alberta agreement on mineral development. Geological Survey of Canada Bulletin 500, 107-132.

CHAVEZ, P.S., JR., KWARTENG, A.Y., 1989. Extracting spectral contrast in Landsat Thematic Mapper image data using selective principal component analysis. Photogrammetric Engineering & Remote Sensing, v. 55, n.3, 339-348.

CHEESMAN, S., MACLEOD, I., HOLLYER, G., 1998. A new, rapid, automated grid stitching algorithm. Exploration Geophysics, v. 29, 301-305.

CHOPIN, G.R., 1988, Humics and radionuclide migration. Radiochima Acta, v.44/45, 23-28.

CLARK, R.B., DUVAL, J.S. Jr., ADAMS, J.A.S., 1972. Computer Simulation of an Airborne Gamma ray Spectrometer. Journal of Geophysical Research, v. 77,n. 17, 3021-3031.

COOK, S.E., CORNER, R.J., GROVES, P.R., GREALISH, G.J., 1996. Use of airborne gamma radiometric data for soil mapping. Aust. J. Soil Res., v. 34, 183-194.

COX, J.R., 1995. "Radiation detection of buried shielded sources in vehicles loaded with scrap steel." IAEA-TECDOC-827, IAEA, Vienna, 315-318.

CRAIG, M., DICKINSON, B., RODRIGUES, S., 1999. Correcting aerial gamma ray survey data for aircraft altitude. Exploration Geophysics, v. 30, 161-166.

DARCE, M., 1990. Mineralogic Alteration Patterns in Volcanic Rocks of the La Libertad Gold Mining District and its Surroundings, Nicaragua. Economic Geology, v. 85, 1059-1071.

DARNLEY, A.G., 1996. "Uranium exploration data and global geochemical baselines: The need for coordinated action," In Uranium Exploration Data and Techniques Applied to the Preparation of Radioelement Maps, IAEA-TECDOC-980, IAEA, Vienna.

DARNLEY, A.G., BJÖRKLUND, A., BØLVIKEN, B., GUSTAVSSON, N., KOVAL, P.V., PLANT, J.A., STEENFELT, A., TAUCHID, M., XUEJING, X., 1995. A Global Geochemical Database for Environmental and Resource Management. Final Report of IGCP Project 259, UNESCO Publishing, Paris.

DICKSON, B.L., SCOTT, K.M., 1997. Interpretation of aerial gamma ray surveys-adding the geochemical factors. AGSO Journal of Australian Geology & Geophysics, v. 17, n.2, 187-200.

DICKSON, B.L., 2001. Improving the quality of aerial gamma ray surveys. Extended Abstracts, 15th Geophysical Conference, Australian Society of Exploration Geophysicists.

DONKER, N.H.W., MULDER, N.J., 1976. Analysis of MSS digital imagery with the aid of principal component transform. 13th Congress of the Intern. Soc. Photogrammetry and Remote Sensing, Helsinki (ISP Commission VII).

DRURY, S.A., 1992. Image Interpretation in Geology. 2nd edition, Allen and Unwin, London, 243 p.

DURRANCE, E.M., 1986. Radioactivity in Geology: Principles and Application. Ellis and Horwood, Chichester.

EBERLE, D., 1993, Geological mapping based on multivariate statistical analysis of airborne geophysical data. ITC Journal 1993-2, 173-178.

FORD, K.L., SAVARD, M., DESSAU, J.-C., PELLERIN, E., CHARBONNEAU, B.W., SHIVES, R.B.K., 2000. The role of gamma ray spectrometry in radon risk evaluation: A case history from Oka, Quebec. GeoCanada 2000 Abstracts CD-ROM.

FULLAGAR, P.K., FALLON, G.N., 1997. Geophysics in metalliferous mines for ore body delineation and rock mass characterisation. *In* "Proceedings of Exploration 97: Fourth Decennial Conference on Mineral Exploration" edited by A.G. Gubins, 573-584.

GILLESPIE, A.R., KAHLE, A.B., WALKER, R.E., 1986. Colour enhancement of highly correlated images. Decorrelation and IHS contrast stretches, Remote Sensing and Environment, v. 20, 209-235.

GIVENS, W.W., MILLS, W.R., DENNIS, C.L., 1976. Uranium assay logging using a pulsed 14 MeV neutron source and detection of delayed fission neutrons. Geophysics, v. 41, n. 3, 468-490.

GNOJEK, I., PRICHYSTAL, A., 1985. A new zinc mineralization detected by airborne gamma ray spectrometry in Northern Moravia (Czechoslovakia). Geoexploranium, 23, 491-502.

GOOSENS, M.A., 1992. Petrogenesis of the mineralised granitic intrusion near Los Santos, Spain, and remote sensing and data integration as a tool in regional exploration for granite related mineralization. PhD Thesis, 148 p.

GRAHAM, D.F., BONHAM-CARTER, G.F., 1993. Airborne radiometric data: a tool for reconnaissance geological mapping using a GIS. Photogrammetric Engineering and Remote Sensing, v.58, n.8, 1243-1249.

GRANT, J.A., 1998. Ten things the textbooks don't tell you about processing and archiving airborne gamma ray spectrometric data. *In* Current Research 1998 D. Geological Survey of Canada, Ottawa, 83-87.

GRASTY, R.L., 1979. Gamma ray spectrometric methods in uranium exploration – Theory and operational procedures. *In* Geophysics and Geochemistry in the Search for Metallic Ores, edited by P.J. Hood, Geological Survey of Canada Economic Geology Report 31, 147-161.

GRASTY, R.L., 1982. Direct snow-water equivalent measurement by airborne gamma ray spectrometry. Journal of Hydrology, v. 55, 213-235.

GRASTY, R.L., 1987. The design, construction and application of airborne gamma ray spectrometer calibration pads – Thailand. Geological Survey of Canada Paper 87-10.

GRASTY, R.L., 1997. Radon emanation and soil moisture effects on airborne gamma ray measurements. Geophysics, v. 62, n. 5, 1379-1385.

GRASTY, R.L., 2001. Spectral component analysis applied to portable gamma ray spectrometry. Extended Abstracts, 15th Geophysical Conference, Australian Society of Exploration Geophysicists.

GRASTY, R.L., CARSON, J.M., Charbonneau, B.W., Holman, P.B., 1984. Natural Background Radiation in Canada. Geol. Surv. Can. Bull. 360.

GRASTY, R.L., COX, J.R., 1997. A car-borne gamma ray spectrometer system for natural radioactivity mapping and environmental monitoring. *In* RESUME 95, Rapid Environmental Surveying Using Mobile Equipment, Report, Nordic Nuclear Safety Research Secretariat, 71-90.

GRASTY, R.L., HOLMAN, P.B., BLANCHARD, Y., 1991. Transportable calibration pads for ground and airborne gamma ray spectrometers. Geol. Survey. Can. Paper (1991) 90-23.

GRASTY, R.L., LAMARRE, J., Environmental Monitoring at Nuclear Power Plant Using 3×3 inch Sodium Iodide Gamma ray Spectrometer. A paper, personal communication.

GRASTY, R.L., MINTY B.R.S., 1995. A guide to the technical specifications for airborne gamma–ray surveys. Australian Geological Survey Organisation Record 1995/60.

GRASTY, R.L., SANDER, L., 2001. Airborne gamma ray surveys over Canadian nuclear sites. Expanded Abstracts, 63rd Annual Conference, European Association of Geoscientists and Engineers.

GRASTY, R.L., SHIVES, R.B.K., 1997. Applications of gamma ray spectrometry to mineral exploration and geological mapping, Workshop presented at Exploration 97: Fourth Decennial Conference on Mineral Exploration.

GRASTY, R.L., TAUCHID, M., TORRES, M., 1995. "Standardization of old gamma ray survey data," Application of Uranium Exploration Data and Techniques in Environmental Studies, IAEA-TECDOC-827, IAEA, Vienna, 35-45.

GREEN, A.A., 1987. Leveling airborne gamma-radiation data using between-channel correlation information. Geophysics, v. 52, 1557-1562.

GREEN, A.A., BERMAN, M., SWITZER, P., CRAIG, M.D., 1988. A transformation for ordering multispectral data in terms of image quality with implications for noise removal. IEEE Trans. Geosci. and Remote Sensing, GE-26, 65-74.

GREEN, B.M.R., HUGHES, J.S., LOMAS, P.R., 1993. Radiation Atlas. Natural Sources of Ionizing Radiation in Europe, CEC, Luxemburg.

GRUMER, W.K., CAMPBELL, F.R., KNIGHT, G.B., RICARD, J.L., 1980. COSMOS 954, The occurrence and nature of recovered debris. Canadian Atomic Energy Control Board, INFO-0006, May, 1980.

GUNN, P.J., 1978. Inversion of airborne radiometric data. Geophysics, v. 43, 133-142.

GUNN, P.J., ALMOND, R., 1997. A method for calculating equivalent layers corresponding to large aeromagnetic and radiometric grids. Exploration Geophysics, v. 28, 72-79.

GUNN, P.J., FITZGERALD, D., YASSI, N., DART, P., 1997. New algorithms for visually enhancing airborne geophysical data. Exploration Geophysics, v. 28, 220-224.

HARRIS, J.R., 1989. Clustering of gamma ray spectrometer data using a computer image analysis system. *In* Statistical Applications in the Earth Sciences, edited by Agterberg and Bonham-Carter, Geological Survey of Canada, Paper 89-9, 19-31.

HARRIS, J.R., MURRAY, R., HIROSE, T., 1990. IHS Transform for the integration of Radar imagery and other remotely sensed data. Photogrammetric Engineering & Remote Sensing, v. 56, n.12, 1631-1641.

HARRIS, J.R., BOWIE, C., RENCZ, A.N., GRAHAM, D., 1994. Computer enhancement techniques for the integration of remotely sensed, geophysical, and thematic data for the geosciences. Canadian Journal of Remote Sensing, v. 20, n.3, 210-221.

HEATH, R.L., 1964. Scintillation spectrometry. Gamma ray spectrum catalogue, 2nd Edition, Volumes 1 and 2: U.S.A.E.C. Research and Development Report IDO–16880–1, Physics T.I.D. – 4500 (31st Edition).

HORSFALL, K.R., 1997 Airborne magnetic and gamma ray data acquisition. AGSO Journal of Australian Geology & Geophysics, v.17, n.2, 159-174.

HOVGAARD, J., AND GRASTY, R.L., 1997. Reducing statistical noise in airborne gamma ray data through spectral component analysis. *In* "Proceedings of Exploration 97: Fourth Decennial Conference on Mineral Exploration" edited by A.G. Gubins, 753-764.

INTERNATIONAL ATOMIC ENERGY AGENCY, 1976. Radiometric Reporting Methods and Calibration in Uranium Exploration, Technical Reports Series No. 174, IAEA, Vienna.

INTERNATIONAL ATOMIC ENERGY AGENCY, 1979. Gamma Ray Surveys in Uranium Exploration, Technical Reports Series No. 186, IAEA, Vienna.

INTERNATIONAL ATOMIC ENERGY AGENCY, 1987. Preparation and Certification of IAEA Gamma ray Spectrometry Reference Materials RGU-1, RGTh-1 and RGK-1, Techn. Report-IAEA/RL/148, IAEA, Vienna.

INTERNATIONAL ATOMIC ENERGY AGENCY, 1989. Construction and Use of Calibration Facilities for Radiometric Field Equipment, Technical Reports Series No. 309, IAEA, Vienna.

INTERNATIONAL ATOMIC ENERGY AGENCY, 1990. The Use of Gamma Ray Data to Define the Natural Radiation Environment, IAEA-TECDOC-566, Vienna.

INTERNATIONAL ATOMIC ENERGY AGENCY, 1991. Airborne Gamma Ray Spectrometer Surveying, Technical Reports Series, No. 323, IAEA, Vienna.

INTERNATIONAL ATOMIC ENERGY AGENCY, 1995. Application of Uranium Exploration Data and Techniques in Environmental Studies. IAEA-TECDOC-827, Vienna.

INTERNATIONAL ATOMIC ENERGY AGENCY, 1997. Uranium Exploration Data and Techniques Applied to the Preparation of Radioelement Maps. IAEA-TECDOC-980, Vienna.

ICRP, 1991. ICRP Publication 60, Recommendations of the International Commission on Radiological Protection, Pergamon Press, Oxford.

ICRP, 1993. ICRP Publication 65, Protection against Radon-222 at Home and Work, International Commission on Radiological Protection, Pergamon Press, Oxford.

ICRU, 1994. Gamma ray Spectrometry in the Environment, ICRU Report 53, International Commission On Radiation Units And Measurements, Bethesda, USA.

ISO, 1992a. Atomic and Nuclear Physics, ISO 31-9.

ISO, 1992b. Nuclear Reactions and Ionizing Radiation, ISO 31-10.

IVANOVICH, M., HARMON, R.S., 1982. Uranium Series Disequilibrium: Applications to Environmental Problems, Clarendon Press, Oxford.

JAQUES, A.L., WELLMAN, P., WHITAKER, A., WYBORN, D., 1997. High resolution geophysics in modern geological mapping. AGSO Journal of Australian Geology & Geophysics, v. 17, n.2, 159-174.

JAYAWARDHANA, P.M., SHEARD, S.N., 1997. The use of airborne gamma ray spectrometry by M.I.M. Exploration – A case study from the Mount Isa Inlier, northwest Queensland, Australia. *In* Proceedings of Exploration 97: Fourth Decennial Conference on Mineral Exploration" edited by A.G. Gubins, 765-774 (reprinted in 2000, Geophysics, v. 65, n. 6, 1993-2000).

JONES, E.J.W., 1999. Marine Geophysics, John Wiley & Sons Ltd., Chichester, 466 p.

KARLSSON, S., MELLANDER, H., LINDGREN, J., FINCK, R., LAURITZEN, B., 2000. RESUME 99, Rapid Environmental Surveying Using Mobile Equipment, Report from the NKS/BOK-1.2 Project Group Mobile Measurements and Measurement Strategies, NKS-15, Nordic Nuclear Safety Research Secretariat, 78 p.

KILLEEN, P.G., 1979. Gamma ray spectrometric methods in uranium exploration – Application and interpretation. *In* Geophysics and Geochemistry in the Search for Metallic Ores, edited by P.J. Hood, Geological Survey of Canada Economic Geology Report 31, 163-230.

KILLEEN, P.G., 1986. A system of deep test holes and calibration facilities for developing and testing new borehole geophysical techniques. *In* "Proceedings of Borehole Geophysics for Mining and Geotechnical Applications", edited by P.G. Killeen, Geological Survey of Canada Paper 85-27, 29-46.

KILLEEN, P.G., 1997a. Borehole geophysics: Exploring the third dimension. *In* "Proceedings of Exploration 97: Fourth Decennial Conference on Mineral Exploration" edited by A.G. Gubins, 31-42.

KILLEEN, P.G., 1997b. Nuclear techniques for ore grade estimation. *In* "Proceedings of Exploration 97: Fourth Decennial Conference on Mineral Exploration" edited by A.G. Gubins, 677-684.

KIRKEGAARD & LOVBORG, 1974, Computer modelling of terrestrial gamma-radiation fields. Riso Report No. 303.

KOGAN, R.M., NAZAROV, I.M., FRIDMAN, S.D., 1971. Gamma spectrometry of Natural Environments and Formations. Israel Programme for Scientific Translations.

KORUN, M., LIKAR, A., LIPOGLAVSEK, M., MARTINCIC, R., PUCELJ, B., 1993. In-situ Measurement of Cs-distribution in the Soil. Umweltradioaktivitat, Radiookologie, Strahlenwirkungen, Band I., Verlag TUV Rheiland, Koln, 417-421.

KOVARCH, A., FLOOD, P.G., TYNE, E., 1994. Geographical information systems for regional scale geological analysis: the Manilla 1:250,000 map area, a case study. Proceedings of the 7th Australian Remote Sensing Conference, 1076-1083.

KRASNOV, A.I., MATVEEV, A.V., SMIRNOV, G.S., et al., 1975. Airborne gamma ray spectrometric method of weakly manifested uranium deposits exploration (in Russian). Ministry of Geology of USSR, Nedra, Leningrad, 1-156.

KRASNOV, A.I., et al., 1980. Geophysical airborne methods of uranium deposits prognostication (in Russian). Atomisdat, Moscow, 1-128.

KRISHNASWAMI, S., 1999. Thorium. *In* Encyclopedia of Geochemistry. Marshall, C.P and Fairbridge, R.W. (editors), Kluwer Academic Publishers, London, 712 p.

LAHTI, M., JONES, D.G., MULTALA, J., RAINEY, M.P., 2001. Environmental applications of airborne radiometric surveys. Expanded Abstracts, 63rd Annual Conference, European Association of Geoscientists and Engineers.

LANNE, E., 1986. Statistical multivariate analysis of airborne geophysical data on the SE border of the central Laplan greenstone complex. Geophysical Prospecting v. 34, 1111-1128.

LANGMUIR, D., HERMANS, J.S., 1980. The mobility of thorium in natural waters at low temperatures. Geochimica et Cosmochimica Acta, v. 44, 1753-1766.

LEE, J.B., WOODYATT, A.S., BERMAN, M., 1990, Enhancement of high spectral resolution remote-sensing data by a noise-adjusted principal components transform: IEEE Trans. Geosci. and Remote Sensing, v. 28(3), 295-304.

LEE, M.K., PEART, R.J., CUSS, R.J., JONES, D.G., BEAMISH, D., VIRONMAKI, J., 2001. Applications and challenges for high resolution airborne surveys in populated areas. Expanded Abstracts, 63rd Annual Conference, European Association of Geoscientists and Engineers.

LEGAULT, M.I., CHARBONNEAU, B.W., 1993. Geophysical, geochemical and petrological study of Contwoyto Batholith, Lupin Gold Mine area, Northwest Territories. *In* Current Research Part E, Geological Survey of Canada, Paper 93-1E, 207-218.

LeSCHACK, L.A., 1998. Magnetic horizontal gradient intensity (HGI) and radiometric surveys for hydrocarbon exploration in Western Canada: Seven case histories. AAPG Bulletin, v. 82, n. 13.

LILLESAND, T.M., KIEFER, R.W., 1994. Remote Sensing and Image Interpretation. 3rd edition, John Wiley & Sons, Inc. New York, 750 p.

LO, B.H., PITCHER, D.H., 1996. A case history on the use of regional aeromagnetic and radiometric data sets for lode gold exploration in Ghana. Annual Meeting Expanded Abstracts, Society of Exploration Geophysicists, 592-595.

LØVBORG, L., KIRKEGAARD, P., & ROSE-HANSEN, J., 1972. Quantitative interpretation of the gamma ray spectra from geologic formations. In The Natural Radiation Environment II, Adams, J.A.S., Lowder, W.M., and Gesell, T.F. (eds.), U.S. Dept. of Commerce, Springfield, Va., 155-180.

LØVBORG, L., 1984. The calibration of portable and airborne gamma ray spectrometers - theory, problems and facilities. Report Riso-M-2456, Roskilde.

LØVBORG, L., MOSE, E., 1987. Counting statistics in radioelement assaying with a portable spectrometer. Geophysics, v. 52, n.4, 555-563.

LØVBORG, L., NYEGAARD, P., CHRISTIANSEN, E.M., NIELSEN, B.L., 1980. Borehole logging for uranium by gamma ray spectrometry. Geophysics, v. 45, 1077-1090.

LUBECKI, A., WOLF, R., 1978. Status report about the development of a XRF borehole probe for uranium determination. Paper presented at the NEA/IAEA workshop on uranium borehole logging, Grand Junction, February 1978.

LUYENDYK, A.P.J., 1997. Processing of airborne magnetic data. AGSO Journal of Australian Geology & Geophysics, v. 17, n. 2, 31-38.

MANOVA, M., MATOLIN, M., 1995. Radiometric map of the Czech Republic 1:500000. Czech Geol. Survey, Prague.

MARES, S., et al., 1984. Introduction to Applied Geophysics. D. Reidel Publ. Comp., Dordrecht, Holland.

MATOLIN, M., 1980. Prospection Aerienne par Spectrometrie Gamma. Rapport au Gouvernement Marocain, AT Rapport No. 1705, WP/5/1705, AIEA, Vienne. Report of a three month IAEA expert mission in Rabat, Morocco, 1 June – 31 August 1980 under an IAEA TC Project MOR/3/005, 12 pages.

MATOLIN, M., 1991. Uranium Exploration - Field gamma ray spectrometry. Report to the Government of the Republic of Nicaragua, IAEA TC-Project NIC/3/003-02, IAEA, Vienna. Report of a two month IAEA expert mission to Managua, Nicaragua, 27 June – 26 August 1991, 18 pages.

MATOLIN, M., 1994. Uranium Favourability and Evaluation in Mongolia. Report to the Government of Mongolia, IAEA TC-Project MON/3/002-03, IAEA, Vienna.

MATOLIN, M., 1995. "Progress in gamma and radon detection methods in geophysical investigation," Recent Developments in Uranium Resources and Supply, IAEA-TECDOC-823, IAEA, Vienna, 91-95.

MATOLIN, M., 1997a. "Terrestrial gamma dose rate maps, their compilation and verification radiometric map of the Czech Republic," Uranium Exploration Data and Techniques Applied to the Preparation of Radioelement Maps, IAEA-TECDOC-980, Vienna, 53-57.

MATOLIN, M., 1997b. "Radiometric map of the Czech Republic and uranium mineralization," Changes and events in uranium deposits, development, exploration, resources, production and the world supply-demand relationship, IAEA-TECDOC-961, Vienna, 207-212.

MATOLIN, M., et al., 1993. Investigation of distribution of natural and anthropogenic substances in the area of eastern Ore Mountains - an ecosystem at the traverse Cinovec – Teplice. Report, Charles University, Faculty of Science, Prague (in Czech).

McDONOUGH, M.R., GROVER, T.W., McNICOLL, V.J., LINDSAY, D.D., KELLY, K.L. and GUERSTEIN, P.G., 1994d, Geology Mercredi Lake, Alberta – Northwest Territories (75/M15). Geological survey of Canada, Calgary, Open File 2904, scale 1:50,000.

McLACHLAN, G.J., 1992. Discriminant Analysis and Statistical Pattern Recognition. New York, Wiley, 300 p.

MELLANDER, H., 1989. Airborne gamma spectrometric measurements of the fall-out over Sweden after the nuclear reactor accident at Chernobyl, USSR. IAEA Report NM-89-1, IAEA, Vienna.

MELLANDER, H., 1995. “The role of mobile gamma spectrometry in the Swedish emergency response programme for nuclear accidents – experience and future plans,” Application of Uranium Exploration Data and Techniques in Environmental Studies, IAEA-TECDOC-827, IAEA, Vienna, 187-195.

MENDE, A., 1993. Chemical and Radiochemical Investigations on a Rock Pile of the Hard Coal Mining in the Area Dohlener Becken, Umweltsradioaktivität, Radiookologie, Strahlenwirkungen, Band I., Verlag TUV Rheiland, Köln ,11-16.

MERRIAM, D.F., 1969. Computer applications in the earth sciences, Plenum, New York, 281 p.

MILLIGAN, P., GUNN, P., 1997. Enhancement and interpretation of airborne geophysical data, AGSO Journal of Australian Geology & Geophysics, v.17, n.2, 63-75.

MINTY, B.R.S., 1991. Simple micro-levelling for aeromagnetic data (short note). Exploration Geophysics, v. 22, 591-592.

MINTY, B.R.S., 1997. Fundamentals of airborne gamma ray spectrometry. AGSO Journal of Australian Geology and Geophysics, v. 17, n. 2, 39-50.

MINTY, B.R.S. 1998a. Multichannel models for the estimation of radon background in airborne gamma ray spectrometry. Geophysics, v. 63, n. 6, 1986-1996.

MINTY, B.R.S. 1998b. Recent developments in the processing of airborne gamma ray spectrometric data. Preview, Issue n. 75.

MINTY, B.R.S., 2000a. Automatic merging of gridded airborne gamma ray spectrometric surveys. Exploration Geophysics, v. 31, 47-51.

MINTY, B.R.S. 2000b. Reducing noise in airborne gamma ray spectra. Preview, Issue n. 89.

MINTY, B.R.S., HOVGAARD, J. 2001. Spectral methods for reducing noise in gamma ray spectrometry. Extended Abstracts, 15th Geophysical Conference, Australian Society of Exploration Geophysicists.

MINTY, B., LUYENDYK, A., BRODIE, R., 1997. Calibration and data processing for airborne gamma ray spectrometry. AGSO Journal of Australian Geology and Geophysics, v. 17, n. 2, 51-62.

MINTY, B.R.S., McFADDEN, P., 1998. Improved NASVD smoothing of airborne gamma ray spectra. Exploration Geophysics, v. 29, n. 3/4, 516-523.

MITTLEFEHLDT, D.W., 1999. Potassium. *In* Encyclopedia of Geochemistry, Marshall, C.P and Fairbridge, R.W. (editors), Kluwer Academic Publishers, London, 712 p.

MUNDIGL, S., BRUMMER, Ch., WINKELMANN, I., 1994. Vergleichsmessungen der Bodenkontamination mit Hilfe der In-situ-Gamma-spektrometrie. BfS Jahresbericht 1993, Salzgitter, 153-156.

MUSSAKOWSKI, R., TROWELL, N.F., HEATHER, K.B., 1991. Digital integration of remote sensing and geoscience data for the Goudreau-Lochalsh area, Wawa, Ontario. Canadian Journal of Remote Sensing, v.17, n.2, 162-173.

NASH, C., LEEMING, P., KOTASEK, H., CAREY, R., 1996. Integrated interpretation of imaged airborne geophysical survey and remote sensing data with the aid of vectorised CAD/GIS coverages: Halls Creek mobile Belt, Australia. *In* Proceedings of the Eleventh Thematic Conference on Geologic Remote Sensing, 27-29 February, 1996, Las Vegas, Nevada, USA, v. 1, 343-352.

NIBLACK, W., 1986. An introduction to digital image processing. Prentice/Hall International, London, 215 p.

NKS, 1997. RESUME 95, Rapid Environmental Surveying Using Mobile Equipment, Report, Nordic Nuclear Safety Research Secretariat, 440 p.

NOVOTNA, J., 1986. Review of Irradiation Sources to Population. Protection at work with sources of ionizing radiation in national economy, Centr. Inf. Centre for Nucl. Progr., Zbraslav, 62-68 (in Czech).

OTTON, J.K., et al., 1995. "Uranium resource assessment and exploration data for geologic radon potential assessment in the United States," Application of Uranium Exploration Data and Techniques in Environmental Studies, IAEA-TECDOC-827, IAEA, Vienna, 135-137.

PARADELLA, W.R., BIGNELLI, P.A., VENEZIANI, P., PIETSCH, R.W., TOUTIN, T., 1997. Airborne and spaceborne synthetic aperture radar (SAR) integration with Landsat TM and gamma ray spectrometry data for geological mapping in a tropical rainforest environment. Carajas Mineral Province, Brazil, International Journal of Remote Sensing, v.18, n.7, 1483-1502.

PAVLIK, B., BOTTOS, F., CUNEEN, P.J., JURZA, P., HOESCHL, V., 1997. "Airborne and truck-borne "radiation footprints" of areas producing, storing, using or being exposed to nuclear materials," Uranium Exploration Data and Techniques Applied to the Preparation of Radioelement Maps. IAEA-TECDOC-980, IAEA, Vienna, 269-277.

PFEISTER, H., PAULY, H., 1980. External Radiation Exposure due to Natural Radionuclides in Phosphate Fertilisers in the Federal Republic of Germany. Seminar on the Radiological Burden of Man from Natural Radioactivity in the Countries of European Communities, CEC Report V/2408/80, 447-467.

PGW, CPRM, GSC, 1997. The Brazil Airborne Radiometric Mapping Project. Report by Paterson, Grant & Watson Limited and Companhia de Pesquisa de Recursos Minerais (Geological Survey of Brazil) and Geological Survey of Canada.

PITCHER, W.S., 1993. The nature and origin of granites. 321 p. Blackie Academic & Professional, Chapman and Hall, Glasgow, 321 p.

PRESS, S.J., 1972. Applied Multivariate Analysis. Holt, Rinehart and Winston Inc., 521p.

REFORD, S.W., GUPTA, V.K., PATERSON, N.R., KWAN, K.C.H., MACLEOD, I.N., 1990. The Ontario master aeromagnetic grid: a blueprint for detailed magnetic compilation on a regional scale. Annual Meeting Expanded Abstracts, Society of Exploration Geophysicists, 617-619.

RICHARDSON, L.M., 2000. Errors in digital elevation models derived from airborne geophysical data. Australian Geological Survey Organisation, Record 2000/37.

ROBERTSON, P.K. & O'CALLAGHAN, J.F., 1988. The application of perceptual colour spaces to the display of remotely sensed data. IEEE Transaction on geoscience and remote sensing, v. 26, n.1, 49-59.

ROBSON, D., 1998. Positive impacts and future direction of Discovery 2000. Exploration Geophysics, v. 29, 584-591.

ROSSI, B.B., STAUB, H.H., 1949. Ionization Chambers and Counters. McGraw-Hill Book Comp., New York.

RUBIN, R.M., LEGGET, D., WELLS, M.B., 1980. Effects of Overburden, Biomass and Atmospheric Inversions on Energy and Angular Distribution of Gamma Rays from U, K, Th and Airborne Radon Sources. Radiation Res. Associates, Report GJBX-141 81, Fort Worth.

RYBACH, L., 1976. Radioactive heat production in rocks and its relation to other petrophysical parameters. Pure and Applied Geophysics, v. 114, 309-318.

SANDERSON, D.C.W., ALLYSON, J.D., TYLER, A.N., SCOTT, E.M., 1995. "Environmental applications of airborne gamma ray spectrometry," Application of Uranium Exploration Data and Techniques in Environmental Studies, IAEA-TECDOC-827, IAEA, Vienna, 71-79.

SANDERSON, D.C.W., FERGUSON, J.M., 1997. The European capability for environmental airborne gamma ray spectrometry. Radiation Protection Dosimetry, v. 73, 213-218.

SAUNDERS, D.F., BURSON, K.R., BRANCH, J.F., THOMPSON, C.K., 1993. Relation of thorium-normalized surface and aerial radiometric data to subsurface petroleum accumulations. Geophysics, v. 58, 1417-1427.

SAUNDERS, D.F., BRANCH, J.F., THOMPSON, C.K., 1994. Tests of Australian aerial radiometric data for use in petroleum reconnaissance. Geophysics, v. 59, 411-419.

SAUNDERS, D.F., BURSON, K.R., THOMPSON, C.K., 1999. Model for hydrocarbon microseepage and related near-surface alterations. AAPG Bulletin, v. 83, n. 1, 170-185.

SCHETSELAAR, E.M., 2002. Petrogenetic interpretation from gamma ray specterometry and geological data: the Arch Lake zoned peraluminous granite intrusion, Western Canadian Shield. Exploration Geophysics v. 33, 35-43.

SCHETSELAAR, E.M., 2001. On preserving spectral balance in image fusion and its advantages for geological image interpretation. Photogrammetric Engineering and Remote Sensing v. 67, n. 8, 925-934.

SCHETSELAAR, E.M., CHUNG, C.F., KIM, K., 2000. Classification of bedrock units in vegetated granite-gneiss terrain by the integration of airborne geophysical images and primary field data. Remote Sensing of Environment v. 71, 89-105.

SCHETSELAAR, E.M., 1998. Fusion by the IHS transform: should we use cylindrical or spherical coordinates. International Journal of Remote Sensing, v.19, n. 4, 759-765.

SCHETTIGARA, V.K., 1992. A generalised component substitution technique for spatial enhancement of multispectral images using higher resolution data. Photogrammetric Engineering and Remote Sensing, v.58, n.5, 561-567.

SCHMID, K., OLSCHEWSKI, K., 1986. Practical aspects and experience resulting from borehole models for gamma ray logging in uranium exploration. *In* "Proceedings of Borehole Geophysics for Mining and Geotechnical Applications", edited by P.G. Killeen, Geological Survey of Canada Paper 85-27, 47-52.

SCHUMACHER, D., 2000. Surface geochemical exploration for petroleum. Chapter 18 *in* Exploring for Oil and Gas Traps edited by E.A. Beaumont and N.H. Foster, Treatise of Petroleum Geology, Handbook of Petroleum Geology, American Association of Petroleum Geologists.

SCHWARZ, G.F., KLINGELE, E.E., RYBACH, L., 1992. How to handle rugged topography in airborne gamma ray spectrometry surveys. First Break, v. 10, n. 1, 11-17.

SHIVES, R.B.K., FORD, K.L., CHARBONNEAU, B.W., 1995. Geological Survey of Canada Workshop Manual: Applications of Gamma ray Spectrometric/Magnetic/VLF-EM Surveys. Geological Survey of Canada, Open File 3061, 85 p.

SHIVES, R.B.K., CHARBONNEAU, B.W., FORD, K.L., 1997. The detection of potassic alteration by gamma ray spectrometry - Recognition of alteration related to mineralisation. *In* Proceedings of Exploration 97: Fourth Decennial Conference on Mineral Exploration, edited by A.G. Gubins, 741-752 (reprinted in 2000, Geophysics, v. 65, n. 6, 2001-2011).

SMITH, G.W., 1977. Status report on the development of a prompt fission neutron uranium borehole logging technique. Sandia Laboratories, SAND 77-0336, 1-55.

STEINMAN, D.K., et al., 1976. Californium-252-based borehole logging system for in-situ assaying of uranium ore. Exploration for Uranium Ore Deposits, Proceedings of a Joint OECD/NEA-IAEA Sympoisum held in Vienna from 29 March – 2 April 1976, STI/PUB/434, p. 487-498.

SURAN, J., 1998. Evaluation of effectiveness of uranium exploration methods (in Czech). Uhli, rudy, geologicky pruzkum no. 12, Praha, 387-389.

SWITZER, P., & GREEN, A., 1984, Min/max autocorrelation factors for multivariate spatial imagery: Dept. of Statistics, Stanford University, Tech. Rep. 6.

TARLOWSKI, C., SIMONIS, F., WHITAKER, A., MILLIGAN, P., 1992. The magnetic anomaly map of Australia. Exploration Geophysics, v. 23, 339-342.

TELFORD, W.M., GELDART, L.P., SHERIFF, R.E., 1990. Applied Geophysics, Second Edition, Cambridge University Press, Cambridge, 770 p.

TOIVONEN, H., 1997. Detection of hidden sources – Prompt reports by airborne teams in RESUME 95. *In* RESUME 95, Rapid Environmental Surveying Using Mobile Equipment, Report, Nordic Nuclear Safety Research Secretariat, 323-339.

TOMPKINS, R., CLARK, J.R., ZIEGLER, D., 2000. Enzyme leach^{SM} geochemistry: A significant advancement in hydrocarbon exploration. AAPG Bulletin, v. 84, n. 13.

TYAPKIN, O.K., SHAPAR, A.G., YTOYAN, J.G., 2001. The prediction of changes of a radiological situation of industrial advanced regions of NIS. Expanded Abstracts, 63rd Annual Conference, European Association of Geoscientists and Engineers.

UNSCEAR, 1982. Ionizing Radiation Sources and Biological Effects, Report, United Nations Scientific Committee On The Effects Of Atomic Radiation.

UNSCEAR, 1988. Exposures from Natural Sources of Radiation, Report, United Nations Scientific Committee On The Effects Of Atomic Radiation.

UNSCEAR, 1993. Sources and Effects of Ionizing Radiation. Report, United Nations Scientific Committee On The Effects Of Atomic Radiation, New York.

VERSTEEG, J.K., PATERSON, N.R., 1997. Report on re-evaluation of airborne geophysical anomalies, Guaniamo area, Venezuela. Paterson, Grant & Watson Limited, confidential report.

VULKAN, U., SHIRAV, M., 1997. "Radiometric Maps of Israel - Partial Contribution to the Understanding of Potential Radon Emanations," Uranium Exploration Data and Techniques Applied to the Preparation of Radioelement Maps. IAEA-TECDOC-980, IAEA, Vienna, 119-124.

WAHL, J.S., 1983. Gamma ray logging. Geophysics, v. 48, 1536-1550.

WELLMAN, P., 1998. Mapping of a granite batholith using geological and remotely sensed data: the Mount Edgar Batholith, Pilbara Craton. Exploration Geophysics, v. 29, 643-648.

WENK, G.J., DICKSON, B.L., 1981. The gamma-logging calibration facility at the Australian Mineral Development Laboratories. Exploration Geophysics, v. 12, no. 3, 37-39.

WILFORD, J.R., 1992. Regolith mapping using integrated Landsat TM imagery and high resolution gamma ray spectrometry – Cape York Peninsula. Australian Geological Survey Organisation, Record 1992/78.

WILFORD, J.R., 1995. Airborne gamma ray spectrometry as a tool for assessing relative landscape activity and weathering development of regolith, including soils. AGSO Res. News, v. 22, 12-14.

WILFORD, J.R., BIERWIRTH, P.N., CRAIG, M.A., 1997. Application of airborne gamma ray spectrometry in soil/regolith mapping and applied geomorphology. AGSO Journal of Australian Geology and Geophysics, v. 17, n. 2, 201-216.

GLOSSARY

absorption of gamma rays: The process resulting from interaction of gamma quanta (photons) with matter, caused by photoeffect and pair production.

accuracy of gamma ray spectrometry analyses: The reliability of analyses in the sense of the relationship of resulting data to the true value of the radioelement concentration.

activity: The rate at which nuclear transformations occur in a radioactive material. The SI unit of activity is the reciprocal second (s^{-1}), termed the becquerel (Bq).

airborne gamma ray spectrometer: A high sensitivity gamma ray spectrometer with the capacity to detect gamma rays, analyse and record energy gamma ray spectra in short (s) time intervals within a flight.

airborne gamma ray survey: A survey carried out using an airborne gamma ray spectrometer installed in an aeroplane.

alpha decay: The disintegration of an unstable atom nucleus by emitting an alpha particle.

alpha radiation: The flux of alpha particles, formed by 2 protons and 2 neutrons.

annual effective dose: A measure of the energy deposited by radiation in organs and tissue per year – measures the biological effects of radiation to humans.

anomaly: a variation in radiation level exceeding those fluctuations normally expected because of the statistical nature of radioactive decay.

background radiation: Radiation attributable to all radiation sources other than the one currently of interest.

becquerel: SI unit of activity, equal to one transformation per second.

beta decay: The disintegration of an unstable atom nucleus by emission of a beta particle.

beta radiation: The flux of beta particles, formed by electrons.

calibration: The process by which the response of a radiometric instrument is related to sources of known activity or other defined radioactivity quantities. Calibration of radiometric instruments implies the estimation of instrument sensitivities and other constants.

calibration pads: Concrete cylindrical or rectangular pads, enriched individually by radioelements of interest – usually K, U and Th.

car-borne gamma ray spectrometer: High sensitivity gamma ray spectrometer mounted in a motor vehicle for the detection of gamma-radiation over short (s) time intervals.

Compton continuum: That part of the gamma energy spectrum formed by photons that have lost part of their original energies through Compton scattering.

Compton scattering: The interaction of a photon with an orbit electron of an atom, in which the photon loses part of its energy and changes its direction.

cosmic radiation: The component of natural radiation formed by high energy particles and photons coming from outer space. Intensity of cosmic radiation increases with altitude.

count rate: The response of a radiometric instrument to detected radiation, given in counts per unit time.

counting time: Preselected time for a radiometric instrument to accumulate counts as a measure of radiation.

counts: Recorded response of a radiometric instrument to radiation sources. The response is due to either a detected particle or photon of energy.

daughter products: Radioelements formed in a disintegration series from a mother element.

dead time: The time required for a detector or a radiometric instrument to generate and process a signal (electrical signal) as a response to detected nuclear particle. During this time the instrument is insensitive to other incident particles or photons.

decay: A spontaneous nuclear transition of an unstable atomic nucleus.

decay constant, λ: For a particular radionuclide, $\lambda = dP/dt$, where dP is the probability of a given nucleus undergoing a spontaneous nuclear transition in the time interval dt.

decay product: Newly formed nuclide in a nuclear transition.

deconvolution of a spectrum: The process of decomposition of an energy spectrum to spectral components corresponding to that from individual contributing sources.

detection efficiency: Probability that an incident particle or photon will interact with the detector - the ratio of registered counts to the number of incident particles.

detector: A sensitive sensor having the capacity to register ionizing radiation directly or to transform the energy of incident nuclear particles to electrical quantities.

differential gamma ray spectrometer: Radiometric instrument that registers gamma rays of energies within defined lower and upper limits (in energy channels).

dose: A measure of the energy deposits by radiation in a target.

dose rate: The ratio of the dose deposited by radiation in a target to the exposure time.

effective dose: The quantity E, defined as a summation of the tissue equivalent doses (H_T), each multiplied by the appropriate tissue weighting factor (w_T). $E = \Sigma\, w_T H_T$.

energy calibration: The process of establishing the relationship between energy of recorded gamma rays, and the channel number of a multichannel gamma ray spectrometer.

energy gamma ray spectrum: A graphical presentation of the energies of gamma rays against their frequency (counts per channel). Peaks in the spectrum indicate radionuclide emission lines.

energy resolution: Parameter describing the ability of detector to distinguish gamma ray energies.

energy threshold: An energy below which all particles/photons are ignored.

energy window: A defined energy interval of the gamma ray spectrum. Energy window implies several energy channels.

equivalent uranium, equivalent thorium: The concentration of uranium/thorium estimated by gamma ray spectrometry under the assumption that the U and Th decay series are in secular equilibrium.

fallout: Fallout, nuclear fallout, man-made radioactive isotopes deposited on the earth surface.

gamma ray spectrometry: Radiometric method based on the proportionality between energy of gamma quanta deposited in the detector and pulse amplitudes at the output of the detector, that enables the qualitative and quantitative analyses of gamma ray emitting sources.

gamma rays: Photons of energy that posses neither charge nor mass. Electromagnetic radiation with a frequency of about 3×10^{19}Hz.

gamma ray: Hyphenated when used as an adjective (eg. gamma ray spectrometer).

gamma total count measurements: Measurement of gamma radiation with instruments responding to gamma rays of all energies.

geometric correction: A correction applied to instrument sensitivities estimated from calibrations using calibration pads of limited horizontal and vertical dimensions.

gray: SI unit of kerma and absorbed dose, equal to 1 J/kg.

gridding: The interpolation of irregularly spaced data onto a mesh at regularly spaced intervals.

half-life, $T_{1/2}$: The time required for the activity of a radionuclide to decrease by half.

height correction: The correction of airborne gamma ray spectrometric data for variations in the height of the survey aircraft above the ground.

infinite radiation source: A source of gamma radiation represented by an infinite half-space with homogeneous concentration of a radionuclide or radionuclides.

internal radiation: The term describing the radiation field and absorbed doses from internal sources in the human body.

ionization: The interaction of nuclear radiation with matter resulting in the generation of charged particles.

ionizing radiation: Radiation capable of producing ion pairs in matter.

levelling the data: The normalization of radiometric data measured under different environmental conditions, with various instruments in adjacent areas.

linear attenuation coefficient, μ (m^{-1}): A constant describing the attenuation of a specific radiation in a particular medium - attenuation of the specified radiation per unit distance (m^{-1}).

live time: The counting time corrected for the total dead time of the radiometric measurement.

man-made radiation: Radiation from sources other than natural sources.

mass attenuation coefficient, μ/q (m^2 kg^{-1}): A constant describing the attenuation of specific radiation per unit surface density of absorbing medium. A ratio of linear attenuation coefficient μ to the density ρ of the absorbing medium.

mass number: The number of nucleons (protons and neutrons) in the nucleus of an atom.

multichannel amplitude analyzer: That part of a gamma ray spectrometer that sorts input pulses into channels according to the amplitude (energy) of the input pulses.

natural radiation: Radiation originating from the decay of naturally occurring radionuclides, and cosmic radiation.

normalization of data: A conversion of older (uncalibrated) radiometric data to a new reference level.

nuclear radiation: Radiation originating by disintegration of unstable atomic nuclei.

pair production: The interaction of a gamma ray photon with the nucleus of an atom, in which the photon is absorbed and its energy, $E > 1.02$ MeV, is transformed into an electron-positron pair.

photoeffect: The interaction of an photon with an orbital electron of an atom, in which the photon is absorbed and its energy is used for the release of the orbital electron (kinetic energy).

photopeak: A local maximum in the gamma energy spectrum, representing the emission energy of photons of a source.

point radiation source: A radiation source of limited dimensions.

portable gamma ray spectrometer: A hand-held instrument for detecting and analysing gamma ray emissions.

profile maps: Graphic representation of traverse data as a plot with time or distance along the abscissa.

proton: Principle particle of an atom nucleus. The proton is a positively charged nucleon.

proton number: The number of positively charged nucleons (protons) in the nucleus of an atom.

radiation: A flux of particles or energy originating at transitions of unstable atoms. A physical property of some sources.

radiation flux (see radiation).

radioactive halos: In mineralogy and petrology, micro-areas around radioactive minerals, identifiable in rock thin sections, formed by radiation – particularly alpha radiation.

radioactive minerals: Rock minerals containing natural radioactive elements.

radioactivity: The phenomenon whereby atoms undergo spontaneous random disintegration, usually accompanied by the emission of radiation.

radioelements: A proxy term for measured K, U and Th in gamma ray surveys for geological purposes.

radiometric instrument: A measuring device having the capacity for detecting radiation.

radionuclide: An isotope with unstable atom nuclei.

radon: A noble gas, having radioactive isotopes ^{222}Rn, ^{220}Rn, ^{219}Rn (radon, thoron and actinon).

radon background: The component of background gamma radiation originating in disintegration and gamma radiation of short lived decay products of ^{222}Rn in air, particularly ^{214}Pb and ^{214}Bi.

reference radionuclide: A gamma ray emitting radionuclide used for instrument energy calibration or instrument sensitivity checks.

relaxation mass, β (g/cm^2): A parameter specifying the vertical distribution of gamma emitting radionuclide in the ground, controlling the surface gamma activity.

roentgen, R: Unit of exposure, equal to 2.58 x 10^{-4} C/kg.

scintillation counter: A sensor converting the energy photons or particles of nuclear radiation to voltage pulses, based on luminescence of scintillation matter.

semi-conductor counter: A sensor converting the energy photons or particles of nuclear radiation to voltage pulses, based on induced conductivity in a part of a semiconductor by radiation.

sievert, Sv: SI unit of equivalent dose and effective dose, equal to 1 J/kg.

snow-water equivalent: A term describing the thickness of a snow or water absorbing layer having the same attenuation of gamma rays of the specified energy.

source-detector geometry: Description of mutual geometric relationship between the detector of an instrument and a source of radiation, involving distance, spatial angle of source radiation and source shape and dimensions.

specific activity: A measure of activity of a unit mass, expressed in becquerel per kilogram.

spectrum drift: Phenomenon caused by non-linearity between pulse amplitudes at the detector output and energy of impacting particles into the detector, at very high count rates.

standard: A reference radiation source of known radioelement composition, concentration or activity, with a defined shape, dimensions and matrix composition.

standardization the data: The reprocessing of gamma ray data to the correct level and correct units.

stripping correction: The correction applied to an elemental window count rate to correct for interference from gamma rays due to other elements in that window.

stripping ratios: Numerical parameters, defined by ratios of gamma ray spectrometer sensitivities, applied in the stripping method.

ternary maps: K, U, Th three component colour presentation of natural radioelement concentration in the ground.

terrestrial radiation: Radiation originating from natural radionuclides in the ground.

test-line: A selected airborne traverse used for daily and temporal control of instrument function and stability of environmental radiation.

thermal energy of the Earth: Thermal energy of the Earth is mainly generated by the disintegration of natural radionuclides in the Earth. Thermal energy can be described by the heat production ($\mu W/m^3$) of unit rock volume, or by heat flow (mW/m^2).

threshold gamma ray spectrometer: Radiometric instrument selecting and registering gamma rays of energy exceeding an energy discrimination threshold.

tie-line: Airborne profiles, generally flown perpendicular to regular survey lines - used to level regular survey line data.

uranium equivalent: The amount of uranium that will give the same measured gamma radiation as a particular radionuclide; for example: uranium equivalent of potassium (ppm U/1% K), uranium equivalent of thorium (ppm U/1ppm Th).

Xrays: Electromagnetic radiation of low energy ($E > 40$ keV, approximately).

CONTRIBUTORS TO DRAFTING AND REVIEW

Erdi-Krausz, G.	International Atomic Energy Agency
Matolin, M.	Charles University in Prague, Czech Republic
Minty, B.	B.R.S. Geoscience, Australia
Nicolet, J.-P.	International Atomic Energy Agency
Reford, W.S.	Paterson, Grant & Watson, Limited, Canada
Schetselaar, E.	International Institute for Geoinformation Science and Earth Observation, ITC, Netherlands

Consultants Meetings

Vienna, Austria: 18–20 November 1998; 27–30 September 1999; 5–8 June 2000